People's Democratic Republic of Algeria

Ministry of Higher Education and Scientific Research

University of Khenchela – Abbes Laghrour

Faculty of Technology

Department of Mechanical Engineering

Ph.D Thesis

Presented to fulfill the requirements to obtain:

ACADIMIC Ph.D DEGREE

Field: Sciences and Technology

Option: Mechanical engineering

Specialty: Energetics

Subject

Study of geothermal energy piles performances using CFD (Etude des performances des pieux à énergie géothermique par utilisation de la CFD)

Presented by:

BOUDJAZA Samia

Defended on :16/12/2025

Committee members:

M. BELGHAR Nourreddine	Prof.	University of Khenchela	President
M. CHEHHAT Abdelmadjid	MCA.	University of Khenchela	Supervisor
M. REBAI Billal	MCA.	University of Khenchela	Co-Supervisor
M. KADJA Mahfoud	Prof.	University of Constantine	Examiner
M. SI-AMEUR Mohamed	Prof.	University of Batna 2	Examiner
M. MAACHE Mouna	Prof.	University of Khenchela	Examiner

Academic Year: 2024/2025

Dedications

I dedicate this humble work to my beloved family, the source of my happiness:

To my soul and heart, the light of my life, my mother and father.

To my source of strength and support in this life , my dear brothers

I hope this work serves as a sincere and humble tribute to my love for my family , my success

reflects their boundless love and unwavering support.

SAMIA BOUDJAZA

Acknowledgments

بِسْمِ اللَّهِ الرَّحْمَٰنِ الرَّحِيمِ

(وَلَقَدْ آتَيْنَا لُقْمَانَ الْحِكْمَةَ أَنِ اشْكُرْ لِلَّهِ ۚ وَمَن يَشْكُرْ فَإِنَّمَا يَشْكُرُ لِنَفْسِهِ ۖ وَمَن كَفَرَ فَإِنَّ اللَّهَ غَنِيٌّ حَمِيدٌ)

[لقمان: 12]

First and foremost, I express my deepest gratitude to Allah for His infinite mercy and guidance throughout this journey, which has made the completion of this thesis possible.

I am profoundly grateful to my supervisor, Dr. Abdelmadjid CHEHHAT, Department of Mechanical Engineering, Faculty of Science and Technology, University of Khenchela, Algeria, for his unwavering support, insightful guidance, and invaluable advice. His dedication to academic excellence and mentorship has been a constant source of inspiration and has profoundly shaped this research.

My sincere thanks go to my co-supervisor, Dr. Billel REBAI, University of Khenchela, Faculty of Science and Technology, Department of Civil Engineering, Algeria, whose expert feedback and constructive criticism greatly enriched this work and encouraged me to achieve higher standards.

I would also like to extend my heartfelt appreciation to Pr. Younes MENNI, University Center Salhi Ahmed Naama, for his generous assistance and continuous support. His expertise, availability, during critical stages of the research were truly invaluable and made a significant impact on the successful progress of this work.

I would like to express my sincere gratitude to the jury president Pr. Noureddine BELGHAR and examiners: Pr. Mahfoud KADJA, Pr. Mohamed SI-AMEUR, and Pr. Mouna MAACHE for their time, insightful comments, and valuable suggestions that greatly contributed to the improvement of this thesis.

Last but not least, I am deeply thankful to my family for their patience, encouragement, and unwavering belief in me, which have been fundamental to the successful completion of this thesis. I also extend my gratitude to everyone who supported and motivated me, even with just a kind word along the way.

Table of contents

List of Tables

List of Figures

List of appendices

Nomenclature

A	Cross-sectional area of the pile	m^2
$C_{1\varepsilon}, C_{2\varepsilon}$	Empirical constants for the turbulence model	-
C_μ	Empirical constant for turbulent viscosity	-
c_p	Specific heat capacity	$J.kg^{-1}.K^{-1}$
c_p	Soil volumetric heat capacity	$J.m^{-3}.K^{-1}$
c_{pf}	Fluid exchanger specific heat capacity	$J.kg^{-1}.K^{-1}$
D_H	Hydraulic diameter	m
Δl	Distance between strain points i and i-1	m
ΔT	Temperature change	K
E	Young's modulus of the pile material	Pa
Ei	Exponential integral function	-
F	Axial load applied to the pile	N
G_k	Production rate of turbulence kinetic energy	$J.kg^{-1}.s^{-1}$
h	Convection coefficient of fluid	$W.m^{-2}.K^{-1}$
k	Turbulence kinetic energy	$m^2.s^{-2}$
L	Length of the pile	m
$\dot{m}$	Mass flow of circulating water	$kg.s^{-1}$
P	Pressure	$N.m^{-2}$
∇p	Pressure gradient	$Pa.m^{-1}$
Q	Heat flux	$W.m^{-2}$
q	Internal heat generation flux in the solid	$W.m^{-2}$
q_r	Radiative heat flux	$W.m^{-2}$
R_b	Conductive thermal resistance for a borehole	$m.K.W^{-1}$
R_c	Concrete thermal resistance	$m.K.W^{-1}$
R_p	Conductive thermal resistance for a single pipe – one leg of the U-tube	$m.K.W^{-1}$
$R_{p,f}$	Inner convective thermal resistance for a single pipe – one leg of the U-tube	$m.K.W^{-1}$
r_c	Radius of the concrete	m
r_{eq}	Equivalent radius of the U-tube legs	m

r_{pi}	Inner radius of the pipe making up the U-tube	m
r_{po}	Outer radius of the pipe making up the U-tube	m
S	Shank spacing i.e. center-to-center distance between two legs of the U-tube	m
T	Temperature	K
T_{in}	Inlet water temperature	K
T_{out}	Outlet water temperature	K
t	Time	s
U	Velocity component	$m.s^{-1}$
u	Fluid velocity	$m.s^{-1}$
u_{trans}	Translational velocity of the solid	$m.s^{-1}$
X	Spatial coordinate	m
∇T	Temperature gradient	$K.m^{-1}$
∇u	Velocity gradient	s^{-1}

Greek Symbols

α	Coefficient of thermal expansion	K^{-1}
α_g	Soil thermal diffusivity	$m^2.s^{-1}$
γ	Euler's constant ($\gamma = 0.5772$)	-
δ	Displacement	m
ε	Dissipation rate of turbulence kinetic energy	$J.kg^{-1}.s^{-1}$
ϵ	Strain	-
ϵ_{res}	Residual strain	-
ϵ_T	Thermal strain	-
ϵ_{T-free}	Free thermal strain	-
λ	Thermal conductivity	$W.m^{-1}.K^{-1}$
λ_s	Thermal conductivity of the solid	$W.m^{-1}.K^{-1}$
λ_f	Thermal conductivity of the water	$W.m^{-1}.K^{-1}$
λ_c	Thermal conductivity of the concrete	$W.m^{-1}.K^{-1}$
λ_p	Thermal conductivity of the pipe	$W.m^{-1}.K^{-1}$
λ_g	Soil thermal conductivity	$W.m^{-1}.K^{-1}$
μ	Dynamic viscosity	$kg.m^{-1}.s^{-1}$

μ_t	Turbulent viscosity	Pa.s
ν	Kinematic viscosity of the fluid	$m^2.s^{-1}$
ρ	Density	$kg.m^{-3}$
σ	Axial temperature stress	$N.m^{-2}$
$\sigma_k, \sigma_\varepsilon$	Turbulent Prandtl numbers	-
σ_{res}	Residual axial stress	$N.m^{-2}$
τ	Stress tensor	Pa
ϕ	Dissipation function	$W.m^{-3}$

Dimensionless numbers

Nu	Nusselt number	-
Pr	Prandtl number	-
Re	Reynolds number	-

Subscripts

b, g	Borehole (soil or ground)
c	Concrete
eq	Equivalent
f	Fluid
i	Inner dimension of pipe
i, j	Indices representing spatial directions
i, k	Index
in	Inlet flow
mech	Mechanical
o	Outer dimension of pipe
out	Outlet flow
p	Pipe
R	Thermal resistance
r	Radiant
res	Residual
s	Solid
T	Temperature

trans	Translational

Abbreviations

BEM	Boundary Element Method
BHEs	Borehole Heat Exchangers
CAE	Computer-Aided Engineering
CEL	Coupled Eulerian–Lagrangian
CFD	Computational Fluid Dynamics
DBP-EP	Deeply Buried Pipe Energy Pile
EICP	Enzyme-Induced Carbonate Precipitation
FBG	Fiber Bragg Grating sensors
FDM	Finite Difference Method
FEM	FEM Finite Element Method
FF	Fluid Flow
FVM	Finite Volume Method
GEPs	Geothermal Energy Piles
GSHP	Ground Source Heat Pump
HCF	Heat Carrier Fluid
HDPE	High-Density Polyethylene
HE	Heat Exchanger
HT	Heat Transfer
HVAC	Heating, Ventilation, and Air Conditioning
NFSEP	Nanofluid-Supplemented Energy Pile
PCMs	Phase Change Materials
PHC	Prestressed High-Strength Concrete
PGP	Pre-bored grouted planted
RANS	Reynolds-Averaged Navier-Stokes
SCW	Standing Column Well
SGES	Shallow Geothermal Energy Systems
SPHXs	Steel Pipe Heat Exchangers
SWHP	Surface Water Heat Pump
TPT	Thermal Performance Test
TRT	Thermal Response Tests

GENERAL INTRODUCTION

BACKGROUND

At present, fossil fuels such as oil, coal, and natural gas remain widely used as primary energy sources. However, these resources are finite and pose significant environmental risks related to their extraction, transportation, and use. Fossil fuels account for approximately 66% of global carbon dioxide and other greenhouse gas emissions [1]. Moreover, with increasing energy demand, Algeria's electricity consumption recently peaked at 19,500 MW on July 21, 2024 [2,3]. These factors highlight the urgent need to transition towards sustainable alternatives.

Renewable energy sources (RESs) are seen as reliable and environmentally friendly solutions to the growing energy crisis. These include wind, solar, marine, hydropower, bioenergy, geothermal, and energy storage technologies, all of which have garnered significant global attention. Among them, Geothermal energy offers a promising solution to environmental challenges while addressing essential heating and cooling needs [4,5].Additionally, it has advantages over other renewable energy sources; it is consistently available regardless of conditions and has a low operating cost compared to other systems [6].

A key innovation in this field is the Geothermal Energy Pile (GEP) foundation system, which integrates shallow geothermal energy capture directly into building foundations to meet heating and cooling demands. Recent research has shown a strong focus on enhancing the thermal performance and efficiency of GEP systems. In particular, the geometrical optimization of energy piles has emerged as a central research area, aiming to improve heat exchange rates and overall system performance, through these coupled thermal and mechanical phenomena must be thoroughly understood to ensure both energy efficiency and structural reliability of GEP installations.

To address these challenges, this thesis leverages recent advancements in numerical modeling, particularly Computational Fluid Dynamics (CFD), which offers a robust and precise framework for simulating the transient thermal behavior of Geothermal Energy Pile (GEP) systems under a range of seasonal and operational scenarios. CFD enables detailed assessment of temperature distribution, heat transfer efficiency, and fluid flow characteristics,

providing critical insights into the system's time-dependent thermal and mechanical responses. Building on this modeling approach, the thesis conducts a comprehensive investigation of key design parameters such as laminar flow rates, heat exchanger geometries (circular, square, triangular), pipe diameters, and spatial configurations, and evaluates their combined effects on both thermal performance and structural behavior including displacement, axial stresses, and shear stresses under summer and winter conditions. By integrating high-fidelity CFD simulations with analytical validation, the thesis aims to develop optimized energy pile configurations that enhance both energy efficiency and structural reliability. Ultimately, this thesis seeks to establish a comprehensive and scalable design framework that supports the practical implementation of GEP systems as a reliable and sustainable solution for renewable heating and cooling in buildings. This multidisciplinary approach bridging geotechnical engineering, heat transfer, and fluid mechanics contributes meaningfully to the advancement of current knowledge while aligning with global efforts toward decarbonization and sustainable energy systems.

SCOPE OF WORK

The scope of this thesis focuses on the investigation, modeling, and optimization of Geothermal Energy Pile (GEP) systems, aiming to improve their thermal response and structural performance under various environmental and design conditions. The study addresses key factors affecting heat transfer characteristics, thermal behavior, and mechanical performance, including seasonal temperature variations, fluid flow characteristics within the laminar regime, and geometric configurations of heat exchangers. Detailed numerical simulations using Computational Fluid Dynamics (CFD) evaluate the thermal response of GEP systems under different operating conditions, such as summer and winter scenarios, with special attention to how laminar fluid flow impacts heat exchange efficiency and thermal response time. The influence of critical design parameters, including the diameter of U-shaped heat exchanger pipes, spacing between the pipes and the concrete pile boundary, angular positioning within the pile cross-section, and overall pile diameter, is also investigated for their effects on thermal performance. Additionally, the research compares various heat exchanger geometries (circular, square, and triangular) to assess their impact on temperature distribution, heat transfer efficiency, and thermal response behavior, as well as thermal-mechanical performance indicators such as pile displacement, axial stress, and shear stress. The findings

of this work aim to provide practical insights and design recommendations for enhancing the energy efficiency, structural integrity, and long-term reliability of geothermal pile systems in real-world construction and infrastructure applications.

THESIS OBJECTIVES

The primary objective of this thesis is to advance the understanding and performance of Geothermal Energy Pile (GEP) systems by enhancing both their thermal efficiency and structural reliability. Through the development, modeling, and optimization of system designs, this research aims to contribute to the integration of GEP systems as a more effective and sustainable renewable energy solution. To achieve this, the thesis focuses on the following specific objectives:

- ☞ Perform detailed numerical simulations using Computational Fluid Dynamics (CFD) to analyze the thermal behavior of GEP systems under varying environmental and operational conditions.
- ☞ Investigate the impact of fluid flow rates within the laminar regime on heat transfer efficiency and thermal response time to determine optimal flow conditions.
- ☞ Evaluate seasonal performance variations by simulating system behavior during both summer and winter, with emphasis on temperature-dependent heat exchange efficiency.
- ☞ Develop thermal models to analyze heat transfer mechanisms within the pile under different heat exchanger configurations and seasonal scenarios.
- ☞ Study the influence of key design parameters, including the diameter of U-shaped heat exchanger pipes, spacing between the heat exchanger and concrete pile boundary, angular positioning of pipes within the pile cross-section, and overall diameter of the pile.
- ☞ Analyze the coupled thermal and mechanical behavior of GEP systems incorporating various heat exchanger geometries (circular, square, and triangular).
- ☞ Evaluate the influence of these geometries on heat transfer efficiency, temperature distribution, pile displacement, axial stress, and shear stress under both summer and

winter conditions, with the aim of identifying the most effective geometric configuration.

- ☞ Validate numerical simulations through analytical modeling to confirm their accuracy and establish a comprehensive framework for optimizing the design and operation of GEP systems.

- ☞ Building upon the comprehensive analysis and the obtained results, the systematic optimization of the GEP system design significantly enhances both its thermal and structural performance, thereby improving the system's overall efficiency, reliability, and long-term sustainability in geothermal energy applications.

THESIS OUTLINES

This thesis is organized in accordance with the research objectives and is divided into four chapters and three appendices. The content of each chapter is structured as follows:

CHAPTER I provides the general context of the study. It begins with an introduction to geothermal energy, followed by a historical overview of its development in Algeria. The chapter then introduces the concept of the Geothermal Energy Pile (GEP) system and discusses the various techniques used for its implementation. Finally, it concludes with a summary of the key elements discussed.

CHAPTER II presents a literature review of research related to pile foundations, including review articles, experimental studies, and numerical analyses. It explores key topics such as the thermal performance and thermo-mechanical behavior of pile foundations and offers an overview of implemented thermo-active geostructure projects worldwide. The chapter concludes with a summary of the main findings.

Chapter III is dedicated to the analytical modeling and numerical simulation of the problem under study. The numerical simulation section comprehensively presents the physical problem, including the research motivation, conceptual framework, and detailed mathematical formulations accompanied by the relevant boundary conditions. This section further delineates

the numerical methodologies employed and specifies the simulation software utilized to carry out the analyses. Additionally, the analytical solution section rigorously introduces the

governing equations formulated for the GEP system, providing a fundamental basis for validating the calculations.

CHAPTER IV, a fundamental part of this thesis, presents and discusses the results of the various investigations carried out throughout the work. The chapter is organized into three parts, each addressing key aspects of the research. The first part explores the thermal response of GEPs under different seasonal conditions, employing CFD simulations to analyze the influence of fluid flow rates. The second part investigates critical design parameters affecting thermal exchange efficiency, such as pile and pipe dimensions, spacing, and geometric arrangements. The third part focuses on a comprehensive thermomechanical analysis, evaluating and comparing heat transfer efficiency, temperature distribution, and mechanical responses such as displacement and stress across different heat exchanger geometries within the GEP systems.

CHAPTER I : INTRODUCTION AND OVERVIEW

III.1 Introduction

The growing demand for clean and sustainable energy sources has positioned geothermal energy as a highly promising solution for generating environmentally friendly and renewable energy. CHAPTER I introduces the fundamental concepts and definitions related to geothermal energy and provides a historical overview of its development in Algeria. In addition, it explores the underlying mechanisms of heat transfer and examines the various applications of geothermal energy, with particular emphasis on low-enthalpy geothermal systems, which are the most commonly employed in building environments for heating and cooling purposes.

The overall objective of CHAPTER I is to provide a comprehensive overview of the most relevant technological applications of geothermal energy in the construction sector, particularly for heating and cooling purposes. Special focus is placed on geothermal energy pile (GEP) systems, which integrate the structural function of deep foundations with the thermal exchange capabilities of ground-source heat pumps. This chapter addresses the definition of GEP systems, their structural and functional components, the principles governing their thermal operation, and the practical methods used for their implementation.

III.2 Geothermal energy

IV.2.1 Definition

Geothermal energy, also referred to as ground energy, a key renewable energy source, has garnered increasing global attention due to its reliability, sustainability, and minimal environmental impact. Derived from the Greek words geo (earth) and thermy (heat), geothermal energy refers to the heat stored within the Earth's crust, originating from the planet's core approximately 6000 km below the surface, where temperatures can reach up to 5000°C. This thermal energy is continuously regenerated through the radiogenic decay of naturally occurring isotopes such as potassium, uranium, and thorium, making it a truly renewable resource. As the temperature decreases gradually from the earth's interior to about 10°C at the surface, a constant flow of heat moves upward, forming a gradient that enables energy extraction at various depths. Geothermal systems are generally classified into shallow systems, extending from a few tens to a few hundred meters below ground, and deep systems, which range from several km to regions containing high temperature molten rock. While shallow systems are commonly used for

heating and cooling, deep systems can be harnessed for electricity generation and industrial applications, making geothermal energy a versatile component of the global transition to clean energy.[7]

IV.2.2 A historical overview of geothermal energy development in Algeria

The history of geothermal energy development in Algeria dates back to the pre-independence period, when geothermal springs were used informally for bathing and swimming in Roman-era pools. Systematic exploration began post-independence, with the launch of a national geothermal program in 1967 by Sonatrach. Initial geochemical and geophysical investigations were carried out between 1966 and 1979, followed by gradient drilling in areas such as Guelma and Sidi Zid. In the early 1980s, focused exploration in the Constantinois Oriental region led to the identification of over 200 hot springs and the first geothermal resource map of Algeria. Collaboration between Sonelgaz and the Italian company ENEL further advanced studies in the eastern and northern regions. From the 1980s to the mid-1990s, geothermal applications were primarily limited to balneology and greenhouse heating, with an estimated thermal power capacity reaching around 100 MWt. However, between 1996 and 2005, geothermal activity stagnated, with few studies published, and reported energy use figures varied across sources. By the early 2000s, low-enthalpy resources dominated, with over 240 springs recorded, yet most applications remained limited to bathing. Diversification began in the 2000s, including fish farming and a few small-scale heating and cooling projects. By 2015, the number of application categories had increased, though total installed capacity declined, indicating infrastructure and maintenance challenges. Despite Algeria's considerable geothermal potential, especially in the Albian aquifer in the Sahara, development has remained limited due to the country's focus on fossil fuel resources and the lack of strategic prioritization of geothermal energy within its renewable energy policies. Table 1 presents a chronological summary of this historical development [8].

Table I. 1. Chronological review of historical development of geothermal energy in Algeria [8].

Year	Key Contents	References
Before 1962	• Geothermal springs were used only for bathing and swimming in the ancient Roman pools.	[9]
1967	• Geothermal exploration program was started-up by the national company Sonatrach.	[9,10]
1978-1979	• The first geophysical prospection in the northeastern part of the country. • The first geothermal well was drilled in Guelma area.	[9]
1980-1982	• Geothermal exploration program was conducted focusing on the Constantino is Oriental area. • The national company Sonelgaz conducted geothermal identifications tudies in the eastern and northern regions of the country. • An inventory of more than 200 hot springs was counted in Algeria.	[10,11]
1983	• Geothermal resources activities have been continued by the Algerian Centre of Renewable Energies Development and the program has been extended to the entire northern part of the country	[10]
1992	• The first installation of greenhouse heating system for 18 greenhouses with a total area of 7200 m^2 using the Albian geothermal water in Ouargla and Touggourt regions.	[12,13]
1995	• Updated inventory with more than 240 identified thermal springs in the country.	[13,14]

2005	• An investigation was carried out through the recorded 240 hot springs and all were identified as low enthalpy resources with maximum reservoir temperature of 120°C. • Geothermal space heating was first installed in Hammam Bouhnifia and Hammam Meskhoutine	[15,16]
2008	• The first fish farms were installed in Saida, Ouargla and Ghardaia locations.	[17,18]
2010	• The first residential geothermal heat pump system was installed in a primary school of Saida city. Starting the installation of the first binary cycle power plant in Guelma region.	[17,18]
2015	• The first air conditioning system was installed in Algeria.	[19,20]
2018	• The updated inventory identified more than 282 hot springs in the country.	[21]

Geothermal energy development in Algeria has experienced fluctuations over the past few decades, reflecting shifts in national priorities and investment in renewable energy. The evolution of installed capacity for direct-use applications highlights both the potential and the challenges associated with geothermal resource utilization in the country. Figure 1 presents a bar chart illustrating the evolution of direct-use geothermal capacity in Algeria over the period from 1995 to 2020. Between 1995 and 2000, the geothermal thermal capacity remained stable at approximately 100 MWt. A significant peak was recorded in 2005, with capacity reaching 152.3 MWt. This was followed by a gradual decline: by 2010, the capacity had decreased by 85.46 MWt relative to the 2005 peak, and by 2015, it had declined further by an additional 97.66 MWt compared to 2005. By 2020, the capacity had reached 77.7 MWt.

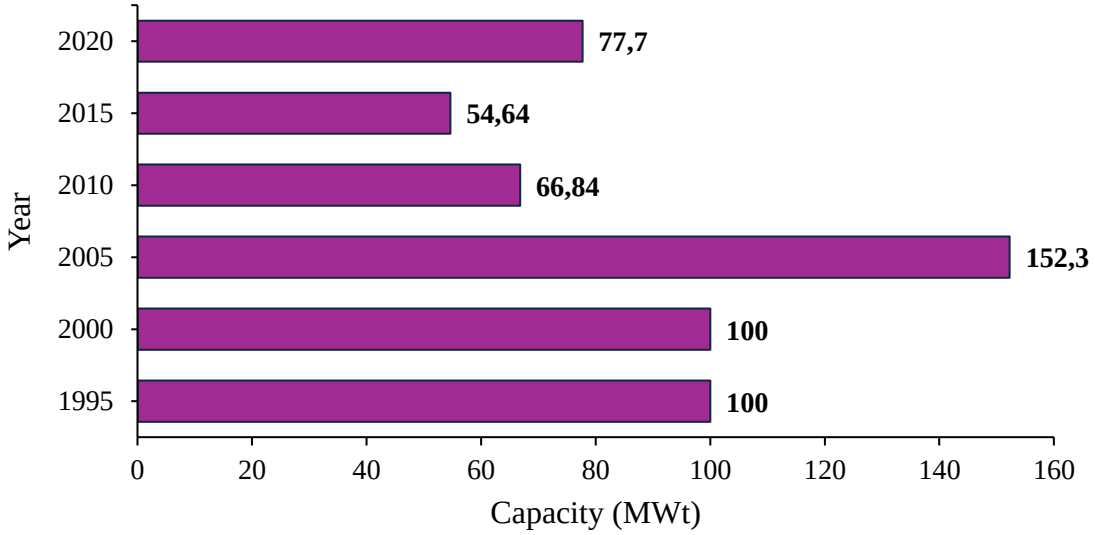

Figure I. 1. Bar chart of direct-use geothermal capacity in Algeria [8,22].

In Algeria, geothermal water is primarily utilized for balneology, space heating, and greenhouse heating. A notable example of successful direct-use application is a fish farming project in the Saharan region, where geothermal water at 60 °C supports aquaculture operations. Similarly, eighteen greenhouses covering a total area of 7,200 m² are heated using geothermal water at 57°C. In the northwestern region of the country, a geothermal heat pump system was implemented in a primary school in Sidi Ben Saleh (Saïda) for both heating and cooling purposes. As of 2020, the distribution of geothermal direct-use applications in Algeria included individual space heating (2.0 MWt, 26 TJ/year), greenhouse heating (1.2 MWt, 5.0 TJ/year), fish farming (15.0 MWt, 300.5 TJ/year), balneology (58.3 MWt, 1955.4 TJ/year), air conditioning (0.5 MWt, 3.2 TJ/year), and geothermal heat pumps (0.7 MWt, 85 TJ/year). The

total installed thermal capacity for direct-use applications was estimated at 77.7 MWt, with an annual energy use of approximately 2,375.1 TJ and a capacity factor of 0.969, indicating efficient and continuous utilization of geothermal resources across multiple sectors. Figure 2 illustrates the distribution of installed geothermal capacity by direct-use application types in Algeria for the year 2020 [16].

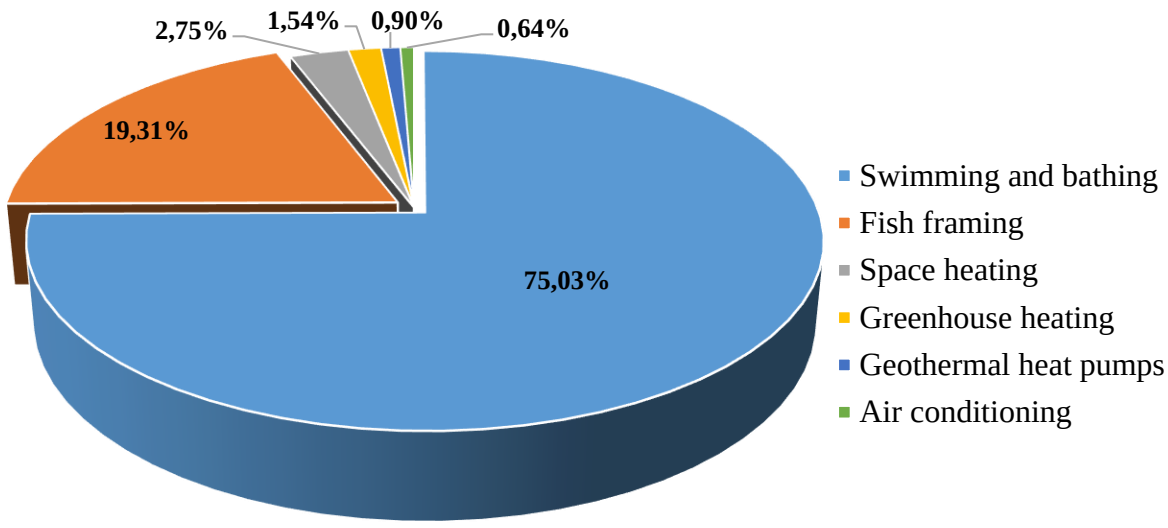

Figure I. 2. Distribution of installed geothermal capacity by direct-use applications in Algeria (2020) [22].

III.3 Low-enthalpy ground energy utilization technologies

Geothermal energy sources are classified based on ground temperature into three categories: low-temperature (below 90 °C), medium-temperature (90–150 °C), and high-temperature (above 150 °C) resources. These temperature levels determine their practical applications. High- and medium-temperature resources are mainly used for electricity production, while low-temperature resources are ideal for heating and cooling buildings**.**

Geothermal systems are generally divided into open-loop and closed-loop types. The open-loop system**,** also known as a geothermal doublet, uses two wells: one to extract groundwater and another to re-inject it after heat exchange. This system is highly efficient, up to eight times more than closed systems, and is suitable where a reliable aquifer is available. In contrast, the closed-loop system uses sealed pipes filled with a heat transfer fluid that circulates underground, absorbing heat and delivering it to a heat pump**.** Unlike open systems, closed

loops do not require groundwater and can be installed vertically or horizontally, depending on site conditions (see Figure 3) .

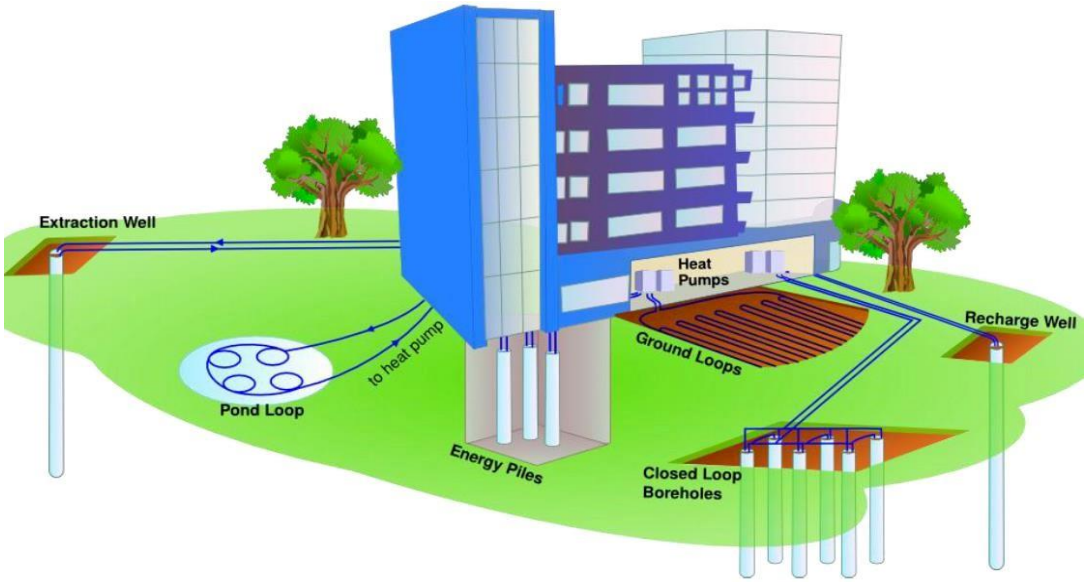

Figure I. 3. Schematic of low-temperature geothermal energy systems [23].

I.3.1 Open-loop ground energy systems

In open-loop geothermal systems, thermal energy is exchanged directly with groundwater. This process involves extracting groundwater through a pumping well, after which the water is either reinjected into the same aquifer or discharged into nearby surface water bodies, such as lakes, rivers, or canals. The performance and feasibility of these systems depend largely on the availability and characteristics of local aquifers, as well as on environmental and regulatory constraints. As shown in Figure 4, groundwater abstraction and discharge can be implemented in several configurations, depending on system design and site-specific legal requirements:

- **Well doublet system:** This configuration includes two separate wells—one for groundwater extraction and another for reinjection into the aquifer.

- **Groundwater heat pump with surface water discharge:** In this case, extracted groundwater is used for heat exchange and subsequently discharged into surface water bodies, in compliance with environmental regulations.
- **Standing column well (SCW):** This design employs a single well for both extraction and reinjection, with water circulating within the same borehole, allowing for efficient thermal exchange while minimizing surface impact.

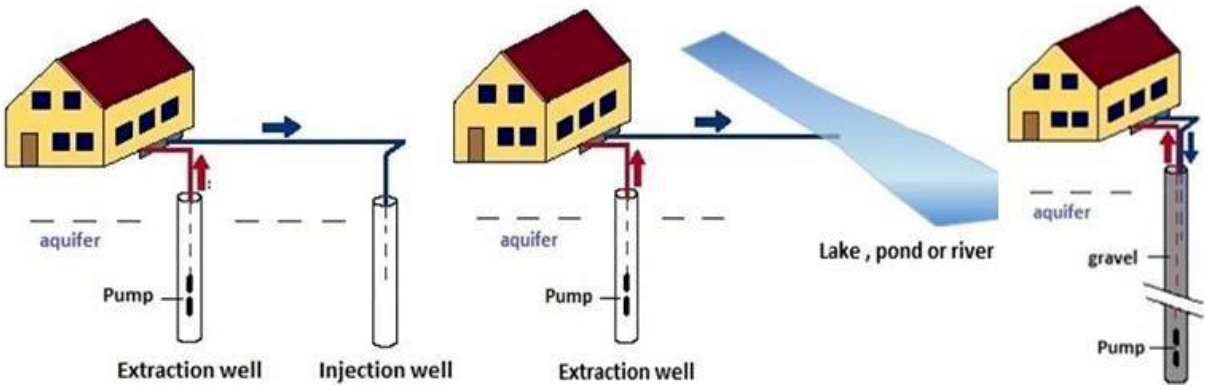

Figure I. 4. Open-loop configuration of groundwater heat pump systems (source: Polytechnic of Turin) [24].

I.3.2 Closed-loop ground energy systems

Closed-loop geothermal systems operate based on conductive heat transfer between the ground and a circulating heat carrier fluid contained within a sealed hydraulic circuit. The fluid either absorbs or releases heat to the ground depending on whether the system is operating in heating or cooling mode. These systems typically involve a single looped pipe, where the fluid enters through one path and returns via the opposite direction in the same circuit. The design and implementation of closed-loop systems can vary, most commonly configured in either horizontal or vertical orientations, depending on site-specific factors such as ground thermal properties, available land area, and the required energy output.

Ground heat exchangers used in closed-loop systems are generally classified into three main categories as shown in Figure 5:

- **Shallow horizontal collectors**, including configurations such as earth coils, serpentine loops, and geothermal baskets, which are installed at relatively shallow depths and require substantial surface area (see Figure 5(A));
- **Borehole heat exchangers (BHEs)**, which are vertically drilled systems and represent the most widely used and efficient configuration, especially in areas with limited surface space (see Figure 5(B));

- **Geothermal piles and energy geo-structures**, where heat exchanger pipes are integrated into structural elements such as building foundations, retaining walls, or piles, allowing for a dual structural and energy function (see Figure 5(C)).

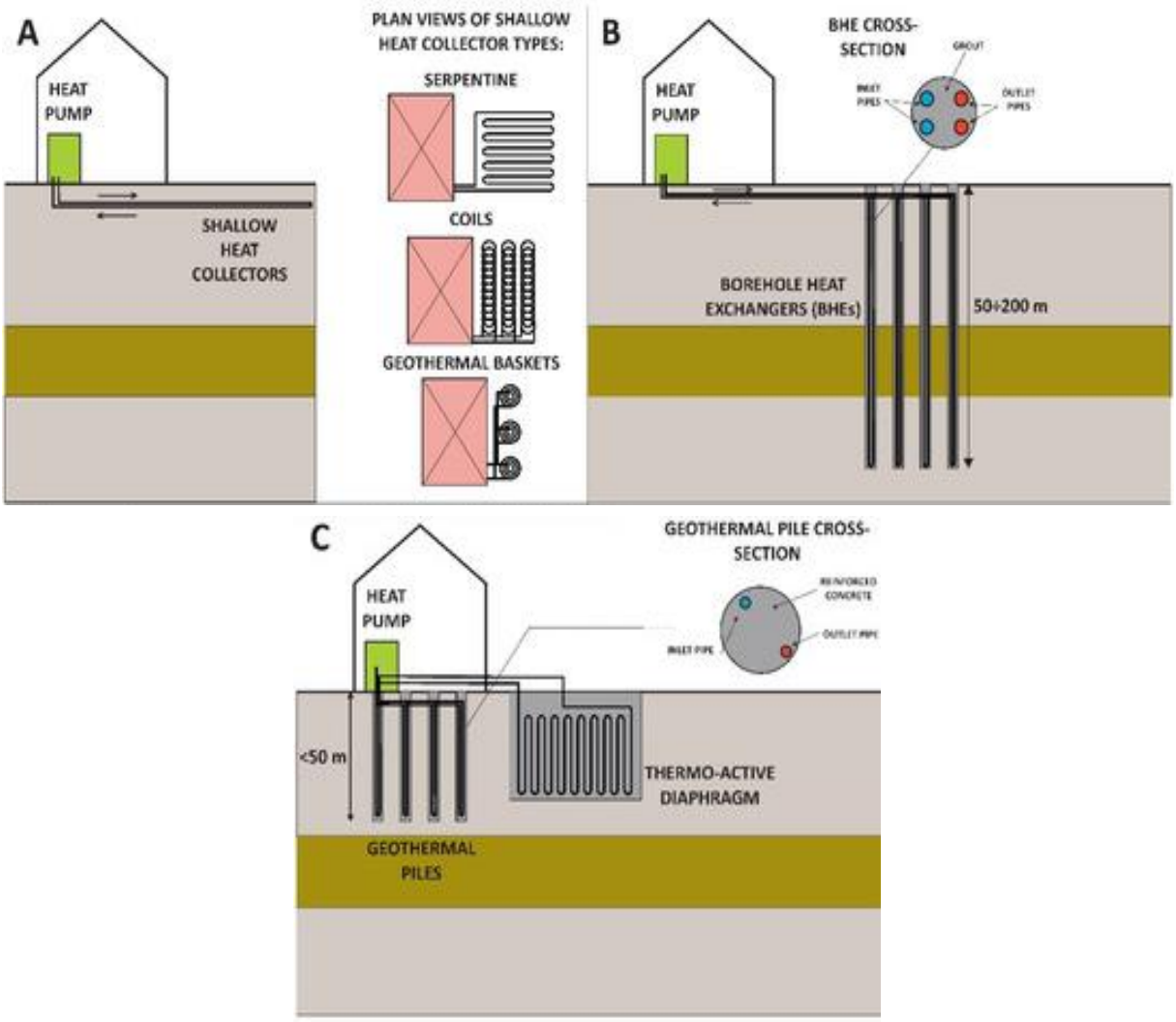

Figure I. 5. Typology of closed-loop ground heat exchangers [25].

I.3.3 Surface water heat pump

Surface water heat pump (SWHP) systems can be implemented using either open-loop or closed-loop configurations. In an open-loop SWHP system, water is directly extracted from a surface water body, circulated through a heat pump for thermal exchange, and subsequently discharged back into the same or a different surface water source (Figure 6(a)). Conversely, closed-loop SWHP systems employ submerged heat exchangers, such as slinky coils, high-density polyethylene (HDPE) pipes, metallic panels, or other specialized configurations,

installed within the surface water body. These components facilitate indirect thermal exchange without direct water withdrawal (Figure 2(b)).

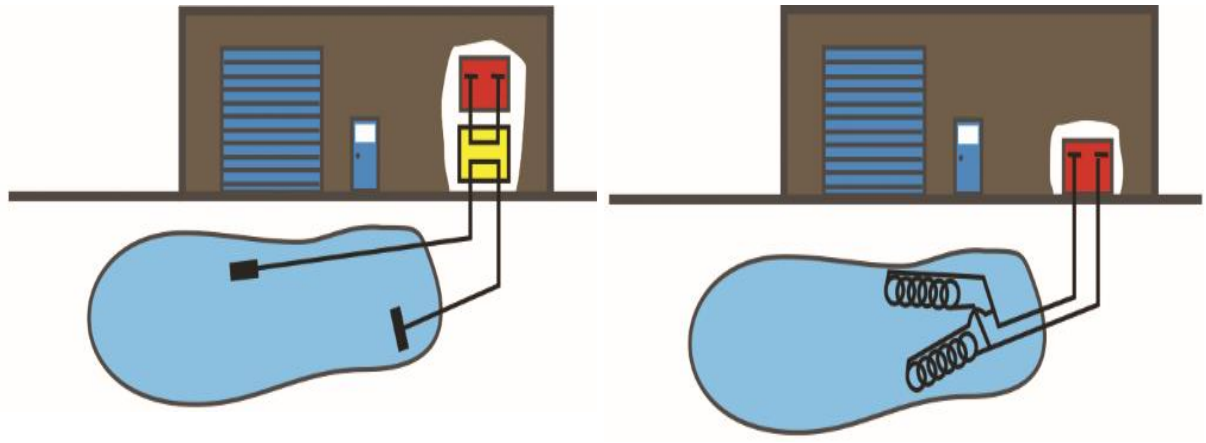

(a) Open loop **(b) Closed loop**

Figure I. 6. Configurations of surface water heat pump (SWHP) systems [26].

Geothermal energy piles (GEPs), also known as thermo-active geostructures, the most common type of energy geo-structures, compared with conventional GSHP systems, GEPs save a lot of installation costs and have become increasingly popular around the world [27,28].

III.4 Geothermal energy pile GEP system

I.4.1 Definition

Geothermal energy piles also known as thermal piles or heat exchanging piles are an innovative way of incorporating the concrete pile foundation element of a building with closed-circuit heat exchanging loops, and coupled with a heat pump system, to exchange the heat energy present within the shallow earth surface **[23,24]** (see Figure 7). This system comprises the process of coupling ground heat exchangers with heat pump units to harness the low-grade heat energy within the shallow earth surface for the purpose of space heating and/or cooling in buildings. The system installation involves incorporating ground energy loops, made from high density polyethylene (HDPE) plastic, within the foundation element(s) often referred to as ground heat exchangers or pile heat exchangers. Inside the HDPE pipes, heat carrier fluid (HCF) is circulated to exchange heat energy with the ground. In winter, the system extracts heat from the ground and transfers it to the building for space heating, whereas the process is reversed in summer to achieve space cooling. The working principle of the system relies on the difference between the ambient air temperature and the ground temperature to transfer the energy between

the two mediums. Thus, to ensure the longevity and sustainability of the system, researchers advised that the system should not be subjected to extreme operating conditions such as extreme monotonic or monodirectional thermal loading [31,32].

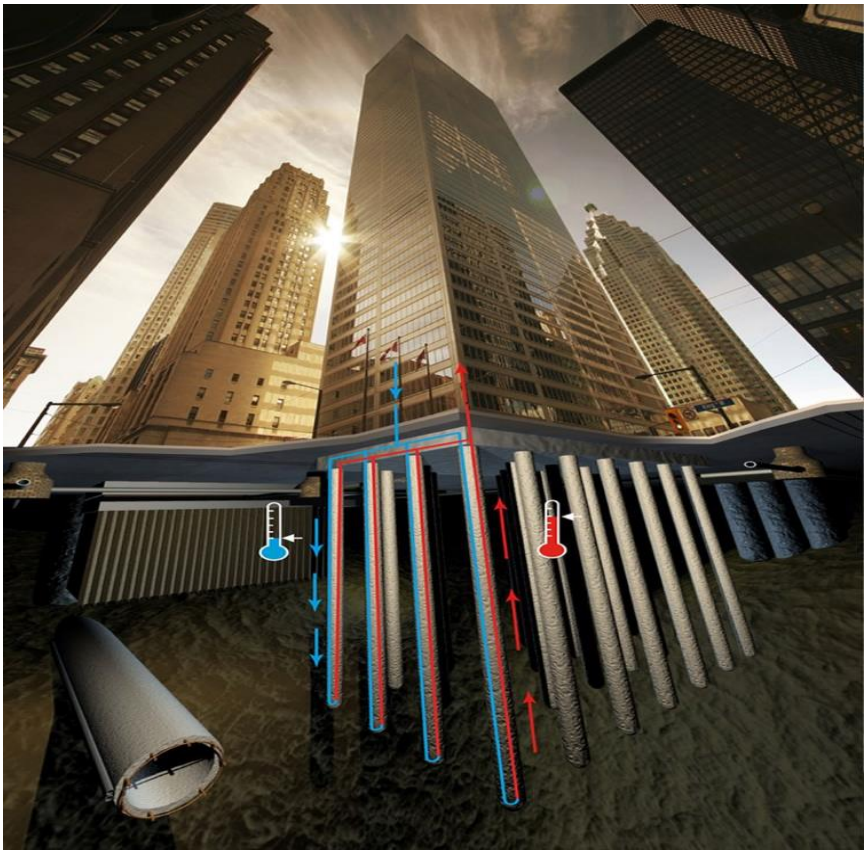

Figure I. 7. GEP system (source: EPF Lausanne) [33].

I.4.2 Structural and functional components of GEP systems

Figure 8 provides a schematic representation of a typical pile foundation system, illustrating the integration of structural foundation elements with subsurface thermal exchange mechanisms. This system exemplifies the dual-function nature of energy geo-structures, serving simultaneously as load-bearing foundations and as ground-coupled heat exchangers for heating and cooling applications.

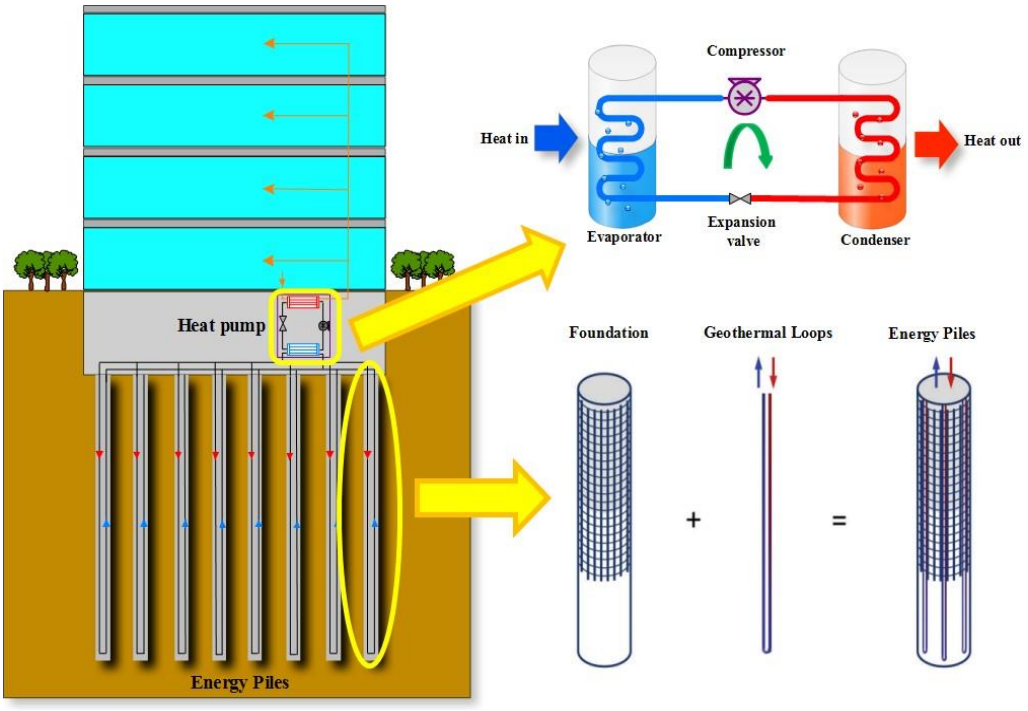

Figure I. 8. Schematic representation of a typical GEP System [34].

To better understand the system's internal organization, Figure 9 presents the three main structural and functional units of a GEP system, as defined in the literature [31]:

- **The primary unit**, which includes the heat exchange loops embedded within the structural piles;
- **The secondary unit,** composed of the underfloor piping network that distributes thermal energy within the building;
- **The heat pump unit**, which enables the transfer of heat between the ground and the building's thermal distribution system.

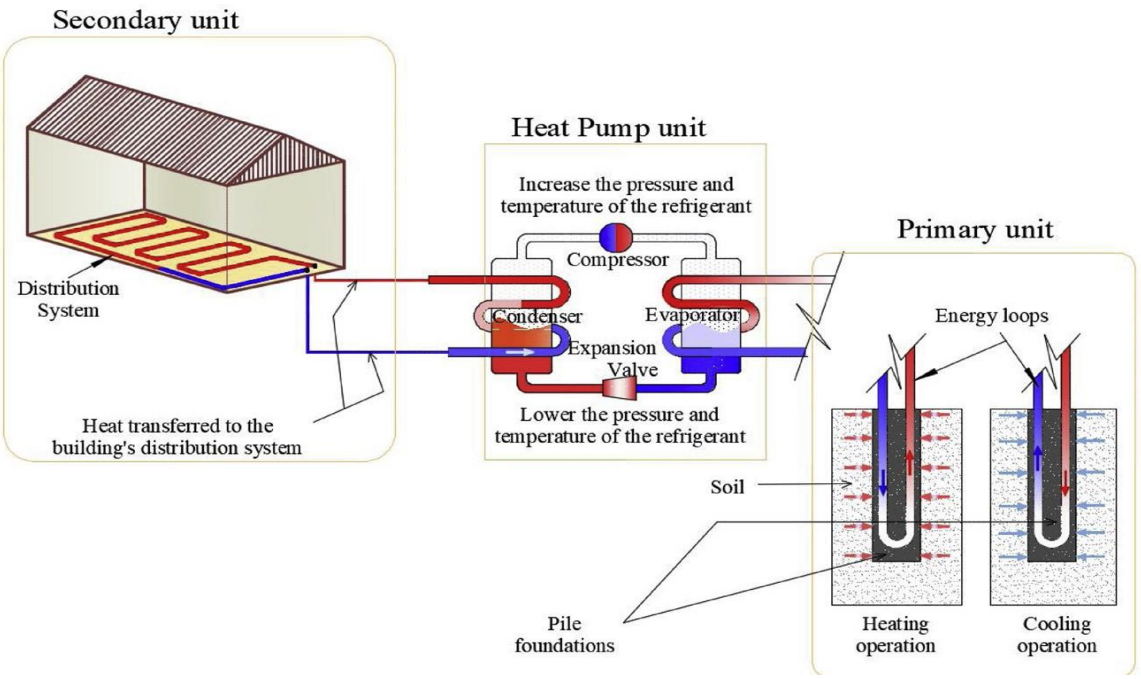

Figure I. 9. Components of GEP system [35].

I.4.2.1 Primary unit

The primary unit of a GEP system consists of heat exchange loops embedded within the structural foundation piles. These loops, typically made of HDPE, are installed during pile construction and serve as the interface for thermal energy transfer between the ground and the circulating fluid. By integrating geothermal functionality into structural elements, this design eliminates the need for separate boreholes, offering a cost-effective and space-efficient solution.

The configuration of the pipe loops plays a critical role in the thermal efficiency of the system. Commonly reported configurations in the literature include the single U-shape, double U-shape, triple U-shape, W-shape, spiral (or helical) shape, as well as direct and indirect double-pipe types [37-41]. These configurations, illustrated in Figure 10, are selected based on key design factors, as the choice of pipe geometry directly influences the overall heat exchange capacity and operational efficiency of the GEP system.

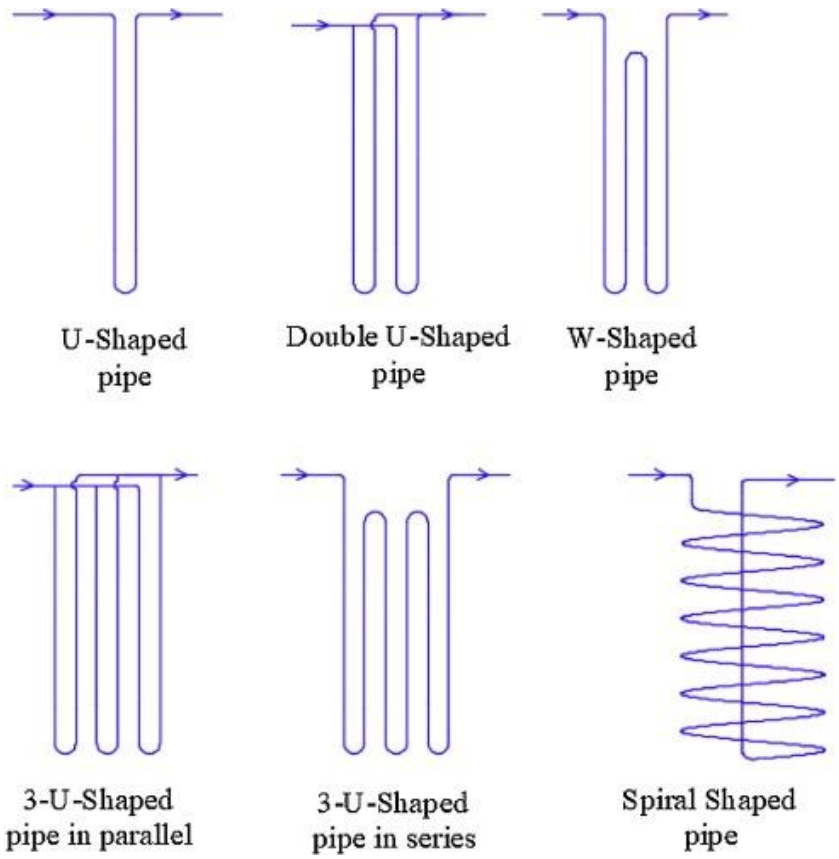

Figure I. 10. Schematic representation of different heat exchange loop designs in GEP system [35].

I.4.2.2 Secondary unit

The secondary unit comprises the internal piping network, often installed in floors or walls, that distributes thermal energy throughout the building. It facilitates the delivery of heating or cooling generated by the GEP system to various zones within the structure. This component ensures effective thermal comfort and energy efficiency by coupling the building's envelope with the heat pump system through low-temperature distribution circuits.

I.4.2.3 Heat pump system

A heat pump is a mechanical system designed to elevate the temperature of thermal energy extracted from the ground, making it suitable for space heating, and conversely, to provide cooling when needed. This is achieved by circulating a HCF, typically a mixture of water and antifreeze, through a closed-loop piping network. The operating principle of the heat pump is analogous to that of a refrigerator working in reverse. As illustrated in Figure 9, a

conventional heat pump consists of four main components: the evaporator, compressor, condenser, and expansion valve.

During heating operation, the heat carrier fluid, typically a mixture of water and antifreeze, is pumped through the pipe loops embedded within the geothermal energy piles (GEPs), where it absorbs geothermal energy from the ground. This warmed fluid is then directed into the evaporator of the heat pump, where it transfers its thermal energy to a refrigerant. As the refrigerant absorbs heat, it evaporates and increases in temperature. The resulting vapor is compressed by the compressor, raising its pressure and temperature to produce a high-energy fluid. This high-temperature vapor then flows into the condenser, where it releases its heat to the building's internal thermal distribution system, commonly referred to as the secondary unit, thereby providing space heating. After releasing heat, the refrigerant condenses back into a liquid and passes through the expansion valve, which reduces its pressure and temperature. The cooled refrigerant then returns to the evaporator, allowing the cycle to begin again. For cooling purposes, the entire process operates in reverse, extracting heat from the building and transferring it back into the ground [42].

I.4.3 Thermal operating principle of GEP systems

Geothermal energy, as previously defined, is a renewable and virtually inexhaustible resource. The operation of a geothermal system is based on a cyclical thermal exchange between the ground and the building (see Figure 11): during the winter, geothermal probes (or ground heat exchangers) extract heat from the earth and inject cooler temperatures back into it; in summer, this process is reversed, as the system absorbs excess heat from the building and transfers it into the ground, thereby cooling the structure and recharging the subsurface with thermal energy. This thermal cycling is essential to maintaining the long-term performance and sustainability of the system. Without the reinjection of heat during summer, the soil’s thermal energy would gradually deplete, leading to a local drop in ground temperature and reduced heating capacity during winter. Conversely, extracting heat only in winter without replenishing the ground in summer can cause freezing of the soil over time, potentially rendering the system ineffective or even damaging to the subsurface environment. To prevent such thermal imbalances, geothermal systems are commonly designed with seasonal thermal energy storage capabilities, also referred to as geothermal heat storage. In this approach, excess heat is stored underground during the summer and recovered during the winter via heat pumps. This

regenerative thermal cycle not only sustains the system's operational balance but also enhances energy efficiency and protects the long-term thermal integrity of the ground.

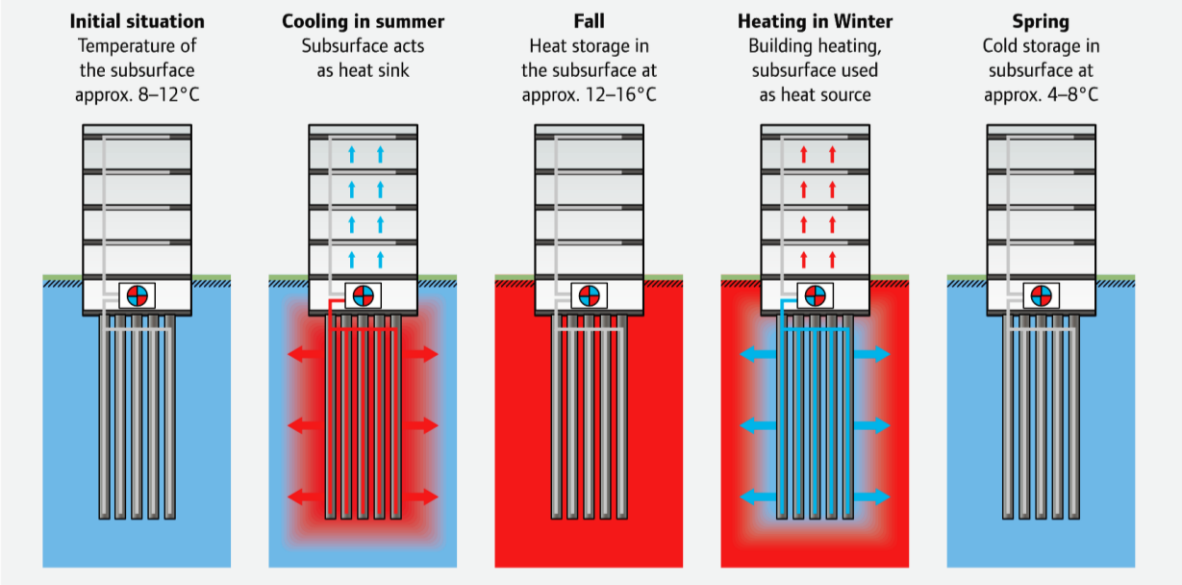

Figure I. 11. Thermal operating principle of GEP systems showing seasonal heat exchange between the building and the ground (source: Technical Information) [43].

I.4.4 Implementation of GEP systems

The implementation of GEP systems involves various construction techniques, depending on site conditions, structural requirements, and the type of heat exchange system to be integrated. Table 2 outlines the main methods used for the installation of geothermal piles, including their descriptions, key characteristics, and typical applications or advantages.

Among these, bored pile techniques are the most widely adopted in France due to their compatibility with a broad range of soil conditions, their adaptability to urban environments, and their ability to accommodate large-diameter piles with integrated heat exchangers. While bored piles are the predominant method, other types such as driven piles and screw piles are also employed in specific contexts.

Table I. 2. Summary of foundation pile types used in GEP systems (source: Technical Information) [43].

Foundation Type	Description	Key Characteristics	Applications / Advantages
Bored Piles (Hollow-Spun Piles)	Cylindrical concrete piles drilled into the ground using various techniques.	• Transfers loads to deeper, more stable soil layers. • Variable length, diameter, and layout.	• Deep foundations. • Excavation support. • Groundwater control.
Hollow-Spun Concrete Ram Piles	Ductile cast iron pipe segments rammed into the ground using hydraulic hammers.	• Quick installation with minimal vibration. • Can be end-bearing or pressure-grouted.	• Suitable for confined construction sites. • Flexible applications.
Pressed Massive Concrete Piles	Precast reinforced concrete sections hydraulically pressed into the ground.	• Excavation possible through hollow core. • Vibration-free installation. • Suitable for low headroom areas.	• Underpinning existing foundations. • Restricted access zones.

Pre-Fabricated Concrete Piles	Solid, fully reinforced concrete piles with circular or square cross-sections.	• Load transfer via skin friction and end bearing. • Installed using hydraulic hammers.	• Cost-effective and technically sound foundation alternative.
Pre-Fabricated Ram Piles (Subtype)	Installed with hydraulic hammers; cutting after installation risks damaging heat exchanger.	• Almost vibration-free installation.	• Risk of pipe damage if cut after installation
In-Situ Piles	Large-diameter piles formed by drilling, soil removal, and casting concrete in place.	• Steel reinforcement inserted before concrete pouring. • Suitable for high-load, deep foundations.	• High-rise buildings and complex foundations.
Slotted Walls (General)	Deep in-situ concrete walls with minimal deformation and high watertightness.	• Low noise/vibration during installation. • Highly watertight.	

I.4.4.1 Installation technique of bored piles (Hollow-spun piles)

❖ **Bored piles with drilling mud**

The construction of a bored geothermal pile involves several key steps. Drilling is carried out using an auger or a bucket under the protection of bentonite-based or polymer-based drilling mud. This technique maintains pressure on the borehole walls, preventing them from collapsing during the drilling process. It also requires the installation of a drilling mud plant, along with a system for recovering and recycling the used mud.

Below is a detailed overview of the step-by-step process (see Figure 12):

Step 1 : Installation of the casing and drilling under mud

A surface casing is installed at the borehole entrance to guide the drilling tools. Drilling is then performed using an auger or bucket while circulating drilling mud to stabilize the borehole walls and facilitate the removal of cuttings.

Step 2 : Cleaning of the borehole

After reaching the desired depth, the borehole is cleaned to eliminate residual cuttings and loose materials, ensuring a clean base for the next construction phases.

Step 3 : Desanding

The used drilling mud, now mixed with sand and soil particles, undergoes a desanding process. This step separates solids from the fluid, allowing the cleaned mud to be recycled back into the drilling operation.

Step 4 : Placement of the reinforcement cage and heat exchanger

A reinforcement cage is lowered into the borehole. Attached to this cage is the geothermal heat exchanger—typically consisting of U-shaped pipes—which enables thermal energy exchange between the ground and the building systems.

Step 5 : Insertion of the concreting pipe (Tremie pipe)

A tremie pipe is inserted to allow for bottom-up concrete placement. This technique prevents segregation of concrete and maintains borehole stability during casting.

Step 6 : Concreting

Concrete is poured through the tremie pipe from the bottom upward, gradually displacing the drilling mud. The displaced mud is collected, treated, and reused as needed.

Step 7 : Withdrawal of the tremie pipe and casing

Once concreting is completed, both the tremie pipe and the temporary surface casing are withdrawn carefully to avoid disturbing the fresh concrete.

Step 8 : Completed geothermal pile

The final product is a reinforced concrete pile equipped with a geothermal heat exchanger. It serves both as a structural foundation element and as a component of the building's energy system.

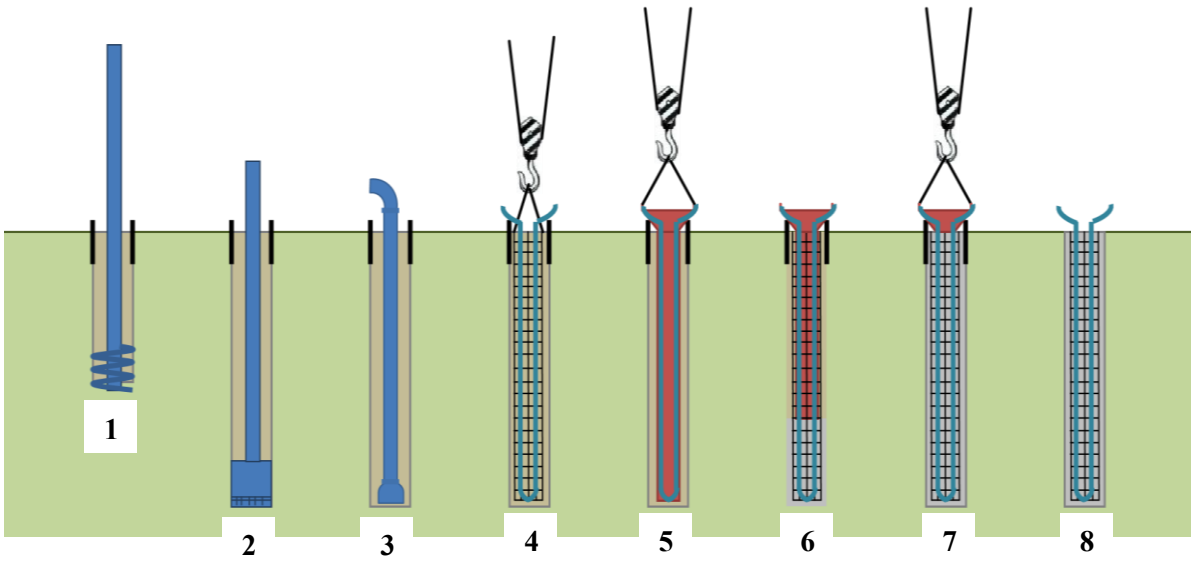

Figure I. 12. Diagram of the different phases of bored pile installation using drilling mud (source: Technical Information) [43].

❖ **Cased bored piles**

This method involves the use of a temporary casing tube during the drilling and concreting phases. Compared to other techniques, cased bored piles generally exhibit lower lateral friction performance, and the soil–pile contact is less direct, which can reduce the overall thermal exchange efficiency.

Below is a step-by-step outline of the process illustrated in the figure 13:

Step 1 : Driving the casing tube

A steel casing is driven into the ground to provide initial support and guide the drilling operation.

Step 2 : Drilling with auger inside the casing

Drilling is carried out inside the casing using a continuous or short-flight auger to reach the required depth.

Step 3 : Placement of reinforcement cage and heat exchanger

The reinforcement cage is lowered into the borehole, along with the geothermal heat exchanger—typically made of U-shaped pipes used for thermal energy transfer.

Step 4 : Concreting

Concrete is poured into the borehole through a tremie or directly into the casing, filling the space around the reinforcement and exchanger.

Step 5: Extraction of the casing tube

Once concreting is complete, the casing is gradually withdrawn. This must be done carefully to avoid disturbing the fresh concrete.

Step 6 : Completed geothermal pile

The result is a reinforced concrete pile with an integrated geothermal heat exchanger, though the thermal contact with the surrounding soil may be less effective than in other methods due to the casing's influence during construction.

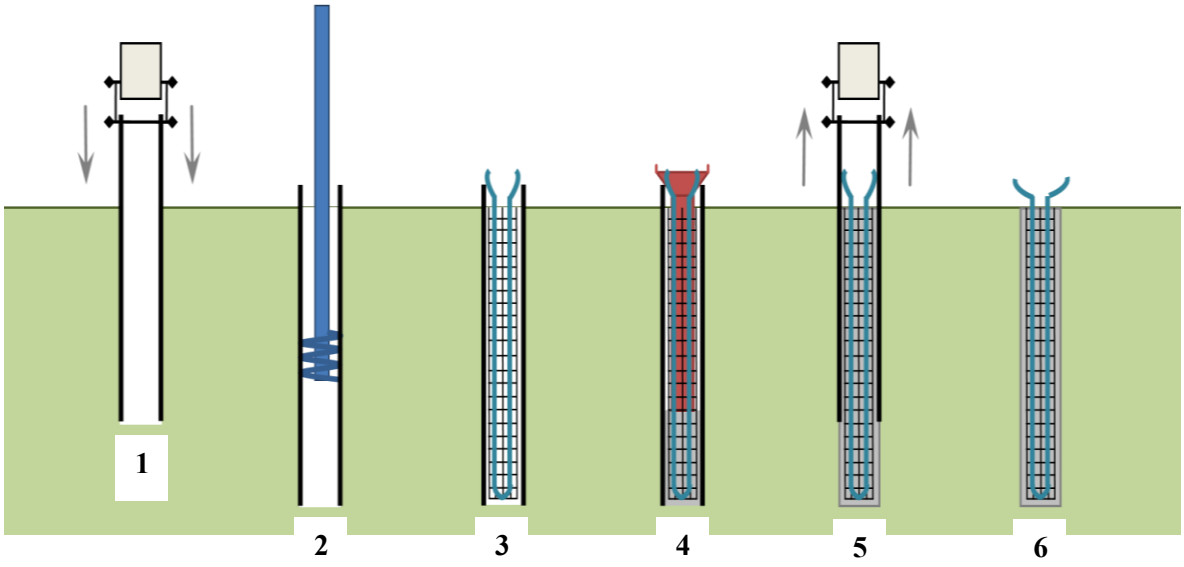

Figure I. 13. Diagram of the different phases in the installation of cased bored piles (source: Technical Information) [43].

❖ **Hollow auger bored piles**

In this technique, the pile is formed using a continuous flight auger that drills into the soil without the need for temporary casing or drilling mud. Concrete is then pumped through the hollow stem of the auger as it is withdrawn, and the reinforcement cage is inserted afterward into the fresh concrete.

One important aspect of this method is that the concrete must have specific rheological properties to ensure it can support the insertion of the reinforcement cage without segregation or collapse of the borehole.

Below is a step-by-step interpretation of the process shown in the figure 14:

Step 1 : Drilling

A continuous flight auger drills into the ground to the required depth, with the soil conveyed upward along the auger flights.

Step 2 : Anchoring

Once the desired depth is reached, the auger is held in place temporarily to ensure borehole stability and anchoring at the base.

Step 3 : Concreting

Concrete is pumped through the hollow stem of the auger from the bottom up, as the auger is slowly withdrawn. This ensures a continuous and compact concrete column is formed.

Step 4 : Spoil Removal

The excavated soil removed during drilling is collected and evacuated from the site.

Step 5 : Placement of reinforcement and heat exchanger

The reinforcement cage and the geothermal heat exchanger pipes are inserted into the fresh concrete while it is still workable.

Step 6: Completed Pile

The final result is a structural pile with integrated geothermal capabilities, ready for use as part of the building’s energy and foundation system.

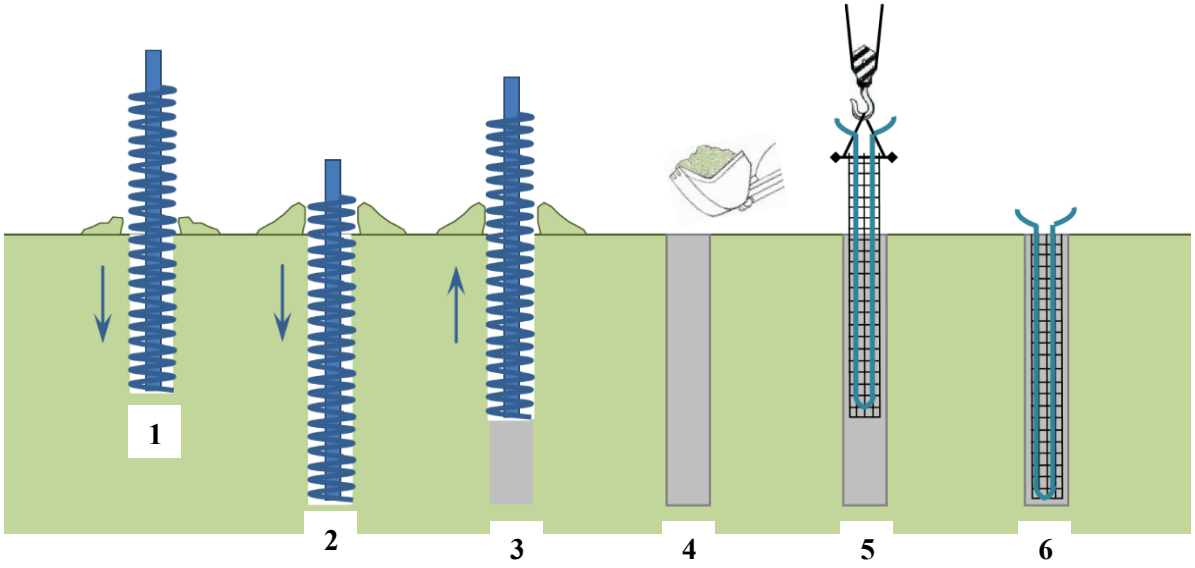

Figure I. 14. Diagram of the different phases in the installation of hollow auger bored piles (source: Technical Information) [43].

III.5 Conclusion

In conclusion, this chapter provided a foundational overview of geothermal energy as a clean and renewable resource, positioning it as a viable alternative to conventional energy systems in the context of sustainable development. It began with the definitions and key concepts of geothermal energy, followed by a historical overview of its development in Algeria. Emphasis was placed on understanding the fundamental heat transfer mechanisms that govern the operation of geothermal systems, particularly within the framework of low-enthalpy applications suitable for buildings. The chapter also highlighted the increasing relevance of geothermal technologies in the construction sector, focusing specifically on GEP systems. These systems, which combine structural and thermal exchange functions, were explored in terms of their definition, components, operating principles, and implementation techniques. The knowledge presented in this chapter lays the groundwork for the more detailed technical, thermal, and structural analyses developed in the subsequent sections of this study.

CHAPTER II : LITERATURE REVIEW

II.1 Introduction

This chapter presents a comprehensive and critical review of the current state of research on geothermal energy pile systems. The review encompasses a broad spectrum of studies focusing on the thermo-mechanical and energy performance of GEPs, highlighting both foundational concepts and recent advances. Particular emphasis is placed on the various factors that govern system performance, including soil thermal conductivity and diffusivity, initial ground temperature conditions, groundwater flow dynamics, and heat transfer mechanisms within the soil–pile interface. Additionally, this chapter examines the impact of structural design parameters such as pile geometry, pipe configurations, and installation methods, as well as the integration of novel technologies such as phase change materials, nanofluids, and advanced modeling techniques. An overview of implemented thermo-active geostructure projects worldwide is also provided, showcasing a diverse range of applications in different climatic and geological contexts. Through this synthesis, the chapter aims to provide a well-structured understanding of how environmental conditions, material properties, and engineering innovations collectively influence the thermal efficiency, mechanical stability, and long-term operational reliability of GEP systems.

II.2 Literature review

II.2.1 Overview of research on geothermal energy piles

The study of geothermal energy piles (GEPs), also known as pile foundations, has witnessed substantial growth over recent decades, driven by the increasing global emphasis on sustainable building technologies and renewable energy systems. The literature in this field demonstrates a progressive evolution from foundational theoretical models to sophisticated numerical simulations and practical field applications. This study underscores a growing recognition of GEPs as a viable solution for enhancing energy efficiency in building systems while addressing structural and geotechnical demands.

Table II.1 presents a chronological overview of the most influential review articles on geothermal energy piles published between 2016 and 2025, forming the core of this bibliographic investigation. This body of research highlights the significant potential of GEPs as sustainable solutions for building heating and cooling.

The reviewed studies cover a broad spectrum of topics, including design methodologies, numerical modeling, experimental testing, and the incorporation of advanced materials such as phase change materials (PCMs) and nanofluids. This synthesized overview provides critical insights into both the historical progression and the current state of research, offering a structured framework for understanding key themes and emerging trends. Consequently, it serves as a valuable reference point for researchers and practitioners aiming to advance further investigations, optimize system performance, or promote the practical deployment of geothermal energy pile technologies.

The following section highlights influential studies that have played a pivotal role in advancing our understanding of thermo-mechanical interactions and in optimizing the performance of pile foundation systems.

Table II. 1. Chronological review of research studies on geothermal energy piles.

Author(s)	Year	Key Contents
Zagorščak et al. [44]	2016	Reviews the performance of energy piles and their impact on surrounding soil; synthesizes findings from field, lab, and numerical studies; highlights how heat transfer affects both thermal efficiency and stress distribution in soil and structural elements; identifies gaps and proposes future research directions to improve understanding of soil–structure–thermal interaction.
Fadejev et al. [45]	2017	Comprehensive review of energy pile systems, including design principles, thermal behavior, and modelling techniques; analysis of thermal response tests (TRT); evaluation of analytical and numerical models; emphasis on the limitations of current software tools and the need for more accurate ground-surface boundary condition modelling.
Gondal et al. [5]	2017	Review of global geothermal technologies with a focus on development pathways and current status in Pakistan; highlights the country's untapped potential in hydrothermal and hot dry rock resources; points out lack of progress in shallow geothermal and direct-use systems; emphasizes the role of geothermal energy in meeting HVAC and process heat demands; proposes policy and institutional recommendations to accelerate adoption of geothermal technologies in developing countries.
Nujid et al. [46]	2018	Reviews numerical modeling of shallow geothermal energy piles, focusing on design, operation, and soil–pile interaction; identifies key parameters for simulations (geometry, soil/thermal properties, boundary conditions);

		highlights use of 3D finite element modeling; concludes W-shaped pipe configuration is most efficient for moderate flow rate and thermal performance.
Sani et al. [4]	2019	Comprehensive review of GEP design, performance, and applications; highlights influence of factors like number of loops, pile length, and soil thermal properties; discusses structural integrity affected by thermal loads and mechanical behavior by pile restraint types; includes global case studies demonstrating benefits, limitations, and energy performance; emphasizes proper design and installation for optimal performance and sustainability.
Cherati et al. [47]	2021	Study on the potential of energy piles in Iran as a sustainable alternative for heating and cooling buildings; addresses the high initial cost of GSHPs by promoting integration with structural elements (e.g., energy piles); reviews international case studies to extract lessons learned; outlines design, construction, and implementation guidance tailored to Iran's economic and environmental conditions; identifies key disadvantages and engineering challenges; proposes practical strategies to overcome regulatory, technical, and awareness-related barriers to adoption in developing countries.
Mohamad et al. [48]	2021	Reviews current knowledge on thermal and thermo-mechanical behavior of energy piles; analyzes design factors like pipe layout, pile dimensions, fluid properties, and concrete mix; finds thermal performance improves with more pipes and thermally enhanced concrete; discusses optimization methods and recommends multi-objective optimization using 4E criteria (energy, exergy, economy, environment) for efficient and safe GEP systems.
Cunha et al. [49]	2022	Reviews shallow geothermal energy systems (SGES) as sustainable solutions for building climate control; synthesizes laboratory, field, and numerical studies; discusses challenges and key factors for effective GEP use;

		emphasizes the need for public and private sector support to expand technology adoption; highlights potential for reducing greenhouse gas emissions.
Zayed et al. [50]	2023	Reviews recent advancements in geothermal reservoir modeling and design of energy piles; outlines thermo-fluid numerical models (FEM, FDM, FVM); analyzes heat extraction performance based on pipe geometry, soil properties, and pile dimensions; discusses coupling of geothermal reservoirs with wells and energy piles; highlights modeling challenges and proposes integrated approaches for better design and optimization of sustainable geothermal systems.
Baffa et al. [51]	2024	Overview of field studies on GEP systems; highlights long-term thermal performance and thermo-mechanical behavior; shows GEPs reduce seasonal energy use compared to conventional systems; axial thermal strains remain within safe limits; stresses from thermal loading are influenced by pile end restraints and soil type; concludes that well-designed and installed GEPs offer a reliable, sustainable energy alternative.
Dokmak et al. [52]	2024	Brief review of geothermal energy piles focusing on key design aspects, challenges, and innovations; discusses use of PCMs and nanofluids as heat transfer media; highlights the impact of pile geometry on performance; provides a concise overview of current developments and outlines future research directions.
Baffa et al. [53]	2025	Bibliometric and systematic review of 72 studies on GEPs; identifies key research trends and variables affecting thermal and thermo-mechanical performance (e.g., heat exchange rate, flow rate, temperature gradient, pile settlement, axial stress); reports practical design challenges, highlights the need to consider thermal loads in structural design, and outlines future research directions.

Ciapala et al. [54]	2025	Reviews and compares TRT, TPT, and operational tests for energy piles/foundations; highlights lack of testing in several global regions; shows key factors affecting thermal performance (e.g., flow rate, inlet temperature, groundwater, pile size); stresses the need for standardized testing protocols and proposes unified frameworks for future research and system design.
Onaizi et al. [55]	2025	Systematic review of PCM use in GEPs; examines experimental and numerical studies on thermal and mechanical impacts; reports major benefits (70% increase in heat extraction, 30% cost savings); identifies challenges such as reduced mechanical strength, material compatibility, and encapsulation issues; highlights research gaps in thermal response, durability, and long-term performance.

II.2.2 Thermo-mechanical behavior of GEP

Thermomechanical studies constitute a critical area of research in GEP foundation systems due to the intricate interactions between mechanical structural behavior and heat transfer phenomena inherent in these systems. Foundational work by Zhang et al. [56] employed multiphysics simulations to investigate the thermo-mechanical behavior of energy piles subjected to seasonal thermal loads. Their results revealed that winter conditions induced an 11.5% reduction in axial compressive stress accompanied by a 47.7% increase in pile head settlement. Conversely, summer conditions resulted in a 12% increase in compressive stress and a 7.2% decrease in settlement. This study underscores the significant influence of seasonal thermo-mechanical coupling on the performance of energy piles.

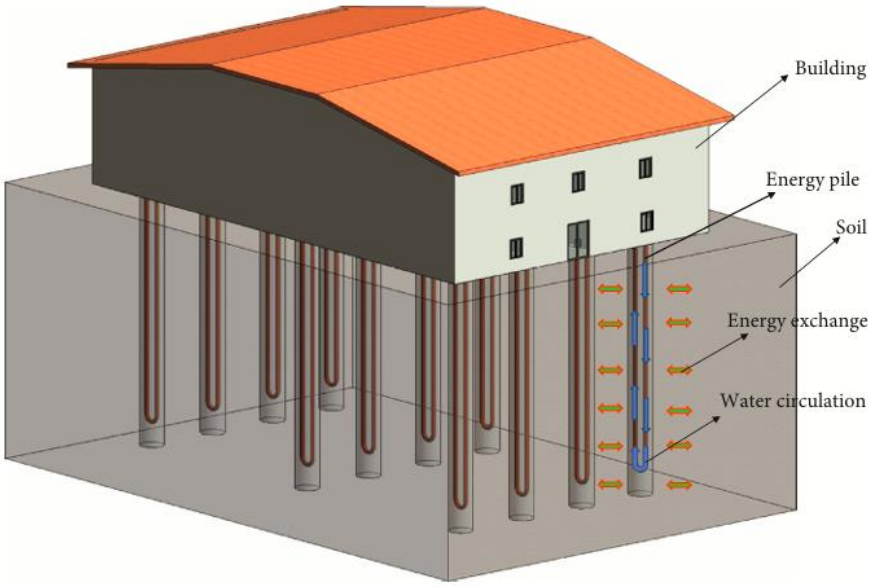

Figure II. 1. Schematic of the energy pile [56].

Furthermore, building on this foundational research, Xu et al. [57] conducted a comprehensive multiphysics simulation to assess the thermo-mechanical behavior of energy piles under varying structural and environmental conditions. Using COMSOL Multiphysics, twelve models were developed featuring different pipe configurations (U-shaped and spiral), pile types (solid and tubular), heat storage materials, and soil treatments incorporating carbon fiber–based enzyme-induced carbonate precipitation (EICP). Results showed that spiral pipes with thermal storage materials enhanced temperature regulation, while EICP-treated soil significantly improved heat transfer and increased soil strength up to 1419.4 kPa. Distinct stress distributions under combined thermal and mechanical loads highlighted the effectiveness of

integrated thermomechanical strategies for improving energy pile performance and sustainability.

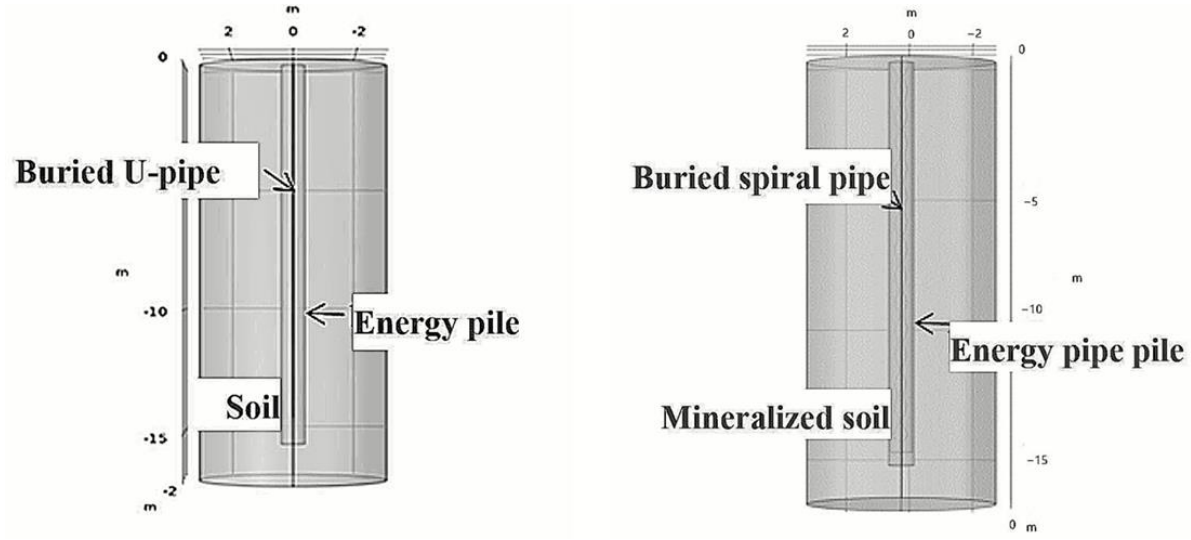

Solid concrete pile **Hollow concrete pile**

Figure II. 2. Structural models of solid and hollow energy piles with different pipe arrangements [57]

Table 2. Summary of Recent Studies (2020–2025) presents key developments in the understanding of the thermo-mechanical behavior of GEP. The reviewed literature underscores the critical influence of coupled thermal and mechanical effects on stress distribution, settlement, and the overall structural performance of GEP systems. Particular attention is given to the roles of soil conditions, pile installation techniques, and thermal loading regimes. Recent innovations such as high-fidelity numerical simulations, machine learning applications, and the incorporation of advanced materials including phase change materials and nanofluids have demonstrated significant potential to enhance both thermal efficiency and mechanical stability. Collectively, these studies contribute to the advancement of more resilient, energy-efficient, and sustainable energy pile foundation designs.

Table II. 2. Recent advances in thermo-mechanical behavior studies of geothermal energy piles.

Author(s)	Year	Aim (s)	Key Contents
Du et al. [58]	2020	To investigate the thermo-mechanical performance of a phase change energy pile with macro-encapsulated PCM under thermal cycles and loading.	Developed and validated a 3D numerical model simulating PC pile behavior. Compared PC and ordinary piles in saturated sand under the same conditions. PC piles showed lower temperature, strain, and displacement. Higher thermal loads increased residual strain and plastic deformation.
Bao et al. [59]	2020	To experimentally investigate the thermo-mechanical behavior of a large-cross-section energy pile in saturated sandy soil.	Conducted model tests on a 0.2 m diameter, 1.5 m long concrete energy pile in saturated sand under controlled thermal cycles. Monitored temperature, pore pressure, soil pressure, and displacement. Found uneven strain and permanent displacement due to thermal plastic strain and soil consolidation.
Li et al. [60]	2021	To investigate the thermomechanical behavior of energy pile-raft foundations under combined building load and cooling thermal load through full-scale in situ testing.	The study shows that the building basement acts as a thermal insulator, reducing the influence of air temperature on subsoil. Ground thermal conductivity, pile-end restraints, and temperature variation significantly affect pile behavior. Cooling induces axial tensile stresses and negative skin friction, but all stresses remain within safe limits. Raft structures experienced minor deformations, confirming the structural stability of the system under operational thermal cycles.

Jiang et al. [61]	2021	To investigate the full-scale thermomechanical behavior of driven energy piles under various mechanical loads and thermal cycles.	Conducted full-scale thermomechanical load tests on driven energy piles. Evaluated behavior under different levels of mechanical loading and thermal cycling (heating and cooling). Compared driven piles (which densify surrounding soil) to bored piles (which loosen it). Found that mechanical loading affects settlement during thermal cycles, and driven piles show distinct behavior due to construction effects.
Moradshahi et al. [62]	2021	To investigate and model the cross-sectional thermo-mechanical responses of concrete energy piles at field scale.	Developed and validated a numerical model using field-measured cross-sectional temperatures and strains from a 0.6 m × 10 m energy pile. Studied effects of fluid temperature, soil properties, and pile spacing. Found center of pile has highest thermal stress and temperature. Current design methods may overestimate stress by up to 2 MPa.
Lou et al. [63]	2022	To experimentally investigate the thermo-mechanical behavior of pre-bored grouted planted (PGP) geothermal energy piles under different restraint conditions.	nstalled a PGP GEP with FBG sensors to measure temperature and strain during two heating tests (with and without building load). Results showed nonuniform thermal stress due to uneven temperature distribution. End restraints significantly affected pile behavior. Compared PGP GEPs with other GEP types.
Pei et al. [64]	2022	To develop a machine learning model for predicting long-term thermomechanical displacement of	Created an artificial neural network trained with validated numerical simulation data covering 60 typical thermal loads from different Chinese regions. The model achieved high accuracy and significantly reduced

		energy piles under various thermal load scenarios.	computational time, making it an efficient alternative to traditional simulations in long-term energy pile design.
Ding et al. [65]	2022	To investigate the thermo-mechanical behavior of energy piles in overconsolidated saturated clay under varying mechanical loads and thermal cycles.	Conducted model-scale experiments with three loading scenarios (0%, 25%, and 50% of ultimate bearing capacity) over ten cooling-heating cycles. Found that higher mechanical loads increased irreversible settlement (up to 1.19%) and reduced bearing capacity (555 N to 520 N). Elevated loads also caused stress redistribution and increased internal tension. Provides insights for long-term performance and design of energy piles under cyclic thermal and structural loads.
Yang et al. [66]	2023	To evaluate the impact of soil type, pile spacing, pile material, and arrangement on the thermo-mechanical behavior of a 3×3 energy pile group using 3D numerical simulations.	Found that increasing pile spacing improves thermal efficiency and reduces displacement but increases axial force. Rock-soil showed the best thermal performance; sand caused the largest displacements. Higher thermal conductivity in piles boosts heat transfer but raises thermal stress and displacement. Cross arrangement enhances heat exchange per unit volume but intensifies soil temperature variation and pile displacement.
Ai and Ye [67]	2023	To develop a coupled BEM–FEM method for analyzing thermo-mechanical behavior of pipe energy piles in layered cross-anisotropic soils.	The pipe pile is modeled using FEM; soil-pile interaction is captured by BEM, ensuring deformation compatibility. Results show pipe wall thickness and soil anisotropy significantly affect thermal stress. Cooling is more sensitive to soil anisotropy than heating. Soft surface layers reduce

			axial force. Provides guidance for designing pipe energy piles in complex soils.
Ding et al. [68]	2024	To investigate the thermo-mechanical behavior of a 2×2 energy pile group in dry sand under horizontal loads via model testing.	Thermal load on a single pile increased bending moments, especially at the upper part. Horizontal loads strongly affected rotational angles and horizontal displacements, which decreased with depth. Temperature rise enhanced pile-soil interaction, increasing pressure in upper soil and decreasing it deeper down.
Feng et al. [69]	2024	Propose an improved thermomechanical load-transfer method that includes soil coupling effects for better prediction of energy pile behavior.	Experimental validation showed that ignoring soil-structure interaction can underestimate pile head settlement by up to 48.8%. The method also identifies irreversible behavior under cyclic thermal loading and high axial stress.
Sun et al. [70]	2024	Investigate the thermomechanical response of driven energy piles under cyclic thermal loading in sandy soils using CEL and axisymmetric FEM.	Validated by centrifuge tests, it highlights how installation-induced axial forces and skin friction reduce over cycles due to interface contraction. Bored piles show greater settlement due to reduced shaft resistance.
Liu et al. [71]	2024	Introduce a novel method to directly compute the thermomechanical response of energy piles and locate the	Uses a boundary shape function combined with a load-transfer framework; validated by field tests. Explores effects of pile-end restraints, soil constraints, and thermal/mechanical loads on null point movement.

		null point (zero thermal displacement) without prior assumptions.	
Yuan et al. [72]	2025	To investigate the thermal–mechanical behavior of deeply buried pipe energy pile (DBP-EP) groups in sand using model testing.	Studied DBP-EP piles with varying cross-sections and heat exchanger configurations. Found higher temperature changes at pile toe, strain decreasing from center outward, and axial earth pressure highest at both ends. Pile top displacement increased with inlet temperature. Group effect reduced heat transfer efficiency and friction compared to single piles.
Zhuang et al. [73]	2025	To investigate the influence of non-uniform initial ground temperature on the thermo-mechanical behavior of energy piles.	Used a validated 3D finite element model in COMSOL to simulate energy piles in the Yellow River floodplain. Found that ignoring vertical ground temperature variation leads to significant errors in heat exchange efficiency, pile head displacement, and axial stress under seasonal thermal loads (heating/cooling).
He et al. [74]	2025	To investigate the thermo-mechanical behavior of a full-scale energy pile under different thermal loading conditions.	Conducted field tests in Jiangsu Province to analyze how different heating/cooling conditions affect pile behavior at various depths. Found middle depth experienced the highest thermal stress due to soil constraints. Intermittent heating/cooling significantly reduced stress levels compared to continuous operation.
Chang et al. [75]	2025	Investigate the thermomechanical behavior of full-scale prestressed high-	Field tests and simulations showed temperature causes compressive/tensile stresses, shifting the neutral point downward; the pile-soil stress ratio

		strength concrete (PHC) energy piles with a flexible cushion layer constraint.	changes with temperature; and cushion strength moderately increases pile constraint.
Song et al. [76]	2025	Introduce a new load transfer method for analyzing thermomechanical performance of dissimilar energy pile groups (different lengths or diameters).	Considers pile–soil, pile–slab, and pile–pile interactions. Validated with experiments and FEM (<5% error). Shows how spacing, diameter, and length affect axial stress and displacement. Fills gap in modeling non-uniform pile groups.
You et al. [77]	2025	Propose a novel thermomechanical energy pile system combining phase change materials (PCMs) and nanofluids (PCM/NFSEP) to improve heat transfer and reduce stress.	Experimental and numerical results show a 56.6% increase in heat transfer rate and reduction in thermomechanical displacement (0.66 mm to 0.19 mm). Enhances thermal efficiency, reduces soil heat buildup, and improves structural stability. Offers design guidance for advanced energy piles.
Chen et al. [78]	2025	Investigate the thermo-mechanical behavior of energy piles with phase change material (PCM) tubes.	PCM tubes increased heat exchange capacity by up to 7.6% and reduced thermally induced stress by up to 30.8%. Positioning of PCM tubes significantly affects performance. PCMs improve thermal efficiency and reduce stress without affecting pile-soil interaction, helping reduce soil heat buildup under uneven thermal loads.
He et al. [79]	2025	Analyze the thermo-mechanical response of a full-scale energy pile under varying thermal loads.	Temperature response sensitivity constant across inlet temps. Middle sections had the highest thermal stress due to structural constraints; the bottom had the least. Intermittent heating reduced compressive stress by

			37.9%, and intermittent cooling lowered tensile stress by 63.3%. Provides insights for depth-specific design and operation.
Liu et al. [80]	2025	Simplify analysis of the thermo-mechanical response of a single energy pile within a group.	Models temperature distribution with exponential (radial) and polyline (axial) functions. Thermal loads change skin friction and axial stress: heating lowers friction near the pile head and raises it near the toe. Thermal effects reach up to 5× pile diameter. Highlights need to consider temperature in design and stability.

II.2.3 The thermal performance of GEP

Recent research (2022-2025) has identified several key factors influencing the thermal performance of geothermal energy piles (GEPs). Studies by Ding et al. [81], Farajollahi et al. [82], Lee et al. [83], and Haridy et al. [84] have examined the effects of geometric parameters, heat exchanger design, flow rates, and material properties on heat transfer efficiency. The use of phase change materials (PCMs) to enhance thermal regulation and system restoration under cyclic thermal loads has been demonstrated by Shahidi et al. [85] and Hu et al. [86,89]. Furthermore, Alqawasmeh et al. [87,90] highlighted the critical influence of geological heterogeneity and hydrothermal spatial variability on GEP performance, underscoring the necessity for site-specific data in accurate modeling. Additionally, Ten Bosch et al. [88] validated the application of GEPs in hot climates, while Guo et al. [91] showed that open-ended tube configurations offer improved heat exchange efficiency and faster thermal responses compared to conventional designs. These comprehensive findings and their detailed analyses are summarized in Table 3, which provides a structured overview of the reviewed studies, including their objectives, methodologies, and key results. This overview offers valuable insight into the interplay between system design, environmental factors, and modeling approaches, helping to guide future development and optimization of GEP technologies.

Table II. 3. Summary of key studies on the thermal performance of GEPs.

Author(s)	Year	Aim (s)	Key Contents
Ding et al. [81]	2022	Assess heat transfer performance of energy piles in frozen and nonfrozen soils using lab tests and simulations.	Developed a 3D heat transfer model based on ground temperature. Found max heat exchange of 125 W/m. Pile length, concrete conductivity, fluid flow rate, and pipe type strongly affect heat transfer. Pile diameter and cover thickness have minor impact. Suggested further research on pipe diameter effects.
Farajollahi et al. [82]	2022	To analyze the thermal performance of an energy pile equipped with a novel triple helix ground heat exchanger.	Developed a 3D CFD model to study design parameters (helix pitch, diameter, etc.) on system performance. The triple helix design improved performance by 24% over conventional systems. Helix pitch was the most influential factor. Thermal interaction between pipes and surrounding soil significantly affected heat transfer efficiency.
Lee et al. [83]	2022	To evaluate the thermal performance of cast-in-place energy piles using steel pipe heat exchangers (SPHXs).	Conducted field tests and CFD modeling on energy piles using steel pipes as both reinforcement and heat exchangers. Found that thermal performance is influenced by concrete and ground conductivity. Optimal flow rate identified as 11.35 L/min. Excessive pipe quantity doesn't proportionally improve performance due to borehole volume constraints.

Haridy et al. [84]	2023	Investigate factors affecting thermal conductance of energy piles as ground heat exchangers using response surface methodology.	Examined 8 factors: number of U-tubes, pile diameter, tube diameter, tube thickness, pile/tube thermal conductivity, soil conductivity, and water flow velocity. Found tube thickness, water velocity, and soil conductivity had little effect. Number of U-tubes, pile/tube diameter, and material thermal conductivities significantly impact thermal conductance. Results help optimize energy pile thermal performance for HVAC systems.
Shahidi et al. [85]	2023	To experimentally investigate the effect of lauric acid-based PCM on the thermal performance of energy piles in sandy soil under warm climate conditions.	Small-scale physical model tests were conducted on energy piles with and without 1.5% lauric acid PCM. PCM reduced temperature fluctuations by up to 13% (dry) and 10% (saturated), and excess pore pressure by 2.14×. PCM piles showed improved power extraction with increased thermal loading, demonstrating better thermal performance.
Hu et al. [86]	2024	To numerically investigate the heat restoration and thermal performance of energy piles backfilled with PCM under various operational and material parameters.	Studied effects of PCM properties (melting temp., latent heat, conductivity) and operation modes on heat transfer. Found high latent heat/conductivity improves Qm, but lower latent heat aids full PCM restoration. Optimal melting temp. should match initial soil temp. Alternate heating/cooling improved Qm by 32.7% and wall temp. recovery by 52.5%.
Alqawasmeh et al. [87]	2024	Assess the impact of soil layering and groundwater flow on the thermal	Shows that assuming homogeneous soil leads to underestimating thermal yield by up to 19.6% over 25 years, especially with unbalanced thermal loads. Proposes an empirical formula to correct effective thermal

		performance of energy piles using a 3D hydro-thermal finite element model.	conductivity in layered soils. Groundwater seepage enhances heat exchange, but inaccurate estimation of seepage, especially at low to moderate Darcy velocities, critically affects predictions.
Ten Bosch et al. [88]	2024	Assess the feasibility and performance of energy piles in hot-dominated climates using a Dubai case study.	Uses 3D numerical modeling validated by experiments to evaluate thermal performance under cooling-dominated conditions. Energy piles can supply 40% of building cooling demand. Temperature rise in heat carrier fluid stabilizes, supporting long-term (50 years) viability. Sensitivity analysis shows proper system sizing keeps heat pump temperatures within limits, confirming energy piles' suitability for hot climates.
Hu et al. [89]	2025	To numerically optimize the restoration performance of phase change pipe energy piles during winter operation.	Investigated optimal PCM properties and inlet temperatures for efficient long-term operation. Found that a high PCM melting point (16.3 °C) and thermal conductivity (1.65 W/m·K) enhance performance. After 30 days, 99.2% of initial heat transfer rate and 99.1% of soil temperature were restored using 12h heating/cooling cycles at 27.4 °C.
Alqawasmeh et al. [90]	2025	Study the impact of ground hydrothermal spatial variability on the thermal performance of energy pile groups.	Used validated 3D finite element modeling with Monte Carlo simulations to include variability in thermal conductivity and permeability. Ignoring spatial variability causes large prediction errors—up to 33% less mean energy output and ±5°C uncertainty in temperature cycles. Emphasizes the

			need for detailed site-specific hydrogeological data and accounting for vertical permeability heterogeneity in design.
Guo et al. [91]	2025	Investigate the thermal performance of open-tube energy piles.	Experimental and analytical study comparing open-ended tubes with conventional U-tubes. Open-tube piles showed higher heat exchange efficiency and stronger temperature responses. Developed and validated a Laplace-transform-based analytical model for full-scale conditions. Thermophysical properties of pile and soil affect heat transfer differently. Open-tube systems are a promising way to improve energy pile efficiency.

II.2.4 Overview of the global implementation of thermo-active geostructures

Thermo-active geostructures, first introduced in Europe during the 1980s as pile foundations and later as diaphragm walls, represent an innovative and sustainable technology that harnesses ground-source energy to reduce reliance on conventional energy systems and lower CO_2 emissions.

Since 2000, their application has expanded significantly, particularly in developed countries with temperate climates such as Austria, Switzerland, and the UK. These systems are implemented in various forms, including energy piles, tunnels, heat exchanger anchors, and energy walls, with energy piles being the most prevalent. In Germany, for example, where 223 piles were installed for the Main Tower in Frankfurt, these figures illustrate the installation process

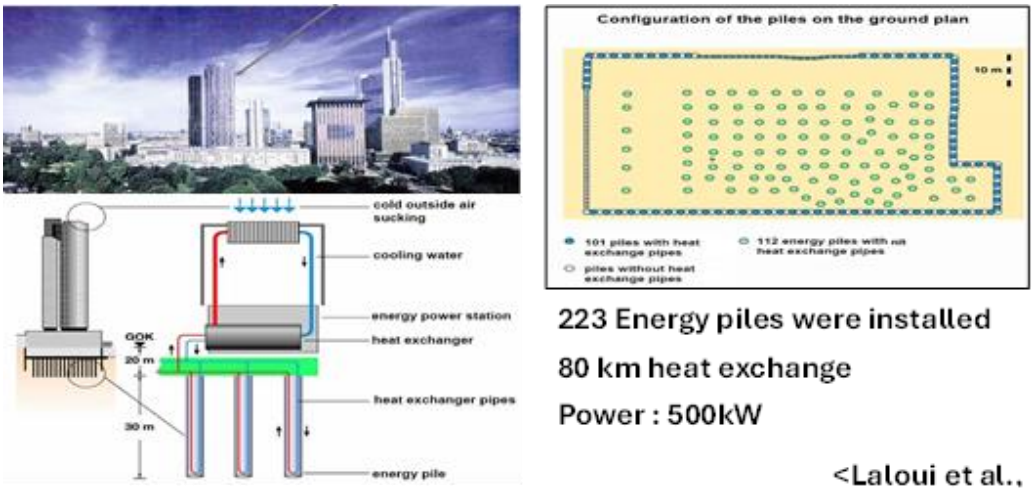

Figure II. 3. MainTower Frankfurt project am Main [94].

Figure II. 4. Preparing work steps [94].

Figure II. 5. Assembly of reinforcement cage [94].

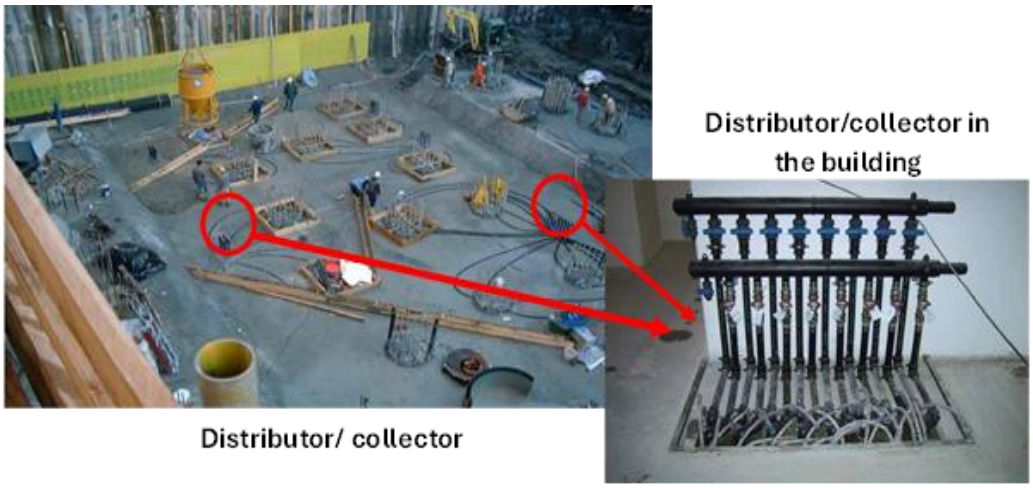

Figure II. 6. Installation the distributor in buildings [94].

The data presented in Table 4 highlight the widespread adoption of thermo-active geostructures across various projects and countries, detailing key parameters such as the year of implementation, energy output (in MWh/year), and the type of structure used. These data underscore the growing importance of thermo-active systems not only in the structural role of foundations but also in meeting the thermal energy demands for heating and cooling in buildings.

Table II. 4. Overview of implemented thermo-active geostructure projects worldwide.

Project	Country	Year	Energy (MWh/year)	Type of structure
Samsung Electronics, Seoul [94]	Korea	1997	/	11150 m^2 of floor plate layout
The Keble College, Oxford [94]	Great Britain	2002	133 (heating)	83 energy piles
STRABAG Headquarters, Vienna [94]	Austria	2003	840 (heating) 1450 (cooling)	245 energy piles and 6000 m^2 of floor plate layout
Uniqa Tower, Vienna [94]	Austria	2003	468 (heating) 530 (cooling)	7800 m^2 diaphragm wall
Dock Midfield Zurich Terminal Airport [92,93]	Switzerland	2003	1170 (cooling)	306 energy piles
Lainzer Tunnel [92,93]	Austria	2004	/	Heat exchanger anchors, Tunnel lining
Dalham Hall Stud, Newmarket [94]	Great Britain	2008	288 (heating) 80 (cooling)	147 energy piles

European Central Bank, Frankfurt [94]	Germany	2009	290 (heating) 176 (cooling)	223 energy piles
Hospital Valle Belbo, NizzaMonferrato [94]	Italia	2010	341 (heating) 318 (cooling)	450 energy piles
Hotel Sofitel, Viena [94]	Austria	2010	960 (heating) 600 (cooling)	100 energy piles and 253 m diaphragm wall
Condominium Great morning, Einsiedeln [94]	Switzerland	2011	262 (heating)	270 energy piles
Financial Building, Wuxi [94]	China	2011	4140 (heating) 5600 (cooling)	513 energy piles
Office Building Timber Port, Hamburg [94]	Germany	2011	1170 (heating) 967 (cooling)	770 energy piles
Omega-Computers and Peripherals, Vienna [94]	Austria	2012	104 (heating) 84 (cooling)	3100 m^2 of floor plate layout
People’s hospital, Yangzhou [94]	China	2014	8260 (heating) 6740 (cooling)	434 energy piles

II.3 Conclusion

The growing emphasis on sustainable foundation systems has driven notable advancements in the research and practical deployment of geothermal energy piles (GEPs). This chapter has presented a critical synthesis of the field's evolution, highlighting how experimental investigations, theoretical frameworks, and advanced numerical modeling have collectively deepened our understanding of the thermal and thermo-mechanical behavior of GEPs. The factors affecting system performance in these studies, such as subsurface heterogeneity, groundwater dynamics, pile geometry, thermal properties of construction materials, and the integration of innovative technologies including phase change materials (PCMs) and nanofluids, have been thoroughly examined. Collectively, these investigations offer valuable insights into improving thermal efficiency and ensuring mechanical stability across a variety of ground conditions. Additionally, an overview of implemented thermo-active geostructure projects worldwide has been provided, illustrating the practical application and energy performance of these systems across different countries and climates. The findings compiled in this review provide a foundational reference for guiding future research efforts and for optimizing the design, implementation, and long-term performance of GEP systems in geotechnical and building engineering applications.

CHAPTER III : MODELING TECHNIQUES

III.1 Introduction

A comprehensive numerical investigation is conducted using Ansys Fluent's Computational Fluid Dynamics (CFD) to analyze the impact of key design parameters on the performance of geothermal energy piles during both winter (heating mode) and summer (cooling mode). The study focuses on the detailed heat transfer behavior within various pile foundation configurations, evaluated under realistic thermal boundary conditions. The primary objective is to develop an optimized GEP design that balances thermal efficiency with mechanical integrity. Critical parameters examined include fluid flow characteristics, heat exchanger diameter, the spacing between the HE and the pile perimeter, angular positioning, overall pile diameter, and the cross-sectional shape of the HE. These factors are systematically varied to assess their influence on heat exchange rates and temperature distribution. Through advanced CFD modeling of fluid dynamics and thermal interactions, the analysis provides valuable insights into the seasonal thermal performance of GEP systems. In addition, a supporting mathematical framework is introduced to enhance the accuracy of simulation results and validate the numerical models against real-world operating conditions. Collectively, these approaches support the development of more energy-efficient, structurally resilient, and operationally robust GEP designs for sustainable building applications.

III.2 Computational fluid dynamics for applied engineering

Computational Fluid Dynamics (CFD) is one of the most advanced areas within Computer-Aided Engineering (CAE), employing numerical methods and algorithms to simulate and analyze fluid flow, heat transfer, and related physical phenomena. Over time, CFD has become an essential tool across a wide range of industries, including aerospace, automotive, energy, and chemical engineering, highlighting its broad impact, versatility, and vital role in modern engineering analysis and design. Among the numerical methods used to implement CFD, the FVM has gained particular prominence due to its conservation properties and effectiveness in handling complex geometries and boundary conditions.

III.3 Finite volume method

The Finite Volume Method (FVM) is a numerical technique that transforms the partial differential equations representing conservation laws over differential volumes into discrete

algebraic equations over finite volumes (or elements or cells). In a similar fashion to the finite difference or finite element method, the first step in the solution process is the discretization of the geometric domain, which, in the FVM, is discretized into non-overlapping elements or finite volumes. The partial differential equations are then discretized/transformed into algebraic equations by integrating them over each discrete element. The system of algebraic equations is then solved to compute the values of the dependent variable for each of the elements [95].

In the finite volume method, some of the terms in the conservation equation are turned into face fluxes and evaluated at the finite volume faces. Because the flux entering a given volume is identical to that leaving the adjacent volume, the FVM is strictly conservative. This inherent conservation property of the FVM makes it the preferred method in CFD. Another important attribute of the FVM is that it can be formulated in the physical space on unstructured polygonal meshes. Finally in the FVM it is quite easy to implement a variety of boundary conditions in a non-invasive manner, since the unknown variables are evaluated at the centroids of the volume elements, not at their boundary faces [95].

These characteristics have made the Finite Volume Method quite suitable for the numerical simulation of a variety of applications involving fluid flow and heat and mass transfer, and developments in the method have been closely entwined with advances in CFD. From a limited potential at inception confined to solving simple physics and geometry over structured grids, the FVM is now capable of dealing with all kinds of complex physics and applications [95].

III.4 Numerical solution

III.4.1 Problem description

III.4.1.1 Heat transfer model

Figure 1 showcases the structural configuration and dimensions of the proposed HT model associated with the GEP system. The model is made up of four interplaying elements, with each playing an individual role in the thermal exchange between the GEP and the surrounding environment. The system begins with the ground domain, taken as a cylindrical column of soil 6.6 m wide and 18 m deep.

This domain simulates the geological medium through which heat exchange occurs. Centrally embedded within the soil is the concrete energy pile, constituting the second major component. This pile extends 15 m vertically downward from the ground surface and features a diameter of 0.4 m. It functions both as a structural foundation and a thermal conduit. The third component, a U-shaped HE tube constructed from HDPE, is embedded within the concrete pile. It extends down to a depth level of 14.5 m and consists of an internal diameter of 0.020 m as well as an outer diameter of 0.025 m. It serves as the channel through which the HT fluid, typically water, circulates. The final element of the system is the fluid domain, encompassing the circulating water within the HDPE tube. This domain facilitates the transfer of thermal energy between the pile and the subsurface environment.

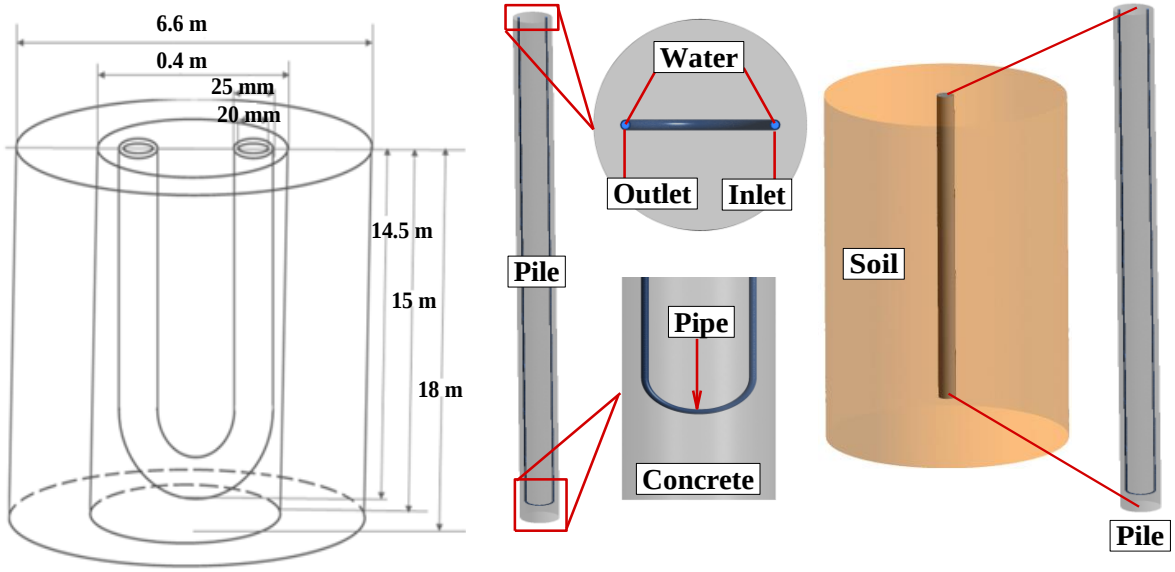

a. Schematic of a GEP [96]. **b.** Physical model of a GEP.

Figure III. 1. Geothermal energy pile (GEP) system.

A detailed summary of the principal physical dimensions associated with each component is provided in Table 1. The geometric and material parameters employed in this work are adopted from Zhang et al. [56], providing a consistent foundation for system design and ensuring the reliability of the results.

Table III. 1. Specifications of physical properties used in the model [56,96].

Material	Density (ρ) (kg/m^3)	Specific Heat (C_p) (J/kg.K)	Thermal Conductivity (λ) (W/m.K)
HDPE	950	2300	0.44
Concrete	2300	850	1.54
Clay soil	2000	1644	1.877
Water	998.2	4182	0.6

III.4.1.2 Mechanics model

To examine the mechanical reaction of the GEP system under applied loads, a precise mechanical model was constructed, as shown in Figure 2. Simulation was aimed to assess both patterns of displacement and stress distribution for the pile as well as around the surrounding soil. A compressive force of 1,600,000 N was applied vertically directly on the surface of the pile, with the underlying medium soil assumed to be fully constrained, which equivalently simulates a fixed boundary condition. The interaction at the pile–soil interface was modeled as a fully bonded contact, incorporating both frictional resistance and normal contact pressure to realistically capture load transfer mechanisms. The mechanical properties of the materials used in this analysis, including elastic modulus, Poisson's ratio, and density, are detailed in Table 2, as reported by Zhang et al. [56].

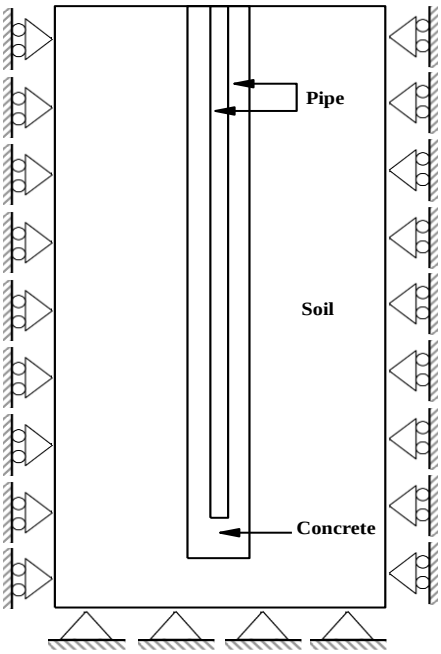

Figure III. 2. Schematic of mechanics model of a GEP [96].

Table III. 2. Specifications of mechanical property parameters used in the study [56,96].

Material	Elastic moduls (GPa)	Poisson's ratio	Expansion angle (°)	Internal friction angle (°)	Thermal expansion coefficient ($°C^{-1}$)
HDPE	1.1	0.42	-	-	0.00023
Concrete	30	0.20	-	-	10^{-5}
Clay soil	0.015	0.33	0	31	-

III.4.2 Research motivation and structure

The main objective of this research is to enhance the thermal performance and energy efficiency of GEP systems by optimizing their design and identifying critical parameters that influence thermal behavior. Particular attention is given to the temperature distribution within the system and the rate of heat exchange between the pile and the surrounding ground. Comprehensive parametric studies were conducted to assess the impact of various physical configurations, specifically those related to the heat exchanger, on overall system performance, with the aim of contributing to the development of more efficient and sustainable geothermal energy technologies. These studies are detailed as follows:

Part 1 : CFD Analysis of the Time-Dependent Thermal Performance of Geothermal Energy Piles During Summer and Winter Periods. This study investigates the effect of fluid flow rate and the thermal response time of the Geothermal Energy Pile (GEP) system. Using Computational Fluid Dynamics (CFD), the analysis focuses on how these parameters influence the system's heat exchange efficiency under both summer and winter operating conditions.

Part 2 : Optimization of Geothermal Energy Pile (GEP) Systems through a Combined Analytical and Numerical Study of Various Heat Exchanger Configurations Under Winter and Summer Conditions. This part examines the influence of key design parameters, including:

- Variations in the diameter of the U-shaped pipe,
- The distance between the outer wall of the heat exchanger and the perimeter of the concrete pile,
- The angular positioning of the heat exchanger within the cross-section of the pile,

- The diameter of pile .

Part 3 : Thermomechanical Analysis of the Response of an Geothermal Energy Pile (GEP) System : Cross-Sectional Impact of Heat Exchanger Geometry on Performance and Heat Transfer under winter under summer. This section investigates how different heat exchanger shapes (circular, square, and triangular) affect both heat transfer efficiency and mechanical stress within the pile. Using coupled thermal and mechanical simulations under winter and summer conditions, the study evaluates the impact of these geometries on the system's overall performance and structural integrity.

III.4.3 Mathematical formulation

This section presents the mathematical framework used to describe the thermomechanical behavior of geothermal energy piles (GEP). The formulation is based on the fundamental principles of thermomechanical coupling, which account for the interaction between thermal and mechanical fields. Specifically, it addresses how temperature variations within the pile and surrounding soil influence stress distribution, strain development, and structural deformation. These equations provide a theoretical basis for understanding and predicting the response of GEPs under thermal loading conditions.

III.4.3.1 Governing equations

This section introduces the fundamental governing equations that describe the coupled interaction between thermal and mechanical fields. Seasonal temperature variations, such as expansion during summer and contraction during winter, induce mechanical stresses and deformations, while mechanical loads influence heat transfer processes. A comprehensive analytical understanding of these equations is essential for accurately predicting the behavior of systems where thermal expansion and mechanical stresses coexist, thereby ensuring enhanced performance and structural integrity.

III.4.3.1.1 Analysis of the fundamentals of thermomechanical coupling

In this section, we present the governing equations for the HT and mechanical models based on the study conducted by Xu et al. [57]. These equations form the foundation for analyzing the interaction between thermal and mechanical fields within the coupled system.

a) Heat transfer equations

This study identifies two modes of heat transfer: one involving the transfer of heat through a solid material, and the other referring to the heat transfer between a solid surface and a fluid.

The heat transfer through a solid material is defined as conduction, which is expressed by Fourier's equation:

$$Q = -\lambda \nabla T \tag{III.1}$$

The equation of transient heat transfer in solids, based on the first law of thermodynamics (conservation of energy), is:

$$\rho_s C_{ps} \left(\frac{\partial T}{\partial t} + u_{trans} \nabla T \right) + \nabla (q + q_r) = Q \tag{III.2}$$

Where u_{trans}: velocity vector of the solid's translational motion; q_r: radiative heat flux; and Q: other external heat sources.

Heat transfer in fluids includes convection and other thermal effects. The governing equation for heat transfer in fluids is:

$$\rho_f C_{pf} \left(\frac{\partial T}{\partial t} + u \nabla T \right) + \nabla (q + q_r) = \alpha_f T \left(\frac{\partial p}{\partial t} + u \nabla p \right) + \tau : \nabla u + Q \tag{III.3}$$

Where α_f is the thermal expansion coefficient of the fluid, defined as ($\alpha_f = -\frac{1}{\rho_f}\left(\frac{\partial p}{\partial T}\right)$; $\alpha_f T \left(\frac{\partial p}{\partial t} + u \nabla p \right)$: represents pressure work.

The previous equation is simplified by neglecting the effects of pressure work because the volume of water changes very little, and is as follows:

$$\rho_f C_{pf} \frac{\partial T}{\partial t} + \rho_f C_{pf}\, u\, \nabla T + \nabla (-\lambda \nabla T) = Q \tag{III.4}$$

b) Mechanical equation

In this study, we focus on the axial stress and displacement under pure mechanical load, as well as under the coupled effects of load and temperature. In this part, we present the following equations relevant to this study [57].

The displacement at a point i under the influence of temperature T is calculated using the model by Melissa A. Stewart [97]] as follows :

$$\delta_{T,i} = \delta_{T,i-1} + \frac{1}{2}\left(\epsilon_{T,i-1} + \epsilon_{T,i}\right) \Delta l \tag{III.5}$$

The mechanical displacement of the pile in the direction of the axial load:

$$\delta_{mech} = \frac{FL}{EA} \tag{III.6}$$

The total displacement along the pile can be expressed as:

$$\delta_{Total,i} = \delta_{mech} + \delta_{T,i} \tag{III.7}$$

The formula for the free thermal strain ,caused by temperature change if the material were free to expand or contract without any external constraints (like the surrounding soil) is as follows:

$$\epsilon_{T-free} = \alpha\, \Delta T \tag{III.8}$$

The axial temperature stress σ in the pile, when the bottom is on the bearing layer and the top supports the building load, is given by:

$$\sigma = E\, \epsilon_{T-free} \tag{III.9}$$

$$\sigma = E\, \alpha\, \Delta T \tag{III.10}$$

Where ϵ_{T-free} thermal strain under free conditions, ignoring the thermal load acting on the pile due to soil stiffness. According to geotechnical engineering conventions, compressive strain is defined as positive.

The axial force F caused by temperature change in a pile can be calculated using the following equation:

$$F = \sigma A \tag{III.11}$$

$$F = E\ \alpha\ \Delta T A \tag{III.12}$$

Where E Young's modulus (modulus of elasticity) of the pile body.

The residual strain represents the thermal strain of the pile that is constrained by the surrounding soil . It is given by the following relation:

$$\epsilon_{res} = \epsilon_{T-free} - \epsilon_T \tag{III.13}$$

Where ϵ_{T-free} denotes the upper limit of free thermal strain of the pile.

The axial stress caused by temperature changes in a pile, when it is constrained by the surrounding soil, can be expressed as follows:

$$\sigma_{res} = E\ \epsilon_{res} = E\left(\epsilon_{T-free} - \epsilon_T\right) = E(\alpha\ \Delta T - \epsilon_T) \tag{III.14}$$

III.4.4 Initial and boundary conditions

The reliability of the computational simulations performed in this investigation depends on the precise specification of boundary conditions for both the fluid and soil domains, which vary in response to seasonal temperature fluctuations. The computational domain consists of a U-shaped tube embedded within a soil medium, where the flow of water is governed by a set of temperature and velocity parameters that change in response to seasonal heating and cooling variations. The boundary conditions of the studied GEP model for the winter and summer seasons are depicted in Figure 3.

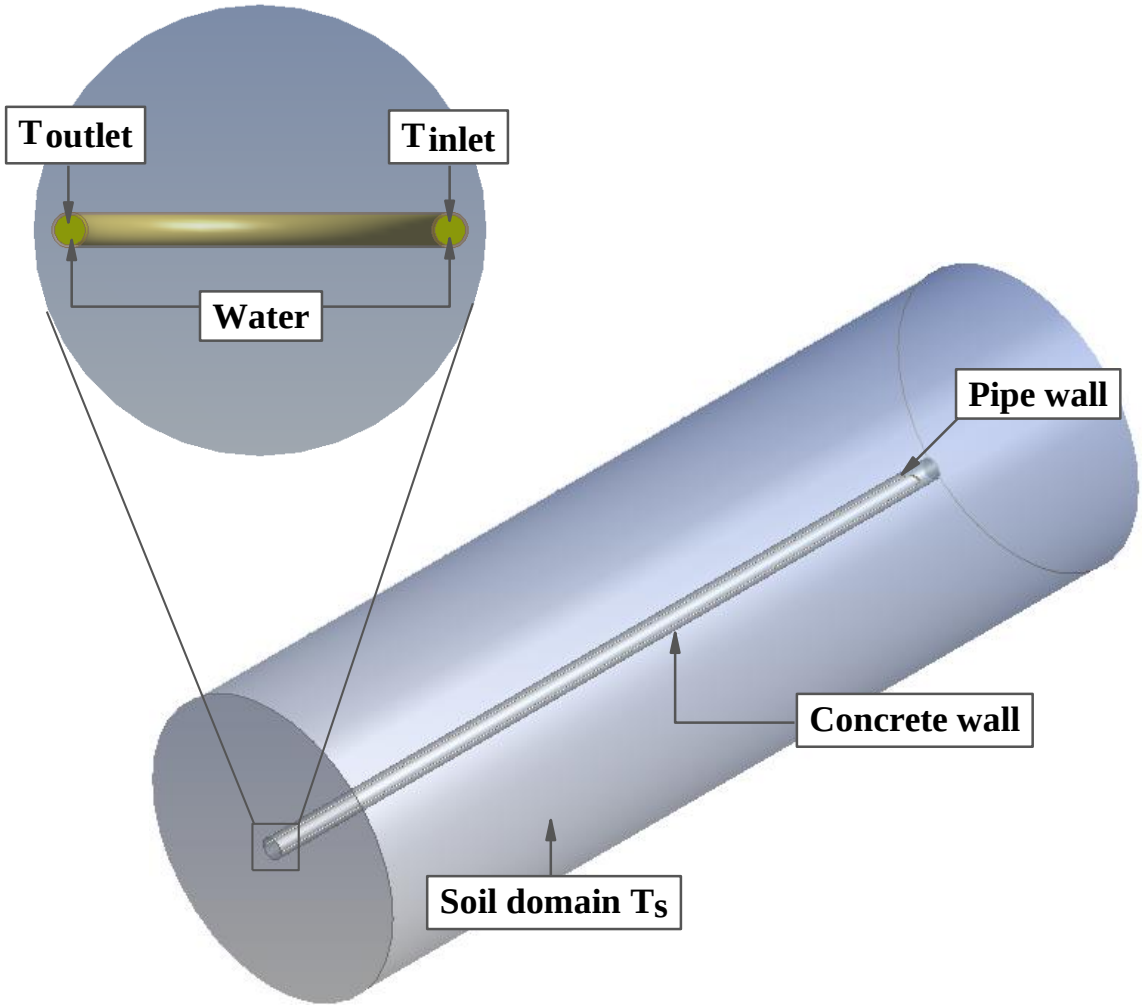

Figure III. 3. Boundary conditions of the physical model.

a) Inlet condition

For the fluid regime, the inlet boundary conditions are necessary to simulate the HT and FF precisely. In both winter and summer simulation cases, the inlet flow velocity is consistently maintained at 0.6 m/s, thereby establishing a stable and uniform flow regime throughout the U-shaped duct. In addition to the velocity, the temperature at the inlet is specified differently for the two seasons to account for the thermal variations:

- Winter simulation: The inlet temperature is set to 278.15 K, representing colder environmental conditions, where the fluid is heated as it flows through the system
- Summer simulation: In contrast, the inlet temperature is set to 318.15 K, simulating a cooling scenario where the fluid is at a higher temperature due to external environmental heat.

b) Outlet condition

The outlet is defined by an outlet flow condition,the water temperature at the outlet is calculated during the course of the analysis as a result of convective heat transfer within the system.

c) Pipe wall condition

The pipe walls are in direct contact with the concrete, and the initial temperature of the pipe is assumed to be the same as that of the concrete. Therefore, the boundary condition for the heat exchanger is defined by the wall temperature.

d) Concrete wall condition

The concrete walls are in direct contact with the surrounding soil, and the initial temperature of the concrete is assumed to be governed by the temperature of the adjacent soil.

e) Soil domain condition

The soil domain surrounding the pile is modeled with a fixed temperature, which remains constant throughout the simulation. This fixed temperature represents the average thermal condition of the soil, assuming that the soil medium's temperature does not vary drastically over the short-term simulation period. For both seasonal scenarios, the soil temperature is maintained at 291.89 K, representing an average ground temperature that remains largely unaffected by seasonal variations in fluid temperature.

The boundary conditions for both fluid and soil domains are summarized in Tables 1 and 2, which provide a clear overview of the parameters used in the winter and summer simulations.

Table III. 3. Boundary conditions for the computational domain: winter period [56].

Boundary	Boundary condition	Value	Mode
Inlet	Velocity inlet	0.6 [m/s]	Heating
	Temperature inlet	278.15 [K]	
Domain soil	Temperature	291.89 [K]	

Table III. 4. Boundary conditions for the computational domain: summer period [56].

Boundary	Boundary condition	Value	Mode
Inlet	Velocity inlet	0.6 [m/s]	Cooling
	Temperature inlet	318.15 [K]	
Domain soil	Temperature	291.89 [K]	

III.5 Numerical procedure

To simulate fluid flow and heat transfer around a geothermal energy pile (GEP), the continuity equation, the Reynolds-Averaged Navier-Stokes (RANS) equations, and the energy equation are solved to obtain the velocity and temperature fields. To accurately capture the influence of turbulence, the standard k–ε turbulence model is employed. Accordingly, the transport equations for two additional quantities namely, the turbulent kinetic energy (k) and its dissipation rate (ε) are solved simultaneously with the governing equations. The following section introduces the k–ε turbulence model, with particular attention to its application in geothermal energy piles.

III.5.1 Turbulence model

In the context of GEP systems, transient fluid flow and heat transfer processes are inherently turbulent due to the high Re numbers typically involved. Capturing the complex interactions between velocity, pressure, and temperature fields under turbulent conditions requires a reliable turbulence model that accounts for viscous and diffusive effects across all governing equations. For this investigation, the standard $k-\varepsilon$ turbulence model [98] was selected. This model is widely recognized for its balance of computational efficiency and robustness in representing turbulent behavior in engineering applications. The simulation was carried out using the ANSYS Fluent CFD platform, which offers comprehensive tools for resolving the coupled mass, momentum, and energy equations in turbulent regimes. The mathematical framework governing the flow includes:

Continuity (mass) equation:

$$\frac{\partial U_i}{\partial X_i} = 0 \tag{III.15}$$

Momentum equation:

$$\rho_f \left(\frac{\partial U_i}{\partial t} + U_j \frac{\partial U_i}{\partial x_j} \right) = -\frac{\partial P}{\partial x_i} + (\mu + \mu_t) \frac{\partial^2 U_i}{\partial x_j \partial x_j} \quad \text{(III.16)}$$

Energy equation:

$$\rho_f C_{pf} \left(\frac{\partial T}{\partial t} + U_j \frac{\partial T}{\partial x_j} \right) = \frac{\partial}{\partial x_j} \left((\lambda + \lambda_t) \frac{\partial T}{\partial x_j} + \phi \right) \quad \text{(III.17)}$$

$$\lambda_t = \frac{\mu_t C_{pf}}{Pr_t}$$

Turbulence kinetic energy equation:

$$\frac{\partial}{\partial t}(\rho_f k) + \frac{\partial}{\partial x_j}(\rho_f k U_j) = \frac{\partial}{\partial x_j} \left[\left(\mu + \frac{\mu_t}{\delta_k} \right) \frac{\partial K}{\partial x_j} \right] + G_k + G_b - \rho_f \varepsilon - Y_M + S_k \quad \text{(III.18)}$$

Turbulent dissipation rate equation:

$$\frac{\partial}{\partial t}(\rho_f \varepsilon) + \frac{\partial}{\partial x_j}(\rho_f \varepsilon U_j) = \frac{\partial}{\partial x_j} \left[\left(\mu + \frac{\mu_t}{\delta_\varepsilon} \right) \frac{\partial \varepsilon}{\partial x_j} \right] + \rho_f C_1 S \varepsilon - C_2 \rho_f \frac{\varepsilon^2}{k + \sqrt{\nu \varepsilon}} + C_{1\varepsilon} \frac{\varepsilon}{k} C_{3\varepsilon} G_b + S_\varepsilon \quad \text{(III.19)}$$

Turbulent viscosity (μ_t) determined by:

$$\mu_t = C_\mu \, \rho_f \frac{k^2}{\varepsilon} \quad \text{(III.20)}$$

Production rate (G_k) computed by:

$$G_k = \mu_t \frac{\partial U_i}{\partial x_j} \left(\frac{\partial U_i}{\partial x_j} + \frac{\partial U_j}{\partial x_i} \right) \quad \text{(III.21)}$$

The equations associated with the $k - \varepsilon$ formulation are supplemented by the following model constants :$C_{1\varepsilon} = 1.44$, $C_{2\varepsilon} = 1.92$, and $C_\mu = 0.09$, the turbulent Prandtl numbers of turbulent kinetic energy k and dissipation rate ε are $\delta_k = 1.0$ and $\delta_\varepsilon = 1.3$, respectively. More information regarding the model's equations can be discovered in reference [98].

III.5.2 Numerical simulation software for engineers

ANSYS Fluent is a state-of-the-art computer program for modeling fluid flow, heat transfer, and chemical reactions in complex geometries. It is written in the C computer language

and makes full use of the flexibility and power offered by the language. Consequently, true dynamic memory allocation, efficient data structures, and flexible solver control are all possible. In addition, ANSYS Fluent uses a client/server architecture, which enables it to run as separate simultaneous processes on client desktop workstations and powerful compute servers. This architecture allows for efficient execution, interactive control, and complete flexibility between different types of machines or operating systems. ANSYS Fluent provides complete mesh flexibility, including the ability to solve your flow problems using unstructured meshes that can be generated about complex geometries with relative ease. Supported mesh types include 2D triangular/quadrilateral, 3D tetrahedral/hexahedral/pyramid/wedge/polyhedral, and mixed (hybrid) meshes. ANSYS Fluent also enables you to refine or coarsen your mesh based on the flow solution [99].

III.6 Analytical solution

III.6.1 Resistance of fluid to pipe wall

The heat exchange rate of an energy pile is determined by calculating the thermal resistance of the heat transfer medium, which serves as a crucial indicator of its thermal efficiency. This involves computing the time-dependent heat exchange rate based on thermal resistances associated with internal flowing water, HDPE pipe, the pile itself, and the surrounding ground. The overall thermal resistance is derived by summing these individual values, following the methodology outlined by Liu Jun et al. (2009) [100]. Figure 4 shows a cross-section of an energy pile made of polyethylene pipes with U-shaped heat exchangers.

In the convective heat transfer mode, the thermal resistance of fluid is determined by Eq. (III.22):

$$R_{p,f} = \frac{1}{2\pi r_{pi} h_{pi}} \tag{III.22}$$

The convective heat transfer coefficient (h_{pi}) of a fluid is influenced by some parameters such as the viscosity and flow velocity of fluid, and also the surface resistance of the solid part. It can be defined in both turbulent and laminar fluid flows using Eq. (III.23):

$$h_{pi} = \frac{\lambda_f}{D_H} \cdot Nu \tag{III.23}$$

When Nusselt number Nu is given by The Dittus-Boelter correlation as in Eq. (III.24):

$$Nu = 0.023 \cdot Re^{0.8} \cdot Pr^{n} \tag{III.24}$$

Replacing Nu in Eq. (III.23) by its expression**,** the convective heat transfer coefficient becomes as in Eq. (III.25):

$$h_{pi} = \frac{0.023 \cdot Re^{0.8} \cdot Pr^{n}\, \lambda_f}{D_H} \tag{III.25}$$

In this case, the *Pr* number exponent *n* changes with the season: summer *n* = 0.3, winter *n* = 0.4.

The thermal resistance of the pipe given by Eq. (III.26) can be used to determine the conductive thermal resistance of the U-tube pipe mentioned in Figure 4:

$$R_P = \frac{1}{2\pi\lambda_p} . ln\left(\frac{r_{po}}{r_{pi}}\right) \tag{III.26}$$

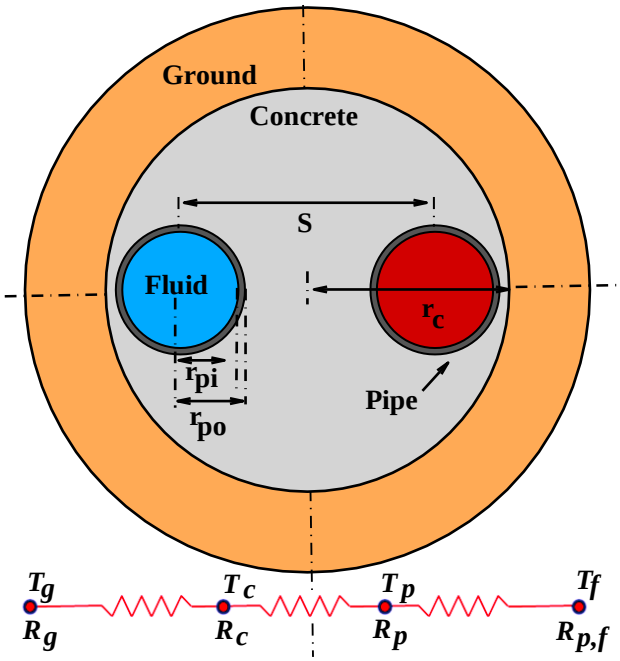

Figure III. 4. Schematic representation of the cross-section of an energy pile with a single U-pipe.

III.6.2 Concrete resistance

For determining the thermal resistance of the grout given by Eq. (III.27)**,** Bose et al [101] and Shonder and Beck [102] employed the equivalent-diameter expression proposed by Claesson and Dunand [103]. This method calculates the equivalent diameter of the pipe while maintaining a total surface area equivalent to the combined area of the two legs of the U-tube. However, this expression does not consider the thermal interaction between the two legs of the U-tube due to the lack of consideration for the spacing between the legs:

$$R_c = \frac{1}{2\pi\lambda_c} \cdot ln\left(\frac{r_c}{r_{eq}}\right) \tag{III.27}$$

The equivalent radius r_{eq} is considered as in Figure 5 and it is calculated using Eq. (III.28) by Gu and O'Neal [104] knowing the distance between the tube legs s of a single U-shaped tube:

$$r_{eq} = \sqrt{r_{po}S} \tag{III.28}$$

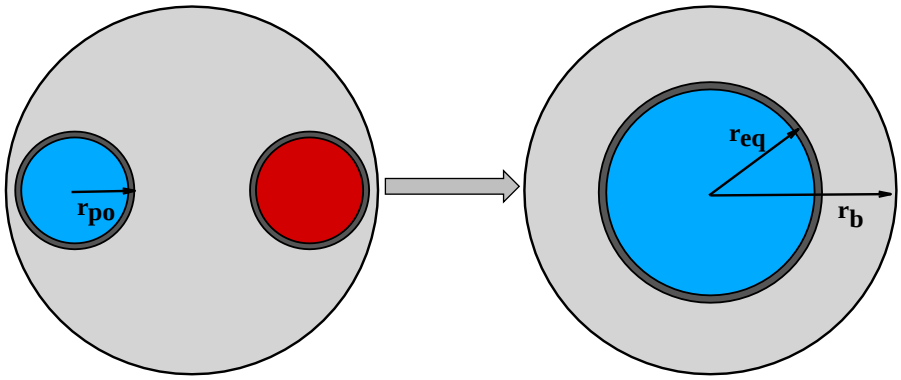

Figure III. 5. Schematic of the equivalent diameter method for a GEP with a single U-pipe.

III.6.3 Ground resistance

The calculation of ground heat resistance around the pile takes into account the isotropic and uniformly distributed thermal properties of the soil. This approach simplifies the analysis by disregarding variations in water content, groundwater flow, and thermal contact resistance with neighboring materials. Kelvin's theory of heat sources and sinks has proven highly

effective in solving heat conduction problems. The Eq. (III.29) for the general line source, as presented by Carlaw and Jaeger, (1959) [105], is provided below:

$$\Delta T = \frac{q}{4\pi\lambda}\int_{r^2/4\alpha_g t}^{\infty}\frac{e^{-u}}{u}du = \frac{q}{4\pi\lambda}Ei\left(\frac{r^2}{4\alpha_g t}\right) \quad \text{(III.29)}$$

The exponential integral *Ei* can be estimated using the following method as determined by Eq. (III.30):

$$Ei\left(\frac{r^2}{4\alpha_g t}\right) = \left[ln\left(\frac{r^2}{4\alpha_g t}\right) - \gamma\right] \quad \text{(III.30)}$$

$$\alpha_g = \frac{\lambda_g}{c_p} \quad \text{(III.31)}$$

$$r = r_b \quad \text{(III.32)}$$

Here, r_b stands for the borehole's radius, α_g for the soil's thermal diffusivity, and t for time.

The thermal resistance of the ground (borehole) is calculated and expressed using Eq. (III.33):

$$R_b(t) = \frac{T_b - T_f}{q} = \frac{1}{4\pi\lambda}\left[ln\left(\frac{4\alpha_g t}{r_b^2}\right) - \gamma\right] \quad \text{(III.33)}$$

III.6.4 Total thermal resistances and heat transfer rates

The overall thermal resistance is provided by Eq. (III.34):

$$\sum R = R_{p,f} + R_p + R_c + R_b \quad \text{(III.34)}$$

The heat transfer rate energy output q is calculated using the Eq. (III.35) as follows:

$$q = \frac{\dot{m}c_{pf}(T_{in} - T_{out})}{L} \quad \text{(III.35)}$$

III.7 Conclusion

Chapter III provided a comprehensive overview of the modeling approaches employed in this study, encompassing both numerical and analytical methods. The numerical modeling was conducted using CFD, with a detailed formulation of the physical system, including governing equations, boundary and initial conditions, and the application of suitable numerical methods. The general-purpose simulation software used for this purpose was also presented.

In parallel, the analytical model offered a theoretical framework that served both to support and validate the numerical findings while also providing additional insight into the system's underlying behavior. This integrated framework ensures a reliable basis for the analysis, evaluation, and interpretation of the study's findings

CHAPTER IV : RESULTS AND DISCUSSION

Part 1: Thermal Response of Geothermal Energy Piles in Different Seasons Using CFD Simulation

IV.1 Thermal Response of Geothermal Energy Piles in Different Seasons Using CFD Simulation

IV.1.1 Objective

The primary objective of this study is to investigate the seasonal thermal response of geothermal energy piles using computational fluid dynamics simulation under varying flow conditions. Geothermal energy piles, which combine structural foundation elements with ground heat exchangers, play a crucial role in sustainable building energy systems by utilizing the relatively stable subsurface temperature of the ground for both heating and cooling applications. This research specifically examines how the thermal performance of these piles changes during summer and winter periods, with a focus on time-dependent heat transfer characteristics. To evaluate the effect of fluid flow on thermal behavior, CFD simulations are performed at different Reynolds numbers: 500, 1000, 1500, and 2000. These values represent a range of laminar flow regimes typically encountered in such systems. By incorporating both seasonal and flow variations, the study aims to provide comprehensive insights into the transient thermal behavior of geothermal energy piles and contribute to the optimization of their design and operational efficiency throughout the year. As an initial step in this research field, this study adopts a general approach to analyzing the thermal phenomena and tests this system configuration to establish a set of foundational numerical results for future investigations.

IV.1.2 Methodology

This study investigates the heat transfer characteristics and thermal response of a geothermal energy pile subjected to both heating and cooling cycles. The system comprises a U-tube heat exchanger embedded within a concrete pile, enabling thermal energy exchange between the circulating fluid and the surrounding soil. The geometry was created using ANSYS Design Modeler, a highly practical and powerful software for constructing complex geometries. As mesh sensitivity analysis is not the primary focus of this study, the default meshing method is employed to discretize the computational domain.

The computational mesh was generated using the ANSYS Meshing module, a robust and widely validated tool for high-fidelity mesh generation in engineering simulations. The model geometry was discretized into four main components, including the U-tube, the fluid

domain, the concrete pile, and the surrounding soil. A default mesh configuration was adopted because it provided a satisfactory balance between computational efficiency and solution accuracy for the intended thermal analysis. Figure 1 shows the mesh configuration of the geothermal energy pile (GEP) components and Table 1 provides a summary of the number of elements and nodes for each domain.

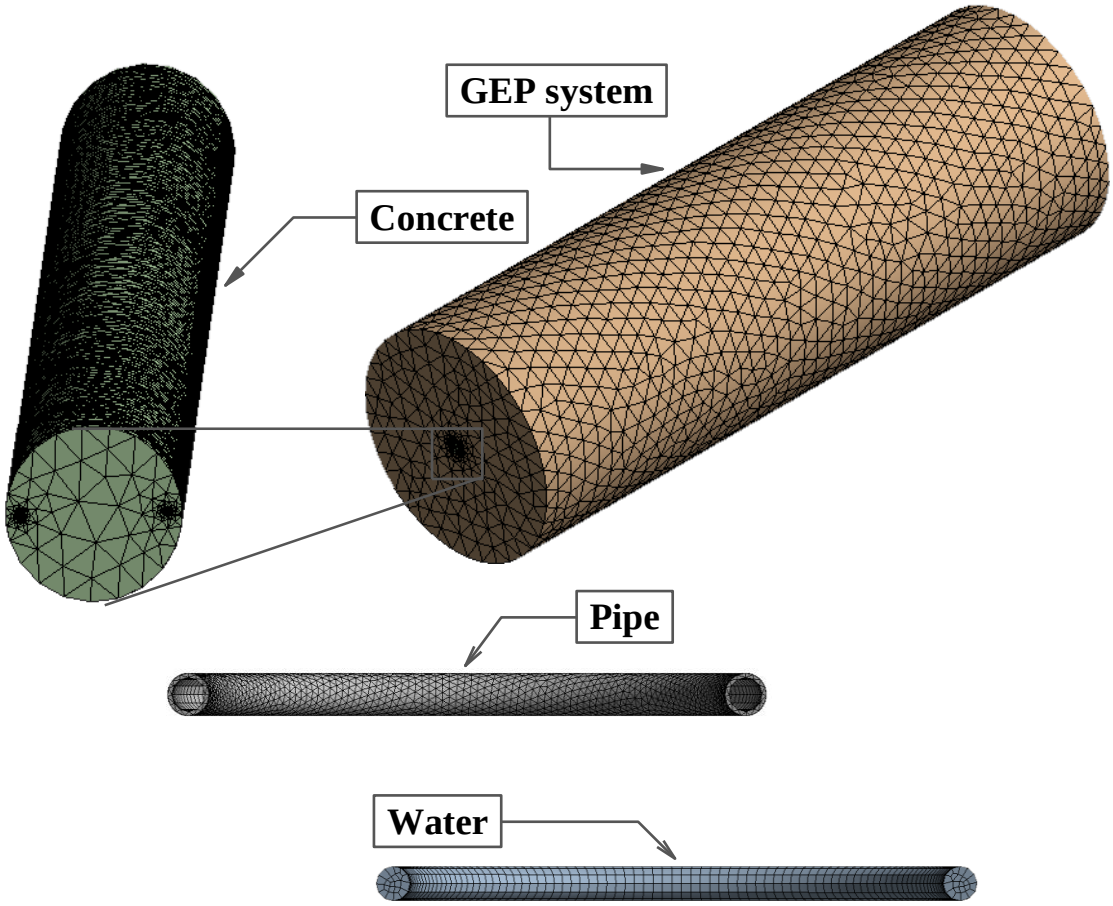

Figure IV. 1. 1. Mesh configuration of the geothermal energy pile (GEP) components.

Table IV. 1. 1. Mesh discretization details of GEP model.

Component	Number of nodes	Number of elements
Soil	25629	121332
Concrete	258449	1241310
U-tube	221437	563344
Fluid	137696	114231
Total Geometry	643211	2040217

In order to investigate the impact of fluid flow on the thermal performance of the system**,** computational fluid dynamics (CFD) simulations were carried out for Reynolds numbers of 500, 1000, 1500, and 2000. These values fall within the laminar flow regime typically encountered in geothermal energy pile applications. By considering seasonal influences and varying flow conditions**,** the study offers a comprehensive analysis of the transient thermal behavior and response of geothermal energy piles, contributing to the optimization of their design and long-term operational efficiency.

The simulations were performed over a total period of 12 hours, with results systematically recorded at critical time intervals of 1 hour, 6 hours, and 12 hours to thoroughly assess the temporal evolution of the thermal field. Boundary conditions were carefully prescribed to emulate typical seasonal operating scenarios, whereby the inlet fluid temperatures were adjusted to represent both summer cooling and winter heating conditions. The initial temperature of the soil was assumed to be uniform and consistent with typical subsurface thermal conditions.

By incorporating both seasonal effects and varying flow conditions, the methodology provides a robust framework for analyzing the thermal performance of geothermal energy piles. The outcomes of this study serve as a reference for future optimization of system design and operation under realistic working conditions.

IV.1.3 Results and discussion

IV.1.3.1 Heating period

Figure 2 illustrates the evolution of thermal contours under winter boundary conditions, with an inlet water temperature of 278 K, for different Reynolds numbers over three operational durations: 1 hour, 6 hours, and 12 hours. The contour plots reveal complex and dynamic spatial temperature distributions within the energy pile system. A key observation across all analyses is the radial expansion of the thermal plume originating from the U-tube heat exchanger, which becomes increasingly pronounced over time. This radial propagation highlights the continuous thermal exchange between the circulating fluid and the surrounding soil. From the 1-hour analysis to the 12-hour time interval, the region affected by heat extraction expands significantly for all Reynolds numbers tested, indicating the cumulative effect of heat transfer between the pile and the soil, as well as a nearly linear relationship between the duration of

operation and the extent of thermal propagation. Such behavior has important implications for understanding the long-term thermal performance and thermal response of energy pile systems, particularly under sustained winter operating conditions.

A comparative analysis of the subfigures in Figure 2 clearly illustrates the significant influence of the Reynolds number on the temperature field distribution around the geothermal energy pile. At higher Reynolds numbers (Re = 1500 and 2000), the thermal contours become more uniform and symmetrically distributed in contrast to the lower Reynolds number case (Re = 500). This behavior is primarily attributed to the increase in fluid velocity associated with higher Reynolds numbers, which enhances convective heat transfer along the pile. Greater flow velocities facilitate more rapid thermal penetration and promote a more extensive and evenly distributed heat diffusion into the surrounding soil. Consequently, elevated Reynolds numbers contribute to a marked improvement in the thermal performance of the GEP system.

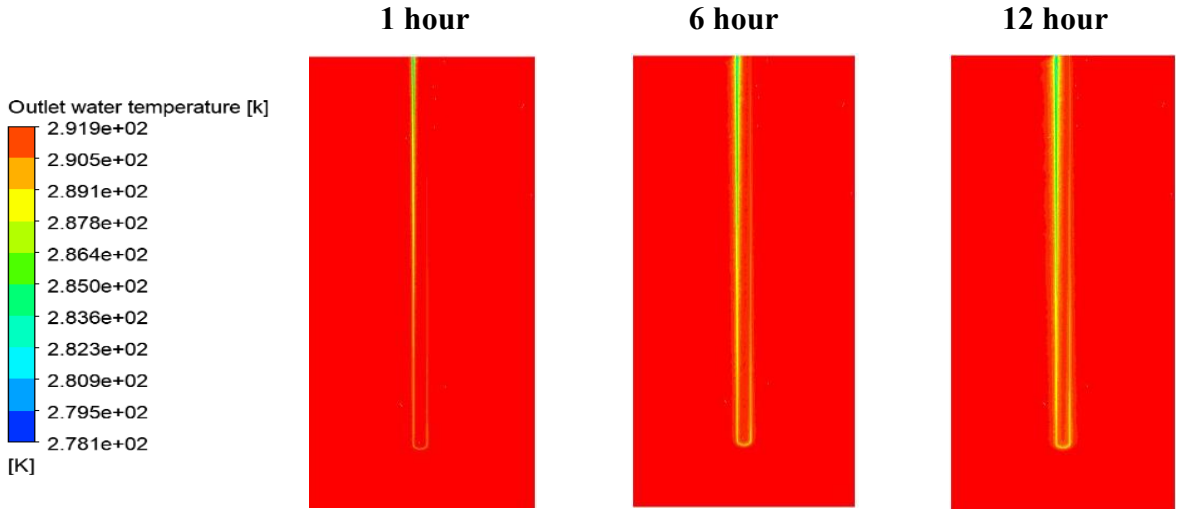

(a)

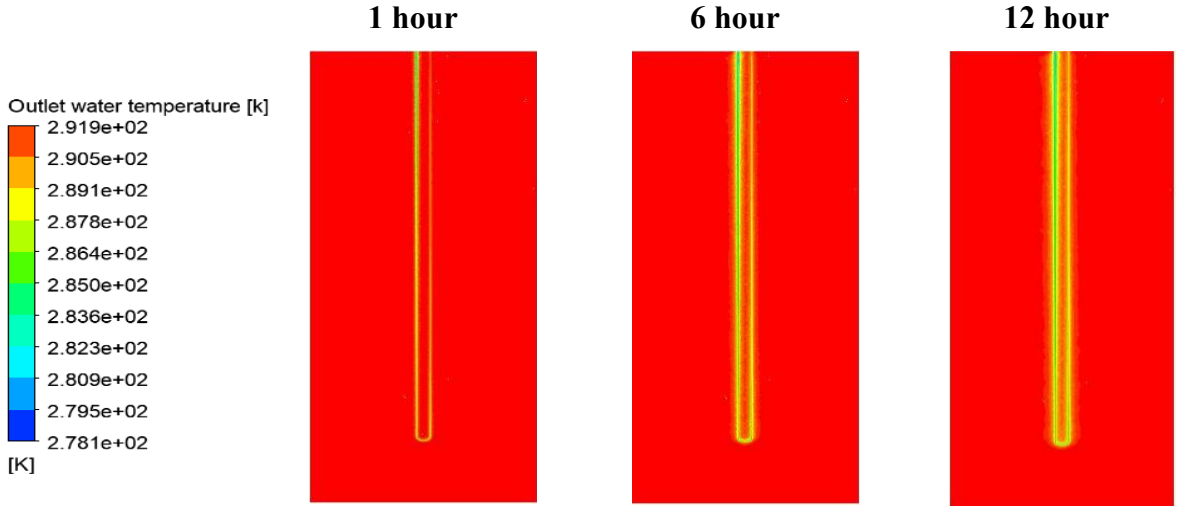

(b)

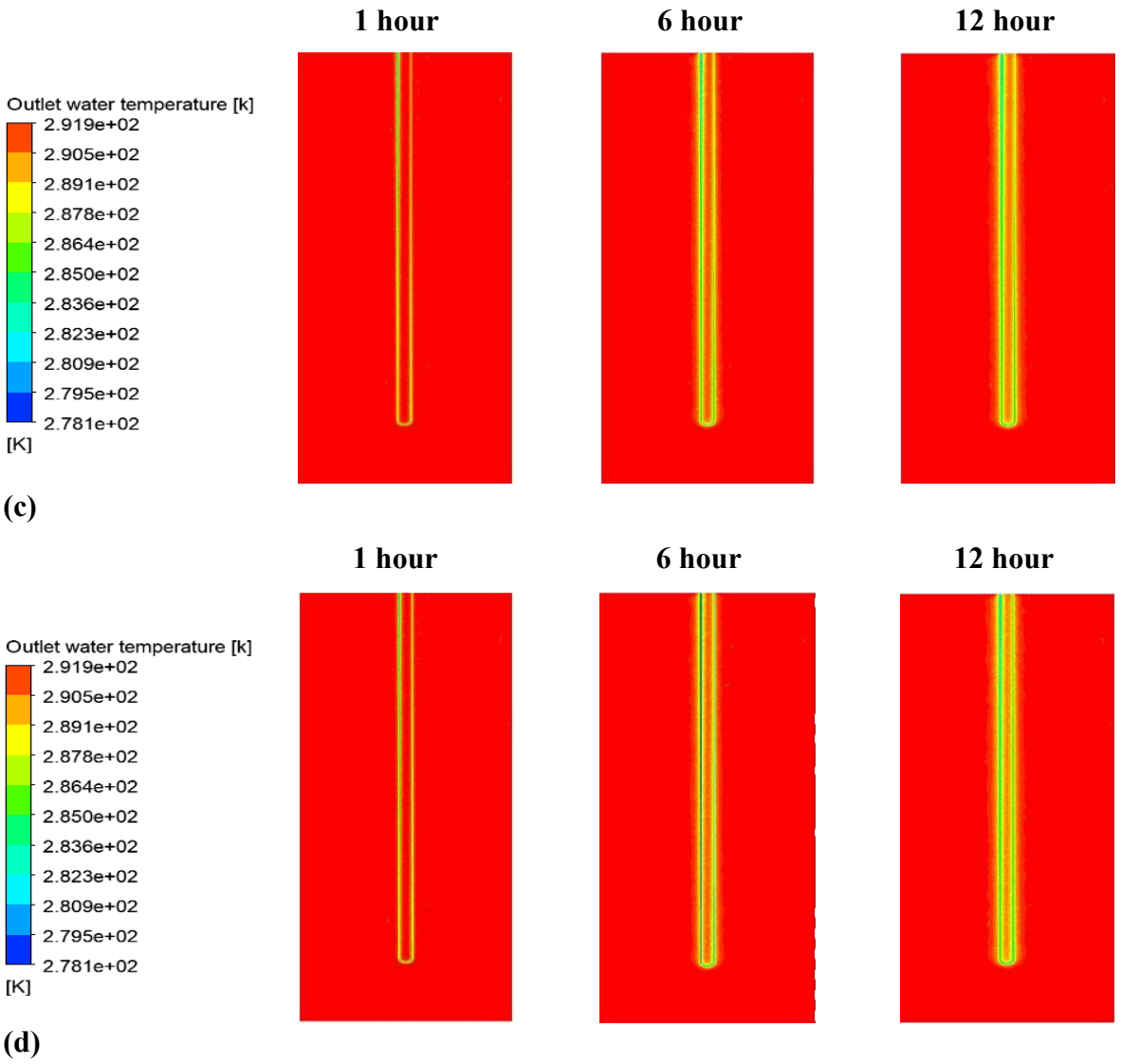

Figure IV. 1. 2. Temperature contour profiles in the GEP during the heating phase for Reynolds numbers of (a) Re = 500, (b) Re = 1000, (c) Re = 1500, and (d) Re = 2000.

Figure 3 presents the time-dependent outlet temperature and heat exchanger rate during the winter heating period with a constant inlet temperature of 278.15 K, for different Reynolds numbers (Re = 500, 1000, 1500, and 2000).

According to the Figure 3(a), the outlet temperature initially rises above the inlet, indicating heat gain from the warmer surrounding soil. Over time, it gradually decreases due to thermal depletion near the pile. Lower Reynolds numbers, such as Re = 500, achieve higher heat transfer efficiency because slower fluid velocity increases residence time and enhances thermal interaction. In contrast, higher Reynolds numbers reduce residence time, limiting heat absorption despite stronger convective effects.

As illustrated in Figure 3(b), there is a clear proportional relationship between the Reynolds number and the heat transfer rate within the GEP system. An increase in the Reynolds number, which represents higher fluid velocity and more turbulent flow, leads to enhanced convective heat transfer. This results in a more efficient exchange of thermal energy between the working fluid and the surrounding soil. The observed trend highlights the critical role of flow dynamics in optimizing the thermal performance of GEP systems. Therefore, controlling the flow rate to maintain a higher Reynolds number can significantly improve the overall efficiency of the heat exchanger.

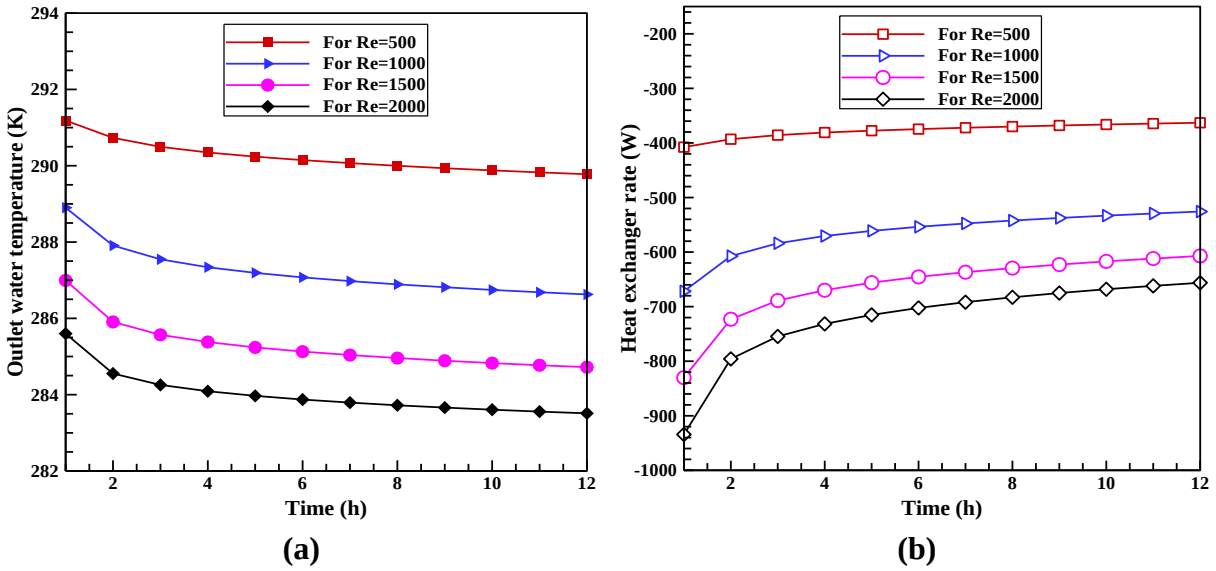

Figure IV. 1. 3. Time-dependent variation of outlet fluid temperature during the heating phase across different Reynolds numbers.

Table 2 shows the effect of the Reynolds number on heat transfer and temperature variation in a GEP system operating in winter mode, with the inlet temperature fixed at 278.15 K. As the Reynolds number increases from 500 to 2000, the outlet temperature decreases from 289.78 K to 283.51 K, causing the temperature difference (ΔT) to drop by 53.9%, from 11.63 K to 5.36 K. Meanwhile, the heat transfer rate rises from 363.04 W to 656.30 W, an increase of 80.9%. This indicates that higher Reynolds numbers, which correspond to increased fluid velocity and flow rate, reduce heat gain per unit mass due to shorter residence time in the system. However, the overall heat extracted increases because the greater fluid flow transports more energy. These findings emphasize the importance of balancing Reynolds number, velocity, and flow rate to optimize thermal efficiency in winter GEP operation.

Table IV. 1. 2. Effect of Reynolds number on thermal performance of a GEP system in winter mode.

Number of Reynolds	T_{inlet} [K]	T_{outlet} [K]	ΔT [K]	Heat exchanger rate [W]
500	278.15	289.78	11.63	363.04
1000		286.63	08.48	525.74
1500		284.72	06.57	607.06
2000		283.51	05.36	656.30

IV.1.3.2 Cooling period

This section investigates the thermal response of GEP during summer operations. Based on the results presented in Figures 4 and 5, the analysis focuses on the temporal evolution of temperature distributions at various Reynolds numbers, emphasizing the interaction between fluid flow and heat transfer to the surrounding soil.

In the summer, with an inlet water temperature of 318.15 K, the figure 4 illustrates temperature contour distributions for Reynolds numbers of 500, 1000, 1500, and 2000 over durations of 1, 6, and 12 hours. The results reveal a progressive transfer of heat from the fluid to the cooler surrounding soil, evidenced by the expanding thermal influence zone over time. This expansion reflects the cumulative nature of heat injection and is consistently observed across all Reynolds numbers. Comparatively, these results show that higher Reynolds numbers (Re = 1500 and 2000) yield smoother and more symmetric thermal fields compared to lower values (Re = 500), due to increased flow velocities that enhance convective heat transfer. These elevated flow rates improve heat rejection efficiency and facilitate broader thermal dispersion, thereby augmenting the cooling performance of the system. Collectively, these findings underscore the dynamic and time-dependent thermal response of energy piles operating under cooling conditions.

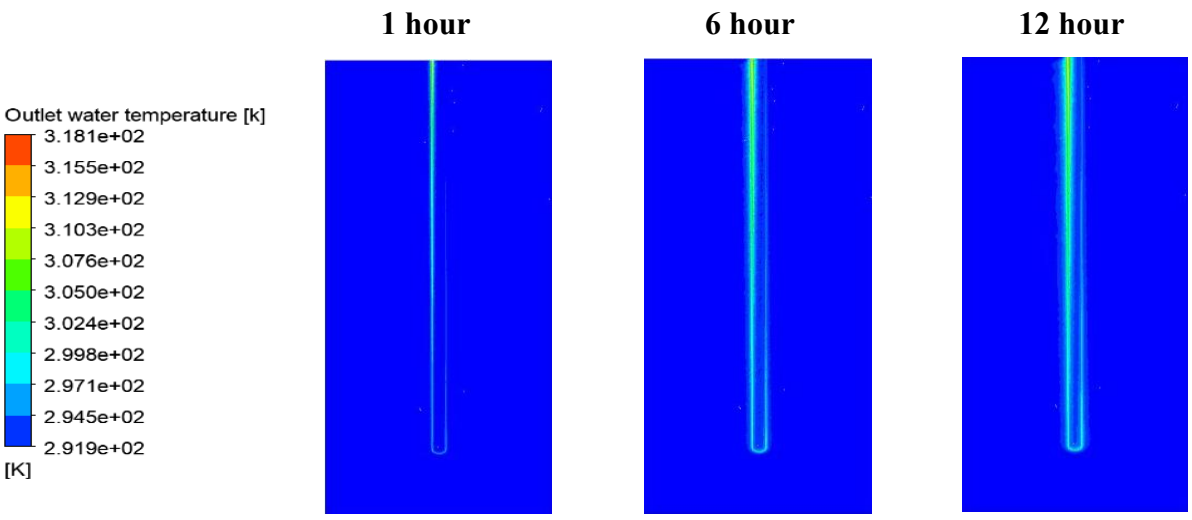
1 hour
6 hour
12 hour
Outlet water temperature [k]
3.181e+02
3.155e+02
3.129e+02
3.103e+02
3.076e+02
3.050e+02
3.024e+02
2.998e+02
2.971e+02
2.945e+02
2.919e+02
[K]

(a)

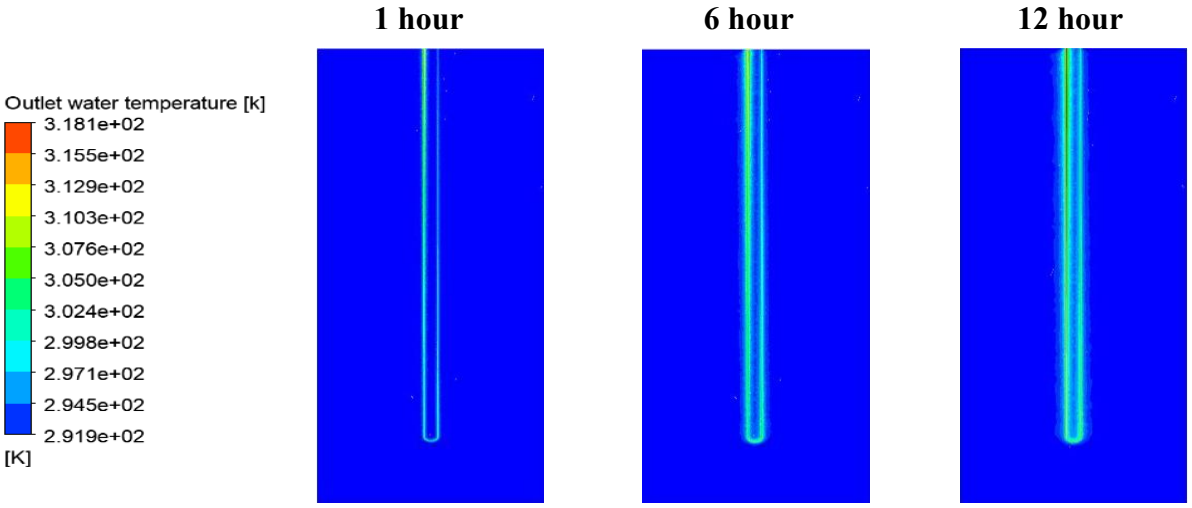
1 hour
6 hour
12 hour
Outlet water temperature [k]
3.181e+02
3.155e+02
3.129e+02
3.103e+02
3.076e+02
3.050e+02
3.024e+02
2.998e+02
2.971e+02
2.945e+02
2.919e+02
[K]

(b)

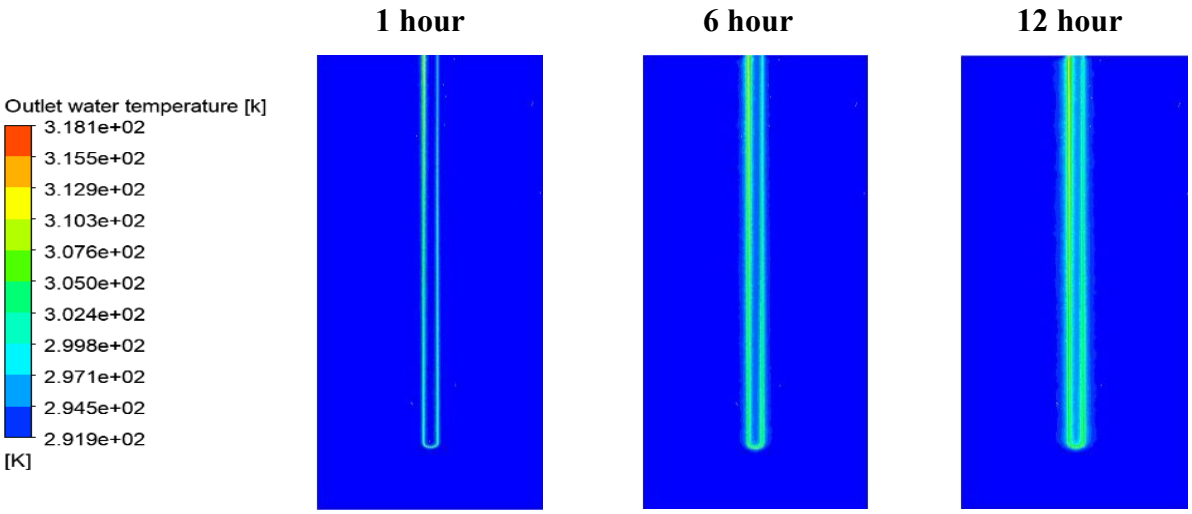
1 hour
6 hour
12 hour
Outlet water temperature [k]
3.181e+02
3.155e+02
3.129e+02
3.103e+02
3.076e+02
3.050e+02
3.024e+02
2.998e+02
2.971e+02
2.945e+02
2.919e+02
[K]

(c)

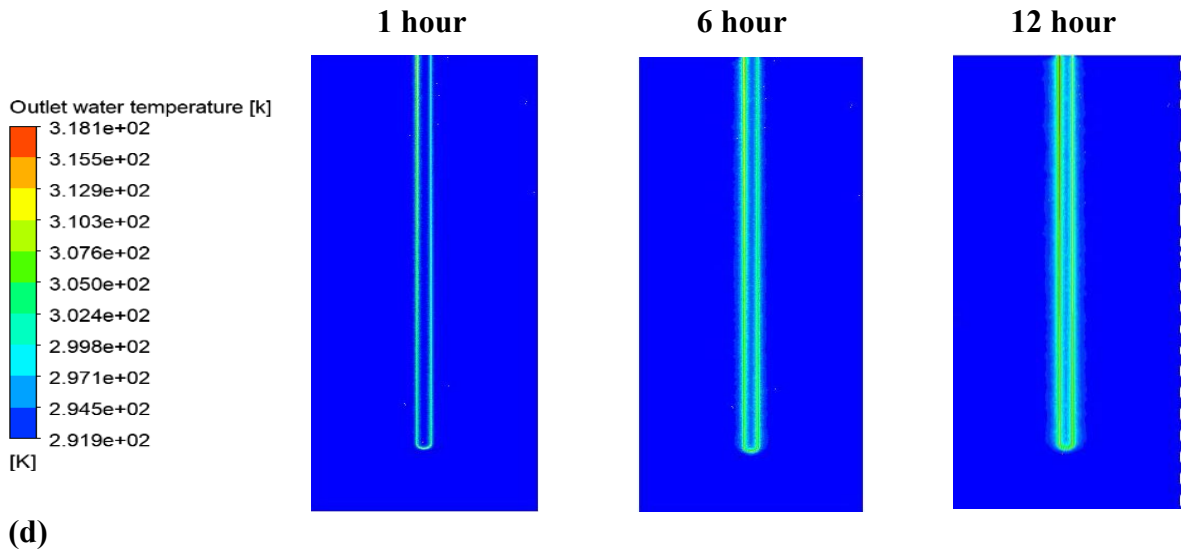

Figure IV. 1. 4. Temperature contour profiles in the GEP during the cooling phase for Reynolds numbers of (a) Re = 500, (b) Re = 1000, (c) Re = 1500, and (d) Re = 2000.

Figure 5 (a) presents the temporal evolution of the outlet temperature during the summer cooling phase, with a constant inlet temperature of 318.15 K, for various Reynolds numbers (Re = 500, 1000, 1500, and 2000). Over time, the outlet temperature increases for all cases, indicating sustained heat transfer from the circulating fluid to the cooler surrounding soil. A comparative analysis of the curves shows that the lowest Reynolds number (Re = 500) is associated with reduced fluid velocity and prolonged residence time, which enhances heat rejection to the soil. In contrast, higher Reynolds numbers (Re = 1000, 1500, and 2000) correspond to shorter residence times, limiting the overall thermal exchange efficiency of the geothermal energy pile system.

Figure 5(b) presents the variation of the heat exchanger rate during the summer cooling phase for different Reynolds numbers (Re = 500, 1000, 1500, and 2000), with a constant inlet temperature of 318.15 K. The results indicate that the heat exchanger rate increases with Reynolds number, reflecting enhanced heat rejection from the circulating fluid to the cooler surrounding soil. Higher Reynolds numbers correspond to greater fluid velocities and increased turbulence, which improve convective heat transfer and thus facilitate more efficient thermal exchange. Conversely, at the lowest Reynolds number (Re = 500), the reduced fluid velocity results in a lower heat exchanger rate despite the longer residence time, due to weaker convective effects. This trend underscores the importance of fluid flow dynamics in maximizing the cooling efficiency of geothermal energy pile systems during summer operation.

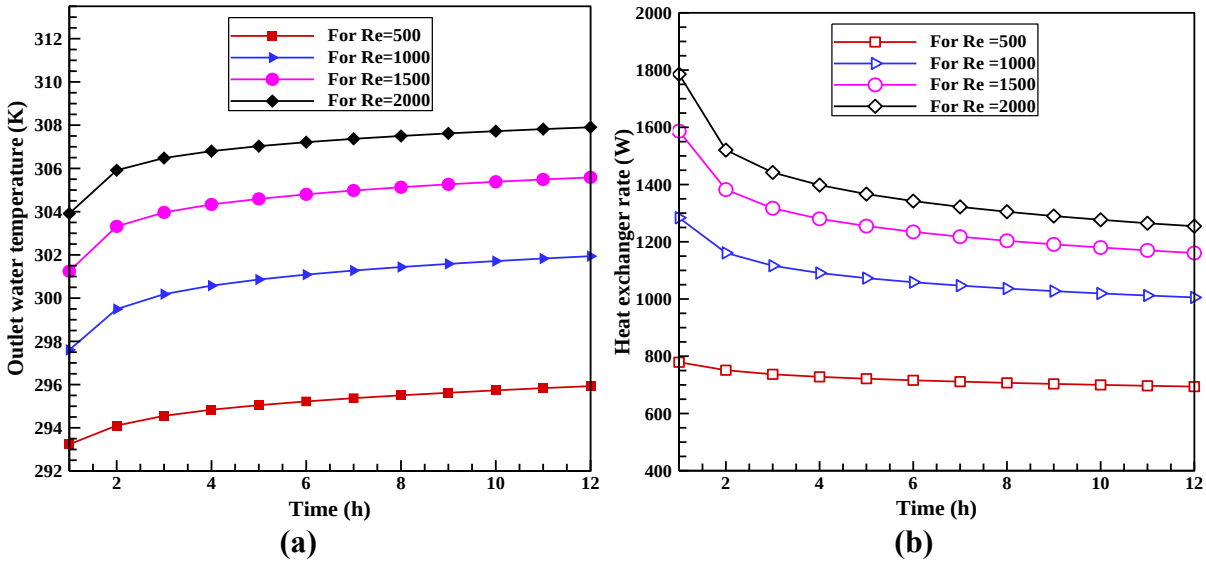

Figure IV. 1. 5. Time-dependent variation of outlet fluid temperature during the cooling phase across different Reynolds numbers.

Table 3 presents the thermal behavior of the GEP system during summer operation with a T_{inlet} fixed at 318.15 K, revealing a clear inverse relationship between the fluid's temperature change and the total heat transfer rate as the Reynolds number increases. Observed that, at a low Reynolds number (Re = 500), the T_{outlet} reaches 295.93 K, yielding a temperature difference (ΔT) of 22.22 K and a corresponding heat transfer rate of 693.86 W. As the Reynolds number increases to 1000, 1500, and 2000, the outlet temperature rises to 301.94 K, 305.59 K, and 307.90 K, while ΔT decreases to 16.21 K, 12.56 K, and 10.25 K, respectively. This represents a 53.9% decrease in ΔT across the range. In contrast, the heat exchanger rate increases steadily with flow rate, reaching 1005.51 W, 1160.86 W, and a maximum of 1254.31 W at Re = 2000, an 80.8% increase compared to the lowest flow condition. This inverse trend can be explained by the fact that, at higher flow rates, the fluid spends less time in the heat exchanger, which reduces the amount of heat it can release per unit mass. However, the increase in flow rate results in a greater overall mass of fluid passing through, which raises the total amount of energy extracted. These results highlight an important design consideration for GEP systems operating during the summer.

Table IV. 1. 3. Effect of Reynolds number on thermal performance of a GEP system in summer mode.

Number of Reynolds	T_{inlet} [K]	T_{outlet} [K]	ΔT [K]	Heat exchanger rate
500	318.15	295.93	22.22	693.86
1000		301.94	16.21	1005.51
1500		305.59	12.56	1160.86
2000		307.90	10.25	1254.31

IV.1.4 Conclusion

This study explored the influence of Reynolds number on the thermal performance and thermal response of GEP systems under both cooling (summer) and heating (winter) operating modes. The results show that variations in Reynolds number have a significant impact on both outlet fluid temperature and heat transfer rate. As the Reynolds number increases, the outlet temperature tends to converge toward the inlet temperature, indicating a reduced capacity for thermal exchange between the fluid and the surrounding soil. This is primarily due to shorter residence times at higher flow velocities, which limit the duration of fluid–soil thermal interaction. In contrast, the heat transfer rate increases with Reynolds number, as greater fluid volumes enhance the total amount of energy exchanged. These findings highlight the critical role of flow regime in shaping the thermal response of GEP systems. Optimizing Reynolds number is therefore essential to balance heat transfer efficiency, system performance, and long-term operational sustainability under varying seasonal demands.

Part 2: Computational Analysis for the Optimization of Geothermal Energy Pile (GEP) Systems Under Winter and Summer Operating Conditions

IV.2 Computational Analysis for the Optimization of Geothermal Energy Pile (GEP) Systems Under Winter and Summer Operating Conditions

IV.2.1 Objective

The present research aims to optimize the thermal performance of geothermal energy pile (GEP) systems through an in-depth investigation of fluid flow and heat transfer behavior, using three-dimensional computational fluid dynamics (CFD) simulations combined with analytical methods under both heating and cooling conditions. The study examines critical design parameters influencing thermal exchange efficiency, including the diameter of the concrete pile, the inner diameter of the heat exchanger pipes, the spacing between the pipe and the concrete boundary, and the angular positioning of the pipes. Following physical model validation, mesh refinement analysis, and verification of consistency between simulation results and analytical solutions, the objective is to determine the most effective configuration to enhance heat transfer and overall system performance. This work ultimately contributes to the design and development of more energy-efficient, cost-effective, and sustainable GEP systems for building heating and cooling applications.

IV.2.2 Problem description

This study investigates the thermal and fluid flow behavior in a geothermal energy pile (GEP) system by analyzing four distinct geometric configurations, each corresponding to a key design parameter. For each case, three-dimensional CFD simulations are performed under both heating and cooling modes to quantify the effects of geometry on heat transfer efficiency and temperature distribution within the pile. The cases examined are as follows:

- **Case 1: Variation in the diameter of the concrete pile**

This case investigates the effect of varying the concrete pile diameter on the thermal performance of the GEP system, specifically in terms of heat exchanger rate and conductive heat transfer to the surrounding soil. Figure 1 presents the different pile diameters evaluated in this study.

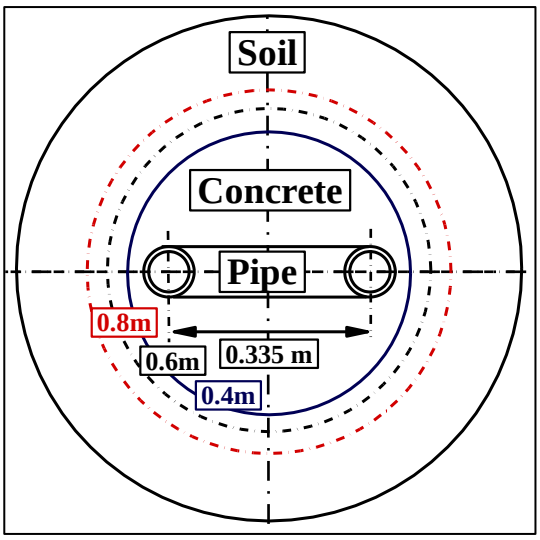

Figure IV. 2. 1. Dimensions and geometric properties of concrete pile diameters.

☞ **Case 2: Variation in the inner diameter of pipe**

This case examines the influence of the pipe's inner diameter on the internal fluid dynamics and heat transfer characteristics within the GEP system. Changes in the inner diameter directly impact the fluid velocity, Reynolds number, and convective heat transfer coefficient, all of which are key parameters affecting the overall thermal performance. The specific inner diameter values considered in this study are summarized in Table 1.

Table IV. 2. 1. Inner diameter values of heat exchanger.

Pipe geometry	Inner diameter of pipe (mm)	Outer diameter of pipe (mm)
U-shaped	14	20
	20	25
	26	32

☞ **Case 3: Variation in the spacing between pipe and concrete boundary**

This case investigates the effect of the spacing between the outer surface of the heat exchanger pipe and the inner boundary of the concrete pile on the thermal behavior of the system. This geometric parameter significantly influences the thermal resistance between the circulating fluid and the surrounding soil, thereby affecting heat dissipation and overall system efficiency. The spacing configurations considered in this study are summarized in Figure 2.

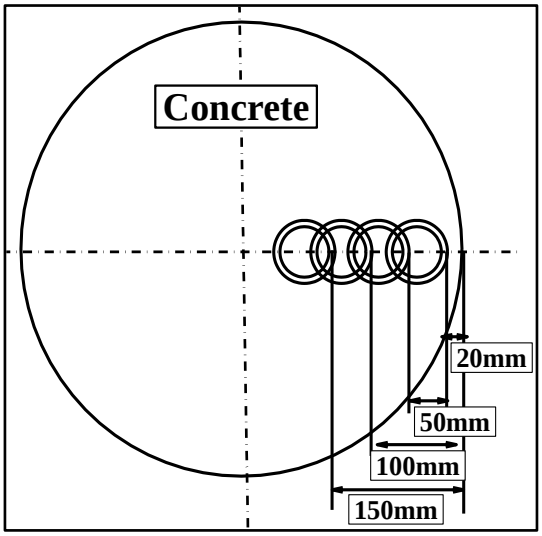

Figure IV. 2. 2. Geometric dimensions of the spacing between the pipe and the concrete wall.

☞ **Case 4: Variation in the angular positioning of the pipe**

This final configuration examines the impact of the angular placement of the heat exchanger pipes within the concrete cross-section on the thermal performance of the GEP system. The relative positioning of the pipes influences the temperature distribution in the concrete, the extent of thermal interference between flow channels, and ultimately the efficiency of heat exchange with the surrounding soil. The angular configurations analyzed in this study are illustrated in Figure 3.

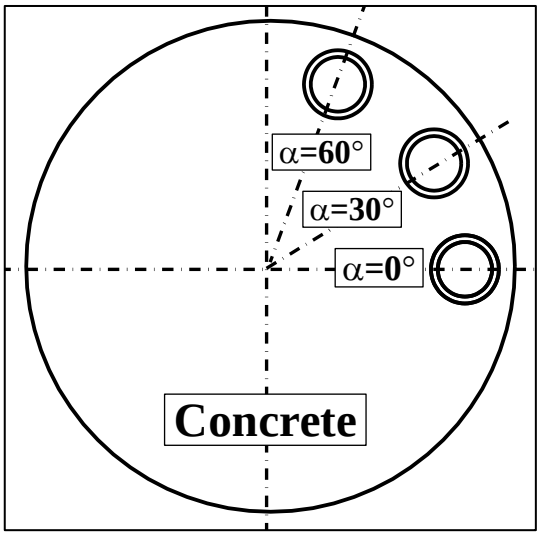

Figure IV. 2. 3. Angular configurations of pipe placement within the concrete cross-section.

IV.2.3 Numerical modelling

IV.2.3.1 Mesh sensitivity test

Grid sensitivity analysis is a crucial step in numerical simulations to ensure reliable predictions and minimize uncertainty, especially in regions near boundaries where gradients are steep. In zones with significant temperature variations, the computational domain was discretized into smaller elements using finer mesh resolutions to capture thermal and flow behavior with greater accuracy. Except for Grid 1, which used the default coarse mesh, all other simulations were performed using the standard k-ε turbulence model with enhanced wall treatment (see Table 2). Wall functions were applied with a Y^+ value close to 1 to accurately represent near-wall regions, thereby improving the reliability of heat transfer predictions across different mesh densities (see Figure 4).

To solve the governing equations, first-order temporal and second-order spatial discretization schemes were employed, balancing numerical accuracy and computational efficiency. The PISO (Pressure Implicit with Splitting of Operators) algorithm was used for pressure–velocity coupling throughout the simulations, offering benefits such as improved stability and better handling of turbulent flow structures.

Following the grid independence study, Mesh 04 was selected for all subsequent simulations due to its balance of accuracy and computational efficiency (see Figure 5). This mesh was further converted to a polyhedral mesh for comparative analysis. According to Table 3, the results demonstrated that the polyhedral mesh not only improved solution precision but also reduced computation time. Additionally, it was observed that further mesh refinement led to increased computational costs without a significant improvement in result accuracy.

Table IV. 2. 2. Mesh sensitivity analysis results.

Grid	Grid 1	Grid 2	Grid 3	Grid 4	Grid 5
Number of elements	2702898	3198148	5730595	8859429	13480156
T_{inlet} [K]	318.15	318.15	318.15	318.15	318.15
T_{outlet} [K]	316.215	316.149	316.141	316.132	316.131
ΔT [K]	1.935	2.001	2.009	2.018	2.019
Computing time	00h46min	01h17min	02h20min	03h50min	05h05min

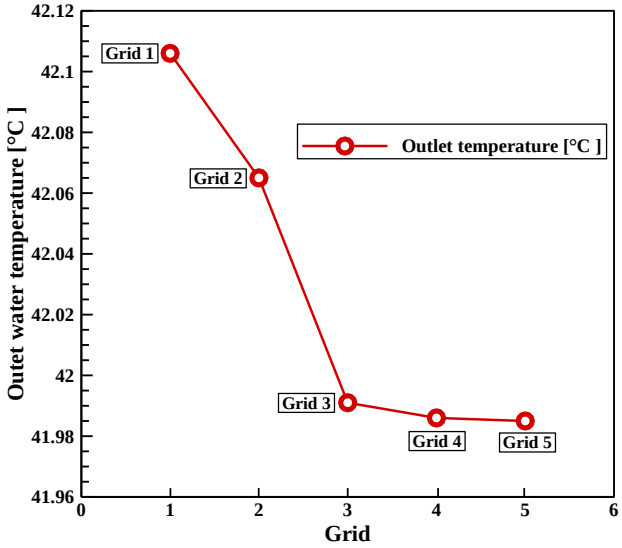

Figure IV. 2. 4. Grid convergence results.

Table IV. 2. 3. Analysis of unstructured and polyhedral meshes.

	Grid 4	
Type	Unstructured	Polyhedral
Number of elements	8859429	3198148
T_{inlet} [K]	318.15	318.15
T_{outlet} [K]	316.132	316.128
ΔT [K]	2.018	2.022
Computing time	03h50min	03h25min

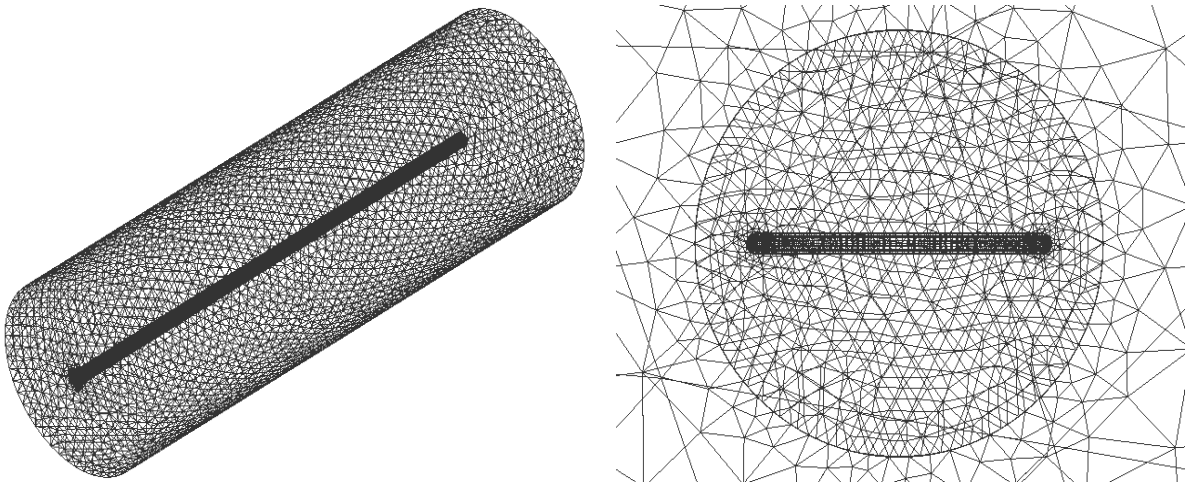

3-D view of unstructured tetrahedral mesh. 2-D view of unstructured tetrahedral mesh.

Figure IV. 2. 5. Results of mesh study.

IV.2.3.2 Validation

To validate the simulation results, a comparative analysis was performed with the recent study by Peng Zhang et al. [56], which focused on a geothermal energy system implemented in a plant project located in Kunshan, Jiangsu Province (see Table 4). The geometric dimensions, material properties of the pipes, concrete, soil, and working fluid, as well as the boundary conditions, were adopted from the referenced study to ensure consistency and comparability.

Table IV. 2. 4. Validation of the numerical model for various parametric case studies against analytical results and literature data.

Authors	Pipe Configuration	Pile Size (m)	Case study	Periods	T_{inlet} (K)	T_{outlet} (K)	Study	Software	t (hours)	ΔT (K)
Zhang et al. [52]	Double U-shaped [56],	Diameter=0.4 Length=15		Summer	318.15	315.35	Numerical	ANSYS Fluent 20.0	36	02.80
				Winter	278.15	279.43				01.28
				Summer	318.15	314.66	Tester			03.49
				Winter	278.15	279.38				01.20
Present study	U-shaped	Diameter=0.4 Length=15	Case 1	Summer	318.15	316.16	Numerical	ANSYS Fluent 20.0	48	01.99
				Winter	278.15	279.19				01.04
				Summer	318.15	315.00	Analytical			03.15
				Winter	278.15	279.81				01.66
			Case 2	Summer	318.15	316.12	Numerical	ANSYS Fluent 20.0		02.03
				Winter	278.15	279.18				01.03
				Summer	318.15	314.81	Analytical			03.34
				Winter	278.15	279.90			48	01.75
			Case 3	Summer	318.15	316.22	Numerical	ANSYS Fluent 20.0		01.93
				Winter	278.15	279.19				01.04
				Summer	318.15	315.20	Analytical		48	02.95
				Winter	278.15	279.70				01.55
			Case 4	Summer	318.15	316.16	Numerical	ANSYS Fluent 20.0		01.99
				Winter	278.15	279.19				01.04
				Summer	318.15	315.27	Analytical		48	02.88
				Winter	278.15	279.66				01.54

According to Table 4, which presents the validation results across several geometric case studies, the numerical and analytical outputs from the present model show strong agreement with the literature. The small deviations observed in all cases confirm that the developed model reliably predicts the thermal response of geothermal energy piles.

These discrepancies can be attributed to several factors, such as differences in heat exchanger configuration, mesh resolution, groundwater effects, soil thermal properties, and variations in software versions or computational platforms. Nevertheless, the consistency observed between numerical simulations and analytical solutions across different configurations reinforces the robustness, accuracy, and overall credibility of the proposed model.

IV.2.4 Results and discussion

IV.2.4.1 Effect of diameter pile change

To analyze the simulation results, Figures 6 and 7 present the transverse temperature profiles in 2-D for the GEP system with varying diameters (400 mm, 600 mm, and 800 mm) after 48 hours of operation under winter and summer conditions, respectively.

These figures effectively illustrate the dual role of the surrounding soil as a heat source in winter and a heat sink in summer, while highlighting the influence of pile diameter on thermal performance. The interaction between the circulating water and the surrounding clayey soil is clearly depicted through color gradients representing temperature variations along the GEP and within the adjacent soil. These profiles offer valuable insights into the thermal behavior of the system under varying seasonal and geometric configurations.

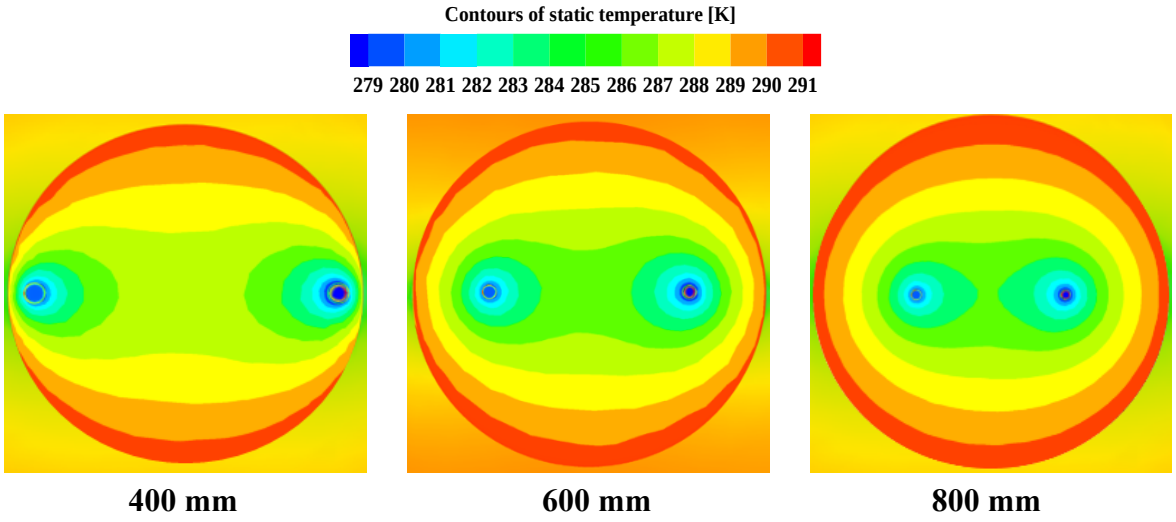

Figure IV. 2. 6. 2-D Temperature distribution for different pile diameters during heating.

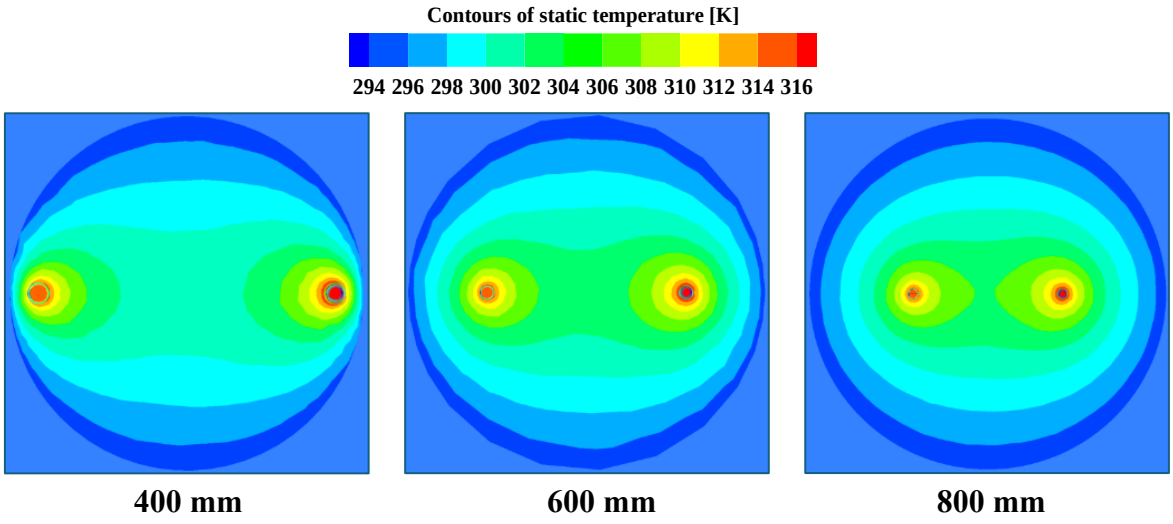

Figure IV. 2. 7. 2-D Temperature distribution for different pile diameters during cooling.

Figures 8 and 9 illustrate the three-dimensional temperature distribution within the GEP system under heating and cooling conditions, respectively. These representations provide a comprehensive view of the thermal exchange between the heat exchanger and the surrounding soil, emphasizing the soil's dual function as a heat source in winter and a heat sink in summer. The spatial gradients depicted in these figures offer valuable insight into the seasonal thermal behavior of the system, reinforcing the trends observed in the two-dimensional analyses.

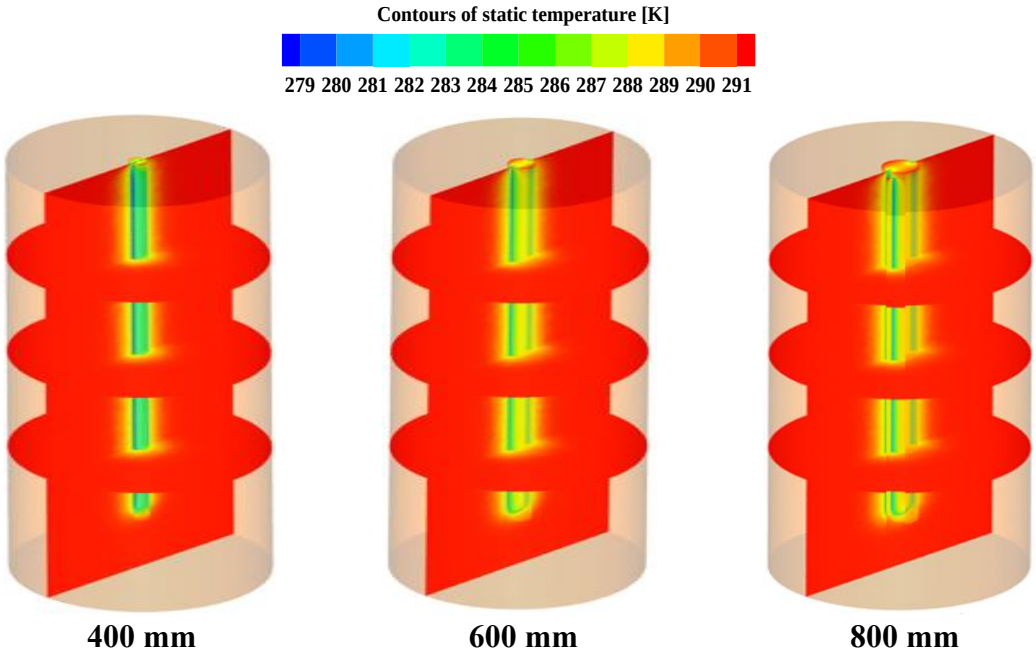

Figure IV. 2. 8. 3-D Temperature distribution for different pile diameters during heating.

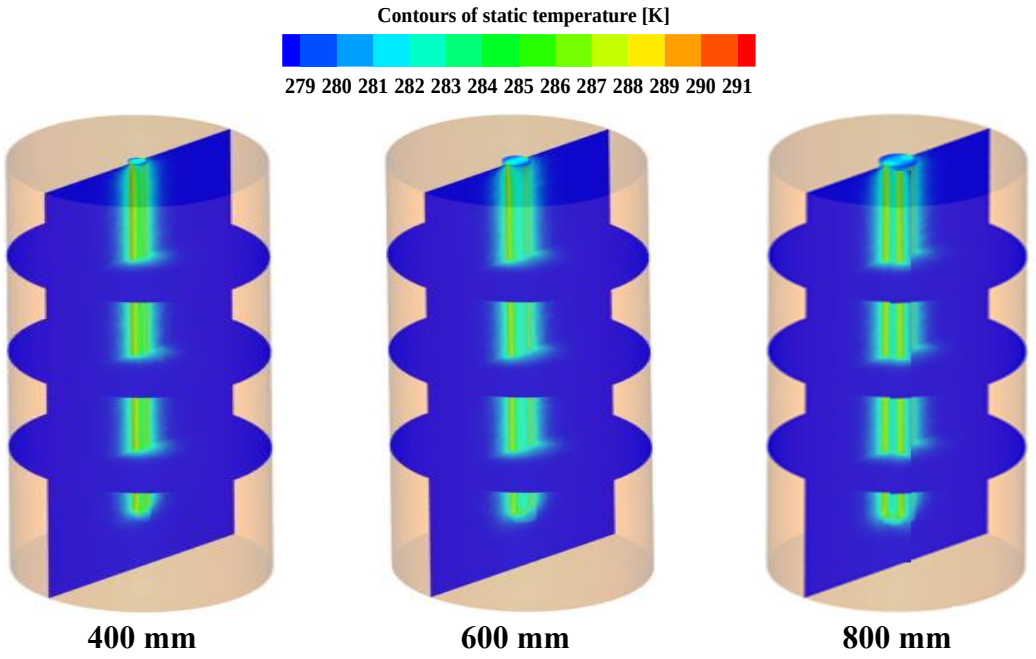

Figure IV. 2. 9. 3-D Temperature distribution for different pile diameters during cooling.

Figure 10 presents a comparison of the variation in water outlet temperature and heat exchanger rate over time under both heating and cooling conditions for energy piles with different diameters (400 mm, 600 mm, and 800 mm), all sharing the same pile foundation physical properties. The comparison of these results during winter and summer shows that the

400 mm diameter pile provides superior heat transfer efficiency compared to larger diameters.

During winter operation (see Figure 10(a)), the 400 mm diameter pile exhibits a modest but consistent thermal advantage, with its water outlet temperature approximately 0.039 K higher than that of the 600 mm pile and 0.086 K higher than the 800 mm pile. Interestingly, despite the higher outlet temperature, the heat exchanger rate of the 400 mm pile is lower by about 8.938 W compared to the 600 mm pile and by 28.737 W relative to the 800 mm pile.

Conversely, under summer cooling conditions (see Figure 10(b)), the 400 mm diameter pile shows a pronounced improvement in thermal extraction. The water outlet temperature from the pipe embedded in the 400 mm diameter concrete pile is 0.095 K cooler than that of the 600 mm pile and 0.161 K cooler than that of the 800 mm pile. In terms of heat exchange rate, the 400 mm diameter pile outperforms the 600 mm and 800 mm piles by approximately 72.457 W and 121.767 W, respectively.

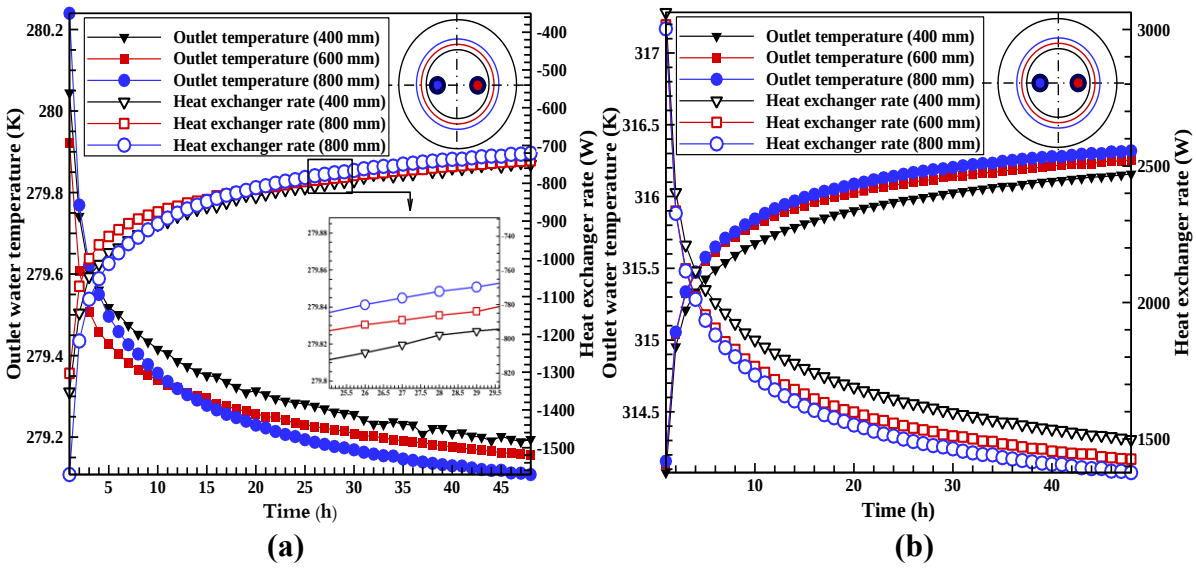

Figure IV. 2. 10. Comparison of outlet water temperature and heat exchange rate for various pile diameters during heating (a) and cooling (b) modes.

To validate the numerical results for outlet water temperature and heat exchanger rate, which indicated that the 400 mm diameter pile is more efficient in heat transfer compared to the 600 mm and 800 mm diameter piles, analytical calculations were performed under identical heating and cooling conditions, material properties, and geometric dimensions of the GEP system. These comparisons, conducted over a continuous 48-hour simulation period, are

presented in Figures 11 and 12. The results demonstrate that the analytical and numerical values for both the outlet water temperature and heat exchanger rate of the 400 mm diameter pile are nearly identical and show excellent agreement throughout the 48-hour period in both winter and summer scenarios. This consistency confirms the robustness and reliability of the numerical simulation model and reinforces the conclusion that the 400 mm diameter pile offers superior heat transfer performance compared to larger diameter piles.

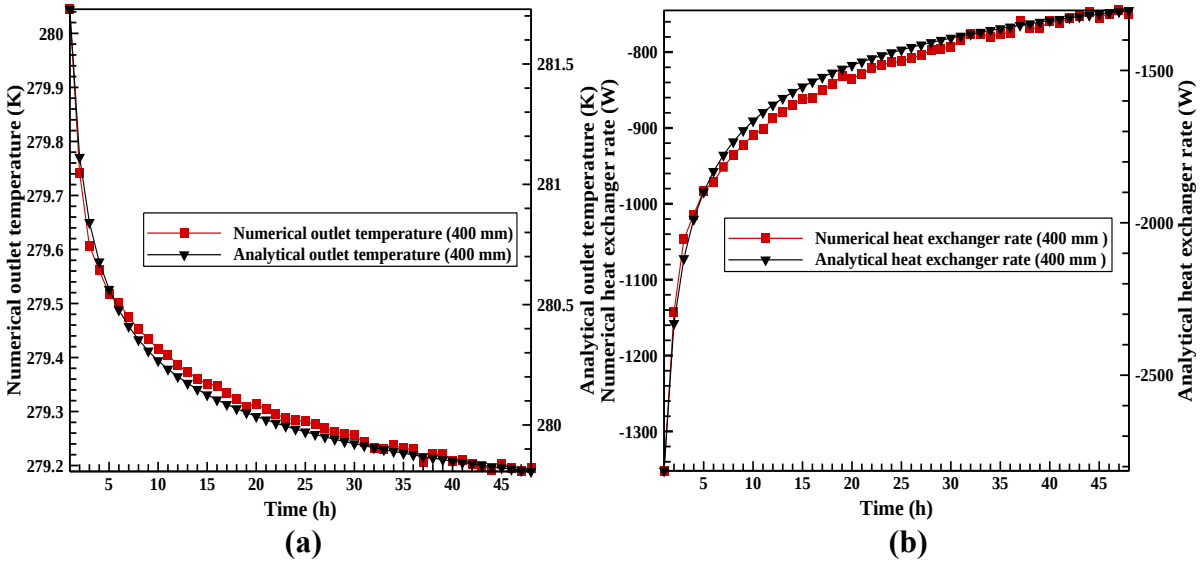

Figure IV. 2. 11. Comparison between analytical and numerical results for the wintertime thermal performance of a 400 mm diameter pile.

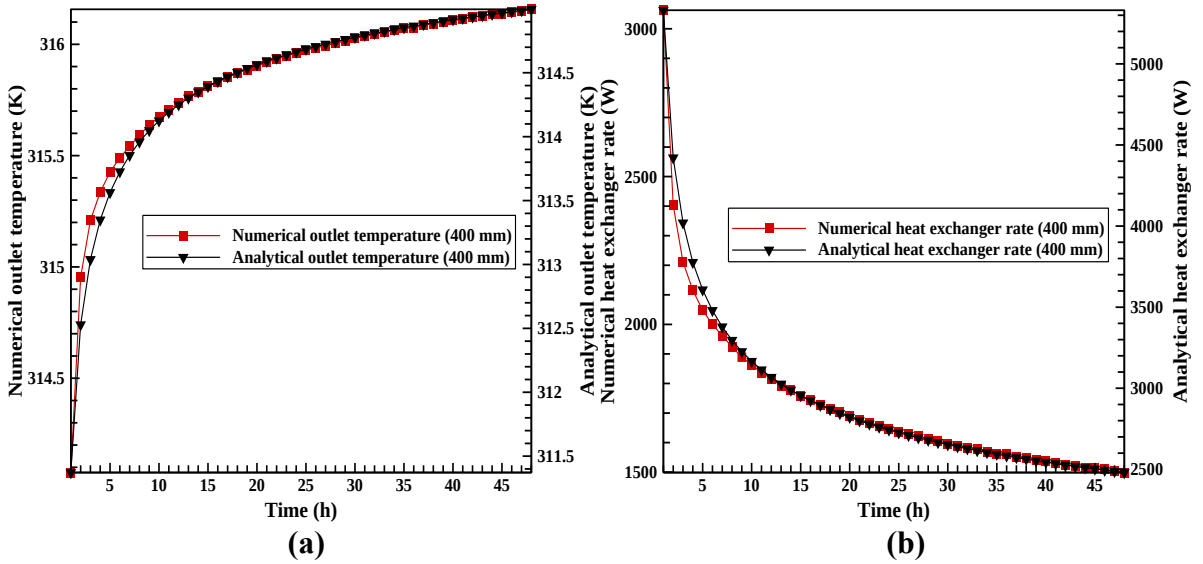

Figure IV. 2. 12. Comparison between analytical and numerical results for the summertime thermal performance of a 400 mm diameter pile.

The numerical investigation of pile diameter variations (400 mm, 600 mm, and 800 mm) revealed a significant influence on the thermal performance of the GEP system under both heating and cooling conditions. With a constant inlet flow rate of 0.188 kg/s over a 48-hour simulation period, the results were evaluated at four distinct time intervals, as presented in Figure 13.

During the heating phase, it achieved the highest outlet fluid temperature (279.195 K) and the maximum heat extraction rate (749.14 W), while the 600 mm and 800 mm piles showed reductions in heat transfer rate of approximately 1.19% and 3.84% respectively.

In the cooling phase, the 400 mm configuration again delivered superior performance, with a heat rejection rate of 1498.61 W, compared to 1426.15 W and 1376.84 W for the 600 mm and 800 mm piles, corresponding to efficiency decreases of about 4.83% and 8.13%. These findings, illustrated in Figure 13, clearly demonstrate that the 400 mm pile diameter provides the most effective thermal interaction with the surrounding soil, making it the optimal choice for enhancing GEP system performance in both seasonal operating modes.

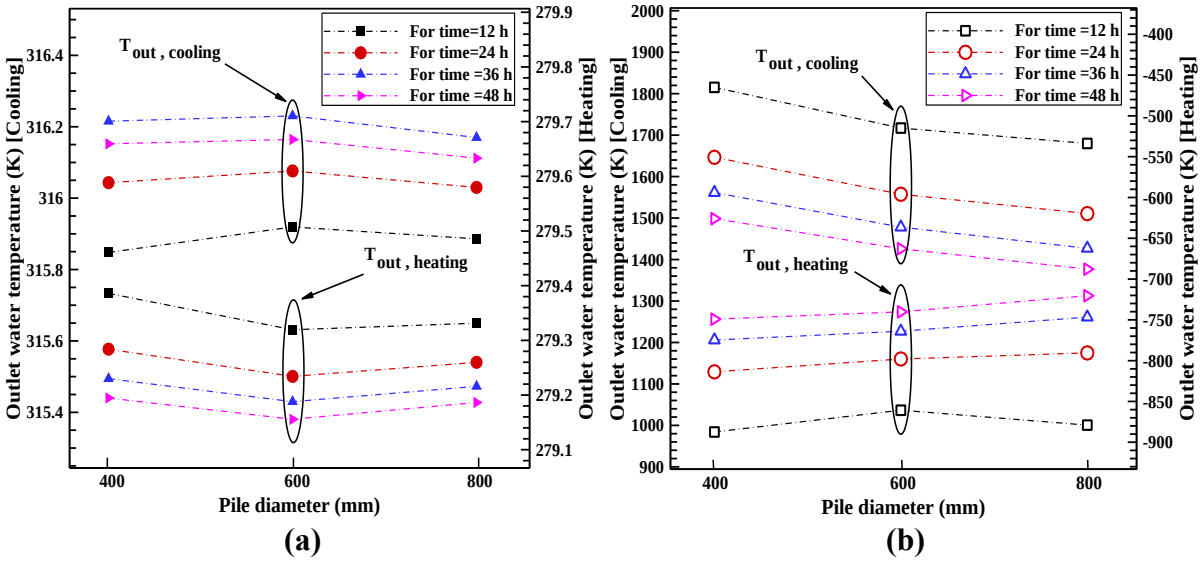

Figure IV. 2. 13. Variation in numerical outlet water temperature and heat transfer rate at different time steps during heating and cooling with pile diameter changes.

IV.2.4.2 Effect of diameter heat exchanger changes

In the final step of the numerical simulations (steady-state conditions), using an inlet flow rate of 0.188 kg/s and varying tube diameters, temperature contour distributions in the

upper horizontal section of the energy piles during both heating and cooling phases are presented in Figures 14 and 15.

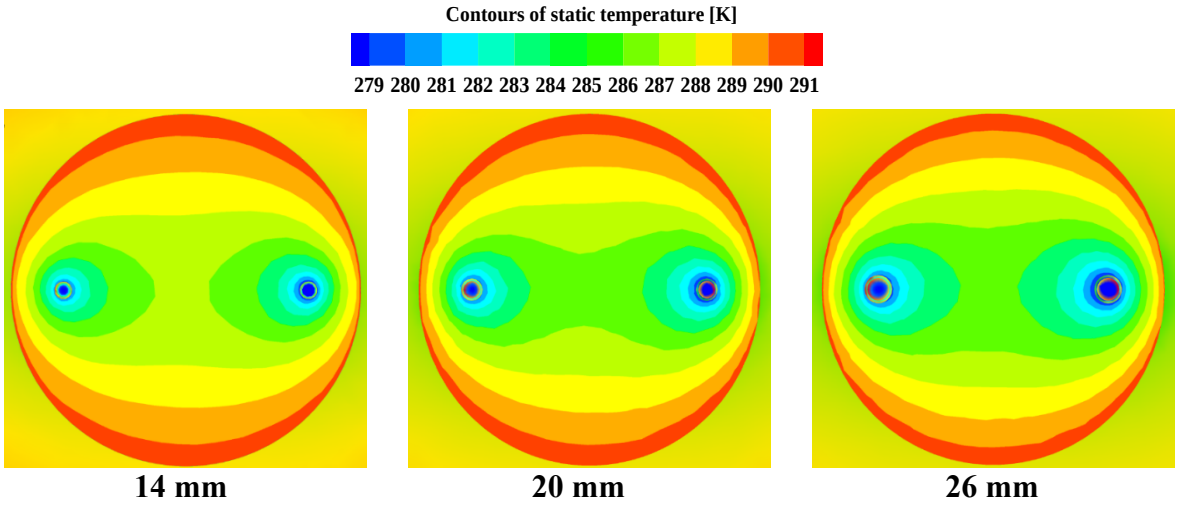

Figure IV. 2. 14. 2-D Contours of static temperature for pipe diameter changes during heating.

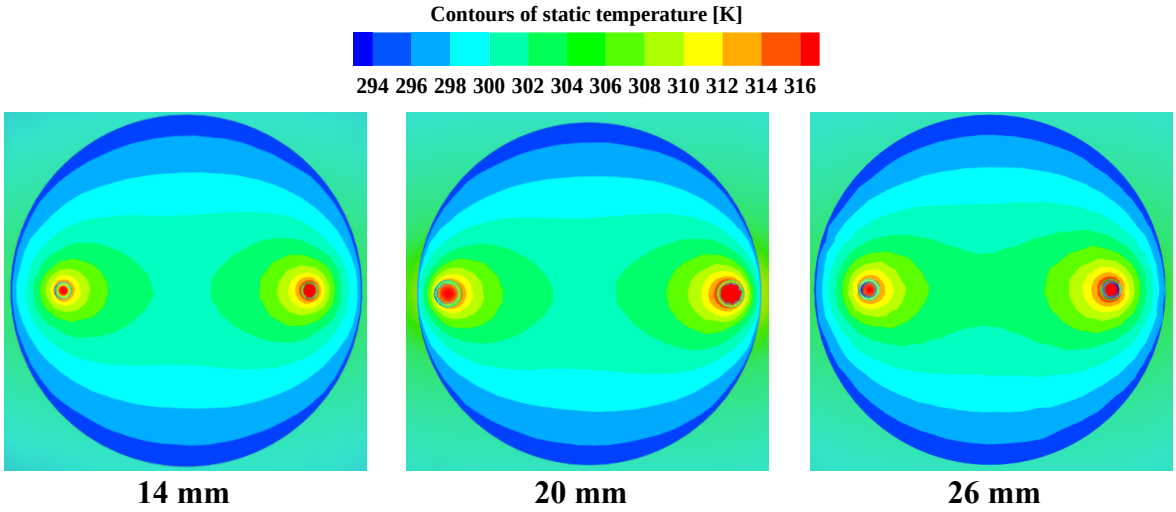

Figure IV. 2. 15. 2-D Contours of static temperature for pipe diameter changes during cooling.

For all tube diameters, a constant inlet water temperature was maintained: 318.15 K for summer and 278.15 K for winter. The heat exchanger with a 26 mm inner diameter showed the greatest temperature variation in both modes. During cooling, the inlet pipe temperature exceeded the return pipe's, while in heating, the inlet temperature was lower.

These results demonstrate that inner diameter variations influence temperature distribution and heat transfer performance, thus affecting the overall efficiency of the GEP system (see Figures 16 and 17).

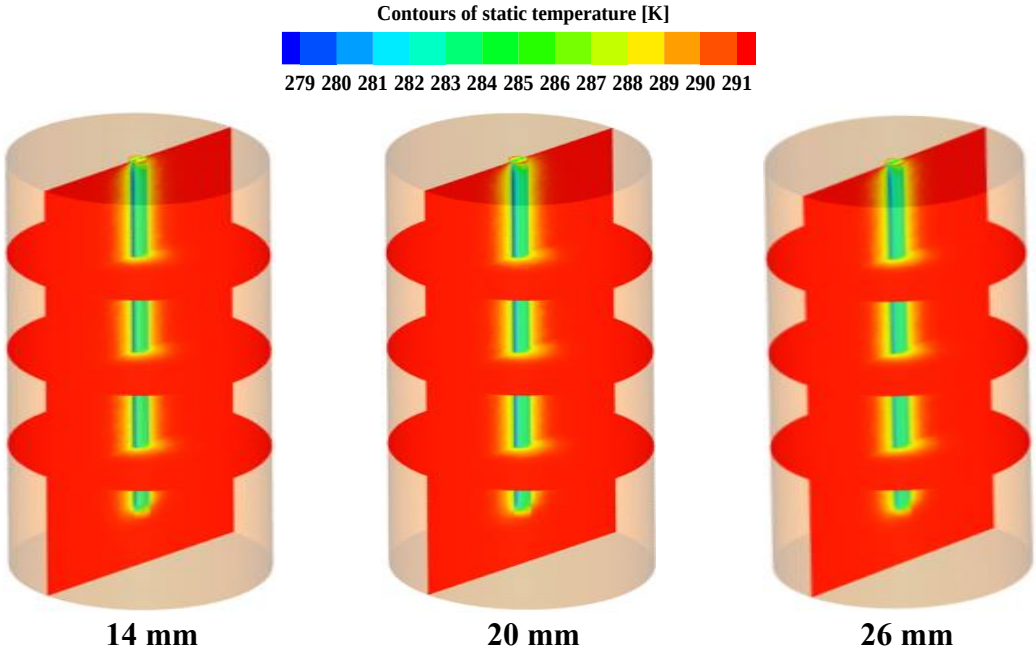

Figure IV. 2. 16. 3-D Contours of temperature distribution along of (GEPs) with varying diameters under winter conditions.

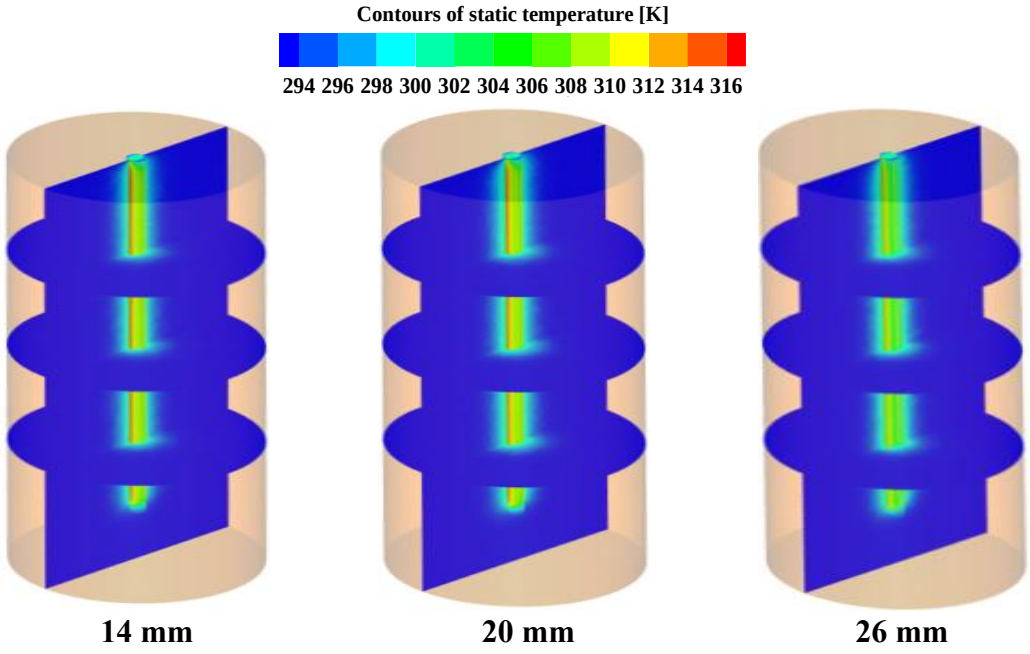

Figure IV. 2. 17. 3-D Contours of temperature distribution along of (GEPs) with varying diameters under summer conditions.

The effect of HE diameter on the performance of the GEP system was investigated in two main parts of this study, and the corresponding results are thoroughly analyzed.

In the first part, variations in outlet water temperature and heat transfer rate were examined over a 48-hour simulation period under both heating and cooling conditions, with a constant flow rate of 0.188 kg/s. The analysis was conducted for HEs with different inner diameters: 14 mm, 20 mm, and 26 mm, as shown in Figures 18 . During the heating phase, the outlet water temperature gradually decreased until thermal equilibrium was reached, whereas under cooling conditions, the temperature increased progressively. The heat transfer rate exhibited an increasing trend during heating and a decreasing trend during cooling, stabilizing in both cases over time. These results demonstrate that the 26 mm inner diameter provides the most efficient thermal performance for the GEP system under both operational modes.

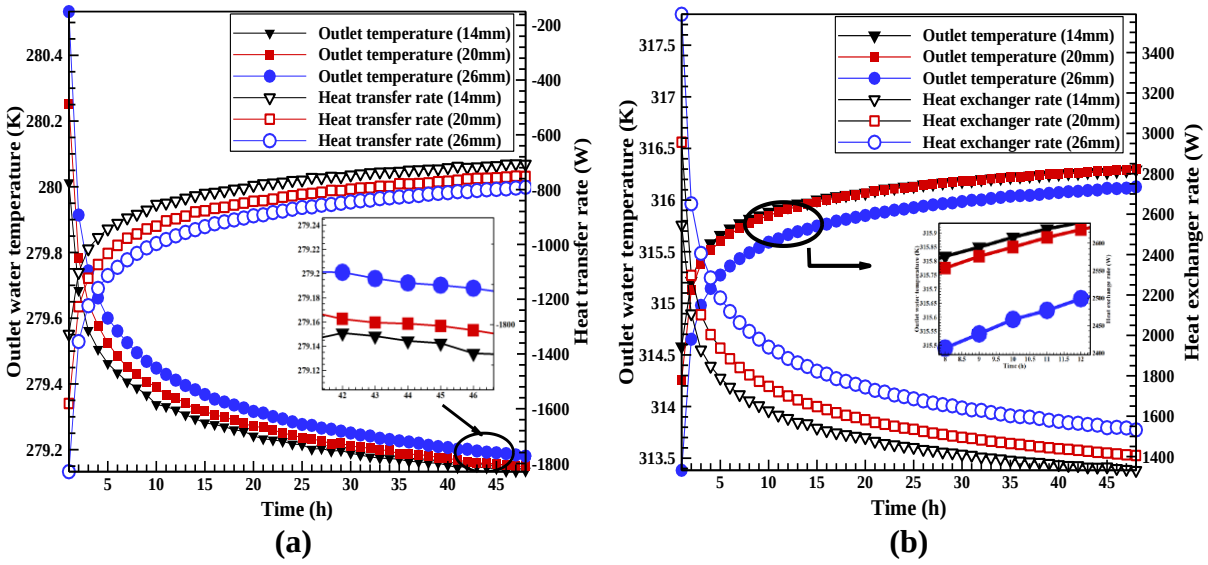

Figure IV. 2. 18. Numerical results for outlet water temperature and heat transfer rate (heating (a) and cooling (b)) in the case of diameter changes.

The second part of the study focuses on analytical validation of the simulation results, specifically for the U-tube with the identified optimal diameter of 26 mm. Figures 19 and 20 present a comparison between analytical and numerical results for outlet water temperature and heat exchanger rate under heating and cooling conditions. In both cases, the results show strong agreement between the numerical simulations and analytical solutions, validating the reliability and accuracy of the simulation model.

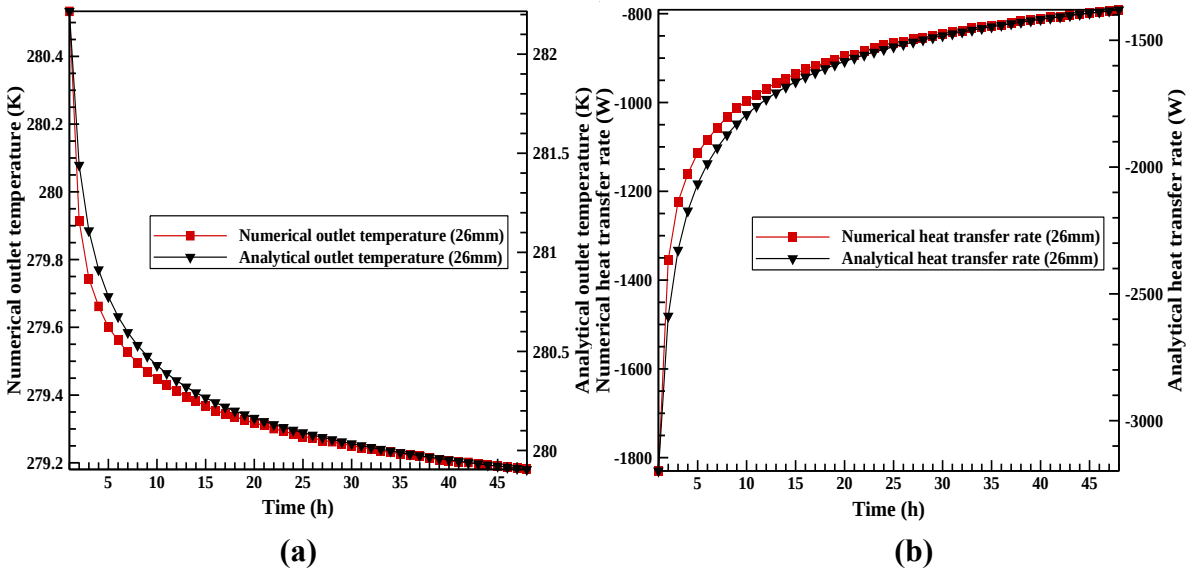

Figure IV. 2. 19. Comparison of analytical and numerical results under winter conditions for the optimal heat exchanger diameter.

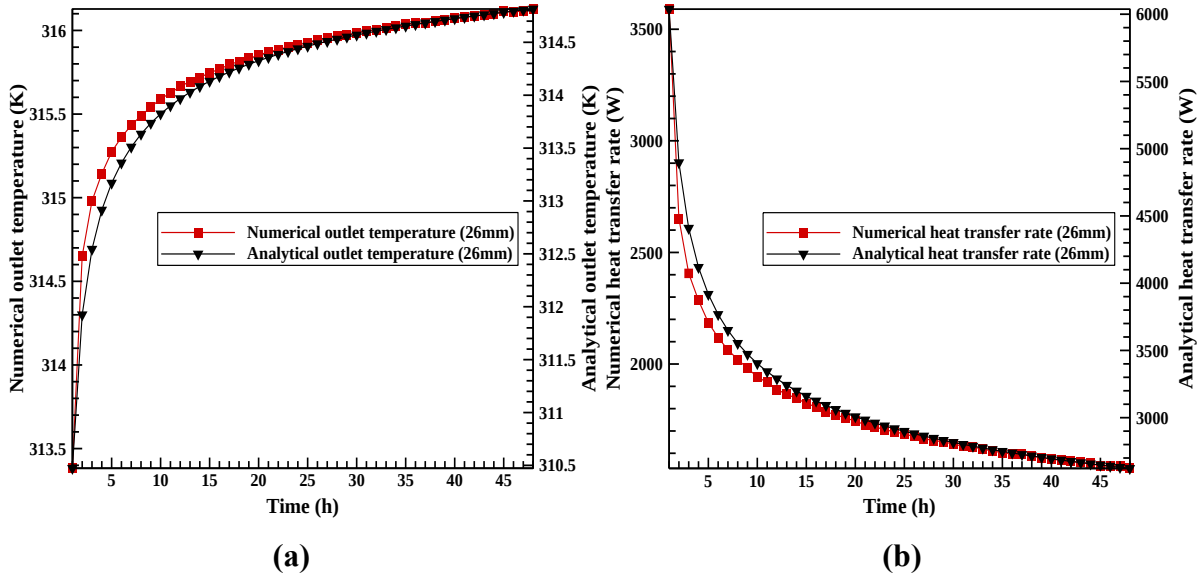

Figure IV. 2. 20. Comparison of analytical and numerical results under summer conditions for the optimal heat exchanger diameter.

Overall, the findings confirm that heat exchange efficiency improves with increased heat exchanger surface area in contact with the thermal source. Among the diameters studied, the 26 mm U-tube heat exchanger demonstrated the highest thermal performance, supporting its identification as the most effective configuration for the GEP system in this work.

Figure 21 presents the results of the numerical model for heat transfer rates, along with a summary of outlet water temperature measurements from the U-tube heat exchanger, recorded at a constant flow rate of 0.188 kg/s during both heating and cooling processes, evaluated at four distinct time intervals.

Over a 48-hour simulation period, the performance of ground heat exchanger pipes with varying inner diameters was assessed under both heating (winter) and cooling (summer) conditions. During heating, the outlet fluid temperature increased by 0.98 K, 1.00 K, and 1.03 K for pipe diameters of 14 mm, 20 mm, and 26 mm, respectively. Correspondingly, the heat extraction rates increased, with a 6.4% improvement observed when increasing the diameter from 14 mm to 20 mm, and an overall increase of approximately 12% when comparing 14 mm to 26 mm. This demonstrates that a larger pipe diameter enhances both the outlet fluid temperature and the system's heat extraction capacity, resulting in improved thermal performance during heating. Similarly, in cooling mode, the outlet temperature decreased by 1.84 K, 1.85 K, and 2.02 K for the same respective diameters. The heat rejection rate improved by approximately 5.5% from 14 mm to 20 mm, and by about 15% from 14 mm to 26 mm. These findings confirm that increasing the pipe diameter enhances thermal exchange with the ground, thereby improving system efficiency in both seasonal modes.

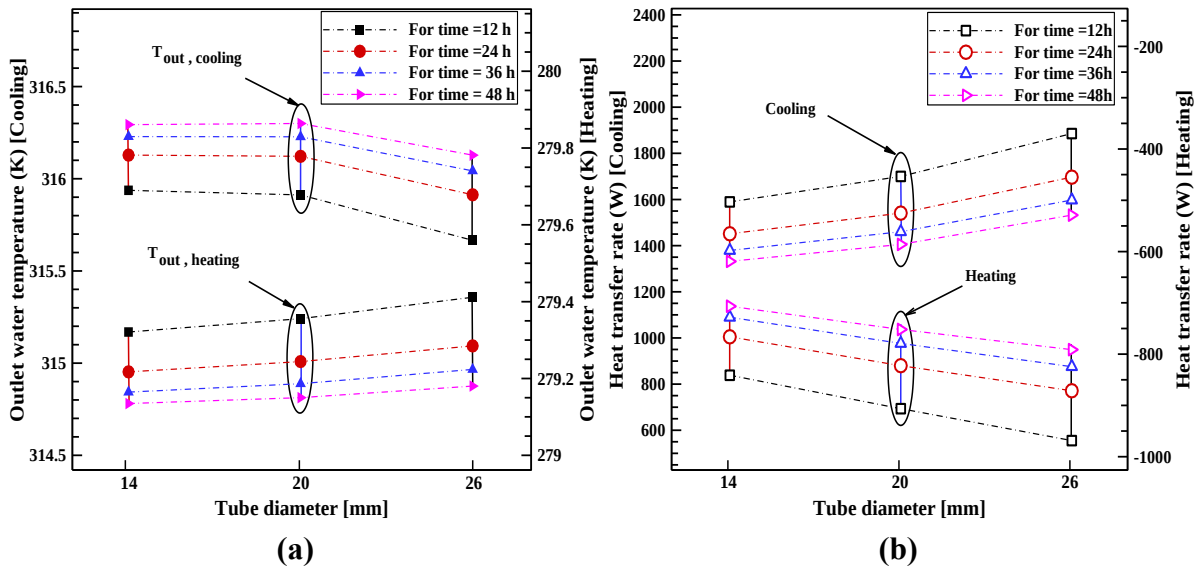

Figure IV. 2. 21. Variation in numerical outlet water temperature and heat transfer rate at different time steps during heating and cooling with diameter changes.

IV.2.4.3 Effect of distance between pipe outer diameter and concrete perimeter

Based on the steady-state contours of static temperature at a 48-hour time step, the effects of varying the distance between the U-shaped heat exchanger and the concrete perimeter (20 mm, 50 mm, 100 mm, and 150 mm) were analyzed under both heating and cooling conditions, with a constant inlet flow rate of 0.188 kg/s, as illustrated in Figures 22 and 23.

The results demonstrate that a spacing of 20 mm between the pipe and the concrete perimeter provides the most favorable heat transfer performance. This finding, further supported by the analysis presented in Figures 24 and 25, suggests that minimizing the distance enhances thermal interaction between the heat exchanger and the surrounding material, thereby improving the overall efficiency of the GEP system.

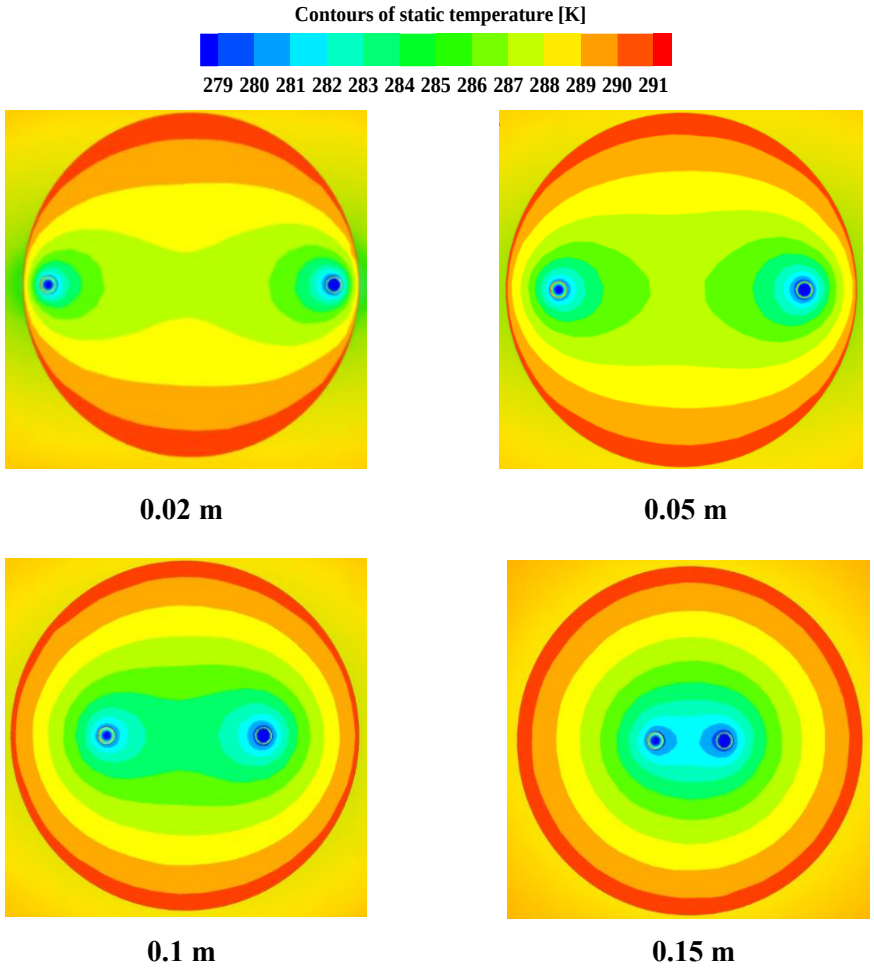

Figure IV. 2. 22. 2-D Contours of static temperature for distance changes during winter.

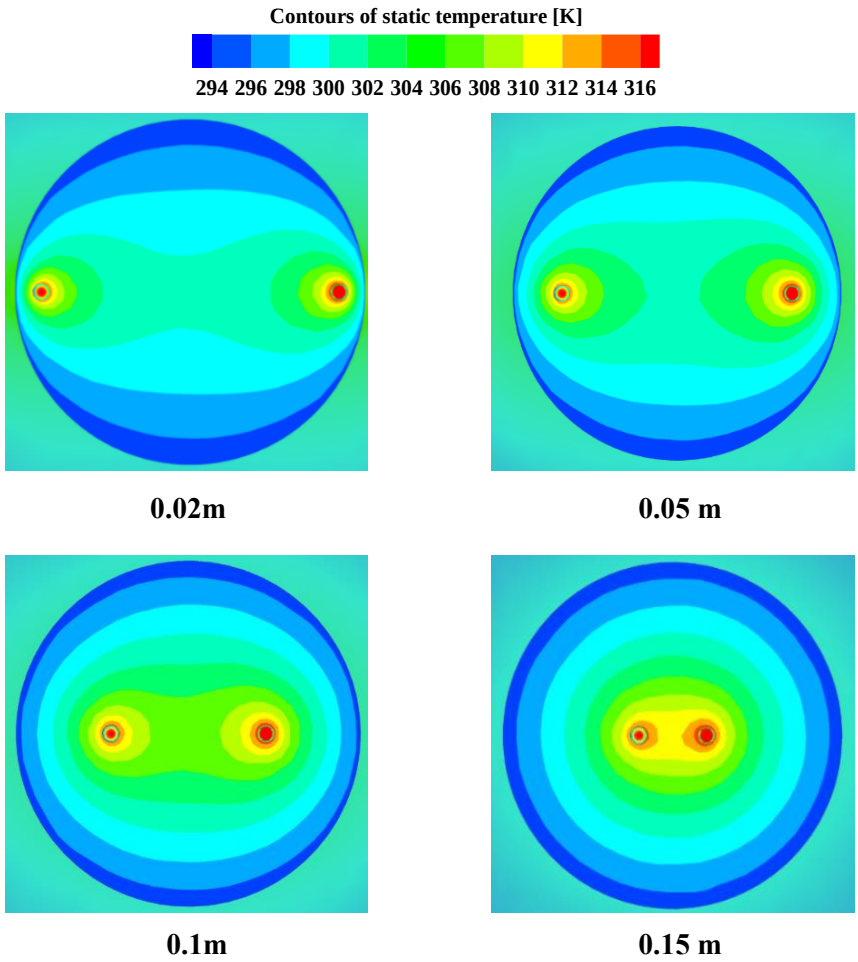

Figure IV. 2. 23. 2-D Contours of static temperature for distance changes during summer.

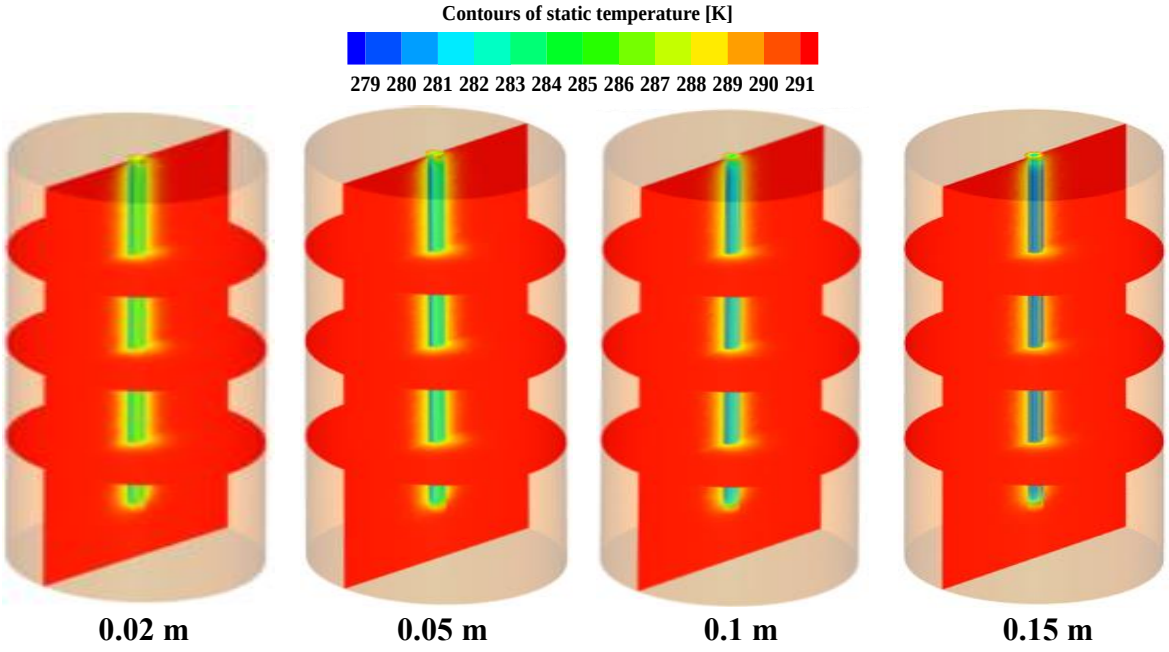

Figure IV. 2. 24. 3-D Contours of static temperature for distance changes during heating.

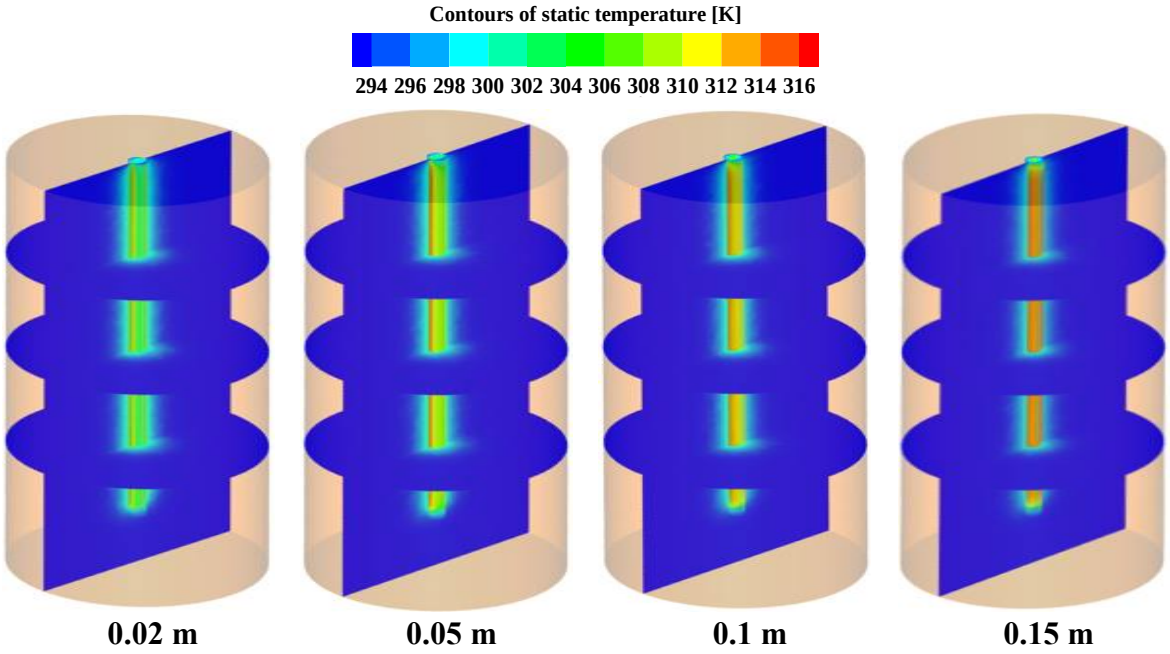

Figure IV. 2. 25. 3-D Contours of static temperature for distance changes during cooling.

An additional key parameter in the 3D thermal analysis of the GEP system is the distance between the outer diameter of the heat exchanger pipe and the surrounding concrete. Distances of 20 mm, 50 mm, 100 mm, and 200 mm were investigated under both summer and winter conditions , as shown in Figure 26.

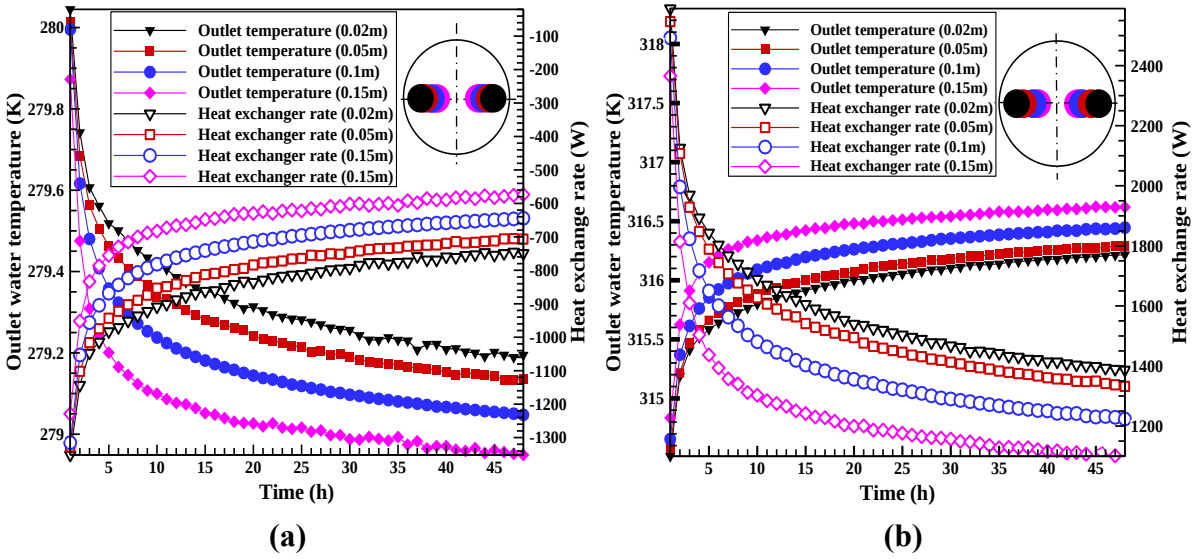

Figure IV. 2. 26. Numerical results for outlet water temperature and heat transfer rate (heating (a) and cooling (b)) in the case of distance changes.

During the heating phase, the heat transfer rate increased progressively until stabilizing, as shown in Figure 26(a). In contrast, during the cooling phase, the outlet water temperature increased while the heat transfer rate decreased, as illustrated in Figure 26(b). The results indicate that a separation distance of 20 mm yielded the most efficient thermal performance, maximizing heat exchange in the GEP system.

Furthermore, the study revealed that increasing the gap between the pipe and the concrete perimeter adversely affected the system's thermal efficiency, reducing performance in both heating and cooling modes. To validate these findings, analytical and numerical comparisons of the outlet water temperature and heat transfer rate were conducted throughout both operational modes over a 48-hour period at the optimal separation distance of 20 mm, as shown in Figure 27 and Figure 28. The close agreement between analytical and numerical results confirms that a 20 mm spacing is optimal and supports the accuracy of the numerical model. These findings contribute to verifying the ideal design parameters for enhancing the performance of GEP systems.

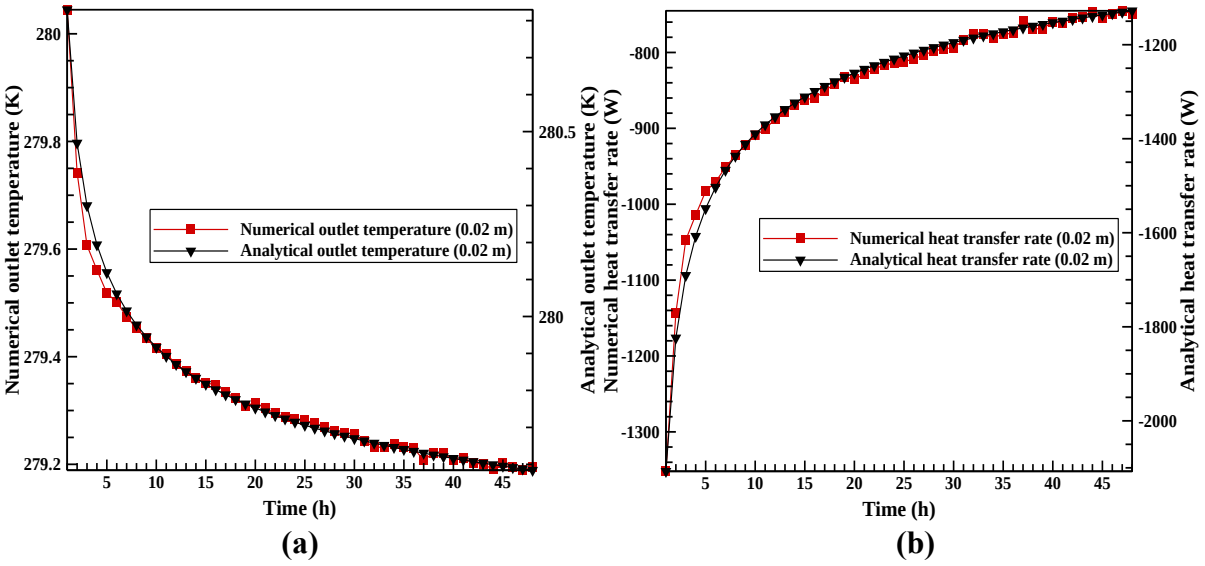

Figure IV. 2. 27. Comparison of analytical and numerical results (a) outlet water temperature and (b) heat transfer rate during winter for the case of optimal distance.

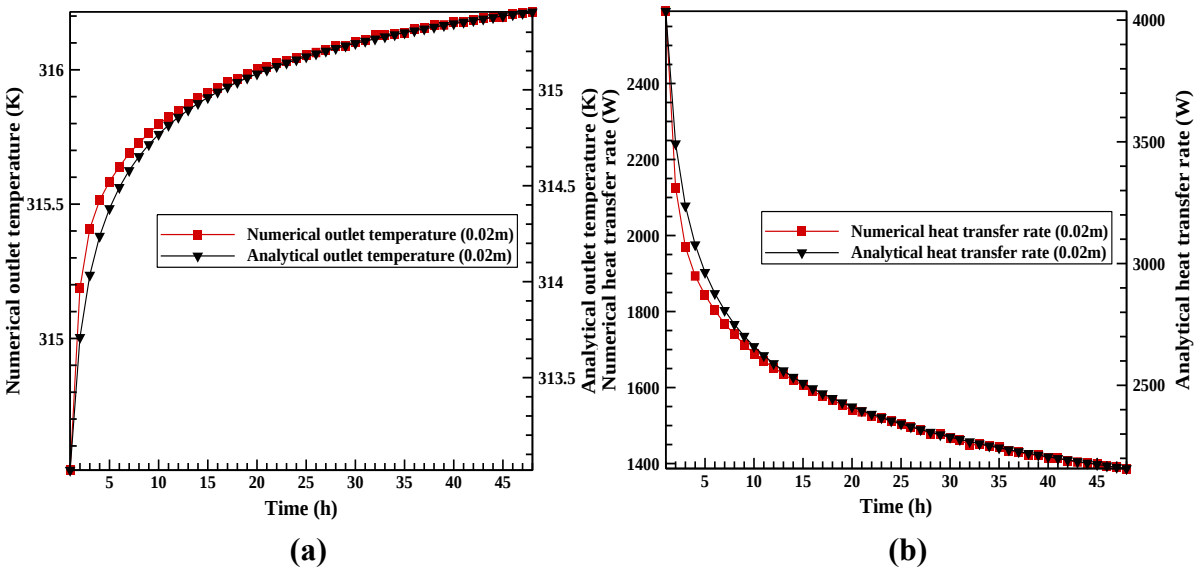

Figure IV. 2. 28. Comparison of analytical and numerical results for (a) outlet water temperature and (b) heat transfer rate during summer for the case of optimal distance.

Figure 29 illustrates the influence of varying distances (20 mm, 50 mm, 100 mm, 150 mm) between the U-tube outlet with an inner diameter of 14 mm and the surrounding concrete on the fluid temperature and heat transfer rate during both heating and cooling phases, under a constant inlet flow rate of 0.188 kg/s.

During the heating phase, the heat exchange rate increased over time, while the outlet fluid temperature progressively decreased as the distance between the heat exchanger and the concrete increased. Specifically, the outlet temperature rise was 1.04 K at 20 mm, 0.98 K at 50 mm, 0.89 K at 100 mm, and 0.79 K at 150 mm. The corresponding heat extraction rate declined by approximately 5.7% when the distance increased from 20 mm to 50 mm, and by about 23.4% when comparing 20 mm to 150 mm .

A similar trend was observed during the cooling phase, where the outlet fluid temperature decreased by 1.93 K, 1.85 K, 1.70 K, and 1.53 K for the respective distances. In this phase, the heat the rejection rate showed a reduction of around 4% percent from 20 mm to 50 mm, and an overall decrease of 20% percent from 20 mm to 150 mm. These findings clearly demonstrate that reducing the distance between the U-tube and the surrounding concrete significantly enhances the heat transfer performance of the ground energy pile system in both heating and cooling modes, thereby improving its overall thermal efficiency.

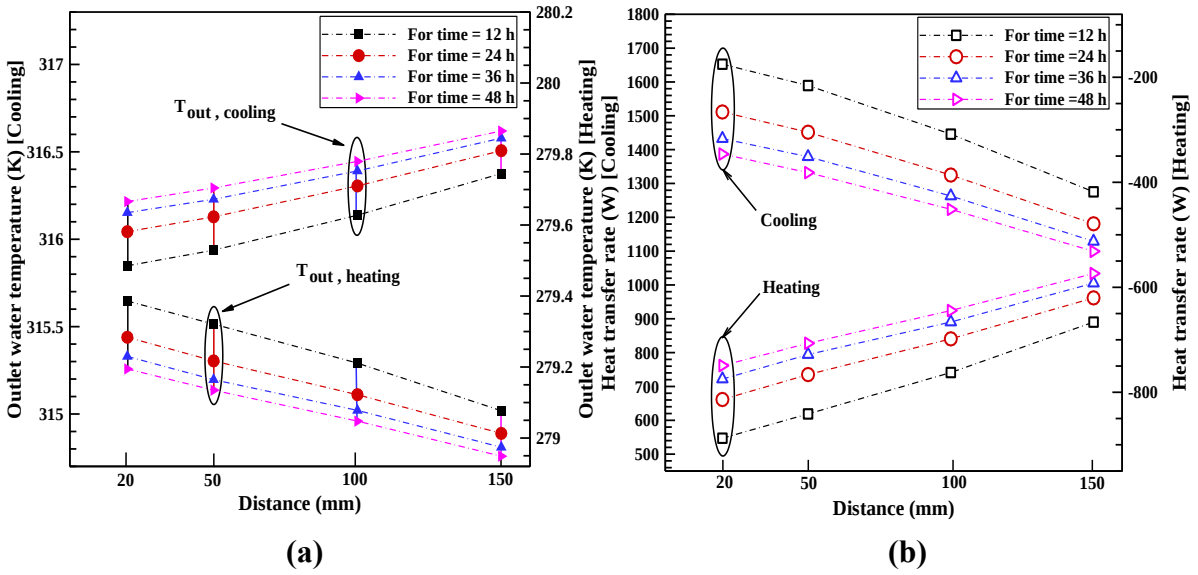

Figure IV. 2. 29. Variation in numerical outlet water temperature and heat transfer rate at different time steps during heating and cooling with distance changes.

IV.2.4.4 Effect of heat exchanger angular position changes

The results of this study highlight the importance of optimizing the angular position of the heat exchanger to improve the heat transfer and thermal distribution efficiency of the GEP system. Figures 30 and 31 present 2D contour plots of the static temperature distribution for different angular positions (0°, 30°, and 60°) over a 48-hour simulation period during both heating and cooling phases.

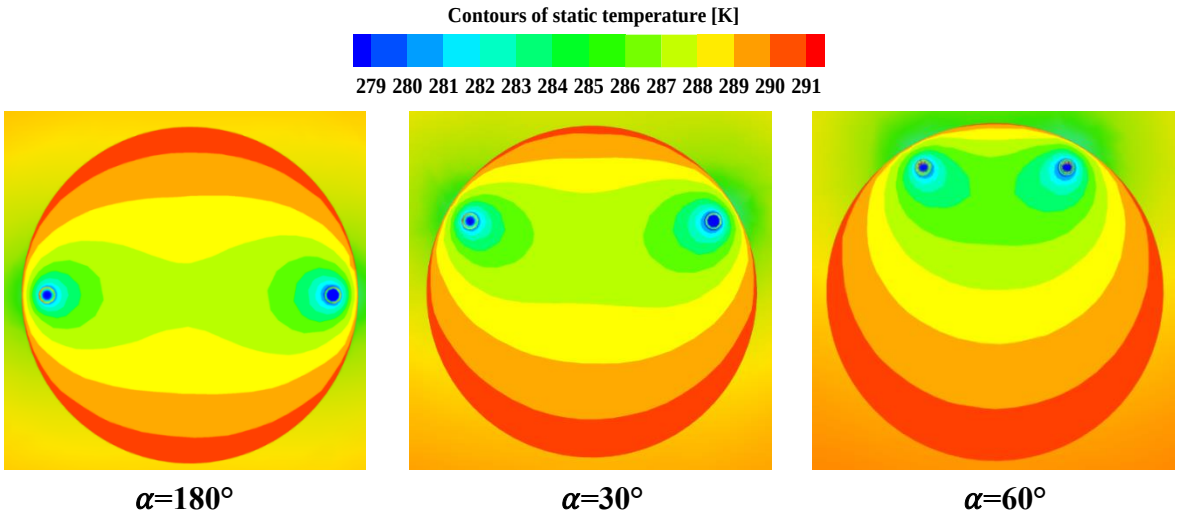

Figure IV. 2. 30. 2-D Contours of static temperature for angle position changes during heating.

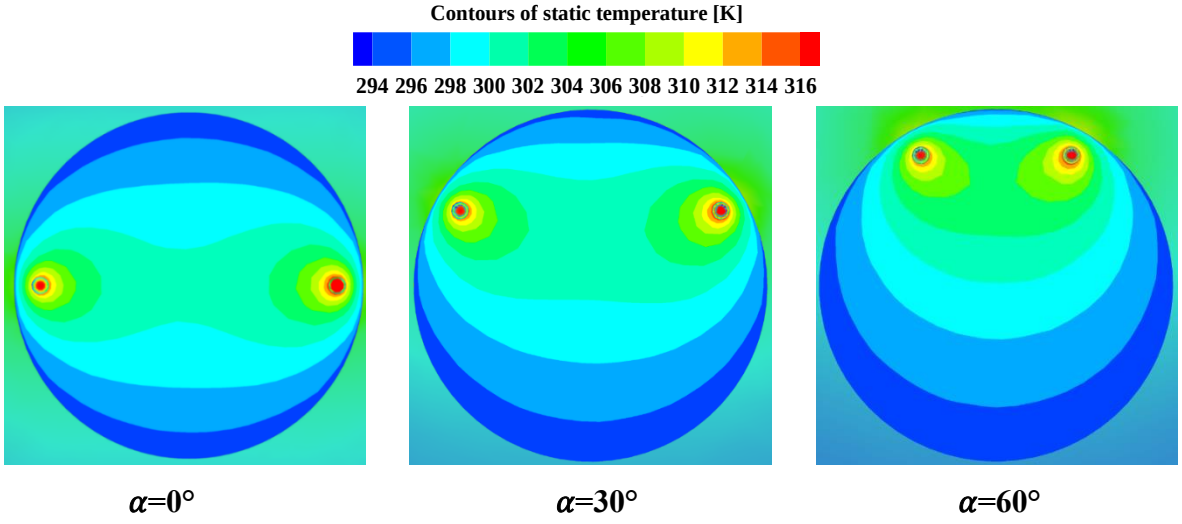

Figure IV. 2. 31. 2-D Contours of static temperature for angle position changes during cooling.

These results show that the 30° configuration offers better performance in terms of thermal distribution compared to the 180° and 60° setups. Additionally, Figures 32 and 33 provide 3D contour visualizations of the temperature distribution under both winter and cooling conditions, respectevely, offering a more comprehensive spatial understanding of the thermal behavior influenced by the exchanger's angular orientation.

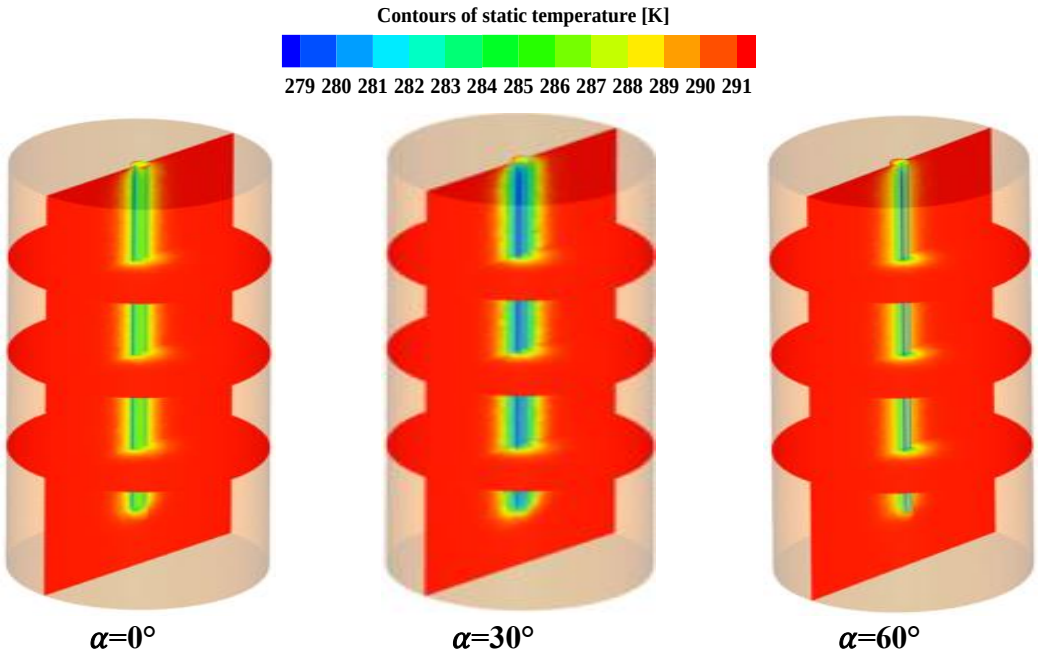

Figure IV. 2. 32. 3-D Contours of temperature distribution of (GEPs) with varying diameters under winter conditions.

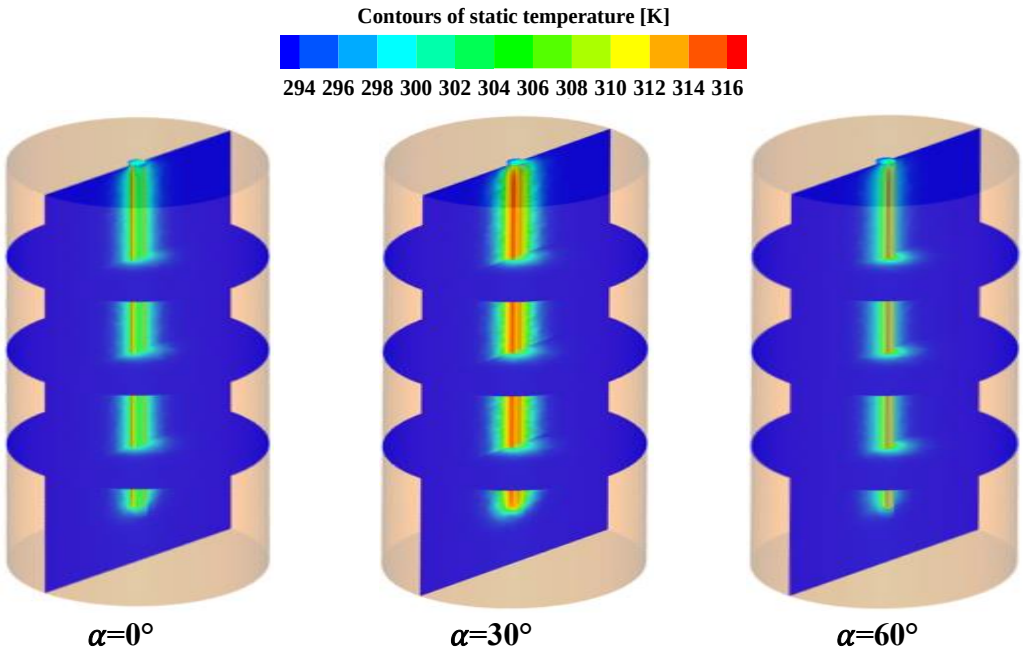

Figure IV. 2. 33. 3-D Contours of temperature distribution of (GEPs) with varying diameters under summer conditions.

The angular position (α) of the heat exchanger plays a critical role in influencing the heat transfer performance of geothermal energy systems. This study investigates the effects of three different angular configurations: 0°, 30°, and 60°, under both heating and cooling conditions, with a constant inlet flow rate of 0.188 kg/s (see Figure 34). The temporal variations of the outlet water temperature and heat transfer rate are analyzed for each angle.

During the heating period, the outlet water temperature exhibits a decreasing trend, while the heat transfer rate increases. Conversely, during the cooling period, the outlet temperature rises, accompanied by a decline in the heat transfer rate. Among the configurations tested, the 30° orientation demonstrates the most favorable heat exchange performance, making it the optimal angle for this application.

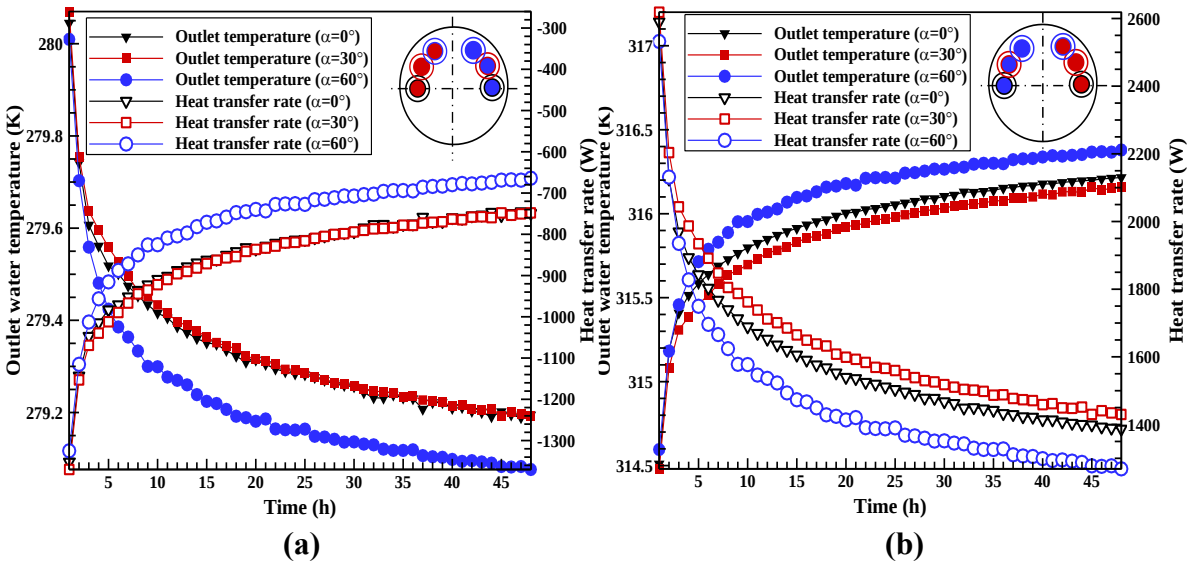

Figure IV. 2. 34. Numerical results for outlet water temperature and heat transfer rate (heating (a) and cooling (b)) in the case of angle position changes.

Numerical and analytical results for the outlet water temperature and heat transfer rate corresponding to the optimal angular position of the heat exchanger (30°) during both the heating and cooling periods are presented in Figure 35 and Figure 36, respectively.

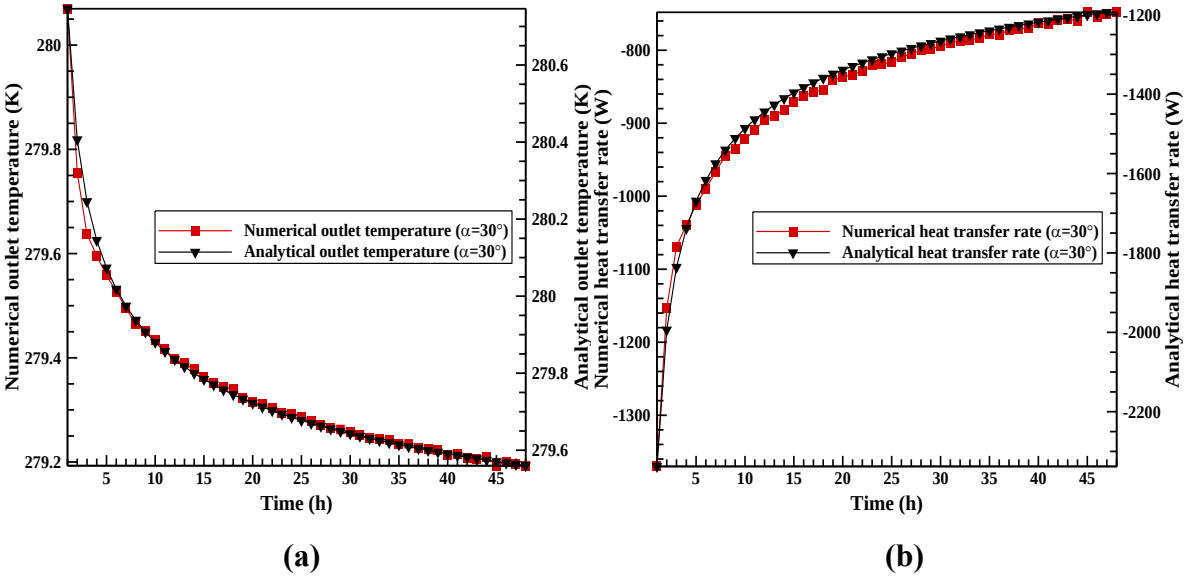

Figure IV. 2. 35. Analytical and numerical comparison of (a) outlet water temperature and (b) heat transfer rate during winter for the optimal angular configuration.

The comparison between the two approaches demonstrates a strong agreement, with only minor discrepancies observed throughout the simulation period. This high level of consistency between numerical and analytical data confirms the accuracy of the numerical

model and reinforces the reliability of the simulation methodology used in this study. The validation of these results provides additional confidence in the identified optimal configuration, supporting the effectiveness of the 30° angular placement in enhancing thermal performance within the GEP system.

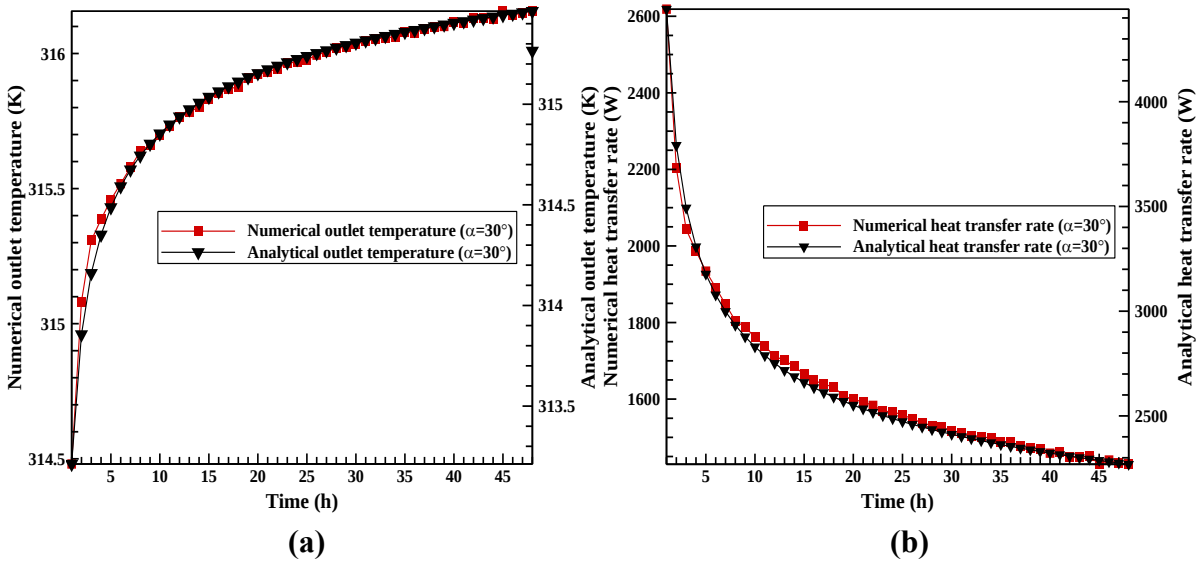

Figure IV. 2. 36. Analytical and numerical comparison of (a) outlet water temperature and (b) heat transfer rate during summer for the optimal angular configuration.

Figure 37 presents the impact of different angular positions of the heat exchanger (0°, 30°, and 60°) on the outlet fluid temperature and heat transfer rate in a U-tube system with an inner diameter of 14 mm, under a constant inlet flow rate of 0.188 kg/s. Simulations were conducted over a 48-hour period for both heating and cooling conditions.

During the heating phase, the outlet fluid temperature increased by 1.04 K at 0°, 1.042 K at 30°, and 0.92 K at 60°. The corresponding heat transfer rates were −749.14 W at 0°, −748.07 W at 30°, and −663.96 W at 60°. The 30° configuration exhibited a negligible decrease of only 0.14% in heat transfer rate compared to the 0° position, indicating nearly equivalent thermal performance. However, the 60° orientation resulted in a reduction of approximately 11.36% in heat transfer efficiency relative to the 0° case.

During the cooling phase, the outlet fluid temperature decreased by 1.39 K at 0°, 1.99 K at 30°, and 1.77 K at 60°. Corresponding heat rejection rates were 1386.82 W at 0°, 1429.71 W at 30°, and 1268.96 W at 60°. In this case, the 30° position demonstrated a 3.09%

improvement in heat transfer rate compared to the 0° configuration, whereas the 60° angle showed a decrease of approximately 8.49%.

These findings clearly demonstrate that the 30° angular position consistently provides superior thermal performance in cooling conditions and performs comparably to the 180° orientation during heating. Therefore, the 30° configuration can be considered the optimal angular placement for enhancing the heat transfer efficiency of the GEP system.

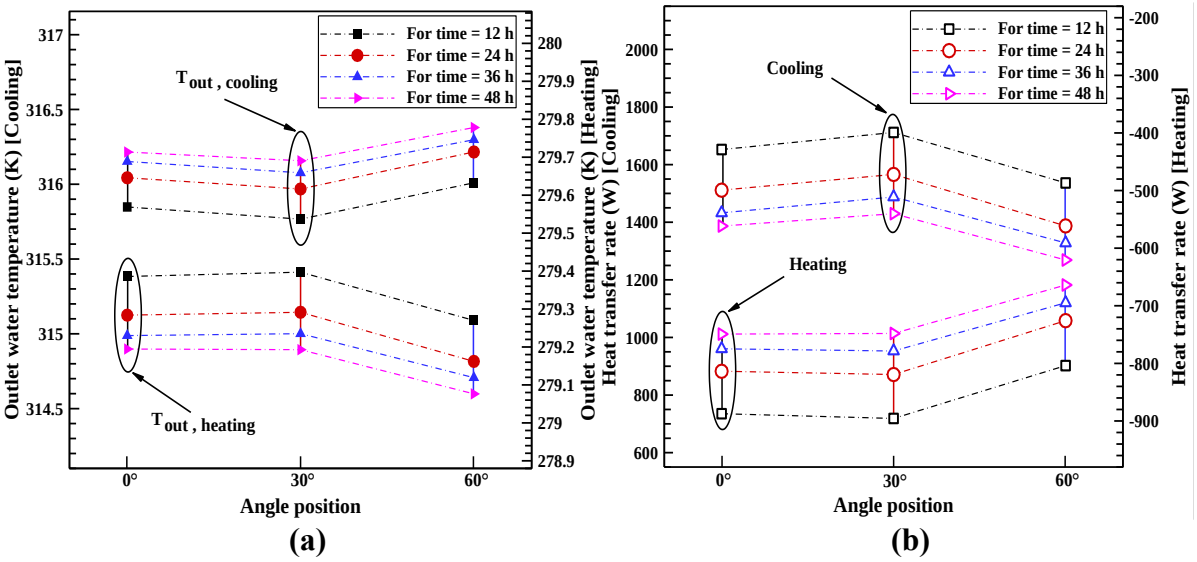

Figure IV. 2. 37. Variation in numerical outlet water temperature and heat transfer rate at different time steps during heating and cooling with angle position changes.

IV.2.5 Conclusion

The objective of this study was to optimize the structural configuration of GEP systems by examining the influence of three key design parameters: the diameter of the pile, the diameter of the heat exchanger, the distance between the heat exchanger and the surrounding concrete, and the angular position of the pipe. These factors were assessed under both heating and cooling conditions using three-dimensional computational fluid dynamics simulations conducted with ANSYS Fluent, alongside a complementary analytical approach. The performance of various configurations was evaluated through the outlet water temperature and heat transfer rates. This work provides practical recommendations for improving GEP design in Algeria and globally. The key conclusions derived from this work are as follows:

❖ The numerical method accurately predicted the thermal performance of the GEP system and proved to be an effective tool for identifying optimal design configurations. Based on the

principles of fluid dynamics and heat transfer, the numerical model offered reliable estimations of system behavior. In parallel, the analytical approach, which also relied on fundamental thermal and fluid flow concepts, produced results that closely matched the numerical data. The strong agreement between both methods reinforces the validity and robustness of the findings across all scenarios studied.

❖ The diameter of the buried pile was found to have a notable effect on heat transfer performance. Among the diameters studied, the pile with a diameter of 400 mm demonstrated superior thermal behavior compared to larger diameters. During winter conditions, the outlet water temperature for the 400 mm pile was approximately 0.039 K and 0.086 K higher than those of 600 mm and 800 mm piles, respectively. These results suggest that reducing the external diameter of the pile may enhance thermal efficiency, likely due to improved thermal interaction with the surrounding soil.

❖ The diameter of the heat exchanger was found to have a significant impact on the thermal performance of the system. Larger diameters led to improved heat transfer rates during the heating phase and greater temperature reductions during the cooling phase. Among the diameters tested, the 26 mm configuration was identified as optimal. It resulted in a temperature increase of 1.03 K during heating and a decrease of 2.02 K during cooling. These results highlight the importance of carefully selecting the exchanger diameter to enhance overall system efficiency.

❖ The spacing between the outer wall of the heat exchanger and the surrounding concrete also played a crucial role. A minimum distance of 20 mm was found to be most effective, achieving a temperature increase of 1.04 K during heating and a decrease of 1.93 K during cooling. As the distance increased to 50 mm, 100 mm, and 150 mm, both the outlet temperature variation and heat transfer rate declined. This demonstrates that minimizing the gap between the pipe and concrete is essential for maximizing heat transfer.

❖ In addition, the angular position of the heat exchanger significantly influenced the thermal response of the GEP system. A 30° orientation yielded the best performance, with a 1.04 K temperature rise during heating and a 1.99 K reduction during cooling. Compared to the 0° and 60° configurations, the 30° angle consistently outperformed the others, particularly under cooling conditions.

In conclusion, this study showed that multiple structural parameters including pile diameter, heat exchanger diameter, spacing from the surrounding concrete, and angular orientation collectively influence the thermal efficiency of GEP systems. The optimal configuration was identified as a 400 mm pile diameter, 26 mm tube diameter, 20 mm spacing, and 30° pipe angle. These findings provide a valuable basis for improving GEP design in practice. Future research may extend this work by examining the effects of climate variability, alternative geometries, dynamic loading conditions and long-term performance to further enhance the reliability and sustainability of geothermal energy systems.

Part 3: Thermomechanical Analysis of the Response of a Geothermal Energy Pile (GEP) System : Cross-Sectional Impact of Heat Exchanger Geometry on Performance and Heat Transfer

IV.3 Thermomechanical Analysis of the Response of a Geothermal Energy Pile (GEP) System : Cross-Sectional Impact of Heat Exchanger Geometry on Performance and Heat Transfer

IV.3.1 Objective

The objective of this thermomechanical study is to evaluate and compare the heat transfer efficiency, temperature distribution, pile displacement, axial stress responses, and shear stress distributions of geothermal energy pile (GEP) systems featuring different heat exchanger (HE) geometries, including circular, square, and triangular configurations. By analyzing these parameters under seasonal thermal loading conditions, the research seeks to deepen understanding of how exchanger geometry influences the overall thermomechanical performance of GEP systems. The results provide valuable insights for optimizing both the thermal and structural behavior of geothermal piles, thereby supporting the development of more energy-efficient and mechanically focused designs. Ultimately, this study aims to advance high-performance, sustainable ground heat exchange technologies, promoting the integration of renewable energy in buildings and infrastructure.

IV.3.2 Problem description

This study comprehensively investigates the influence of heat exchanger (HE) cross-sectional geometry on the thermal and mechanical performance, as well as the energy efficiency, of a GEP system under both heating and cooling conditions. Figure 1 illustrates the cross-sectional configurations of the heat exchangers analyzed in this study. Three distinct geometries, circular, triangular, and square, are evaluated to determine their effects on heat transfer rates, fluid flow dynamics, mechanical behavior, and the thermal interaction between the circulating fluid and the surrounding soil. Three-dimensional numerical simulations using computational fluid dynamics (CFD) are conducted to quantitatively assess the impact of each geometry on the overall system performance.

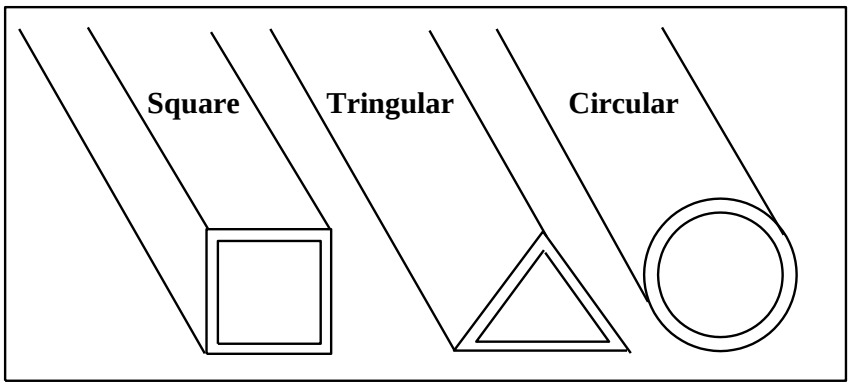

Figure IV. 3. 1. Different cross-section studies.

IV.3.3 Numerical modelling

IV.3.3.1 Numerical procedure

The numerical procedure followed in this study involves several key steps, which are visually summarized in Figure 2 through a detailed flowchart. At the heart of the simulation process is the utilization of ANSYS software, which is integral to solving the governing equations governing the flow dynamics. To obtain the numerical solution, a 3D segregated solver is employed, using an under-relaxation method that ensures stability and convergence. The FVM is implemented implicitly, allowing for efficient discretization of the flow equations. For transient calculations, the algorithm used is a double-precision pressure-based Navier-Stokes solver, ensuring high accuracy in capturing the dynamics of FF over time. For pressure-velocity coupling and transient flow calculations, the PISO algorithm is applied. This method facilitates precise synchronization between the pressure and velocity fields, improving the accuracy of the transient solutions. The discretization of the governing equations employs the SOU scheme, providing a good balance between computational efficiency and solution accuracy. For the transient formulation, a bounded second-order implicit method is used, further enhancing the stability of the numerical results. To ensure reliable and consistent results, all simulations are performed over time intervals of 48 hours, providing sufficient temporal resolution for capturing the evolving flow dynamics. The commercial software ANSYS Fluent serves as the primary tool for executing the entire numerical procedure, offering robust capabilities for FF and HT simulations.

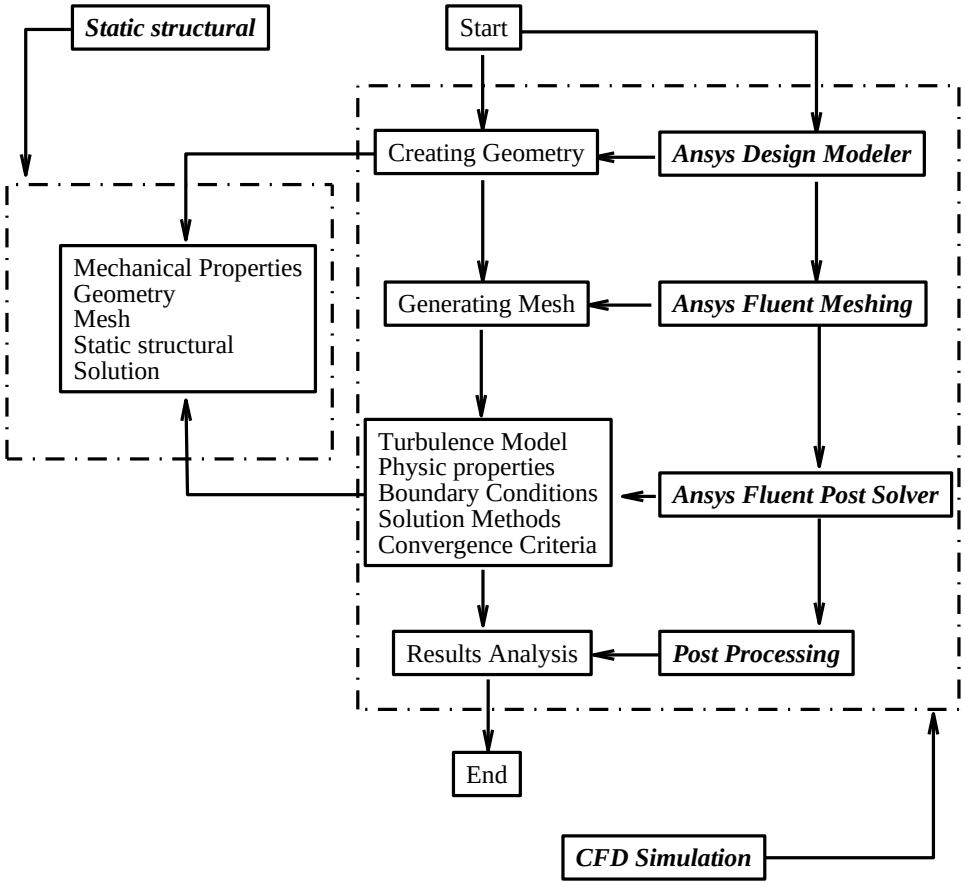

Figure IV. 3. 2. Flowchart of the numerical modeling in this study using ANSYS.

IV.3.3.2 Mesh sensitivity test

To ensure accurate and reliable results, a mesh sensitivity test was conducted using ANSYS Workbench meshing software. Five different grid configurations, each with varying element sizes, were generated for the analysis. Given the complex geometry of the GEP system, a non-structured mesh was selected, utilizing tetrahedral elements complemented by prism layers to capture the system's intricacies effectively. For the simulation, the Enhanced Wall Treatment's wall functions were applied, with a specific emphasis on achieving a y+ value of 1. This was crucial for accurately capturing both wall HT and wall stress.

A comprehensive mesh convergence study was conducted, and the results are detailed in Table 3. Among the five grids tested, Grid 4 emerged as the most suitable, offering an optimal balance between numerical accuracy and computational efficiency. As a result, Grid 4 was adopted as the base mesh and subsequently converted into a polyhedral configuration for all investigated pipe geometries (circular, square, and triangular). This refinement was intended to

further improve simulation stability and reduce computational time without compromising result quality. To illustrate this process, Figure 3 depicts the polyhedral mesh structure used for the circular cross-section case. The polyhedral meshes demonstrated improved solver performance and enhanced numerical precision. Additional mesh refinement beyond this stage was found to deliver only marginal accuracy gains while significantly increasing computational cost, confirming the effectiveness of the selected mesh strategy.

Table IV. 3. 1. Details of grid- solution independence and computing time.

Grid	Geometry	Number of elements	T_{inlet} [K]	T_{outlet} [K]	ΔT [K]	Computing time
Grid 1	Circular	2,702,898	318.15	316.215	1.935	00 h 46 min
	Square	2,721,050		316.148	2.002	00 h 48 min
	Triangular	2,735,800		316.225	1.925	00 h 47 min
Grid 2	Circular	3,198,148	318.15	316.149	2.001	01 h 17 min
	Square	3,200,340		316.122	2.028	01 h 22 min
	Triangular	3,215,900		316.178	1.972	01 h 20 min
Grid 3	Circular	5,730,595	318.15	316.141	2.009	02 h 20 min
	Square	5,695,210		316.110	2.040	02 h 25 min
	Triangular	5,732,880		316.161	1.989	02 h 23 min
Grid 4	Circular	8,859,429	318.15	316.132	2.018	03 h 50 min
	Square	8,765,980		316.105	2.045	03 h 55 min
	Triangular	8,795,610		316.155	1.995	03 h 48 min
Grid 5	Circular	13,480,156	318.15	316.131	2.019	05 h 05 min
	Square	13,482,700		316.104	2.046	05 h 11 min
	Triangular	13,495,600		316.154	1.996	05 h 07 min

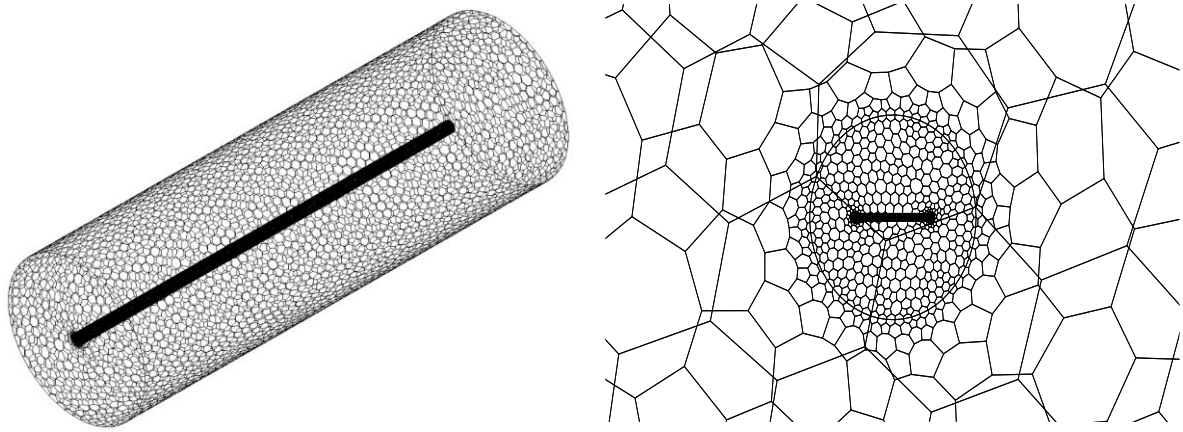

3-D view of polyhedral mesh . 2-D view of polyhedral mesh.

Figure IV. 3. 3. Results of mesh study.

IV.3.3.3 Model confirmation and validation

To ensure the reliability of the computational methodology used in this study, it is essential to validate the results by comparing them with previously published studies under similar research domains and boundary conditions. The present analysis of the geothermal energy pile (GEP) is compared with the numerical and field test findings of Peng Zhang et al. [56] on a plant project in Kunshan, Jiangsu Province. We have taken the geometric parameters and material properties of pipes, concrete, soil, fluids, and boundary conditions from this study to validate the model in both thermal and mechanical analyses, as well as in thermal-mechanical coupling analyses.

The GEP of the referred study is 15 m long and 0.4 m in diameter, made of concrete. The surrounding soil is clay, with a length of 18 m and a diameter of 0.6 m. The heat exchanger is composed of polyethylene and has a double U-shape with a diameter of 0.025 m; however, in the present study, a single U-shaped pipe is used. The inlet fluid temperature is maintained at 278.15 K and 318.15 K during winter and summer conditions, respectively. The soil temperature is fixed at 291.89 K during both heating and cooling operations. A mechanical load of 1,600,000 N is applied to the pile. The results are summarized in Tables 6 and 7.

From the data in Table 2, it can be observed that, according to the results of Zhang et al. paper, under winter conditions, the outlet water temperature increase for the tested and simulated cases was 1.20 K and 1.28 K, respectively. In the present study, the numerical temperature increase was 1.03 K, and the analytical increase was 1.75 K. This results in

differences of 0.25 K and 0.17 K for the numerical values and 0.47 K and 0.55 K for the analytical values compared to the experimental and numerical results of Zhang et al., respectively.

Under summer conditions, the outlet water temperature of the experimental and numerical cases decreased by 3.49 K and 2.80 K, respectively, based on the results of Zhang et al. study. In contrast, in the present study, the numerical temperature decrease was 2.03 K, and the analytical decrease was 3.43 K. In contrast, in the present study, the decrease in numerical temperature was 2.03 K, and in analytical temperature, 3.43 K, resulting in differences of 1.46 K and 0.77 K for numerical values and differences of 0.15 K and 0.54 K for analytical values when compared to the experimental and simulation results of Zhang et al.

Table IV. 3. 2. Comparison of outlet water temperature data.

Authors	Pipe Configuration	Pile Size (m)	Software	Periods	T_{inlet} (K)	T_{outlet} (K)	Study	t (hours)	ΔT (K)
Zhang et al. [56],	Double U-shaped	Diameter=0.4 Length=15	ANSYS Workbench	Summer	318.15	315.35	Numerical	36	02.80
				Winter	278.15	279.43			01.28
				Summer	318.15	314.66	Tester		03.49
				Winter	278.15	279.38			01.20
Present study	U-shaped	Diameter=0.4 Length=15	ANSYS Fluent 20.0	Summer	318.15	316.12	Numerical	48	02.03
				Winter	278.15	279.18			01.03
				Summer	318.15	314.81	Analytical	48	03.34
				Winter	278.15	279.90			01.75

According to the data in Table 3 and the results of Zhang et al. [56], the pile experiences shrinkage under winter conditions, with values of 1.12 mm and 0.79 mm in the tested and numerical cases, respectively. In contrast, in this study, the numerical shrinkage is observed to be 0.09 mm. Under summer conditions, the pile undergoes expansion. Zhang et al. [56], observed an elongation of 0.17 mm in the experimental case and 0.04 mm in the numerical case, while the present study recorded a slight elongation of 0.01 mm.

In mechanical behavior, under the influence of thermo-mechanical coupling in summer conditions, the circular configuration exhibited the highest axial compressive stress in the present study, increasing by about 0.0787 MPa, while decreasing by about 0.0441 MPa in winter conditions. While, from the numerical results calculations of Zhang et al. [56], the highest axial

compressive stress increased by about 2.533 MPa, while decreasing by about 2.583 MPa in summer and winter scenarios, respectively.

Table IV. 3. 3. Comparison of displacement and compressive stress data.

Authors	Pipe Configuration	Pile Size (m)	Software	Condition	Study	Displacement (mm)	Compressive stress (MPa)
Zhang et al. [52]	Double U-shaped [56]	Diameter=0.4 Length=15	ANSYS Workbench	- Pure mechanical load	Numerical	02.45	3.183
				- Thermal coupling at winter		03.24	0.600
				- Thermal coupling at summer		02.41	0.650
				- Pure mechanical load	Tester	02.35	/
				- Thermal coupling at winter		03.47	/
				- Thermal coupling at summer		02.18	/
Present study	U-shaped	Diameter=0.4 Length=15	ANSYS Fluent 20.0	- Pure mechanical load	Numerical	01.76	1.5894
				- Thermal coupling at winter		01.67	1.5453
				- Thermal coupling at summer		01.75	1.5107

The discrepancies observed in the results can be attributed to several factors, including the differences in HE design, mesh sensitivity, groundwater effects, differences in mechanical conditions, and variations in soil layers with differing thermal and mechanical properties, as well as possible computational differences due to the use of different computers and versions of the ANSYS FLUENT software in this study. However, the close agreement between the numerical and analytical values for outlet water temperature and HE performance in this study confirms the reliability of the present numerical method.

IV.3.4 Results and discussion

IV.3.4.1 Study and analysis of thermal performance assessment of geothermal energy pile GEP

The evolution of thermal distribution within the GEP systems, employing U-tube configurations of circular, triangular, and square cross-sections, is depicted in Figures 4 and 5 for winter operation. These figures illustrate both longitudinal and transverse temperature profiles at intervals of 1, 24, and 48 hours.

During the initial hour of heating, a sharp decline in temperature was observed in all configurations, a clear indication of rapid initial heat extraction from the surrounding soil. As

the systems continued operating up to the 24-hours , this downward thermal trend intensified, demonstrating sustained HT. However, by 48 hours, the temperature drop across all geometries became marginal, suggesting a diminished thermal gradient and reduced heat exchange performance, likely due to the thermal saturation of the surrounding soil.

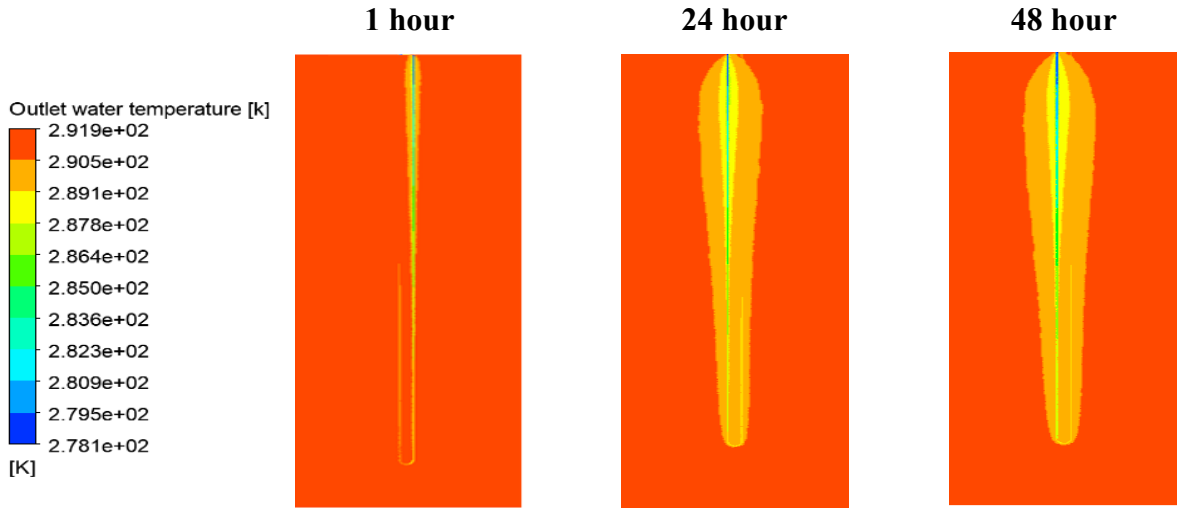

(a)

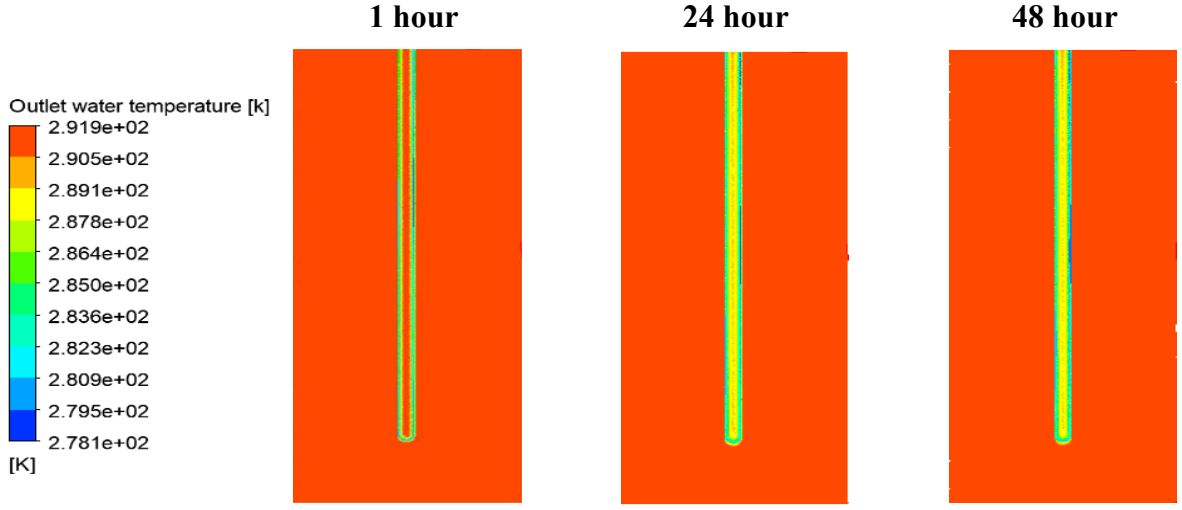

(b)

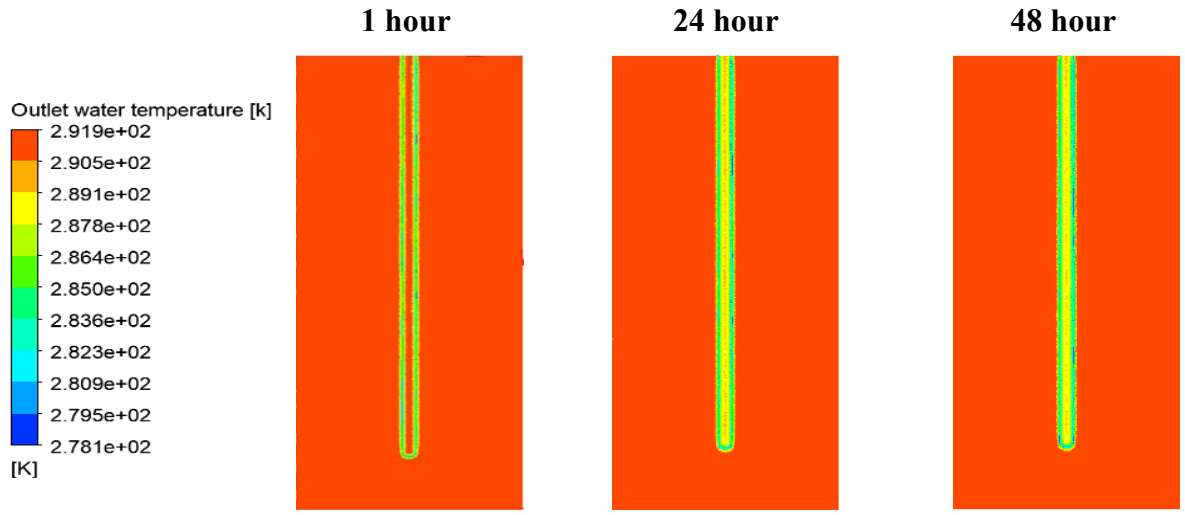

(c)

Figure IV. 3. 4. 2-D contours of temperature distribution along the longitudinal axis of energy piles with circular (a), triangular (b), and square (c) U-pipes in winter.

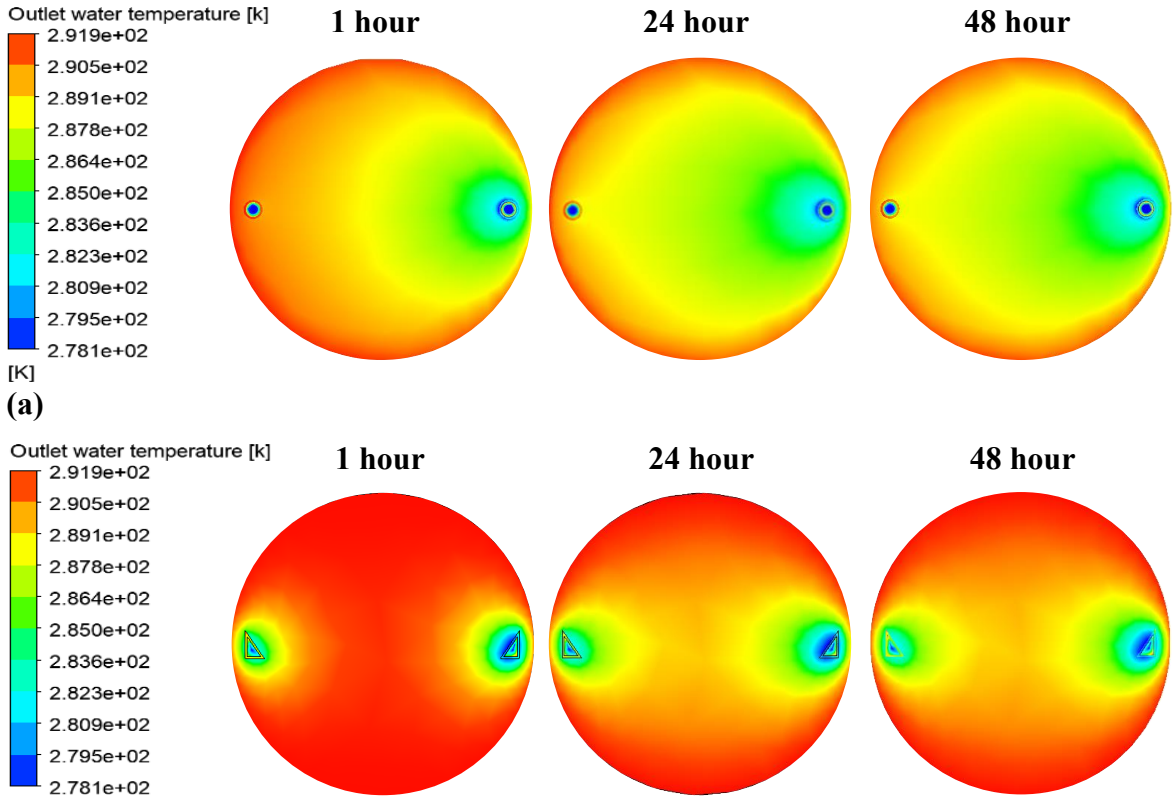

(a)

(b)

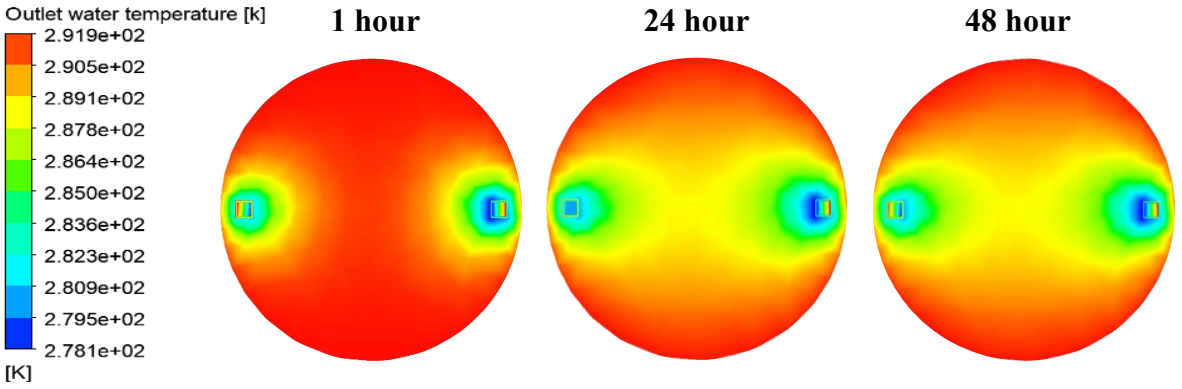

Figure IV. 3. 5. 2-D contours of temperature distribution along the transverse axis of energy piles with circular (a), triangular (b), and square (c) U-pipes in winter.

In contrast, Figures 6 and 7 present the temperature contours for the same GEP shapes during summer-mode operation. Over the first hour of cooling, a discernible rise in soil temperature occurred around all GEP types, pointing to the onset of heat injection into the ground. This temperature continued to increase notably over the following 24 hours, indicating active thermal interaction between the fluid inside the U-tubes and the surrounding earth. By the time the systems reached 48 hours of operation, however, the temperature increment had plateaued. The relatively smaller changes observed beyond the 24-hour mark suggest that thermal diffusion into the ground had slowed, and the rate of HT was less significant compared to the early stages of operation.

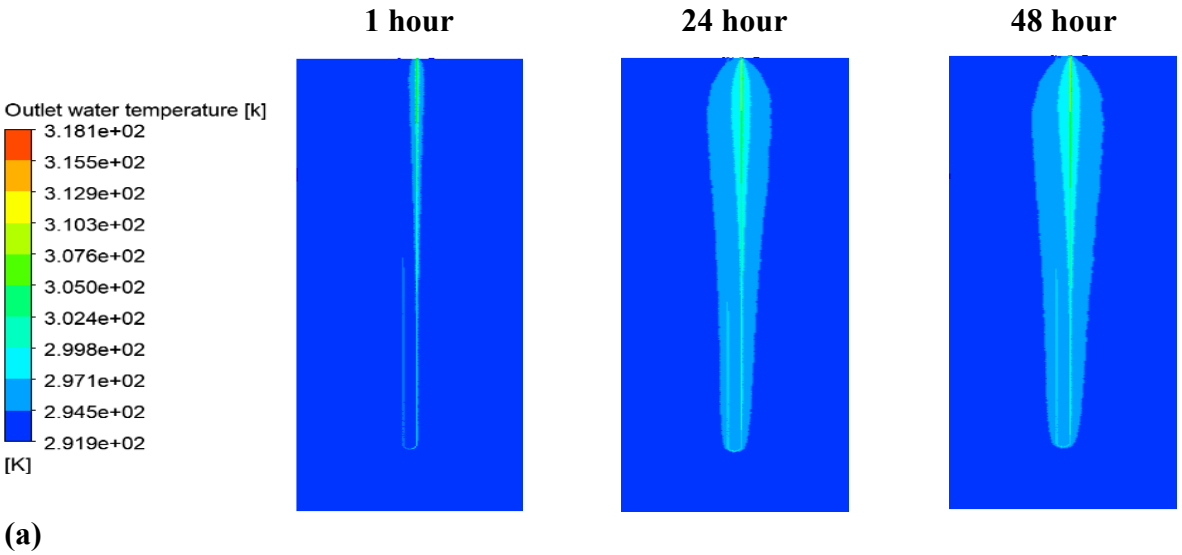

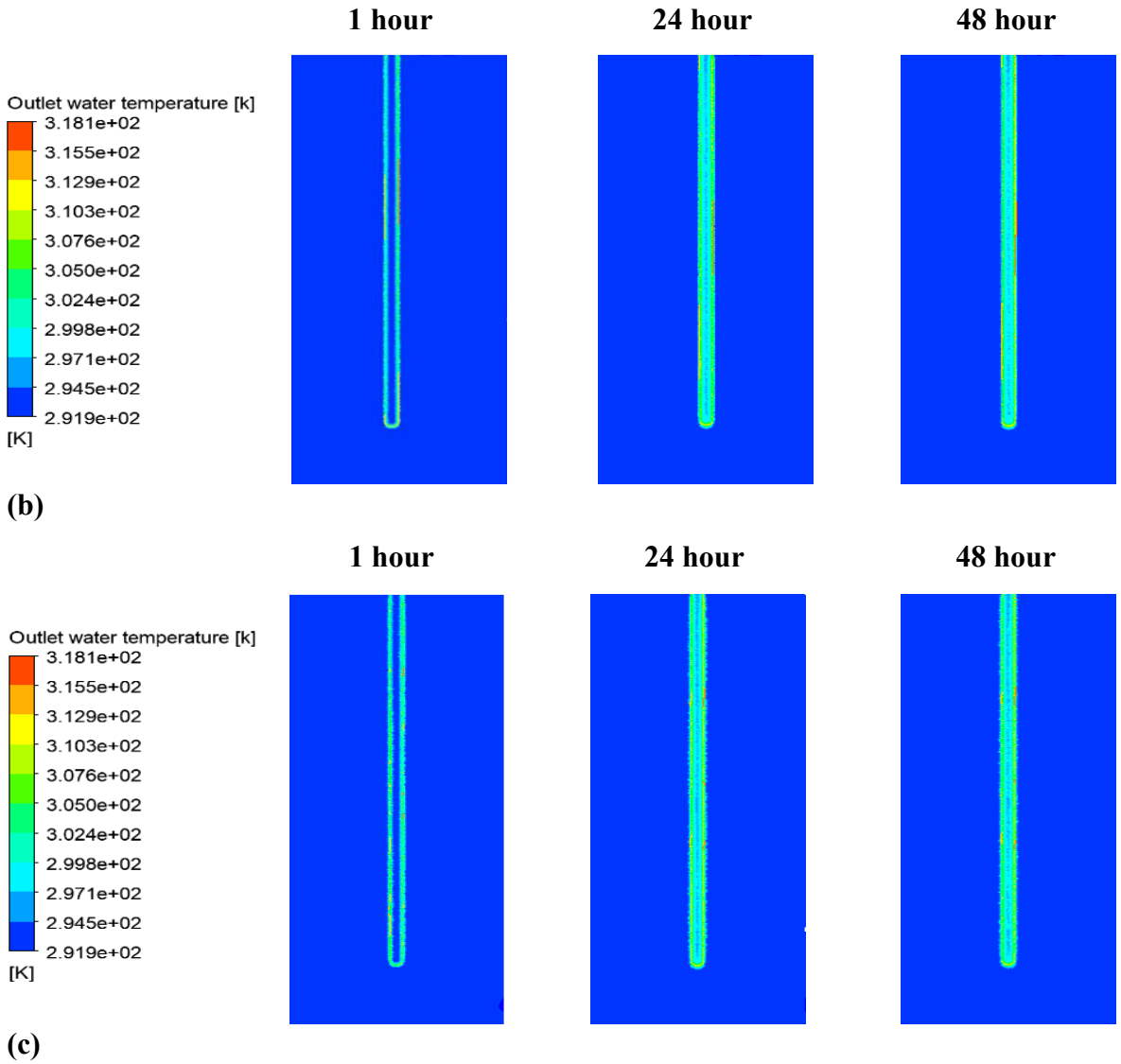

Figure IV. 3. 6. 2-D contours of temperature distribution along the longitudinal axis of energy piles with circular (a), triangular (b), and square (c) U-pipes in summer.

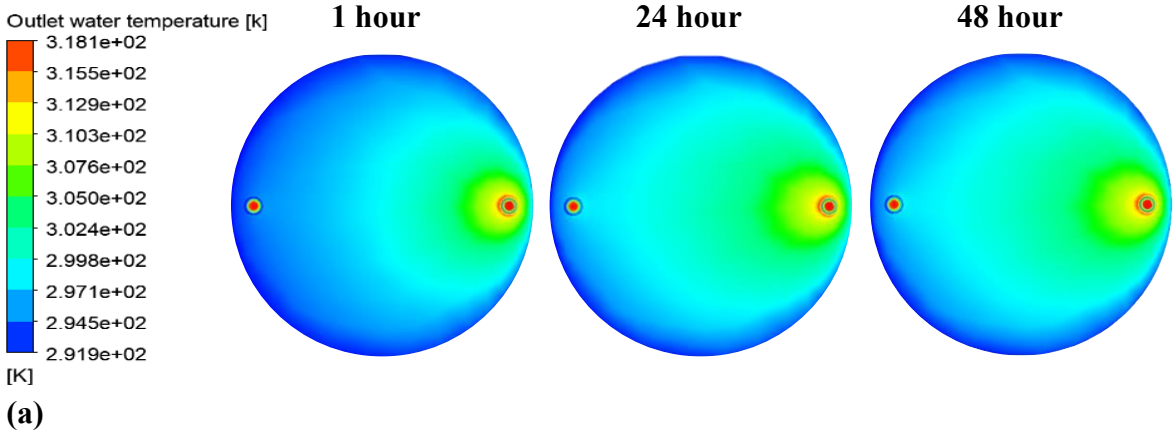

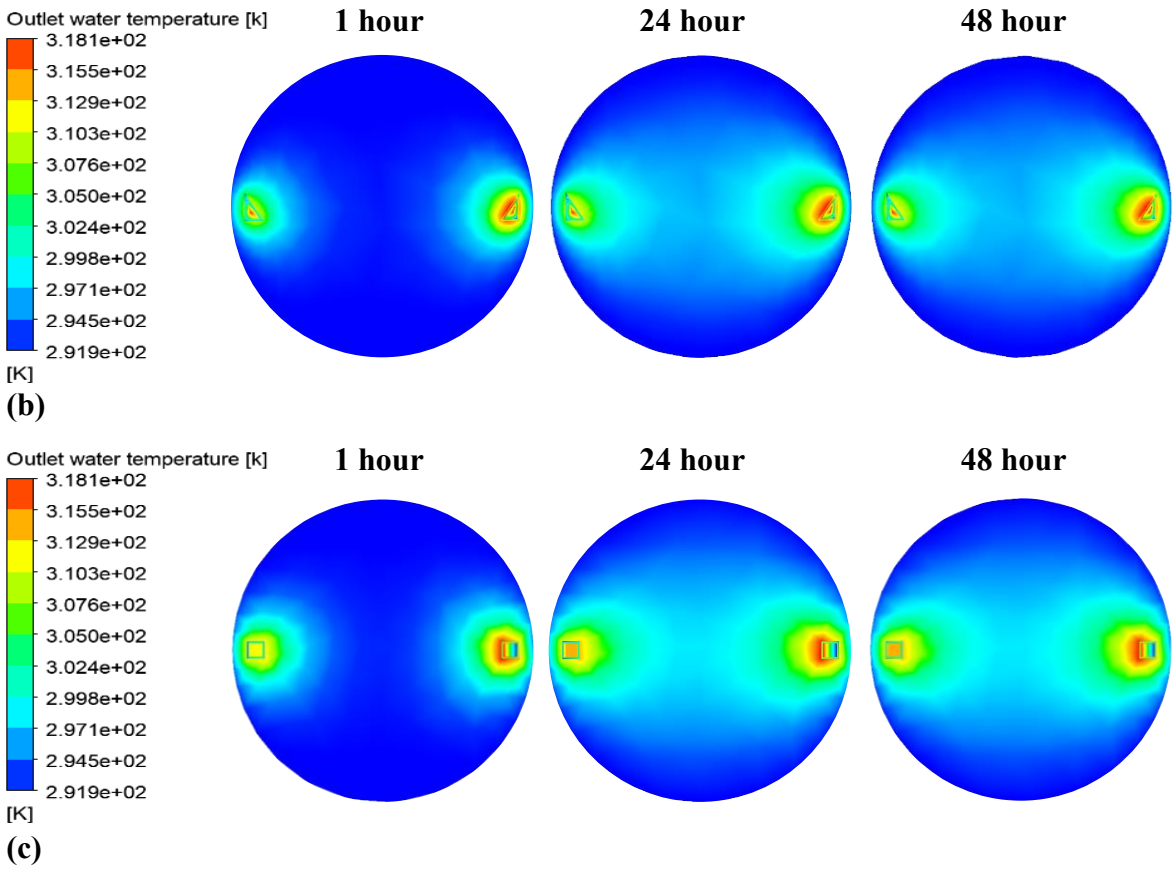

Figure IV. 3. 7. 2-D contours of temperature distribution along the transverse axis of energy piles with circular (a), triangular (b), and square (c) U-pipes in summer.

The thermal response of buried heat exchanger systems follows a distinct operational progression, beginning with an initial phase of rapid heat transfer, followed by a gradual stabilization of thermal conditions over time, observable during both summer and winter operation. At system start-up, all pipe configurations undergo a sharp temperature shift, primarily driven by the significant thermal gradient between the circulating fluid and the undisturbed surrounding soil. This steep gradient promotes highly efficient heat exchange, predominantly via conduction, with a minor contribution from convection. However, this initial high-efficiency phase is inherently transient, gradually diminishing as the system approaches thermal equilibrium. Within approximately 48 hours of continuous operation, temperature profiles begin to stabilize, indicating the formation of a thermal boundary layer around the pipe. In this quasi-steady-state phase, the adjacent soil becomes increasingly saturated with heat during cooling operations or progressively depleted during heating, which reduces the local temperature gradient and thus the driving force for further heat exchange. This characteristic thermal behavior of buried heat exchangers underscores the importance of implementing

operational strategies such as rest intervals or staggered loading cycles to minimize thermal fatigue and improve long-term energy transfer performance.

The thermal dynamics of the U-shaped GEPs equipped with different pipe geometries, circular, triangular, and square, were analyzed through a comprehensive numerical simulation. The resulting soil temperature distributions along the depth of the pile are illustrated in Figure 8 for both heating (winter) and cooling (summer) scenarios.

During the winter cycle, as shown in Figure 8(a), a pronounced temperature gradient is observed within the upper 1.5 m beneath the soil surface, where the soil temperature drops sharply due to active heat extraction. Beyond this region, the rate of temperature decline becomes more gradual and persists uniformly down to 15 m. From 15 to 16 m, the thermal profile begins to plateau, a consequence of the absence of embedded pipes in this lower section, resulting in minimal thermal interaction. This general pattern is consistently observed across all pipe configurations.

In contrast, the summer condition, shown in Figure 8(b), reveals a mirrored behavior: the soil temperature rises sharply within the top 1.5 m as heat is rejected into the ground. This upward trend continues, with minor fluctuations, down to 15 m, illustrating continued heat rejection into the surrounding ground. Below this point, from 15 to 16 m, the temperature curve flattens, eventually stabilizing around 291.89 K.

When comparing the thermal responses across the three pipe geometries, the circular and triangular configurations exhibit nearly identical temperature profiles throughout the entire depth range, indicating similar thermal performance. However, the square pipe displays a markedly different pattern. In winter, it produces a higher soil temperature profile, indicating less effective heat extraction and, therefore, lower heating efficiency. In the summer cycle, it results in a relatively lower soil temperature profile, which implies reduced heat rejection capability and suboptimal cooling performance. In contrast, during the winter-summer cycle, the U-shaped triangular tube configuration exhibits the best thermal behavior compared to other HE configurations studied.

Soil heat absorption and geometric influence on thermal propagation are important factors in buried heat exchanger performance. The soil surrounding U-shaped pipes acts as an effective thermal buffer, facilitating heat absorption and distribution during operation. Under both winter and summer conditions, heat injected into the soil propagates mainly through conduction.

Analysis of temperature distributions shows that triangular pipe geometries promote faster lateral heat propagation compared to other shapes. This enhanced transfer is likely due to the pipe's sharper exterior angles, which concentrate thermal fluxes more intensely into the adjacent soil. Conversely, square pipes exhibit slower and less uniform heat propagation, attributed to geometric confinement and flow channeling effects that impede even thermal spreading. These findings emphasize the critical role of pipe geometry in soil heat absorption, which is vital for optimizing buried heat exchanger design and performance.

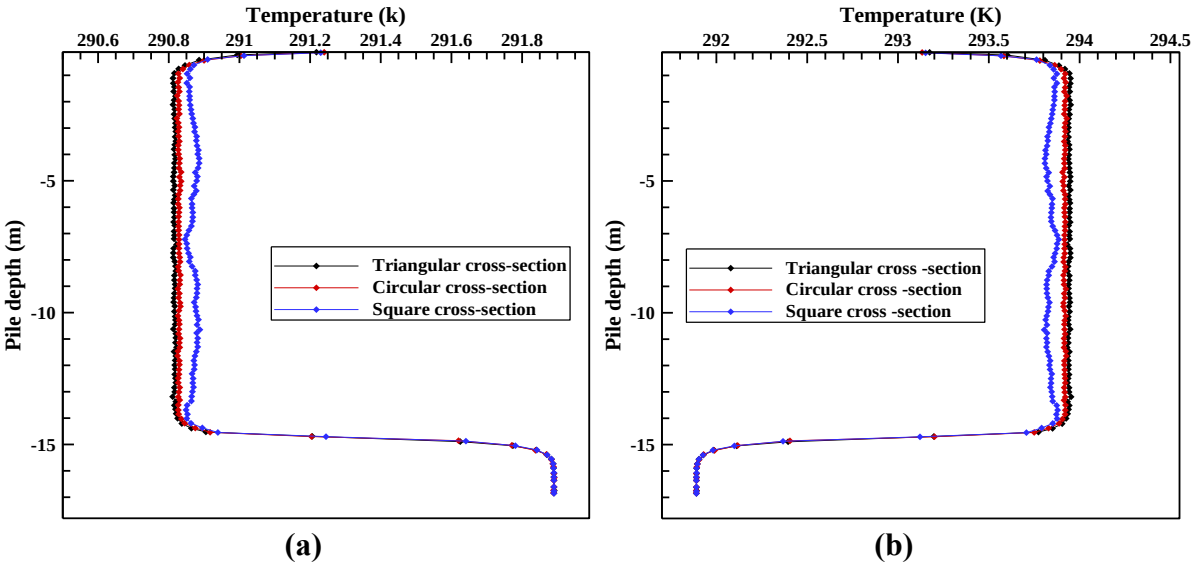

Figure IV. 3. 8. Temperature distribution along the depth of energy piles for different pipe forms (heating (a) and cooling (b)).

Figure 9 presents a comparative analysis of the temporal variation in water outlet temperature and heat exchange rate for GEPs configured with circular, triangular, and square pipe geometries. All piles share identical foundation characteristics and geometric dimensions, ensuring that performance differences are solely attributable to pipe geometry. The results indicate the performance and dynamic thermal behavior under heating (winter) and cooling (summer) conditions for each design.

During winter operation (Figure 9(a)), the triangular tube exhibits a modest but consistent thermal advantage, with its water T_{outlet} approximately 0.34 K higher than that of the circular counterpart and 0.42 K higher than the square configuration. Interestingly, while the water T_{outlet} is elevated, the heat exchange rate for the triangular tube is lower, by about 3.96 W when compared to the circular tube and by 38.93 W relative to the square tube. Although the triangular

tube exhibits a higher outlet temperature, the corresponding reduction in heat transfer rate indicates a limited thermal interaction with the surrounding soil. This behavior is primarily linked to the tube's geometric configuration, which results in a comparatively smaller and uneven contact surface with the soil, thereby restricting the efficiency of conductive heat transfer. Additionally, the angular shape may lead to irregular boundary layer development on the external pipe surface, further impeding effective heat dissipation into the ground. In contrast, the circular pipe, offering the most uniform flow path, supports stable convective flow but lacks the internal turbulence-enhancing characteristics of the triangular configuration, leading to slightly reduced performance compared to heat exchanger with the triangular cross-section.

Conversely, under summer cooling conditions (Figure 9(b)), the triangular configuration exhibits a pronounced improvement in thermal extraction. The water T_{outlet} from the triangular pipe is 0.65 K cooler than the circular pipe and 0.80 K cooler than the square design. In terms of heat exchange rate, the triangular tube surpasses the circular and square tubes by approximately 8.61 W and 74.41 W, respectively, indicating its higher capacity for heat absorption and rejection during cooling cycles. This notable enhancement is likely due to improved internal convective HT dynamics. The sharp corners and angular flow paths inherent in the triangular geometry promote localized turbulence or secondary flows, even at moderate Re numbers, enhancing the convective HT coefficient on the internal surface. As a result, the triangular pipe facilitates more efficient heat rejection to the ground, yielding a cooler T_{outlet} and a higher thermal exchange rate. In contrast, the square geometry, although it has a higher perimeter-to-area ratio, suffers from corner-induced flow recirculation and stagnation, which inhibit effective convective exchange and reduce overall thermal performance. The circular configuration, while providing the most uniform and stable flow path, lacks turbulence-enhancing geometric features, resulting in a slightly lower convective efficiency than the triangular design. Overall, the triangular geometry facilitates more efficient heat rejection to the ground, as evidenced by a lower outlet temperature and a significantly higher thermal exchange rate under summer operating conditions.

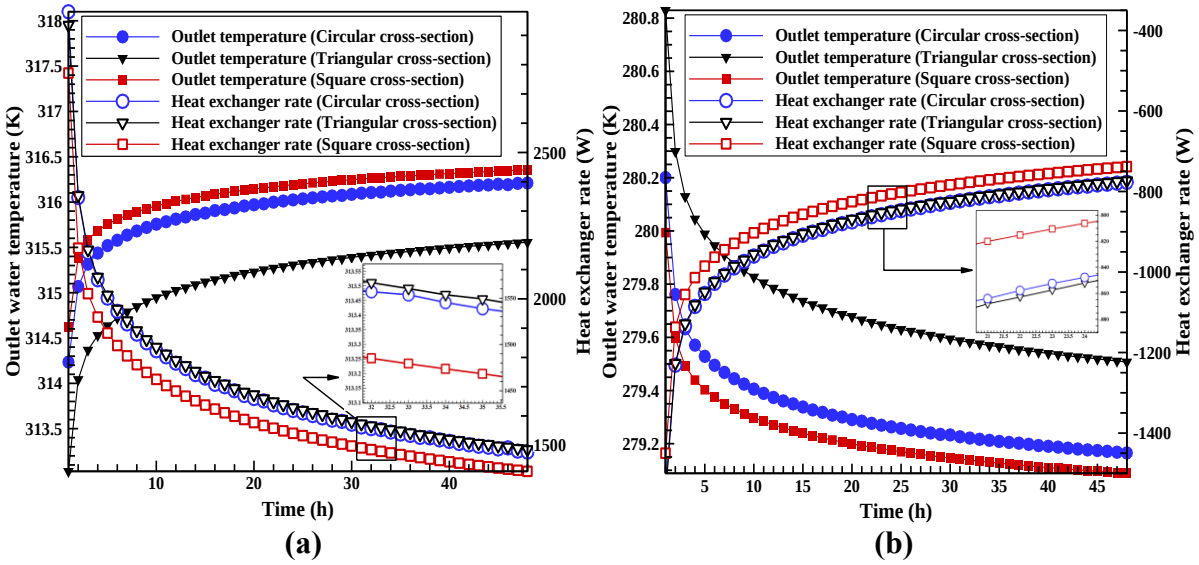

Figure IV. 3. 9. Comparison of outlet water temperature and heat exchanger rate for various pipe cross-sections (heating (a) and cooling (b)).

To validate these numerical findings, the T_{outlet} and heat exchange rates for the triangular pipe configuration were compared with analytical solutions under identical thermal boundary conditions and material parameters across a continuous 48-hour simulation window, as illustrated in Figures 10 and 11 corresponding to winter and summer conditions, respectively.

The results demonstrate remarkable agreement between the numerical simulations and analytical predictions in both winter and summer scenarios. Specifically, the results for the tuple values and heat exchange rates from the numerical and analytical calculations were almost identical over a 48-hour period. This consistency confirms the robustness and reliability of the simulation model applied to the studied GEP system.

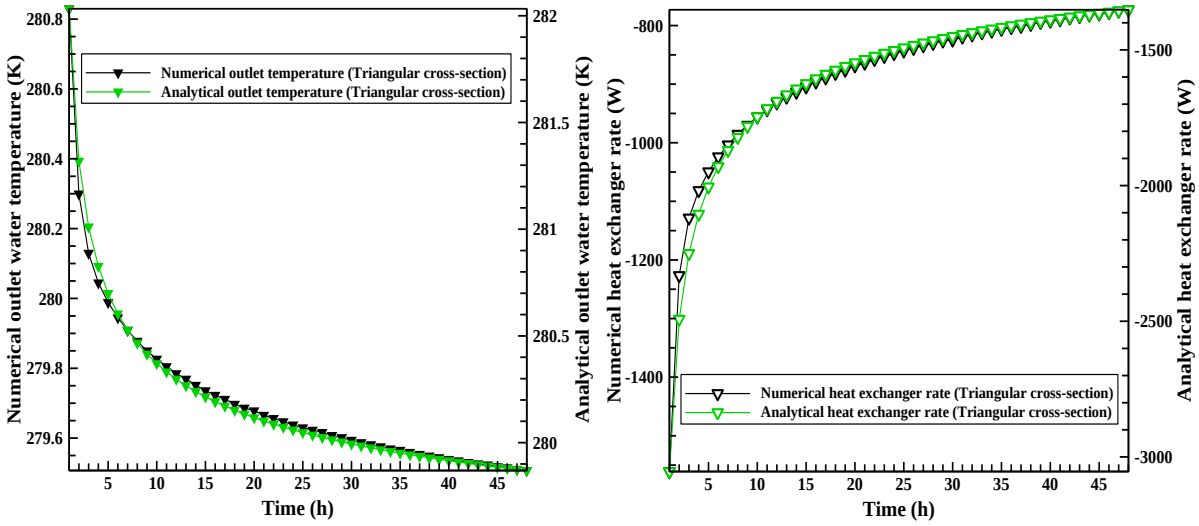

Figure IV. 3. 10. Comparison of analytical and numerical results for outlet water temperature and heat exchanger rate of triangular pipe in winter.

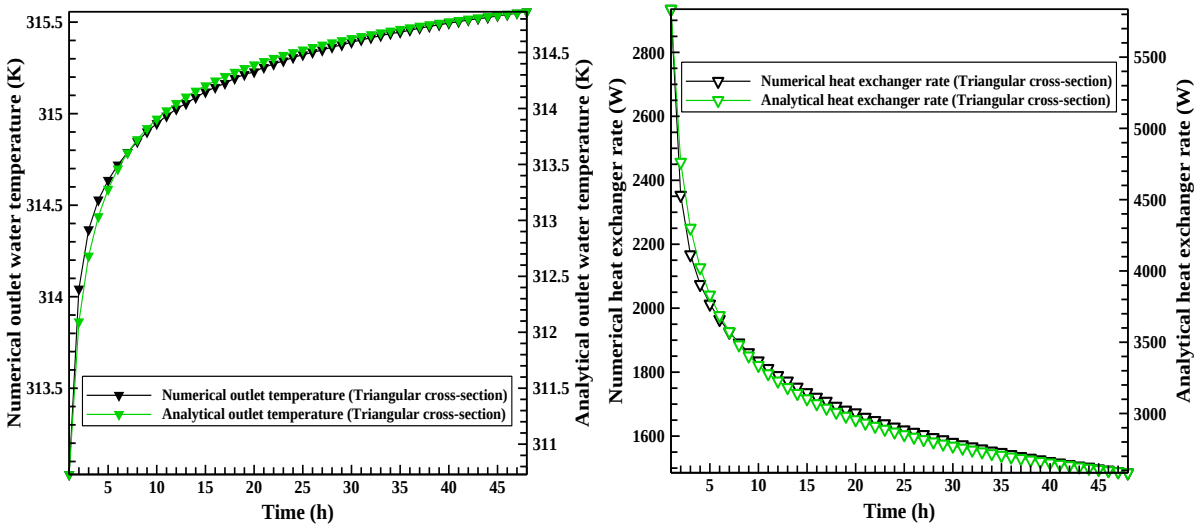

Figure IV. 3. 11. Comparison of analytical and numerical results for outlet water temperature and heat exchanger rate of triangular pipe in summer.

IV.3.4.2 Study and analysis of thermomechanical assessment of geothermal energy pile GEP

Figure 12 presents the vertical displacement profiles of GEPs embedded with internal U-tube HEs of circular, square, and triangular cross-sections, each subjected to a concentrated mechanical load of 1,600,000 N. The results correspond to a purely mechanical analysis excluding thermal effects, specifically those caused by seasonal temperature variations of the circulating fluid within the heat exchanger during winter and summer. This analysis allows for

an evaluation of the mechanical response of the GEP system, thereby providing a clearer understanding of how internal pipe geometry influences the structural performance of the pile.

The simulation results reveal only slight variations in the vertical deformation responses among the different pipe configurations, suggesting that the influence of internal pipe geometry on structural performance is minimal under purely mechanical loading conditions. This finding, from a qualitative and a structural design perspective, indicates that the internal pipe geometry does not introduce any significant disadvantage in terms of settlement or deformation, allowing engineers to prioritize thermal efficiency without compromising mechanical safety.

Specifically, the downward displacements observed at the pile head reached 1.762 mm for the circular pipe design, followed closely by 1.758 mm in the square pipe configuration and 1.764 mm for the triangular pipe. Similarly, at the base of the pile, downward displacements were recorded as 1.269 mm, 1.266 mm, and 1.270 mm for the circular, square, and triangular shapes, respectively. These findings indicate that the geometric variation of the internal piping exerts a negligible influence on the overall displacement response of the energy pile under pure mechanical loading conditions. All three configurations demonstrate comparable deformation profiles, suggesting that pipe shape has a minimal effect on the structural performance of GEPs in this loading scenario.

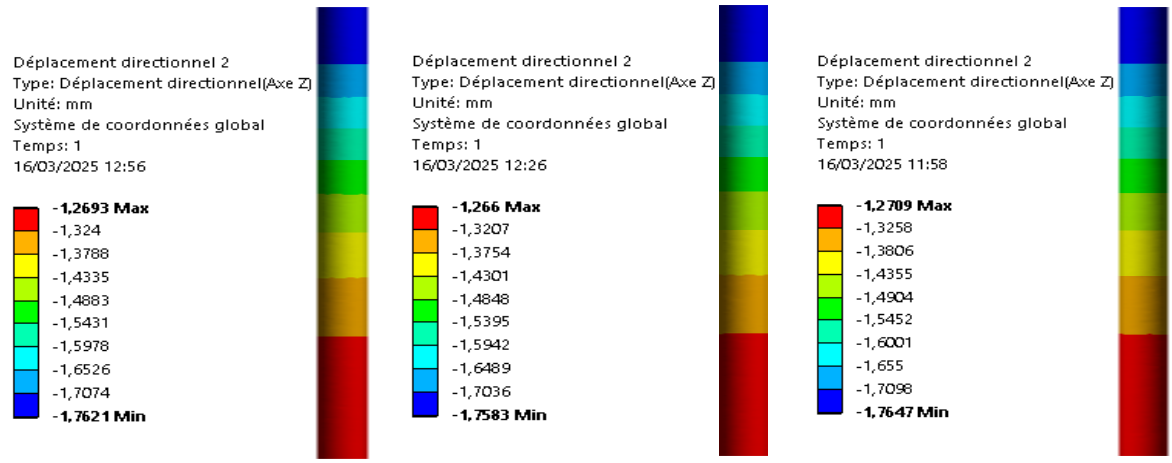

(a) **(b)** **(c)**

Figure IV. 3. 12. Displacement distribution of energy pile under pure mechanical load (pile with circular pipe (a), pile with square pipe (b) and pile with triangular pipe (c)).

Temperature variations inherently induce displacement within the pile structure due to the interaction between thermal expansion and mechanical constraints. Figures 13 and 14 depict

the displacement profiles of piles embedded in soil, each integrated with differently shaped heat exchange pipes, circular, square, and triangular, after 48 hours of operation during winter and summer conditions, respectively.

In the colder winter scenario, as visualized in Figure 13, the distribution of displacement reveals noticeable variations influenced by the pipe geometry. The pile incorporating a circular pipe exhibits a downward displacement of approximately 1.668 mm at the top of the pile and 1.668 mm at the bottom. For the square pipe configuration, these values slightly increase, reaching 1.777 mm at the top and 1.254 mm at the base of the pile. The triangular pipe results in the most pronounced displacement, with 1.787 mm at the top of the pile and 1.256 mm at the bottom, indicating a marginally higher thermal response. Although the numerical differences are small, they reveal that the triangular geometry, known for higher thermal efficiency, also results in slightly greater thermally induced deformation. This indicates a potential trade-off between thermal performance and structural behavior under cyclic temperature conditions that may be relevant in long-term durability assessments of GEP systems.

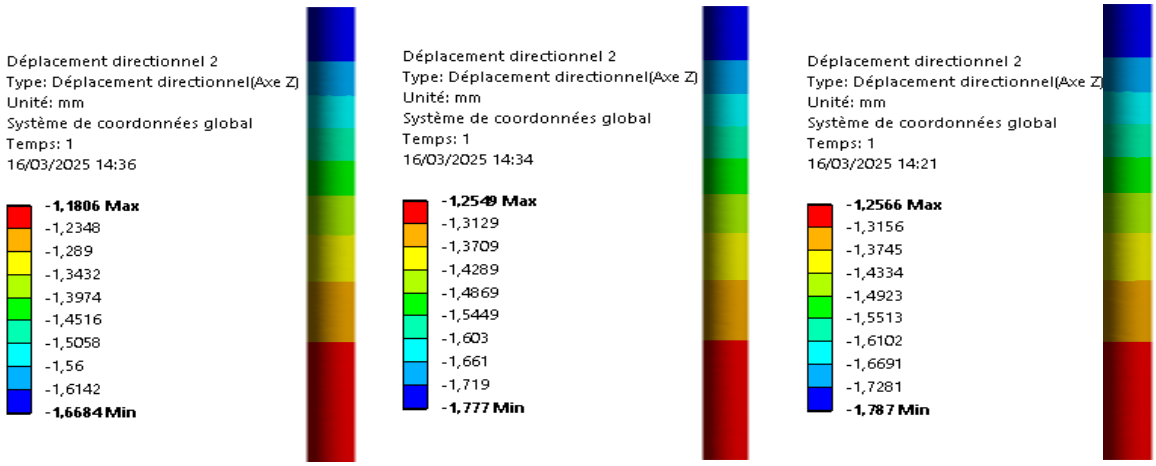

Figure IV. 3. 13. Displacement distribution of energy pile under load and temperature (pile with circular pipe (a), pile with square pipe (b) and pile with triangular pipe (c)) in winter.

As seasonal conditions transition to summer, the thermal behavior subtly shifts, as shown in Figure 14. The pile with the circular pipe experiences a downward displacement of 1.748 mm at the top and 1.281 mm at the base . Comparatively, the square pipe yields a nearly equivalent response,1.742 mm at the top and 1.279 mm at the bottom. The triangular configuration again displays a slightly larger downward displacement, with values of 1.744 mm and 1.286 mm at the top and base of the pile, respectively. These closely aligned values reaffirm

that, although the differences are minimal, the triangular configuration consistently results in slightly greater vertical displacement compared to the other geometries.

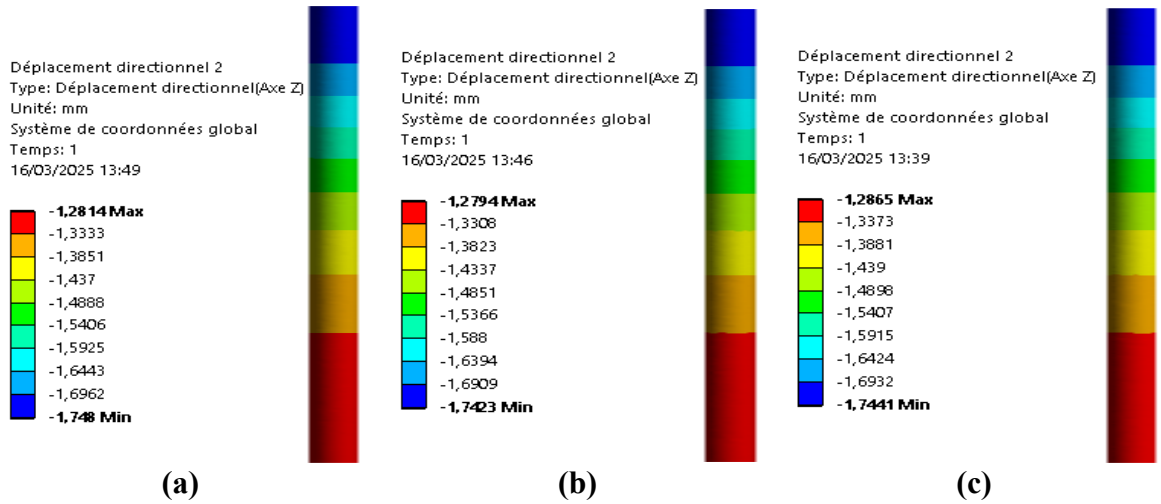

(a) **(b)** **(c)**

Figure IV. 3. 14. Displacement distribution of energy pile under load and temperature (pile with circular pipe (a), pile with square pipe (b) and pile with triangular pipe (c)) in summer.

Figures 15, 16, and 17 illustrates the displacement distribution curves along the length of the GEPs when subjected to thermal-mechanical coupling, during both heating and cooling conditions. These results expand upon the thermal loading induced displacement scenarios previously examined in Figures 13 and 14. For comparison, the displacement behavior under a purely mechanical load of P = 1,600,000 N, as shown in Figure 12, is also included. The analyses were conducted for piles incorporating three distinct pipe geometries: circular (a), square (b), and triangular (c).

Under purely mechanical loading, the pile with circular pipe shape (a) demonstrates a slightly greater basal and vertical displacements than the pile with square shape (b), with a differences of approximately 0.0033 mm and 0.0039 mm, respectively. However, it exhibits a marginally smaller displacement, by about 0.0009 mm at the base and 0.0059 mm at the top of the pile with the triangular shape (c). These variations are minimal, indicating that pipe geometry has little influence on pile behavior under mechanical load alone.

Under winter heating conditions, the impact of thermal effects on displacement becomes more pronounced. The circular pipe configuration exhibits smaller total displacements at both the base and top of the pile approximately 0.0744 mm and 0.1082 mm less, respectively, compared to the square configuration. These displacements are also lower than those observed

in the triangular configuration by about 0.0766 mm at the base and 0.0083 mm at the top. This pattern indicates that, under thermal loading, the triangular pipe induces a more pronounced structural response. This is likely attributable to its enhanced heat transfer characteristics, which result in greater thermally induced expansion or contraction within the pile structure.

In the summer scenario, when the system operates in cooling mode and rejects heat into the ground, displacement differences between pipe configurations are less pronounced but still noticeable. The circular pipe exhibits slightly greater displacement than the square configuration, approximately 0.0019 mm at the base and 0.0060 mm at the top of the pile, yet remains lower than that of the triangular configuration by about 0.0073 mm at the base and 0.0044 mm at the top. These results suggest that, even under reversed thermal gradients, the triangular geometry continues to produce marginally higher deformations. Nonetheless, the overall influence of pipe shape on structural displacement remains relatively modest. This consistent pattern across both seasonal conditions points to a subtle but persistent trade-off between thermal efficiency and structural response.

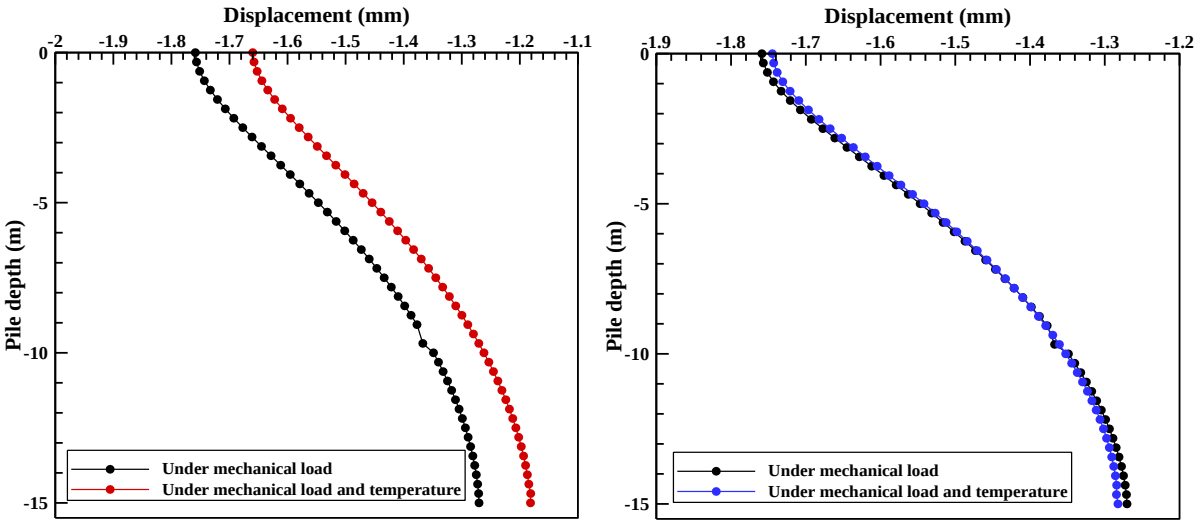

Figure IV. 3. 15. Displacement distribution of pile with circular pipe (heating (a) and cooling (b)).

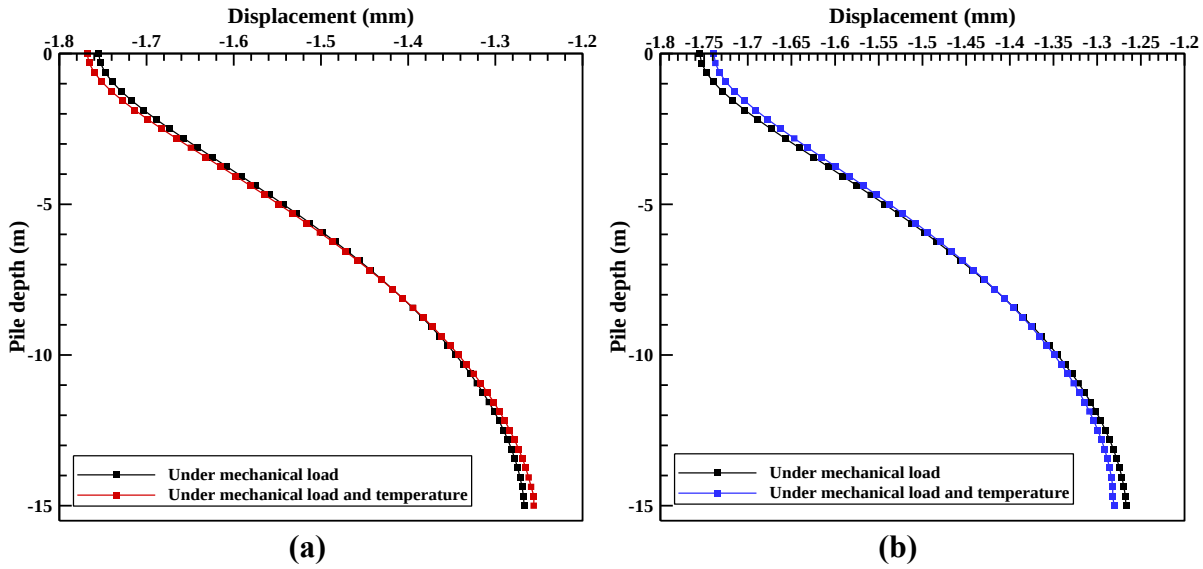

Figure IV. 3. 16. Displacement distribution of pile with square pipe (heating (a) and cooling (b)).

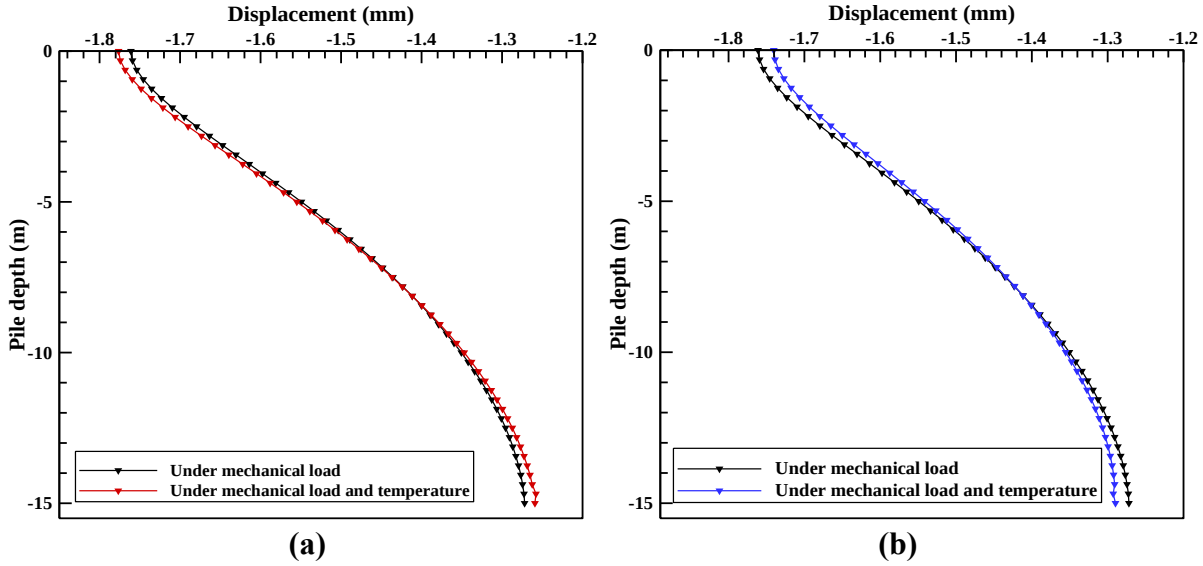

Figure IV. 3. 17. Displacement distribution of pile with triangular pipe (heating (a) and cooling (b)).

This study presents the axial stress distribution along the pile length for three distinct heat exchanger geometries, circular, square, and triangular, under both pure mechanical and thermo-mechanical loads, in corresponding curves depicted in Figures 18, 19, and 20 for heating (winter) and cooling (summer) scenarios.

Under a purely mechanical load of 1,600,000 N, all pile types exhibit their peak axial stress at the pile head. The recorded maximum axial stresses values are 1.5894 MPa for the

circular configuration, 1.5872 MPa for the square, and 1.5911 MPa for the triangular pipe. Toward the base of the pile, the axial stress gradually declines, reaching minimum values of 0.0288 MPa, 0.0253 MPa, and 0.0148 MPa for circular, square, and triangular pipes, respectively.

While the applied load is identical, the results reveal that pipe geometry significantly influences the internal stress distribution. The circular geometry exhibits the highest stress, likely due to its symmetrical shape offering lower structural resistance to axial forces. In contrast, the square configuration distributes stress more uniformly owing to its flat surfaces, resulting in moderately lower stress. The triangular geometry shows the least stress, possibly due to its angular design that promotes more efficient stress dissipation along the pile. These observations highlight that geometric design plays a crucial role in mechanical behavior, as the distribution of internal stresses is influenced by the geometry of the pipes.

When thermal effects are introduced, specifically with the inlet water temperature set at 278.15 K, the stress distribution shifts in this heating (winter) condition, and axial compressive stresses peak around the mid-depth of the pile, tapering off toward both the top and base. The highest stress concentrations are observed at a depth of 3.7500 m below the pile top, with magnitudes of approximately 1.5453 MPa, 1.6499 MPa, and 1.6667 MPa for circular, square, and triangular exchangers, respectively. These results indicate that the triangular configuration induces the highest thermally driven stresses, which may be attributed to its greater heat exchange efficiency and steeper temperature gradients along the pile. This suggests that pipe geometry not only influences mechanical response but also significantly affects thermal stress behavior.

A similar trend emerges under cooling conditions with a water temperature of 318.15 K. Compressive stresses again reach their maximum in the pile's central region and diminish toward both ends. At the same respective depth identified in the cooling scenario in the heating scenario, the stress magnitudes for the circular, square, and triangular configurations are about 1. 4899 MPa, 1.5107 MPa, and 1.5212 MPa, respectively.

This mid-depth stress concentration can be explained by the interaction between thermal dilation and geometric constraints imposed by the surrounding soil, which restricts axial displacement and leads to localized stress accumulation. The triangular configuration consistently exhibits the highest stress values, likely due to stress intensification at angular regions, while the circular shape shows the lowest, indicating a more uniform stress distribution. This consistent mid-depth stress localization highlights the central region of the pile as the most sensitive to thermal deformation, regardless of whether the pile is heating or cooling.

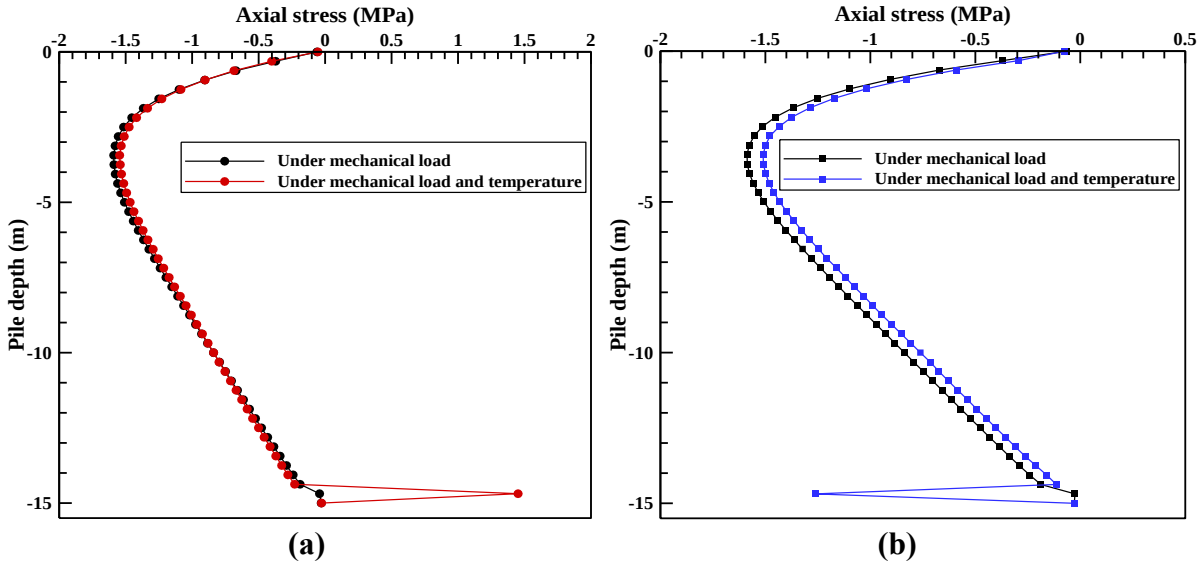

Figure IV. 3. 18. Axial stress distribution of pile with circular pipe (heating (a) and cooling (b)).

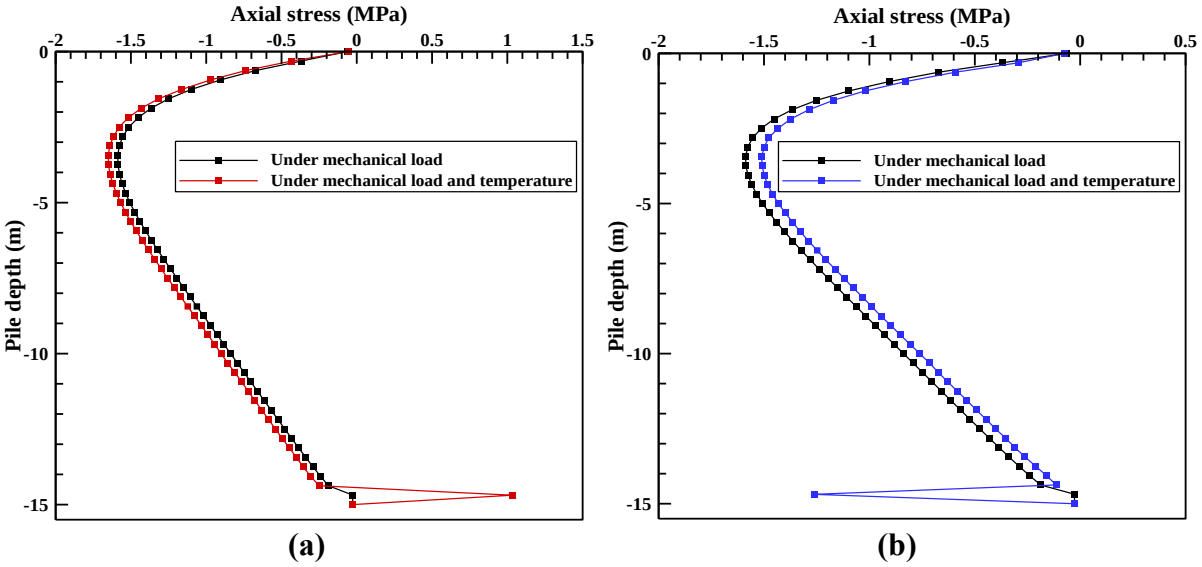

Figure IV. 3. 19. Axial stress distribution of pile with square pipe (heating (a) and cooling (b)).

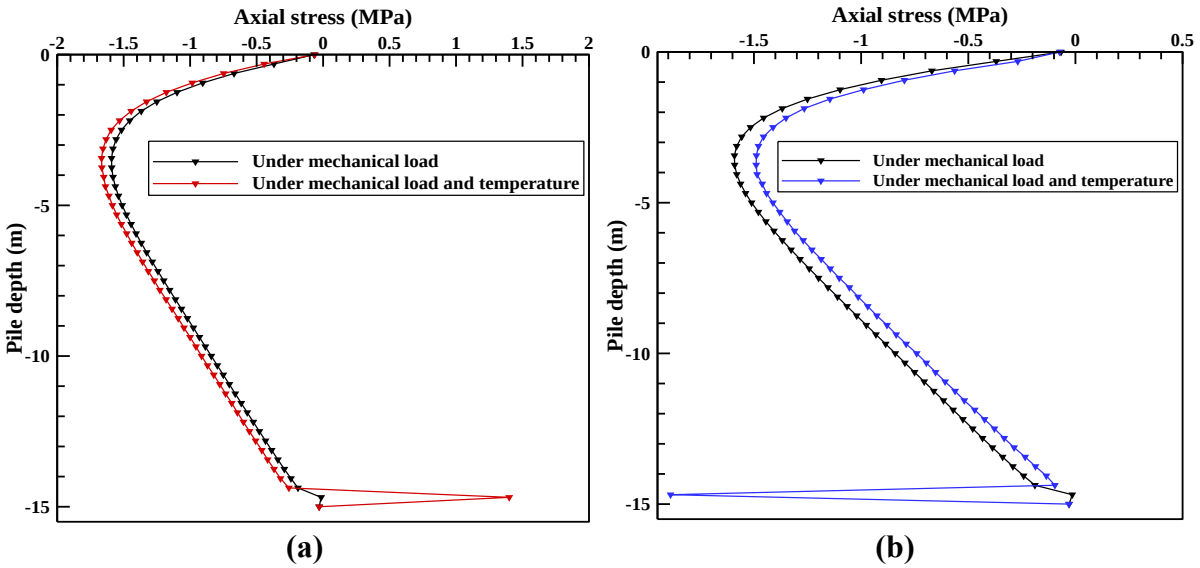

Figure IV. 3. 20. Axial stress distribution of pile with triangular pipe (heating (a) and cooling (b)).

In the simulation of pile foundations GEP, the shear stress interaction between the pile and the surrounding soil is represented as frictional resistance, capturing the mobilization of shear stress under both mechanical and thermal influences. Within this simulation framework, three distinct pile geometries, circular, square, and triangular, were examined to reveal how shear stress unfolds along their depth. As depicted in Figures 21, 22, and 23, these profiles were assessed under a purely mechanical load of 1,600,000 N, as well as under combined thermal-mechanical loading considering both heating and cooling conditions.

A consistent trend emerged across all configurations and scenarios: shear stress is predominantly concentrated within the upper 3.7500 m of the pile. This region serves as the primary zone of pile–soil interaction, where frictional forces are maximized due to higher normal stresses and more effective confinement near the ground surface. As depth increases, the magnitude of shear stress decreases gradually, reflecting the diminishing contact resistance and reduced relative movement between the pile and surrounding soil. This distribution suggests that the effectiveness of shear load transfer is strongly governed by near-surface soil stiffness and confinement conditions, which diminish with depth. The upper portion of the pile acts as the primary load-transfer interface, while deeper segments contribute less significantly to shear resistance due to decreased normal stress and soil-pile bonding.

The abrupt changes in shear stress observed near the bottom of the pile in Figures 21, 22, and 23 under combined thermal and mechanical loading during both heating (summer) and cooling (winter) scenarios can be attributed to the design of the heat exchanger embedded within the pile. Specifically, the pipe does not extend to the full length of the pile and terminates approximately 0.5 m above the pile base. As a result, the lower segment of the pile remains thermally inactive, experiencing no significant temperature-induced expansion or contraction. This creates a sharp transition between the thermally active and inactive regions, where a mismatch in strain develops along the pile length. The abrupt stress variations at this interface are the result of internal adjustments in response to this differential deformation. Additionally, the base of the pile typically experiences greater mechanical constraint due to contact with a stiff soil layer, further amplifying stress redistribution in this region. Together, the absence of thermal influence and the mechanical boundary condition at the pile tip explain the sudden changes in shear stress near the bottom observed in the simulations.

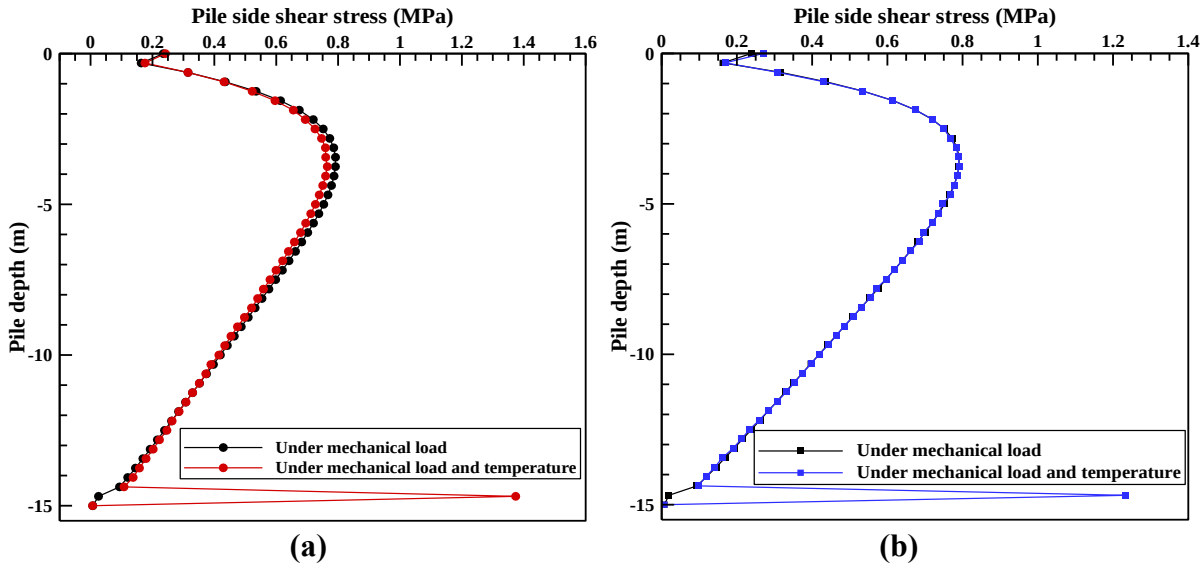

Figure IV. 3. 21. Shear stress distribution of pile with circular pipe (heating (a) and cooling (b)).

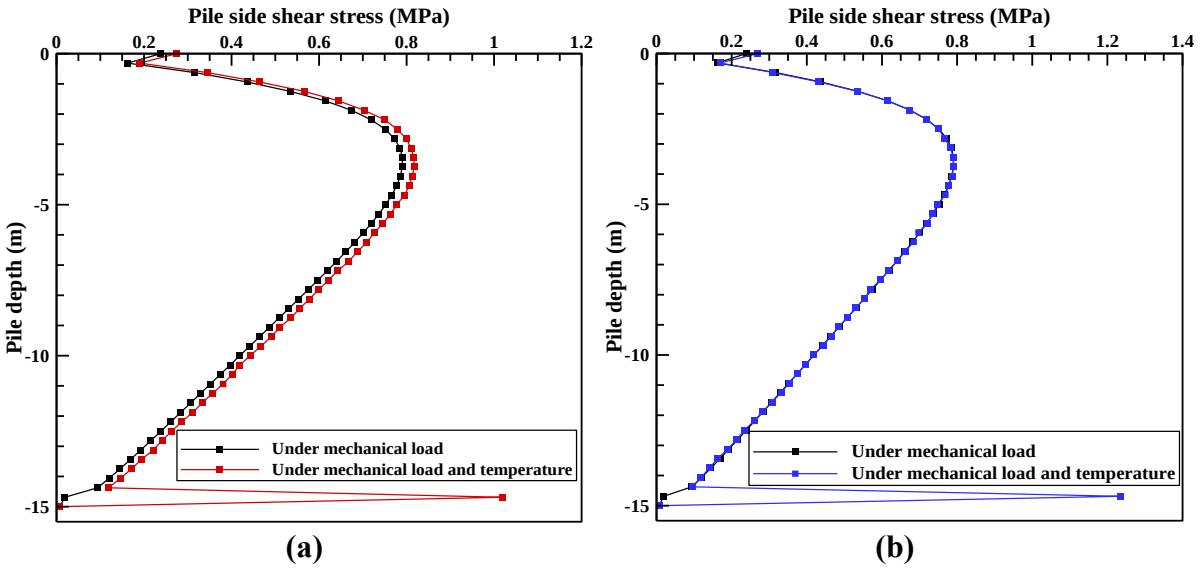

Figure IV. 3. 22. Shear stress distribution of pile with square pipe (heating (a) and cooling (b)).

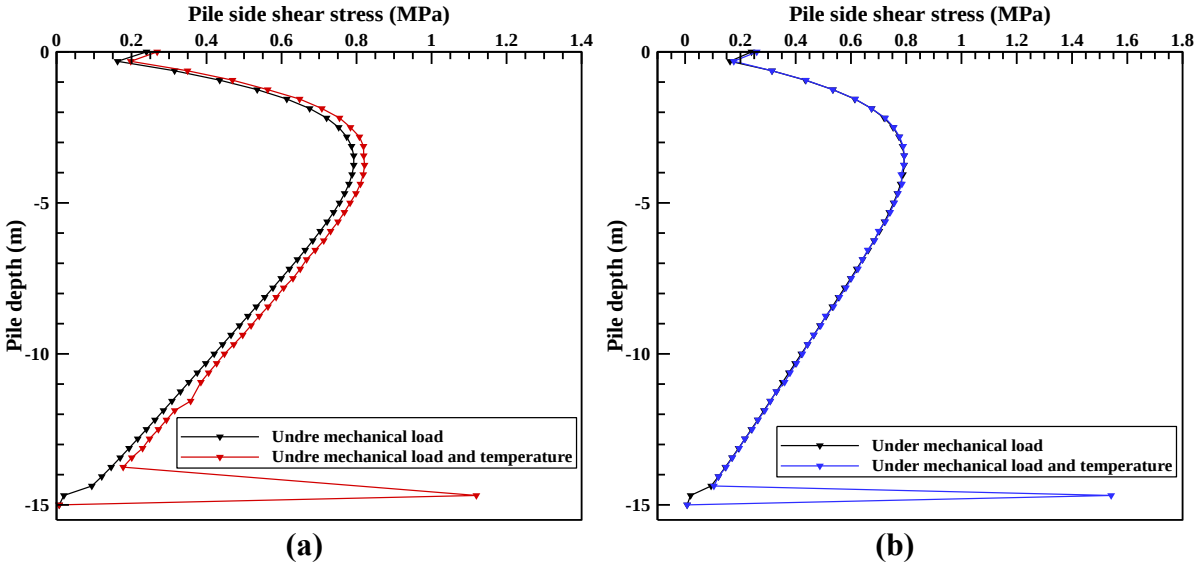

Figure IV. 3. 23. Shear stress distribution of pile with triangular pipe (heating (a) and cooling (b)).

IV.3.5 Conclusion

In this study, the thermomechanical behavior of GEPs equipped with different U-shaped pipe geometries (circular, square, and triangular) under summer and winter operating conditions is investigated through comprehensive numerical simulations. The principal conclusions derived from this analysis are as follows:

❖ Heat exchanger geometry plays a pivotal role in influencing thermal performance. Analytical formulations reveal that the shape of the embedded HE affects HT efficiency, which was numerically validated by simulating three distinct U-shaped configurations subjected to 48-hour operational cycles under both seasonal scenarios.

❖ Seasonal thermal response follows expected physical trends: During summer, the T_{outlet} decreases as the heat is absorbed by the surrounding soil, resulting in an increase in soil temperature along the pile length. In winter, the inverse behavior occurs; fluid temperature rises as heat is drawn from the soil, leading to a decrease in soil temperature.

❖ Triangular pipes outperform other geometries in cooling conditions, while trade-offs exist in heating: Among the geometries tested, the triangular U-pipe configuration demonstrated superior thermal exchange during cooling. Its T_{outlet} was approximately 1.206 K and 1.598 K lower than that of the circular and square configurations, respectively. The corresponding heat exchange rate was 45.727 W and 163.627 W higher. However, in winter, the triangular pipe produced higher outlet fluid temperatures by 0.629 K and 0.836 K compared to the circular and square counterparts, while its heat exchange rate was slightly lower by 25.416 W and 111.03 W, respectively. These findings suggest a more balanced or season-specific design approach may be required depending on operational priorities.

❖ Numerical simulations are in good agreement with theoretical expectations: The temperature and heat exchange behavior predicted for the triangular pipe geometry aligned closely with analytical estimates, reinforcing the reliability of the simulation framework under defined boundary and physical conditions.

❖ The triangular pipe's enhanced performance in cooling mode can be explained by its angular geometry, which promotes flow separation and secondary circulations within the pipe. These flow disturbances enhance convective heat transfer inside the pipe and increase the overall heat exchange surface area due to tighter fluid contact at corners. Conversely, the square geometry, while having a higher perimeter-to-area ratio, suffers from recirculation stagnation in corners, reducing effective convective flow and thus degrading performance.

❖ Axial compressive stress follows a linear profile under mechanical loading: The maximum stress occurs at the pile head and decreases linearly toward the pile base, while

displacement shows an opposite trend, peaking at the bottom. This behavior is consistent with standard geotechnical expectations for axially loaded piles.

❖ Thermal-mechanical coupling impacts pile deformation behavior: Under coupled thermal and mechanical loads, both in cooling and heating scenarios, displacement distribution remains linear. Maximum displacement is observed at the bottom, indicating enhanced safety and structural predictability of the GEP under operating loads.

❖ Stress distribution under thermal cycles is geometry-sensitive: The coupled axial and shear stresses exhibit a distinctive pattern, peaking in the middle of the pile and tapering toward the ends. This distribution arises due to the thermal expansion and contraction effects induced by seasonal loading. These stress concentrations are observed across all pipe geometries, though their magnitude and spread vary, highlighting the importance of pipe shape in structural integrity assessments.

❖ Compared with the pure conventional load state of each pipe, in the mechanical behavior, under the effect of thermal-mechanical coupling in summer conditions, the circular, square, and triangular configurations exhibited the highest axial compressive stress, increasing by approximately 4.29%, 4.82%, and 6.36%, respectively, while they are reduced by about 2.77%, 3.95%, and 4.75% in winter conditions, respectively.

❖ Displacements distributions of GEPs under mechanical load and temperature at the pile base showed minimal variation across geometries, with the circular, square, and triangular piles displaying a 0.57%, 1.14%, and 1.13% decrease in summer and a 5.11%, 1.13%, and 1.70% increase in winter, respectively. All these results are compared with the pure conventional load state of each pipe.

In summary, the results underscore the critical role of pipe geometry in optimizing the thermal and mechanical performance of geothermal energy piles. The triangular pipe configuration presents a promising option for enhancing cooling performance, though careful consideration is warranted for heating applications. Future studies are recommended to further refine GEP design by exploring additional geometric variations, material compositions, soil-structure interactions, and long-term operational behavior under real-world climatic fluctuations.

GENERAL CONCLUSION

This thesis has presented an in-depth investigation into the thermal and mechanical performance of geothermal energy piles (GEPs) using advanced numerical modeling, computational fluid dynamics (CFD) simulations, thermomechanical analysis, and complementary analytical methods. GEPs represent a promising solution in the field of sustainable energy, combining the roles of structural support and ground heat exchange for heating and cooling purposes in buildings. The aim of this work was to improve the understanding of GEP behavior under various operational conditions and to provide clear guidelines for their optimal design, especially in arid and semi-arid climates such as those found in Algeria.

The study was divided into three main parts, each addressing a distinct but complementary aspect of the thermal and mechanical behavior of GEP systems.

In the first part, the research focused on the seasonal thermal response of GEPs under varying flow conditions. The primary objective was to examine how the Reynolds number, representing fluid flow velocity, affects heat transfer efficiency and thermal behavior during summer (cooling mode) and winter (heating mode). CFD simulations were performed for Reynolds numbers of 500, 1000, 1500, and 2000 representing laminar flow regimes typically observed in geothermal applications. The simulations revealed that increasing the Reynolds number led to higher heat transfer rates, primarily because of the increased volume of fluid passing through the system. However, this also caused the outlet temperature to move closer to the inlet temperature, indicating reduced thermal interaction with the surrounding soil due to decreased residence time. This finding suggests a trade-off: while faster flows improve total energy exchange, they may reduce per-unit thermal efficiency. Consequently, optimizing the flow rate is essential to balance heat exchange capacity, efficiency, and operational sustainability over time.

The second part of the thesis investigated the impact of geometric parameters on the thermal performance of GEP systems using three-dimensional CFD modeling in parallel with an analytical model for validation. The key design parameters studied were:

- The diameter of the concrete pile (400 mm, 600 mm, 800 mm),
- The diameter of the heat exchanger pipes (ranging from 14 mm, 20 mm, 26 mm),

- The spacing between the heat exchanger and the concrete wall (20 mm, 50 mm, 100 mm, 150 mm),
- The angular orientation of the embedded U-shaped pipes (30°, 60°, 180°).

Simulation results under both heating and cooling conditions demonstrated the significant influence of each parameter. The optimal configuration for maximizing heat transfer was identified as:

- A 400 mm pile diameter, which enhanced thermal exchange by minimizing the distance between the fluid and the external soil,
- A 26 mm exchanger pipe, which provided a favorable balance between surface area and flow characteristics,
- A 20 mm spacing between the exchanger and the concrete wall, minimizing heat loss through internal conduction,
- A 30° angular pipe placement, which improved flow distribution and thermal interaction.

This part of the research underscores that even small changes in design geometry can produce measurable improvements in thermal performance, offering practical insights for engineers aiming to deploy more efficient and cost-effective GEP systems.

Importantly, the numerical results obtained from the CFD simulations were rigorously validated using an analytical approach. The analytical model, based on fundamental laws of heat transfer and fluid flow, provided theoretical predictions that closely matched the simulation data. This strong agreement confirms the accuracy and reliability of the CFD approach used in this study, reinforcing its value as a predictive tool for optimizing GEP configurations.

The third part of the thesis extended the analysis to a thermomechanical perspective, exploring how different U-pipe geometries (circular, square, and triangular) affect both heat transfer efficiency and mechanical stress distribution under seasonal thermal loading. The simulations focused on temperature profiles, heat exchange rates, axial and shear stress distributions, and vertical displacements within the pile. This coupled analysis is critical

because GEPs not only transfer heat but also serve as structural foundations that must withstand mechanical loading from the building and soil.

Results showed that pipe geometry has a significant effect on both thermal and mechanical performance:

- The triangular U-pipe delivered the best thermal performance during cooling, with a lower outlet temperature and higher heat exchange rates than both circular and square pipes. This improvement is attributed to enhanced internal fluid mixing, secondary flow patterns, and a greater effective contact area.

- During heating, however, the circular geometry slightly outperformed the triangular one, demonstrating that season-specific designs may be needed based on operational priorities (e.g., cooling-dominant vs. heating-dominant climates).

- From a mechanical standpoint, axial stress followed a linear distribution along the pile length, with maximum stress at the top and maximum displacement at the bottom, consistent with geotechnical expectations. The addition of thermal loads increased compressive stress by up to 6.36% in summer and reduced it by 4.75% in winter, depending on pipe geometry.

- The shear stress distribution peaked at mid-length due to thermal expansion/contraction effects, which may influence long-term fatigue behavior.

- Despite geometric differences, displacement variations among pipe shapes were minimal, confirming structural reliability across all configurations.

This part also incorporated validation of the thermal simulation results via analytical methods. The temperature profiles and heat exchange trends obtained from the CFD models showed strong consistency with analytical predictions for each pipe geometry. This validation step confirms that the thermomechanical simulations accurately reflect the expected physical behavior, thus providing confidence in the structural assessments performed.

In conclusion, this thesis has demonstrated the importance of integrating heat transfer, fluid dynamics, and structural mechanics to enhance the design and operation of geothermal energy piles. The proposed numerical and analytical approaches provide a solid foundation for

optimizing thermal and mechanical performance, contributing to the development of more sustainable and cost-effective ground heat exchanger systems. Future work may expand on these results by exploring advanced control strategies, alternative materials, and real-time operational data to further improve system efficiency and resilience in varying environmental conditions.

RECOMMENDATIONS AND PERSPECTIVE

The results and conclusions drawn in this thesis have provided valuable insights into the thermal and mechanical behavior of geothermal energy piles (GEPs). However, the scope of the study remains limited to the defined conditions and assumptions adopted in the numerical models. Based on the encountered limitations and in view of potential improvements, several recommendations and perspectives for future work are proposed:

- **Incorporation of experimental validation:**

Future studies should include laboratory-scale or field-scale experiments to verify the accuracy of CFD and analytical models under real-world conditions.

- **Consideration of groundwater movement:**

The influence of subsurface water flow on thermal behavior should be explored through coupled thermo-hydro models, especially in permeable soils.

- **Study of unsaturated and heterogeneous soils:**

Simulations should include unsaturated, anisotropic, or layered soils to better represent real geological conditions affecting heat exchange.

- **Use of alternative heat transfer fluids:**

Investigating fluids such as glycol, nanofluids, or eco-friendly refrigerants may improve heat transfer efficiency in different climates.

- **Application of advanced AI methods:**

Deep learning and ensemble models could enhance prediction and control of system performance, especially in complex dynamic environments.

- **Mechanical behavior under real loads:**

The response of GEPs under axial, lateral, and combined mechanical loads—including seismic effects—should be thoroughly investigated.

- **Long-term performance and fatigue analysis:**

The effect of repeated thermal cycles on material fatigue, settlement, and degradation must be analyzed for long-term reliability.

- **Hybrid renewable energy integration:**

Combining GEPs with solar PV, solar thermal, or heat pumps can create hybrid systems that improve energy autonomy and sustainability in buildings.

REFERENCES

[1] H. Wang, B.W. Ang, B. Su, “A multi-region structural decomposition analysis of global CO2 emission intensity”, *Ecological Economics*, vol. 142, pp. 163-176, 2017, http://dx.doi.org/10.1016/j.ecolecon.2017.06.023

[2] Sonelgaz. (2024). Press release: Record peak demand for electricity on July 21. https://www.sonelgaz.dz/media/file/2233/21_joyly_2024_669d29e2b17a03.42802169.pdf , accessed on Nov. 3, 2024.

[3] M. Merdassi , M. Aouissi , ”Numerical Simulation and Comparative Analysis of Earth Air Heat Exchanger Designs “, *International Journal of Heat and Technology*, vol. 42, pp. 2143-2156, 2024, https://doi.org/10.18280/ijht.420633.

[4] A. K. Sani, R. M. Singh, T. Amis, and I. Cavarretta, “A review on the performance of geothermal energy pile foundation, its design process and applications,” Renewable and Sustainable Energy Reviews, vol. 106. Elsevier Ltd, pp. 54–78, May 01, 2019. http://dx.doi.org/10.1016/j.rser.2019.02.008

[5] I. A. Gondal, S. A. Masood, and M. Amjad. “Review of geothermal energy development efforts in Pakistan and way forward.” Renewable and Sustainable Energy Reviews, vol. 71. Elsevier Ltd, pp. 687–696, 2017. https://doi.org/10.1016/j.rser.2016.12.097

[6] A. G. Olabi, M. Mahmoud, B. Soudan, T. Wilberforce, and M. Ramadan, “Geothermal based hybrid energy systems, toward eco-friendly energy approaches,” *Renewable Energy*, vol. 147, pp. 2003–2012, 2020, https://doi.org/10.1016/j.renene.2019.09.140.

[7] R. Al-Khoury, “Computational Modeling of Shallow Geothermal Systems”, *Taylor & Francis Group*, vol. 4, 2011. https://doi.org/10.1201/b11462 .

[8] N. Lebbihiat, A. Atia, M. Arıcı, N. Meneceur, “Geothermal energy use in Algeria: A review on the current status compared to the worldwide, utilization opportunities and countermeasures”, *Journal of Cleaner Production* , vol. 302, p. 126950, 2021. https://doi.org/10.1016/j.jclepro.2021.126950 .

[9] A. Fekraoui, “Geothermal resources in Algeria and their possible use”, *Geothermics* , vol.17, pp. 515-519, 1988. https://doi.org/10.1016/0375-6505(88)90080-6 .

[10] H. Saibi, S. Ehara, Y. Fujimitsu, J. Nishijima, “Progress of geothermal devel opment in Algeria”, *Journal of the Geothermal Research Society of Japan*, vol. 28, pp. 383-397, 2006. https://doi.org/10.11367/grsj1979.28.383 .

[11] Y. Himri, A.S. Malik, A.B. Stambouli, S. Himri, B. Draoui,” Review and use of the Algerian renewable energy for sustainable development”, *Renewable and Sustainable Energy Reviews*, vol.13 ,pp. 1584-1591, 2009. https://doi.org/10.1016/j.rser.2008.09.007 .

[12] O. Bellache, M. Hellel, E.H. Abdelmalik, A. Chenak, “Geothermal heating of greenhouses in southern Algeria”, *Proceedings of the World Geothermal Congress 1995, Florence, Italy*, pp. 2285-2290, 1995.

[13] D.H. Freeston, “Direct uses of geothermal energy 1995”, *Geothermics*, vol. 25, pp. 189-214, 1996. https://doi.org/10.1016/0375-6505(95)00051-8 .

[14] A. Fekraoui, M. Abouriche, “Algeria country update report ”, *Proceedings of the World Geothermal Congress 1995, Florence, Italy*, pp. 31-34,1995.

[15] A. Fekraoui, F.Z, Kedaid, “Geothermal resources and uses in Algeria: a country update report”, *Proceedings of the World Geothermal Congress 2005, Ant alya, Turkey*, 2005.

[16] J.W, Lund, D.H, Freeston, T.L, Boyd,” Direct application of geothermal energy: 2005 worldwide review”, *Geothermics*, vol. 34, pp. 691-727, 2005. https://doi.org/10.1016/j.geothermics.2005.09.003 .

[17] A. Fekraoui, “Geothermal activities in Algeria”, *Proceedings of the 2010 World Geothermal Congress, Bali, Indonesia*, pp. 25-29, 2010.

[18] J.W, Lund, D.H, Freeston, T.L, Boyd, “Direct utilization of geothermal energy 2010 worldwide review”, *Geothermics*, vol. 40, pp. 159-180, 2011. https://doi.org/10.1016/j.geothermics.2011.07.004 .

[19] J.W, Lund, T.L, Boyd, “Direct utilization of geothermal energy 2015 worldwide review”, *Geothermics*, vol. 60, pp. 66-93, 2016. https://doi.org/10.1016/j.geothermics.2015.11.004 .

[20] H., Saibi, “Geothermal resources in Algeria, proceedings of the 2015 world geothermal congress, Melbourne, Australia” *International Geothermal Association*, p. 10, 2015.

[21] S. Ouali, M. Hadjiat, A. Ait-Ouali, K. Salhi, A. Malek, ”Cartographie et car acterisation des ressources geothermiques de l’Algerie”, *Revue des Energies Renouvelables*, vol. 21 , pp. 54-61, 2018. https://doi.org/10.54966/jreen.v21i1.669 .

[22] J.W, Lund, G.W, Huttrer, A.N, Toth, “Characteristics and trends in geothermal development and use, 1995 to 2020”, *Geothermics*, vol. 105, p. 102522, 2022. https://doi.org/10.1016/j.geothermics.2022.102522 .

[23] P. Yu , Y. Xu, H. Liu, X. Liu, J. Fu, M. Xu, D. Zhou, “Regional-Scale Assessment of the Potential for Shallow Geothermal Energy Development Using Vertical Ground Source Heat Pumps”, *Energies*, vol.17, p. 4363, 2024. https://doi.org/10.3390/en17174363 .

[24] Source: Polytechnic of Turin https://webthesis.biblio.polito.it/17388/1/tesi.pdf .

[25] A. Casasso, R. Sethi, ”Assessment and Minimization of Potential Environmental Impacts of Ground Source Heat Pump (GSHP) Systems”, *Water*, vol. 11, p. 1573, 2019. https://doi.org/10.3390/w11081573 .

[26] G. Florides, S. Kalogirou, “Ground heat exchangers: A review of systems, models and applications”, *Renewable Energy*, vol. 32, pp. 2461- 2478, 2007. https://doi.org/10.1016/j.renene.2006.12.014

[27] W. Yang, J. Zhou, W. Xu, G. Zhang, “Current status of ground-source heat pumps in China” *Energy Policy*, vol. 38, pp. 323–332, 2010. https://doi.org/10.1016/j.enpol.2009.09.021

[28] M. De Moel, P.M. Bach, A. Bouazza, R.M. Singh, J.O. Sun, “Technological advances and applications of geothermal energy pile foundations and their feasibility in Australia” *Renewable and Sustainable Energy Reviews*, vol. 14, pp. 2683–2696, 2010. https://doi.org/10.1016/j.rser.2010.07.027 .

[29] A.K. Sani, R.M. Singh, I. Cavarretta, S. Bhattacharya, “Heat storage performance of a pile heat exchanger installed in partially saturated swelling clay”, *The 7th International Conference on Unsaturated Soils, Hong Kong*, 2018.

[30] D. Banks, "Introduction to Thermogeology : Ground Source Heating and Cooling", *2nd Editio, John Wiley & Sons*, 2012.

[31] H. Brandl, "Energy foundations and other thermos-active ground structures", *Géotechnique*, vol.56, pp. 81–122, 2006. https://doi.org/10.1680/geot.2006.56.2.81.

[32] A.K. Sani, "Thermo-hydraulic behaviour of geothermal energy piles in unsaturated soils", *University of Surrey*, 2019.

[33] Source Energy piles: a research activity at EPF Lausanne, Study of thermal and mechanical behaviour http://lms.epfl.ch/research/research-fields/energy-geostructures-thermal-piles .

[34] C.G. Olgun, T. Ozudogru, S. Abdelaziz, A. Senol, "Long-term performance of heat exchanger piles", *Acta Geotechnica,* vol. 10, pp. 553–569, 2015. https://doi.org/10.1007/s11440-014-0334-z .

[35] A.K, Sani, R. M., Singh, C.H.C., Tsuha, I., Cavarretta, "Pipe–pipe thermal interaction in a geothermal energy pile", *Geothermics*, vol. 81, pp. 209-223, 2019. https://doi.org/10.1016/j.geothermics.2019.05.004 .

[36] J. Gao , X. Zhang, J. Liu, K. Li, J. Yang, "Numerical and experimental assessment of thermal performance of vertical energy piles: An application", *Applied Energy,* vol. 85, pp. 901–10, 2008. https://doi.org/10.1016/j.apenergy.2008.02.010 .

[37] H. Park, S.R. Lee, S. Yoon, J.C. Choi, "Evaluation of thermal response and performance of PHC energy pile: Field experiments and numerical simulation", *Applied Energy,* vol. 103, pp. 12–24, 2013. https://doi.org/10.1016/j.apenergy.2012.10.012 .

[38] Y. Hamada, H. Saitoh, M. Nakamura, H. Kubota, K. Ochifuji, " Field performance of an energy pile system for space heating", *Energy Building*, vol. 39, pp. 517–24, 2007. https://doi.org/10.1016/j.enbuild.2006.09.006 .

[39] B. Wang, C. Haberfield, S. Baycan, " Field investigation of a geothermal energy pile: Initial observations", *Geotech-FrOrg*, pp. 3415–8, 2013. https://doi.org/10.1179/1937525514Y.0000000002 .

[40] S. You, X. Cheng, H. Guo, Z. Yao, "Experimental study on structural response of CFG energy piles", *Applied Thermal Engineering,* vol. 96, pp. 640–51, 2016. https://doi.org/10.1016/j. applthermaleng.2015.11.127.

[41] A. Zarrella A, M. De Carli, A. Galgaro, "Thermal performance of two types of energy foundation pile: Helical pipe and triple U-tube", *Applied Thermal Engineering*, vol. 61, pp. 301–10, 2013. https://doi.org/10.1016/j.applthermaleng.2013.08.011.

[42] G.A. Akrouch, "Energy piles in cooling dominated climates", *Texas A&M University*, 2014.

[43] Uponor Ground Energy Technical Information 03/2012.

[44] R. Zagorscak, H.R. Thomas, "A review on performance of energy piles and effects on surrounding ground", *Inženjerstvo Okoliša (Environmental Eng),* vol. 3, pp. 33–45, 2016.

[45] J. Fadejev, R. Simson, J. Kurnitski, F. Haghighat, "A review on energy piles design, sizing and modelling", *Energy* , vol. 122, pp. 390-407, 2017. https://doi.org/10.1016/j.energy.2017.01.097 .

[46] M.M. Nujid, J. Idrus, K. A. Hashim, D. A. Tholibon, N. S. Azizan, "A review of shallow geothermal energy pile from numerical study", *AIP Conference Proceedings 2020, 020006 (2018).* https://doi.org/10.1063/1.5062632 .

[47] D.Y. Cherati, O. Ghasemi-Fare, "Practical approaches for implementation of energy piles in Iran based on the lessons learned from the developed countries experiences", *Renewable and Sustainable Energy Reviews*, vol.140, p. 110748, 2021. https://doi.org/10.1016/j.rser.2021.110748 .

[48] Z. Mohamad , F. Fardoun , F. Meftah, "A review on energy piles design, evaluation, and optimization", *Journal of Cleaner Production,* vol. 292, p.125802, 2021. https://doi.org/10.1016/j.jclepro.2021.125802 .

[49] R.P. Cunha, P.J. Bourne-Webb, "A critical review on the current knowledge of geothermal energy piles to sustainably climatize buildings", *Renewable and Sustainable Energy Reviews* vol. 158, p. 112072, 2022. https://doi.org/10.1016/j.rser.2022.112072 .

[50] M.E. Zayed, B. Shboul, H. Yin, J. Zhao, A.A. Zayed, "Recent advances in geothermal energy reservoirs modeling: Challenges and potential of thermo-fluid integrated models for reservoir heat extraction and geothermal energy piles design", Journal of Energy Storage, vol. 62, p.106835, 2023. https://doi.org/10.1016/j.est.2023.106835 .

[51] A.M. Baffa, Z. Mustaffa, N. Rosmawati, M. E. Al-Atroush, "Field Studies on the Application and Performance of Geothermal Energy Piles (GEP) in Buildings: An Overview", *Lecture Notes in Civil Engineering, vol 556. Springer, Singapore*, 2024. https://doi.org/10.1007/978-981-97-8712-8_25

[52] H. Dokmak, K. Faraj, M. Khaled, J. Faraj, C. Castelain, " A short recent review on geothermal energy piles", *Journal of Physics: Conference Series*, vol. 2754, p. 012022, 2024, https://doi.org/10.1088/1742-6596/2754/1/012022 .

[53] M.A. Baffa, Z. Mustaffa, N.R. Ahmad, M.E. El-Atroush, N.S.A. Yaro, M.E. Ben Seghier, "Performance of geothermal energy piles in buildings: A bibliometric analysis and systematic review", *Energy and Buildings*, vol.331, p.115357, 2025. https://doi.org/10.1016/j.enbuild.2025.115357 .

[54] B. Ciapala , G.S. Georgiou, L. Aresti , T. Onoufriou , G. A. Florides , P. Christodoulides, "Thermal performance evaluation of energy piles and energy foundations: A comprehensive review of thermal effectiveness testing methods", *Energy and Buildings*, vol. 346, p. 116181, 2025. https://doi.org/10.1016/j.enbuild.2025.116181

[55] A.M. Onaizi , W. Tang, G. Fahim Huseien , M. Alhassan , S. A. Onaizi , "A systematic review on the application progress of phase change materials in energy piles", *Applied Thermal Engineering*, vol. 274, p.126630, 2025. https://doi.org/10.1016/j.applthermaleng.2025.126630

[56] P. Zhang, M. Liu, Z. Li, Q. Lv, Z. Sun, Q. Zhang, X. Liu, "Simulation and analysis of the thermal-mechanical response of an energy pile" , *Lithosphere*, p. 5506908,2022. https://doi.org/10.2113/2022/5506908 .

[57] C. Xu, Y. Wang, X. Meng, Q. Lv, H. Chen, Q. Wu, "A Multiphysics Simulation Study of the Thermomechanical Coupling Response of Energy Piles", *Buildings*, vol.14, p.1440. 2024. https://doi.org/10.3390/buildings14051440 .

[58] Du, T.; Li, Y.; Bao, X.; Tang, W.; Cui, H. Thermo-Mechanical Performance of a Phase Change Energy Pile in Saturated Sand.Symmetry 2020, 12, 1781. http://dx.doi.org/10.3390/sym12111781

[59] X. Bao, Y. Li, T. Feng, H. Cui, X. Chen, "Investigation on thermo mechanical behavior of reinforced concrete energy pile with large cross-section in saturated sandy soil by model experiments", *Underground Space,* 2020. http://dx.doi.org/10.1016/j.undsp.2019.03.009 .

[60] R. Li , G. Kong , G. Sun , Y. Zhou , Q. Yang , "Thermomechanical characteristics of an energy pile-raft foundation under heating operations", *Renewable Energy,* vol. 175, p.580-592, 2021. https://doi.org/10.1016/j.renene.2021.05.020 .

[61] G. Jiang, C. Lin , D. Shao, M. Huang , H. Lu , G. Chen , C. Zong, "Thermo-mechanical behavior of driven energy piles from full-scale load tests", *Energy and Buildings,* vol. 233, , 110668, 2021. https://doi.org/10.1016/j.enbuild.2020.110668 .

[62] A. Moradshahi, M. Faizal , A. Bouazza ,J.S. McCartney, "Cross-sectional thermo-mechanical responses of energy piles", *Computers and Geotechnics*, vol. 138, p. 104320, 2021. http://dx.doi.org/10.1016/j.compgeo.2021.104320 .

[63] Y. Lou , P. Fang , X. Xie , R. Zhang , C. Shan Anthony Chong , Z. Wang , D. Zhu, "Experimental study on thermo-mechanical responses of pre-bored grouted planted piles with different restraint conditions", *Energy and Buildings*, vol. 268, p. 112232, 2022. http://dx.doi.org/10.1016/j.enbuild.2022.112232 .

[64] H. Pei , H. Song , F. Meng , W. Liu, "Long-term thermomechanical displacement prediction of energy piles using machine learning techniques", *Renewable Energy,* vol. 195, pp. 620-636, 2022, https://doi.org/10.1016/j.renene.2022.06.057 .

[65] X. Ding, D. Zhang , A. Bouazza , C. Wang, G. Kong, "Thermo-mechanical behaviour of energy piles in overconsolidated clay under various mechanical loading levels and thermal cycles", *Renewable Energy*, vol 201, pp. 594-607. 2022. https://doi.org/10.1016/j.renene.2022.10.128

[66] W. Yang , Y. Qiang , L. Ju , F. Wang , A. Liu, "Numerical evaluations on the effects of different factors on thermo- mechanical behaviour of an energy pile group", *Computers and Geotechnics*, vol. 162, 105664, 2023. https://doi.org/10.1016/j.compgeo.2023.105664 .

[67] Z.Y. Ai, J.M. Ye, "Thermo-mechanical analysis of pipe energy piles in layered cross-isotropic soils", *Energy*, vol 277, 127757, 2023. https://doi.org/10.1016/j.energy.2023.127757

[68] X. Ding , Q. Wu, C. Wang , G. Kong, "Thermo–mechanical behavior of energy pile group in dry sand subjected to a horizontal load", *Renewable Energy,* vol. 233, 121170, 2024. https://doi.org/10.1016/j.renene.2024.121170 .

[69] S. Feng , J. Fang , Y. Zhao , Z. Zhang , Y. Wang, "Thermomechanical Analysis of Energy Piles Using a Load-transfer Approach Considering Soil Coupling Effects", *Computers and Geotechnics* ,vol. 168, 106147, 2024. https://doi.org/10.1016/j.compgeo.2024.106147 .

[70] B. Sun , C. Shi , A. Leung, "Numerical Investigation on Thermomechanical Behavior of Driven Energy Piles Subjected to Cyclic Thermal Loading in Sand", *Computers and Geotechnics*, vol. 173, p. 106582, 2024. https://doi.org/10.1016/j.compgeo.2024.106582

[71] K. Liu , Z. Wang, P. Fang , X. Xie , Y. Lou , Z. Meng, "A new method for analyzing the thermomechanical behavior and the null point movement of energy piles", *Computers and Geotechnics*, vol. 165, p. 105867, 2024. https://doi.org/10.1016/j.compgeo.2023.105867 .

[72] J. Yuan, Z. Chen, H Xiao, L. Zheng, W. Li, X. Song, "Thermal-mechanical behavior of deeply buried pipe energy pile group in sand obtained from model test", *Applied Thermal Engineering*, vol. 261, p. 125078, 2025. https://doi.org/10.1016/j.applthermaleng.2024.125078

[73] P.Z. Zhuang, K.X. Wang, X.G. Song , X. Geng , H. Yang , "Thermo mechanical behaviour of energy pile considering non-uniform initial ground temperatures", *Proceedings of the Institution of Civil Engineers-Geotechnical Engineering*, 2025. https://doi.org/10.1680/jgeen.24.00363 .

[74] F. He, H. Liu, C. Wang, A. Bouazza, G. Kong, Z. Sun , "Effects of thermal loading conditions on the thermo-mechanical response of energy pile at different depths", *Geothermics,* vol. 131, p. 103392, 2025. https://doi.org/10.1016/j.geothermics.2025.103392 .

[75] H. Chang , G. Kong , G. Sun , C. Wang , Y. Zhou , Q. Yang , "Thermomechanical response characteristics of full-scale prestressed high-strength concrete energy pile under the flexible constraint of cushion layer", *Energy,* vol. 331, p. 137070, 2025. https://doi.org/10.1016/j.energy.2025.137070 .

[76] H. Song , L. Zheng , Z-J. Cao , K. Cui , H. Pei , W. Liu , S. Zhang, ”Thermomechanical analysis of dissimilar energy pile groups using a load transfer method”, *Renewable Energy* , vol. 254, p. 123708, 2025. https://doi.org/10.1016/j.renene.2025.123708 .

[77] T. You , T. Yan , Y. Huang , S. Huang , H. Cui, “Thermo-mechanical coupling performance analysis of phase change material and nanofluid synergized high-efficiency energy piles for shallow geothermal energy utilization”, *Energy*, vol. 334, p. 137691, 2025. https://doi.org/10.1016/j.energy.2025.137691 .

[78] R. Chen , D. Wu , T. Zhang , G. Kong, J. Fang , “Thermo-mechanical behavior of energy piles equipped with PCM tubes”, *Computers and Geotechnics*, vol. 179, p. 107005, 2025. https://doi.org/10.1016/j.compgeo.2024.107005.

[79] F. He , H. Liu , C. Wang , A. Bouazza , G. Kong , Z. Sun, “Effects of thermal loading conditions on the thermo-mechanical response of energy pile at different depths”, *Geothermics,* vol. 131, p. 103392, 2025. https://doi.org/10.1016/j.geothermics.2025.103392 .

[80] J. Liu , Q. Zhang , K. Xiao , W. Cui , Z. Liu, “Study on the thermo-mechanical response of a single energy pile in pile groups”, *Structures*, vol. 71, p. 108013, 2025. https://doi.org/10.1016/j.istruc.2024.108013 .

[81] X. Ding , C. Peng , C. Wang , G. Kong, “Heat transfer performance of energy piles in seasonally frozen soil areas”, *Renewable Energy*, vol. 190, pp. 903-918, 2022. https://doi.org/10.1016/j.renene.2022.04.004 .

[82] A.H. Farajollahi, B. Asgari , M. Rostami, “Thermal performance analysis of an energy pile with triple helix ground heat exchanger”, *Geothermics,* vol. 104, pp. 102459, 2022. http://dx.doi.org/10.1016/j.geothermics.2022.102459 .

[83] S. Lee, S. Park, D. Ahn, H. Choi, “Thermal performance of novel cast-in place energy piles equipped with multipurpose steel pipe heat exchangers (SPHXs)”, *Geothermics,* vol. 102, pp. 102389, (2022). https://doi.org/10.1016/j.geothermics.2022.102389

[84] S. Haridy , K. Alnaqbi , A. Radwan, M. G. Arab, “Optimizing the thermal performance of energy piles using response surface methodology”. *Case Studies in Thermal Engineering*, vol. 41, p. 102637, 2023. https://doi.org/10.1016/j.csite.2022.102637 .

[85] S. Shahidi, M. Hajialilue-Bonab, H.R. Tohidvand, A. Khosravi, "Experimental investigation on the efficiency of the phase change materials for enhancing the thermal performance of energy piles in sandy soils", *Energy and Buildings*, vol. 298, p. 113544, 2023. http://dx.doi.org/10.1016/j.enbuild.2023.113544 .

[86] C. Hu, H. Gu, J. Luo, D. Tian, "Numerical study on heat restoration cycle performance of energy pile with backfilling PCM", *Case Studies in Thermal Engineering*, vol. 61, p. 105047, 2024. https://doi.org/10.1016/j.csite.2024.105047 .

[87] Q.I. Alqawasmeh, G. A. Narsilio, N. Makasis, M.J. Kreitmair, "The impact of soil layering and groundwater flow on energy pile thermal performance", *Geomechanics for Energy and the Environment ,* vol. 38, p.100538, 2024. https://doi.org/10.1016/j.gete.2024.100538 .

[88] S. Bosch, E. Ravera, L. Laloui, "Performance of energy piles foundation in hot-dominated climate: A case study in Dubai", *Renewable Energy*, vol. 220, p. 119632, 2024. https://doi.org/10.1016/j.renene.2023.119632 .

[89] C. Hu, J. Cui., M. Wang, Y. Zhang, J. Luo, L. Li , "Optimizing the restoration performance of pipe energy piles using energy injection in winter mode: A numerical investigation", *Energy Storage*, vol. 114, p. 115807, 2025. https://doi.org/10.1016/j.est.2025.115807 .

[90] Q. I. Alqawasmeh , M.J. Kreitmair , G. A. Narsilio, " The role of ground hydrothermal spatial variability on energy pile group thermal performance", *Computers and Geotechnics* , vol. 179, p. 106983, 2025. https://doi.org/10.1016/j.compgeo.2024.106983 .

[91] Y. Guo , C. Wang, A. Bouazza, G. Kong , X. Ding, "Thermal performance of pipe-type energy piles with open-ended heat exchange tubes", *Applied Thermal Engineering,* vol. 258, p. 124573, 2025. https://doi.org/10.1016/j.applthermaleng.2024.124573 .

[92] D. Adam, R. Markiewicz, " Energy from earth-coupled structures, foundations, tunnels and sewers" , *Géotechnique,* vol. 59, pp. 229–236. 2009. https://doi.org/10.1680/GEOT.2009.59.3.229

[93] P. Daniel, H. Markus, "Measured Thermal Performances of the Energy Pile System of the Dock Midfield at Zürich Airport", *Procedding European Geothermal Congress 2007*

(Unterhaching, Germany), pp. 1–7. 2007. https://aris.supsi.ch/entities/speech/57c71b74-42a1-4027-9a00-b39224048b4b

[94] Adapted from https://www.enercret.com/

[95] F. Moukalled, L. Mangani, M. Darwish, "The finite volume method in computational fluid dynamics", *Springer,* vol. 113, 2016.

[96] S. Boudjaza, A. Chehhat , A. Kaddour , Y. Menni , S. Larguech , B.M. Alshammari , L. Kolsi, "Three-dimensional thermomechanical modeling of geothermal energy piles with U-tube heat exchangers of different cross-sectional shapes*", Case Studies in Thermal Engineering*, vol. 74, p. 106846, 2025, https://doi.org/10.1016/j.csite.2025.106846

[97] M. A, Stewart, J.S. McCartney, "Centrifuge modeling of soil-structure interaction in energy foundations*", Journal of Geotechnical and Geoenvironmental Engineering*, vol. 140, pp. 04013044, 2014. https://doi.org/10.1061/(ASCE)GT.1943-5606.0001061.

[98] B.E. Launder, D.B. Spalding, "The numerical computation of turbulent flows", *Computer Methods in Applied Mechanics and Engineering,* vol.3, pp. 269-289, 1974. https://doi.org/10.1016/0045-7825(74)90029-2

[99] ANSYS, ANSYS Fluent User's Guide, *ANSYS Inc ed*., 2018.

[100] L. Jun , Z. Xu , G. Jun , Y. Jie, "Evaluation of heat exchanger rate of GHE in geothermal heat pump system", *Renewable Energy,* vol. 34, pp. 2898-2904, 2009. http://dx.doi.org/10.1016/j.renene.2009.04.009

[101] J.E. Bose, J.D. Parker, F.C. McQuiston, "Design/data manual for closed-loop ground-coupled heat pump systems", *American Society of Heating, Refrigerating, and Air-Conditioning Engineers*, 1985.

[102] J.A. Shonder, J.V. Beck, " Field test of a new method for determining soil formation thermal conductivity and borehole resistance", *ASHRAE Trans*, vol.106 , pp. 843–50, 2000.

[103] J. Claesson, A. Dunand. "Heat extraction from the ground by horizontal pipes: a mathematical analysis", *Swedish Council for Building Research*, 1983.

[104] Y. Gu , D.L. O'Neal , "Development of an equivalent diameter expression for vertical U-tubes used in ground-coupled heat pumps", *ASHRAE Trans*, vol. 104, pp.347–55, 1998.

[105] H.S. Carslaw, J.C, Jaeger, " Conduction of heat in solids. Oxford: Clarendon Press", 2nd ed, 1959.

APPENDICES

Appendice A

Appendice A. 1 Analytical Framework and Parametric Calculations (Part 02).

Table A. 1 Results analytical calculations for the optimal pile diameter (400 mm) under heating conditions.

t	α	x	E(x)	R b	Pr	Re	Nu	H	R p,f	Rp	R eq	R c	R tot	m	T out	q	Q
3600	5,70864E-07	0,205511	-2,15946	-0,0916	6,99091	11942,57	91,45756	2743,727	0,005804	0,080755	0,05863	0,126879	0,121839	0,188061	281,7618	-97,9501	-2840,55
7200	5,70864E-07	0,411022	-1,46631	-0,0622	6,99091	11942,57	91,45756	2743,727	0,005804	0,080755	0,05863	0,126879	0,15124	0,188061	281,1359	-80,9773	-2348,34
10800	5,70864E-07	0,616533	-1,06084	-0,045	6,99091	11942,57	91,45756	2743,727	0,005804	0,080755	0,05863	0,126879	0,168439	0,188061	280,8611	-73,5247	-2132,22
14400	5,70864E-07	0,822044	-0,77316	-0,0328	6,99091	11942,57	91,45756	2743,727	0,005804	0,080755	0,05863	0,126879	0,180642	0,188061	280,6949	-69,0179	-2001,52
18000	5,70864E-07	1,027555	-0,55002	-0,02333	6,99091	11942,57	91,45756	2743,727	0,005804	0,080755	0,05863	0,126879	0,190107	0,188061	280,5794	-65,8854	-1910,68
21600	5,70864E-07	1,233066	-0,3677	-0,0156	6,99091	11942,57	91,45756	2743,727	0,005804	0,080755	0,05863	0,126879	0,197841	0,188061	280,4926	-63,5295	-1842,35
25200	5,70864E-07	1,438577	-0,21355	-0,00906	6,99091	11942,57	91,45756	2743,727	0,005804	0,080755	0,05863	0,126879	0,20438	0,188061	280,4238	-61,6651	-1788,29
28800	5,70864E-07	1,644088	-0,08001	-0,00339	6,99091	11942,57	91,45756	2743,727	0,005804	0,080755	0,05863	0,126879	0,210044	0,188061	280,3674	-60,1364	-1743,96
32400	5,70864E-07	1,849599	0,03777	0,001602	6,99091	11942,57	91,45756	2743,727	0,005804	0,080755	0,05863	0,126879	0,21504	0,188061	280,32	-58,8496	-1706,64
36000	5,70864E-07	2,055109	0,14313	0,006071	6,99091	11942,57	91,45756	2743,727	0,005804	0,080755	0,05863	0,126879	0,219509	0,188061	280,2792	-57,7443	-1674,58
39600	5,70864E-07	2,26062	0,23844	0,010114	6,99091	11942,57	91,45756	2743,727	0,005804	0,080755	0,05863	0,126879	0,223552	0,188061	280,2437	-56,7796	-1646,61
43200	5,70864E-07	2,466131	0,32545	0,013805	6,99091	11942,57	91,45756	2743,727	0,005804	0,080755	0,05863	0,126879	0,227242	0,188061	280,2122	-55,9266	-1621,87
46800	5,70864E-07	2,671642	0,40549	0,0172	6,99091	11942,57	91,45756	2743,727	0,005804	0,080755	0,05863	0,126879	0,230638	0,188061	280,1841	-55,1642	-1599,76
50400	5,70864E-07	2,877153	0,4796	0,020344	6,99091	11942,57	91,45756	2743,727	0,005804	0,080755	0,05863	0,126879	0,233781	0,188061	280,1588	-54,4767	-1579,82
54000	5,70864E-07	3,082664	0,54859	0,02327	6,99091	11942,57	91,45756	2743,727	0,005804	0,080755	0,05863	0,126879	0,236708	0,188061	280,1357	-53,8518	-1561,7
57600	5,70864E-07	3,288175	0,61313	0,026008	6,99091	11942,57	91,45756	2743,727	0,005804	0,080755	0,05863	0,126879	0,239445	0,188061	280,1146	-53,2802	-1545,13
61200	5,70864E-07	3,493686	0,67376	0,028579	6,99091	11942,57	91,45756	2743,727	0,005804	0,080755	0,05863	0,126879	0,242017	0,188061	280,0952	-52,7541	-1529,87
64800	5,70864E-07	3,699197	0,73092	0,031004	6,99091	11942,57	91,45756	2743,727	0,005804	0,080755	0,05863	0,126879	0,244441	0,188061	280,0773	-52,2676	-1515,76
68400	5,70864E-07	3,904708	0,78498	0,033297	6,99091	11942,57	91,45756	2743,727	0,005804	0,080755	0,05863	0,126879	0,246735	0,188061	280,0606	-51,8155	-1502,65
72000	5,70864E-07	4,110219	0,83628	0,035473	6,99091	11942,57	91,45756	2743,727	0,005804	0,080755	0,05863	0,126879	0,24891	0,188061	280,0451	-51,3938	-1490,42
75600	5,70864E-07	4,31573	0,88507	0,037542	6,99091	11942,57	91,45756	2743,727	0,005804	0,080755	0,05863	0,126879	0,25098	0,188061	280,0305	-50,999	-1478,97
79200	5,70864E-07	4,521241	0,93159	0,039516	6,99091	11942,57	91,45756	2743,727	0,005804	0,080755	0,05863	0,126879	0,252953	0,188061	280,0168	-50,6282	-1468,22

82800	5,70864E-07	4,726752	0,97604	0,041401	6,99091	11942,57	91,45756	2743,727	0,005804	0,080755	0,05863	0,126879	0,254839	0,188061	280,004	-50,2789	-1458,09
86400	5,70864E-07	4,932263	1,0186	0,043206	6,99091	11942,57	91,45756	2743,727	0,005804	0,080755	0,05863	0,126879	0,256644	0,188061	279,9918	-49,9489	-1448,52
90000	5,70864E-07	5,137774	1,05942	0,044938	6,99091	11942,57	91,45756	2743,727	0,005804	0,080755	0,05863	0,126879	0,258376	0,188061	279,9803	-49,6365	-1439,46
93600	5,70864E-07	5,343285	1,09864	0,046602	6,99091	11942,57	91,45756	2743,727	0,005804	0,080755	0,05863	0,126879	0,260039	0,188061	279,9693	-49,34	-1430,86
97200	5,70864E-07	5,548796	1,13638	0,048203	6,99091	11942,57	91,45756	2743,727	0,005804	0,080755	0,05863	0,126879	0,26164	0,188061	279,9589	-49,0579	-1422,68
100800	5,70864E-07	5,754307	1,17275	0,049745	6,99091	11942,57	91,45756	2743,727	0,005804	0,080755	0,05863	0,126879	0,263183	0,188061	279,949	-48,7892	-1414,89
104400	5,70864E-07	5,959818	1,20784	0,051234	6,99091	11942,57	91,45756	2743,727	0,005804	0,080755	0,05863	0,126879	0,264671	0,188061	279,9396	-48,5327	-1407,45
108000	5,70864E-07	6,165328	1,24174	0,052672	6,99091	11942,57	91,45756	2743,727	0,005804	0,080755	0,05863	0,126879	0,266109	0,188061	279,9305	-48,2874	-1400,34
111600	5,70864E-07	6,370839	1,27453	0,054063	6,99091	11942,57	91,45756	2743,727	0,005804	0,080755	0,05863	0,126879	0,2675	0,188061	279,9219	-48,0525	-1393,52
115200	5,70864E-07	6,57635	1,30628	0,055409	6,99091	11942,57	91,45756	2743,727	0,005804	0,080755	0,05863	0,126879	0,268847	0,188061	279,9136	-47,8273	-1386,99
118800	5,70864E-07	6,781861	1,33705	0,056715	6,99091	11942,57	91,45756	2743,727	0,005804	0,080755	0,05863	0,126879	0,270152	0,188061	279,9056	-47,611	-1380,72
122400	5,70864E-07	6,987372	1,3669	0,057981	6,99091	11942,57	91,45756	2743,727	0,005804	0,080755	0,05863	0,126879	0,271418	0,188061	279,8979	-47,403	-1374,69
126000	5,70864E-07	7,192883	1,39589	0,05921	6,99091	11942,57	91,45756	2743,727	0,005804	0,080755	0,05863	0,126879	0,272648	0,188061	279,8905	-47,2027	-1368,88
129600	5,70864E-07	7,398394	1,42406	0,060405	6,99091	11942,57	91,45756	2743,727	0,005804	0,080755	0,05863	0,126879	0,273843	0,188061	279,8834	-47,0098	-1363,28
133200	5,70864E-07	7,603905	1,45146	0,061568	6,99091	11942,57	91,45756	2743,727	0,005804	0,080755	0,05863	0,126879	0,275005	0,188061	279,8766	-46,8236	-1357,88
136800	5,70864E-07	7,809416	1,47813	0,062699	6,99091	11942,57	91,45756	2743,727	0,005804	0,080755	0,05863	0,126879	0,276136	0,188061	279,8699	-46,6438	-1352,67
140400	5,70864E-07	8,014927	1,50411	0,063801	6,99091	11942,57	91,45756	2743,727	0,005804	0,080755	0,05863	0,126879	0,277238	0,188061	279,8635	-46,4699	-1347,63
144000	5,70864E-07	8,220438	1,52942	0,064874	6,99091	11942,57	91,45756	2743,727	0,005804	0,080755	0,05863	0,126879	0,278312	0,188061	279,8573	-46,3018	-1342,75
147600	5,70864E-07	8,425949	1,55412	0,065922	6,99091	11942,57	91,45756	2743,727	0,005804	0,080755	0,05863	0,126879	0,279359	0,188061	279,8513	-46,1389	-1338,03
151200	5,70864E-07	8,63146	1,57821	0,066944	6,99091	11942,57	91,45756	2743,727	0,005804	0,080755	0,05863	0,126879	0,280382	0,188061	279,8455	-45,9811	-1333,45
154800	5,70864E-07	8,836971	1,60174	0,067942	6,99091	11942,57	91,45756	2743,727	0,005804	0,080755	0,05863	0,126879	0,28138	0,188061	279,8398	-45,828	-1329,01
158400	5,70864E-07	9,042482	1,62473	0,068917	6,99091	11942,57	91,45756	2743,727	0,005804	0,080755	0,05863	0,126879	0,282355	0,188061	279,8344	-45,6794	-1324,7
162000	5,70864E-07	9,247993	1,64721	0,069871	6,99091	11942,57	91,45756	2743,727	0,005804	0,080755	0,05863	0,126879	0,283308	0,188061	279,829	-45,5351	-1320,52
165600	5,70864E-07	9,453504	1,66919	0,070803	6,99091	11942,57	91,45756	2743,727	0,005804	0,080755	0,05863	0,126879	0,28424	0,188061	279,8239	-45,3949	-1316,45
169200	5,70864E-07	9,659015	1,69069	0,071715	6,99091	11942,57	91,45756	2743,727	0,005804	0,080755	0,05863	0,126879	0,285153	0,188061	279,8188	-45,2585	-1312,5
172800	5,70864E-07	9,864526	1,71175	0,072608	6,99091	11942,57	91,45756	2743,727	0,005804	0,080755	0,05863	0,126879	0,286046	0,188061	279,8139	-45,1257	-1308,65

Table A. 2 Results analytical calculations for the optimal pile diameter (400 mm) under cooling conditions.

t	α	x	E(x)	Rb	Pr	Re	Nu	h	R p,f	R p	Req	R c	R tot	m	Tout	q	Q
3600	5,71E-07	0,205511	-2,15946	-0,0916	6,99091	11942,57	75,29502	2258,851	0,007049	0,080755	0,05863	0,126879	0,123084	0,188061	311,3079	185,5551	5381,099
7200	5,71E-07	0,411022	-1,46631	-0,0622	6,99091	11942,57	75,29502	2258,851	0,007049	0,080755	0,05863	0,126879	0,152486	0,188061	312,4849	153,6365	4455,459
10800	5,71E-07	0,616533	-1,06084	-0,045	6,99091	11942,57	75,29502	2258,851	0,007049	0,080755	0,05863	0,126879	0,169685	0,188061	313,0028	139,5904	4048,123
14400	5,71E-07	0,822044	-0,77316	-0,0328	6,99091	11942,57	75,29502	2258,851	0,007049	0,080755	0,05863	0,126879	0,181888	0,188061	313,3163	131,0873	3801,531
18000	5,71E-07	1,027555	-0,55002	-0,02333	6,99091	11942,57	75,29502	2258,851	0,007049	0,080755	0,05863	0,126879	0,191353	0,188061	313,5344	125,1729	3630,015
21600	5,71E-07	1,233066	-0,3677	-0,0156	6,99091	11942,57	75,29502	2258,851	0,007049	0,080755	0,05863	0,126879	0,199087	0,188061	313,6985	120,7226	3500,957
25200	5,71E-07	1,438577	-0,21355	-0,00906	6,99091	11942,57	75,29502	2258,851	0,007049	0,080755	0,05863	0,126879	0,205625	0,188061	313,8284	117,1996	3398,79
28800	5,71E-07	1,644088	-0,08001	-0,00339	6,99091	11942,57	75,29502	2258,851	0,007049	0,080755	0,05863	0,126879	0,211289	0,188061	313,935	114,31	3314,99
32400	5,71E-07	1,849599	0,037769	0,001602	6,99091	11942,57	75,29502	2258,851	0,007049	0,080755	0,05863	0,126879	0,216285	0,188061	314,0247	111,8769	3244,43
36000	5,71E-07	2,055109	0,143129	0,006071	6,99091	11942,57	75,29502	2258,851	0,007049	0,080755	0,05863	0,126879	0,220755	0,188061	314,1018	109,7866	3183,81
39600	5,71E-07	2,26062	0,238439	0,010114	6,99091	11942,57	75,29502	2258,851	0,007049	0,080755	0,05863	0,126879	0,224797	0,188061	314,1691	107,9618	3130,892
43200	5,71E-07	2,466131	0,325451	0,013805	6,99091	11942,57	75,29502	2258,851	0,007049	0,080755	0,05863	0,126879	0,228488	0,188061	314,2286	106,3481	3084,094
46800	5,71E-07	2,671642	0,405493	0,0172	6,99091	11942,57	75,29502	2258,851	0,007049	0,080755	0,05863	0,126879	0,231883	0,188061	314,2818	104,9056	3042,263
50400	5,71E-07	2,877153	0,479601	0,020344	6,99091	11942,57	75,29502	2258,851	0,007049	0,080755	0,05863	0,126879	0,235027	0,188061	314,3297	103,6046	3004,532
54000	5,71E-07	3,082664	0,548594	0,02327	6,99091	11942,57	75,29502	2258,851	0,007049	0,080755	0,05863	0,126879	0,237953	0,188061	314,3733	102,422	2970,238
57600	5,71E-07	3,288175	0,613133	0,026008	6,99091	11942,57	75,29502	2258,851	0,007049	0,080755	0,05863	0,126879	0,240691	0,188061	314,4132	101,3399	2938,858
61200	5,71E-07	3,493686	0,673757	0,028579	6,99091	11942,57	75,29502	2258,851	0,007049	0,080755	0,05863	0,126879	0,243263	0,188061	314,45	100,3441	2909,98
64800	5,71E-07	3,699197	0,730916	0,031004	6,99091	11942,57	75,29502	2258,851	0,007049	0,080755	0,05863	0,126879	0,245687	0,188061	314,4839	99,42304	2883,268
68400	5,71E-07	3,904708	0,784983	0,033297	6,99091	11942,57	75,29502	2258,851	0,007049	0,080755	0,05863	0,126879	0,247981	0,188061	314,5155	98,56717	2858,448
72000	5,71E-07	4,110219	0,836276	0,035473	6,99091	11942,57	75,29502	2258,851	0,007049	0,080755	0,05863	0,126879	0,250156	0,188061	314,5449	97,76873	2835,293
75600	5,71E-07	4,31573	0,885066	0,037542	6,99091	11942,57	75,29502	2258,851	0,007049	0,080755	0,05863	0,126879	0,252226	0,188061	314,5725	97,02116	2813,614
79200	5,71E-07	4,521241	0,931586	0,039516	6,99091	11942,57	75,29502	2258,851	0,007049	0,080755	0,05863	0,126879	0,254199	0,188061	314,5984	96,31895	2793,249
82800	5,71E-07	4,726752	0,976038	0,041401	6,99091	11942,57	75,29502	2258,851	0,007049	0,080755	0,05863	0,126879	0,256085	0,188061	314,6228	95,65739	2774,064
86400	5,71E-07	4,932263	1,018598	0,043206	6,99091	11942,57	75,29502	2258,851	0,007049	0,080755	0,05863	0,126879	0,25789	0,188061	314,6458	95,03244	2755,941
90000	5,71E-07	5,137774	1,05942	0,044938	6,99091	11942,57	75,29502	2258,851	0,007049	0,080755	0,05863	0,126879	0,259621	0,188061	314,6676	94,44064	2738,779
93600	5,71E-07	5,343285	1,098641	0,046602	6,99091	11942,57	75,29502	2258,851	0,007049	0,080755	0,05863	0,126879	0,261285	0,188061	314,6883	93,87895	2722,49

97200	5,71E-07	5,548796	1,136381	0,048203	6,99091	11942,57	75,29502	2258,851	0,007049	0,080755	0,05863	0,126879	0,262886	0,188061	314,708	93,34474	2706,997
100800	5,71E-07	5,754307	1,172749	0,049745	6,99091	11942,57	75,29502	2258,851	0,007049	0,080755	0,05863	0,126879	0,264429	0,188061	314,7268	92,83568	2692,235
104400	5,71E-07	5,959818	1,20784	0,051234	6,99091	11942,57	75,29502	2258,851	0,007049	0,080755	0,05863	0,126879	0,265917	0,188061	314,7447	92,34972	2678,142
108000	5,71E-07	6,165328	1,241741	0,052672	6,99091	11942,57	75,29502	2258,851	0,007049	0,080755	0,05863	0,126879	0,267355	0,188061	314,7619	91,88504	2664,666
111600	5,71E-07	6,370839	1,274531	0,054063	6,99091	11942,57	75,29502	2258,851	0,007049	0,080755	0,05863	0,126879	0,268746	0,188061	314,7783	91,44003	2651,761
115200	5,71E-07	6,57635	1,30628	0,055409	6,99091	11942,57	75,29502	2258,851	0,007049	0,080755	0,05863	0,126879	0,270093	0,188061	314,794	91,01323	2639,384
118800	5,71E-07	6,781861	1,337052	0,056715	6,99091	11942,57	75,29502	2258,851	0,007049	0,080755	0,05863	0,126879	0,271398	0,188061	314,8091	90,60336	2627,497
122400	5,71E-07	6,987372	1,366905	0,057981	6,99091	11942,57	75,29502	2258,851	0,007049	0,080755	0,05863	0,126879	0,272664	0,188061	314,8237	90,20923	2616,068
126000	5,71E-07	7,192883	1,395892	0,05921	6,99091	11942,57	75,29502	2258,851	0,007049	0,080755	0,05863	0,126879	0,273894	0,188061	314,8377	89,8298	2605,064
129600	5,71E-07	7,398394	1,424063	0,060405	6,99091	11942,57	75,29502	2258,851	0,007049	0,080755	0,05863	0,126879	0,275089	0,188061	314,8511	89,46411	2594,459
133200	5,71E-07	7,603905	1,451462	0,061568	6,99091	11942,57	75,29502	2258,851	0,007049	0,080755	0,05863	0,126879	0,276251	0,188061	314,8641	89,11127	2584,227
136800	5,71E-07	7,809416	1,47813	0,062699	6,99091	11942,57	75,29502	2258,851	0,007049	0,080755	0,05863	0,126879	0,277382	0,188061	314,8767	88,77052	2574,345
140400	5,71E-07	8,014927	1,504106	0,063801	6,99091	11942,57	75,29502	2258,851	0,007049	0,080755	0,05863	0,126879	0,278484	0,188061	314,8889	88,4411	2564,792
144000	5,71E-07	8,220438	1,529423	0,064874	6,99091	11942,57	75,29502	2258,851	0,007049	0,080755	0,05863	0,126879	0,279558	0,188061	314,9006	88,12238	2555,549
147600	5,71E-07	8,425949	1,554116	0,065922	6,99091	11942,57	75,29502	2258,851	0,007049	0,080755	0,05863	0,126879	0,280605	0,188061	314,912	87,81373	2546,598
151200	5,71E-07	8,63146	1,578214	0,066944	6,99091	11942,57	75,29502	2258,851	0,007049	0,080755	0,05863	0,126879	0,281627	0,188061	314,923	87,51459	2537,923
154800	5,71E-07	8,836971	1,601744	0,067942	6,99091	11942,57	75,29502	2258,851	0,007049	0,080755	0,05863	0,126879	0,282626	0,188061	314,9337	87,22446	2529,509
158400	5,71E-07	9,042482	1,624734	0,068917	6,99091	11942,57	75,29502	2258,851	0,007049	0,080755	0,05863	0,126879	0,283601	0,188061	314,9441	86,94284	2521,342
162000	5,71E-07	9,247993	1,647207	0,069871	6,99091	11942,57	75,29502	2258,851	0,007049	0,080755	0,05863	0,126879	0,284554	0,188061	314,9542	86,66931	2513,41
165600	5,71E-07	9,453504	1,669185	0,070803	6,99091	11942,57	75,29502	2258,851	0,007049	0,080755	0,05863	0,126879	0,285486	0,188061	314,964	86,40345	2505,7
169200	5,71E-07	9,659015	1,690692	0,071715	6,99091	11942,57	75,29502	2258,851	0,007049	0,080755	0,05863	0,126879	0,286398	0,188061	314,9735	86,14488	2498,202
172800	5,71E-07	9,864526	1,711745	0,072608	6,99091	11942,57	75,29502	2258,851	0,007049	0,080755	0,05863	0,126879	0,287292	0,188061	314,9828	85,89325	2490,904

Table A. 3 Results analytical calculations for the optimal heat exchanger diameter (26 mm) under heating conditions.

t	α	x	E(x)	Rb	Pr	v	Re	Nu	H	R(p,f)	Rp	r(eq)	Rc	R tot	m	Tout	q	Q
3600	5,70864E-07	0,205511	-2,1595	-0,0916	6,99091	0,35503	9186,594	74,14211	1710,972	0,007159	0,075145	0,065483	0,115449	0,106154	0,188061	282,2165	-110,281	-3198,16
7200	5,70864E-07	0,411022	-1,4663	-0,0622	6,99091	0,35503	9186,594	74,14211	1710,972	0,007159	0,075145	0,065483	0,115449	0,135555	0,188061	281,4401	-89,2254	-2587,54
10800	5,70864E-07	0,616533	-1,0608	-0,045	6,99091	0,35503	9186,594	74,14211	1710,972	0,007159	0,075145	0,065483	0,115449	0,152754	0,188061	281,1095	-80,2613	-2327,58
14400	5,70864E-07	0,822044	-0,7732	-0,0328	6,99091	0,35503	9186,594	74,14211	1710,972	0,007159	0,075145	0,065483	0,115449	0,164957	0,188061	280,9126	-74,9208	-2172,7
18000	5,70864E-07	1,027555	-0,55	-0,02333	6,99091	0,35503	9186,594	74,14211	1710,972	0,007159	0,075145	0,065483	0,115449	0,174422	0,188061	280,777	-71,2438	-2066,07
21600	5,70864E-07	1,233066	-0,3677	-0,0156	6,99091	0,35503	9186,594	74,14211	1710,972	0,007159	0,075145	0,065483	0,115449	0,182156	0,188061	280,6757	-68,4971	-1986,42
25200	5,70864E-07	1,438577	-0,2135	-0,00906	6,99091	0,35503	9186,594	74,14211	1710,972	0,007159	0,075145	0,065483	0,115449	0,188694	0,188061	280,596	-66,3348	-1923,71
28800	5,70864E-07	1,644088	-0,08	-0,00339	6,99091	0,35503	9186,594	74,14211	1710,972	0,007159	0,075145	0,065483	0,115449	0,194358	0,188061	280,5309	-64,5691	-1872,5
32400	5,70864E-07	1,849599	0,03777	0,001602	6,99091	0,35503	9186,594	74,14211	1710,972	0,007159	0,075145	0,065483	0,115449	0,199355	0,188061	280,4763	-63,0879	-1829,55
36000	5,70864E-07	2,055109	0,14313	0,006071	6,99091	0,35503	9186,594	74,14211	1710,972	0,007159	0,075145	0,065483	0,115449	0,203824	0,188061	280,4295	-61,8194	-1792,76
39600	5,70864E-07	2,26062	0,23844	0,010114	6,99091	0,35503	9186,594	74,14211	1710,972	0,007159	0,075145	0,065483	0,115449	0,207866	0,188061	280,3888	-60,715	-1760,73
43200	5,70864E-07	2,466131	0,32545	0,013805	6,99091	0,35503	9186,594	74,14211	1710,972	0,007159	0,075145	0,065483	0,115449	0,211557	0,188061	280,3529	-59,7407	-1732,48
46800	5,70864E-07	2,671642	0,40549	0,0172	6,99091	0,35503	9186,594	74,14211	1710,972	0,007159	0,075145	0,065483	0,115449	0,214953	0,188061	280,3208	-58,8716	-1707,28
50400	5,70864E-07	2,877153	0,4796	0,020344	6,99091	0,35503	9186,594	74,14211	1710,972	0,007159	0,075145	0,065483	0,115449	0,218096	0,188061	280,292	-58,0892	-1684,59
54000	5,70864E-07	3,082664	0,54859	0,02327	6,99091	0,35503	9186,594	74,14211	1710,972	0,007159	0,075145	0,065483	0,115449	0,221023	0,188061	280,2658	-57,3793	-1664
57600	5,70864E-07	3,288175	0,61313	0,026008	6,99091	0,35503	9186,594	74,14211	1710,972	0,007159	0,075145	0,065483	0,115449	0,22376	0,188061	280,2419	-56,7307	-1645,19
61200	5,70864E-07	3,493686	0,67376	0,028579	6,99091	0,35503	9186,594	74,14211	1710,972	0,007159	0,075145	0,065483	0,115449	0,226332	0,188061	280,2199	-56,1347	-1627,91
64800	5,70864E-07	3,699197	0,73092	0,031004	6,99091	0,35503	9186,594	74,14211	1710,972	0,007159	0,075145	0,065483	0,115449	0,228756	0,188061	280,1996	-55,5841	-1611,94
68400	5,70864E-07	3,904708	0,78498	0,033297	6,99091	0,35503	9186,594	74,14211	1710,972	0,007159	0,075145	0,065483	0,115449	0,23105	0,188061	280,1807	-55,0732	-1597,12
72000	5,70864E-07	4,110219	0,83628	0,035473	6,99091	0,35503	9186,594	74,14211	1710,972	0,007159	0,075145	0,065483	0,115449	0,233225	0,188061	280,1632	-54,597	-1583,31
75600	5,70864E-07	4,31573	0,88507	0,037542	6,99091	0,35503	9186,594	74,14211	1710,972	0,007159	0,075145	0,065483	0,115449	0,235295	0,188061	280,1468	-54,1517	-1570,4
79200	5,70864E-07	4,521241	0,93159	0,039516	6,99091	0,35503	9186,594	74,14211	1710,972	0,007159	0,075145	0,065483	0,115449	0,237268	0,188061	280,1314	-53,7338	-1558,28
82800	5,70864E-07	4,726752	0,97604	0,041401	6,99091	0,35503	9186,594	74,14211	1710,972	0,007159	0,075145	0,065483	0,115449	0,239154	0,188061	280,1169	-53,3405	-1546,87
86400	5,70864E-07	4,932263	1,0186	0,043206	6,99091	0,35503	9186,594	74,14211	1710,972	0,007159	0,075145	0,065483	0,115449	0,240959	0,188061	280,1032	-52,9693	-1536,11
90000	5,70864E-07	5,137774	1,05942	0,044938	6,99091	0,35503	9186,594	74,14211	1710,972	0,007159	0,075145	0,065483	0,115449	0,242691	0,188061	280,0902	-52,618	-1525,92
93600	5,70864E-07	5,343285	1,09864	0,046602	6,99091	0,35503	9186,594	74,14211	1710,972	0,007159	0,075145	0,065483	0,115449	0,244354	0,188061	280,0779	-52,2849	-1516,26

97200	5,70864E-07	5,548796	1,13638	0,048203	6,99091	0,35503	9186,594	74,14211	1710,972	0,007159	0,075145	0,065483	0,115449	0,245955	0,188061	280,0663	-51,9683	-1507,08
100800	5,70864E-07	5,754307	1,17275	0,049745	6,99091	0,35503	9186,594	74,14211	1710,972	0,007159	0,075145	0,065483	0,115449	0,247498	0,188061	280,0551	-51,6669	-1498,34
104400	5,70864E-07	5,959818	1,20784	0,051234	6,99091	0,35503	9186,594	74,14211	1710,972	0,007159	0,075145	0,065483	0,115449	0,248986	0,188061	280,0445	-51,3793	-1490
108000	5,70864E-07	6,165328	1,24174	0,052672	6,99091	0,35503	9186,594	74,14211	1710,972	0,007159	0,075145	0,065483	0,115449	0,250424	0,188061	280,0344	-51,1045	-1482,03
111600	5,70864E-07	6,370839	1,27453	0,054063	6,99091	0,35503	9186,594	74,14211	1710,972	0,007159	0,075145	0,065483	0,115449	0,251815	0,188061	280,0247	-50,8415	-1474,4
115200	5,70864E-07	6,57635	1,30628	0,055409	6,99091	0,35503	9186,594	74,14211	1710,972	0,007159	0,075145	0,065483	0,115449	0,253162	0,188061	280,0154	-50,5894	-1467,09
118800	5,70864E-07	6,781861	1,33705	0,056715	6,99091	0,35503	9186,594	74,14211	1710,972	0,007159	0,075145	0,065483	0,115449	0,254467	0,188061	280,0065	-50,3474	-1460,08
122400	5,70864E-07	6,987372	1,3669	0,057981	6,99091	0,35503	9186,594	74,14211	1710,972	0,007159	0,075145	0,065483	0,115449	0,255733	0,188061	279,9979	-50,1149	-1453,33
126000	5,70864E-07	7,192883	1,39589	0,05921	6,99091	0,35503	9186,594	74,14211	1710,972	0,007159	0,075145	0,065483	0,115449	0,256963	0,188061	279,9897	-49,8911	-1446,84
129600	5,70864E-07	7,398394	1,42406	0,060405	6,99091	0,35503	9186,594	74,14211	1710,972	0,007159	0,075145	0,065483	0,115449	0,258158	0,188061	279,9817	-49,6756	-1440,59
133200	5,70864E-07	7,603905	1,45146	0,061568	6,99091	0,35503	9186,605	74,14218	1710,973	0,007159	0,075145	0,065483	0,115449	0,25932	0,188061	279,9741	-49,4677	-1434,56
136800	5,70864E-07	7,809416	1,47813	0,062699	6,99091	0,35503	9186,605	74,14218	1710,973	0,007159	0,075145	0,065483	0,115449	0,260451	0,188061	279,9667	-49,2671	-1428,75
140400	5,70864E-07	8,014927	1,50411	0,063801	6,99091	0,35503	9186,605	74,14218	1710,973	0,007159	0,075145	0,065483	0,115449	0,261553	0,188061	279,9595	-49,0732	-1423,12
144000	5,70864E-07	8,220438	1,52942	0,064874	6,99091	0,35503	9186,605	74,14218	1710,973	0,007159	0,075145	0,065483	0,115449	0,262627	0,188061	279,9526	-48,8857	-1417,69
147600	5,70864E-07	8,425949	1,55412	0,065922	6,99091	0,35503	9186,605	74,14218	1710,973	0,007159	0,075145	0,065483	0,115449	0,263674	0,188061	279,9459	-48,7042	-1412,42
151200	5,70864E-07	8,63146	1,57821	0,066944	6,99091	0,35503	9186,605	74,14218	1710,973	0,007159	0,075145	0,065483	0,115449	0,264696	0,188061	279,9394	-48,5284	-1407,32
154800	5,70864E-07	8,836971	1,60174	0,067942	6,99091	0,35503	9186,605	74,14218	1710,973	0,007159	0,075145	0,065483	0,115449	0,265695	0,188061	279,9331	-48,3579	-1402,38
158400	5,70864E-07	9,042482	1,62473	0,068917	6,99091	0,35503	9186,605	74,14218	1710,973	0,007159	0,075145	0,065483	0,115449	0,26667	0,188061	279,927	-48,1925	-1397,58
162000	5,70864E-07	9,247993	1,64721	0,069871	6,99091	0,35503	9186,605	74,14218	1710,973	0,007159	0,075145	0,065483	0,115449	0,267623	0,188061	279,9211	-48,0319	-1392,93
165600	5,70864E-07	9,453504	1,66919	0,070803	6,99091	0,35503	9186,605	74,14218	1710,973	0,007159	0,075145	0,065483	0,115449	0,268555	0,188061	279,9154	-47,8759	-1388,4
169200	5,70864E-07	9,659015	1,69069	0,071715	6,99091	0,35503	9186,605	74,14218	1710,973	0,007159	0,075145	0,065483	0,115449	0,269468	0,188061	279,9098	-47,7242	-1384
172800	5,70864E-07	9,864526	1,71175	0,072608	6,99091	0,35503	9186,605	74,14218	1710,973	0,007159	0,075145	0,065483	0,115449	0,270361	0,188061	279,9043	-47,5766	-1379,72

Table A. 4 Results analytical calculations for the optimal heat exchanger diameter (26 mm) under cooling conditions.

t	α	x	E(x)	Rb	Pr	v	Re	Nu	H	R p,f	R p	Req	R c	R tot	m	Tout	q	Q
3600	5,70864E-07	0,205511	-2,15946	-0,0916	6,99091	0,35503	9186,594	61,03958	1408,606	0,008696	0,075145	0,065483	0,115449	0,10769	0,188061	310,4728	208,2027	6037,88
7200	5,70864E-07	0,411022	-1,46631	-0,0622	6,99091	0,35503	9186,594	61,03958	1408,606	0,008696	0,075145	0,065483	0,115449	0,137092	0,188061	311,9241	168,8434	4896,46
10800	5,70864E-07	0,616533	-1,06084	-0,045	6,99091	0,35503	9186,594	61,03958	1408,606	0,008696	0,075145	0,065483	0,115449	0,154291	0,188061	312,5441	152,0313	4408,909
14400	5,70864E-07	0,822044	-0,77316	-0,0328	6,99091	0,35503	9186,594	61,03958	1408,606	0,008696	0,075145	0,065483	0,115449	0,166494	0,188061	312,914	141,9994	4117,983
18000	5,70864E-07	1,027555	-0,55002	-0,02333	6,99091	0,35503	9186,594	61,03958	1408,606	0,008696	0,075145	0,065483	0,115449	0,175959	0,188061	313,1689	135,0854	3917,476
21600	5,70864E-07	1,233066	-0,3677	-0,0156	6,99091	0,35503	9186,594	61,03958	1408,606	0,008696	0,075145	0,065483	0,115449	0,183692	0,188061	313,3595	129,9169	3767,59
25200	5,70864E-07	1,438577	-0,21355	-0,00906	6,99091	0,35503	9186,594	61,03958	1408,606	0,008696	0,075145	0,065483	0,115449	0,190231	0,188061	313,5096	125,8459	3649,531
28800	5,70864E-07	1,644088	-0,08001	-0,00339	6,99091	0,35503	9186,594	61,03958	1408,606	0,008696	0,075145	0,065483	0,115449	0,195895	0,188061	313,6322	122,5202	3553,086
32400	5,70864E-07	1,849599	0,037769	0,001602	6,99091	0,35503	9186,594	61,03958	1408,606	0,008696	0,075145	0,065483	0,115449	0,200891	0,188061	313,7351	119,7293	3472,15
36000	5,70864E-07	2,055109	0,143129	0,006071	6,99091	0,35503	9186,594	61,03958	1408,606	0,008696	0,075145	0,065483	0,115449	0,20536	0,188061	313,8233	117,3384	3402,813
39600	5,70864E-07	2,26062	0,238439	0,010114	6,99091	0,35503	9186,594	61,03958	1408,606	0,008696	0,075145	0,065483	0,115449	0,209403	0,188061	313,9001	115,2563	3342,433
43200	5,70864E-07	2,466131	0,325451	0,013805	6,99091	0,35503	9186,594	61,03958	1408,606	0,008696	0,075145	0,065483	0,115449	0,213094	0,188061	313,9678	113,419	3289,152
46800	5,70864E-07	2,671642	0,405493	0,0172	6,99091	0,35503	9186,594	61,03958	1408,606	0,008696	0,075145	0,065483	0,115449	0,216489	0,188061	314,0283	111,7799	3241,616
50400	5,70864E-07	2,877153	0,479601	0,020344	6,99091	0,35503	9186,594	61,03958	1408,606	0,008696	0,075145	0,065483	0,115449	0,219633	0,188061	314,0827	110,3039	3198,813
54000	5,70864E-07	3,082664	0,548594	0,02327	6,99091	0,35503	9186,594	61,03958	1408,606	0,008696	0,075145	0,065483	0,115449	0,222559	0,188061	314,1321	108,9644	3159,969
57600	5,70864E-07	3,288175	0,613133	0,026008	6,99091	0,35503	9186,594	61,03958	1408,606	0,008696	0,075145	0,065483	0,115449	0,225297	0,188061	314,1772	107,7406	3124,477
61200	5,70864E-07	3,493686	0,673757	0,028579	6,99091	0,35503	9186,594	61,03958	1408,606	0,008696	0,075145	0,065483	0,115449	0,227868	0,188061	314,2187	106,6157	3091,856
64800	5,70864E-07	3,699197	0,730916	0,031004	6,99091	0,35503	9186,594	61,03958	1408,606	0,008696	0,075145	0,065483	0,115449	0,230293	0,188061	314,257	105,5765	3061,717
68400	5,70864E-07	3,904708	0,784983	0,033297	6,99091	0,35503	9186,594	61,03958	1408,606	0,008696	0,075145	0,065483	0,115449	0,232586	0,188061	314,2926	104,6119	3033,745
72000	5,70864E-07	4,110219	0,836276	0,035473	6,99091	0,35503	9186,594	61,03958	1408,606	0,008696	0,075145	0,065483	0,115449	0,234762	0,188061	314,3257	103,713	3007,676
75600	5,70864E-07	4,31573	0,885066	0,037542	6,99091	0,35503	9186,594	61,03958	1408,606	0,008696	0,075145	0,065483	0,115449	0,236832	0,188061	314,3567	102,8721	2983,291
79200	5,70864E-07	4,521241	0,931586	0,039516	6,99091	0,35503	9186,594	61,03958	1408,606	0,008696	0,075145	0,065483	0,115449	0,238805	0,188061	314,3858	102,083	2960,407
82800	5,70864E-07	4,726752	0,976038	0,041401	6,99091	0,35503	9186,594	61,03958	1408,606	0,008696	0,075145	0,065483	0,115449	0,24069	0,188061	314,4132	101,3402	2938,866
86400	5,70864E-07	4,932263	1,018598	0,043206	6,99091	0,35503	9186,594	61,03958	1408,606	0,008696	0,075145	0,065483	0,115449	0,242496	0,188061	314,4391	100,6391	2918,533
90000	5,70864E-07	5,137774	1,05942	0,044938	6,99091	0,35503	9186,594	61,03958	1408,606	0,008696	0,075145	0,065483	0,115449	0,244227	0,188061	314,4635	99,97562	2899,293
93600	5,70864E-07	5,343285	1,098641	0,046602	6,99091	0,35503	9186,594	61,03958	1408,606	0,008696	0,075145	0,065483	0,115449	0,245891	0,188061	314,4867	99,34638	2881,045

97200	5,70864E-07	5,548796	1,136381	0,048203	6,99091	0,35503	9186,594	61,03958	1408,606	0,008696	0,075145	0,065483	0,115449	0,247492	0,188061	314,5088	98,74833	2863,702
100800	5,70864E-07	5,754307	1,172749	0,049745	6,99091	0,35503	9186,594	61,03958	1408,606	0,008696	0,075145	0,065483	0,115449	0,249034	0,188061	314,5298	98,1788	2847,185
104400	5,70864E-07	5,959818	1,20784	0,051234	6,99091	0,35503	9186,594	61,03958	1408,606	0,008696	0,075145	0,065483	0,115449	0,250523	0,188061	314,5498	97,63546	2831,428
108000	5,70864E-07	6,165328	1,241741	0,052672	6,99091	0,35503	9186,594	61,03958	1408,606	0,008696	0,075145	0,065483	0,115449	0,251961	0,188061	314,569	97,11621	2816,37
111600	5,70864E-07	6,370839	1,274531	0,054063	6,99091	0,35503	9186,594	61,03958	1408,606	0,008696	0,075145	0,065483	0,115449	0,253352	0,188061	314,5873	96,61923	2801,958
115200	5,70864E-07	6,57635	1,30628	0,055409	6,99091	0,35503	9186,594	61,03958	1408,606	0,008696	0,075145	0,065483	0,115449	0,254698	0,188061	314,6049	96,14284	2788,142
118800	5,70864E-07	6,781861	1,337052	0,056715	6,99091	0,35503	9186,594	61,03958	1408,606	0,008696	0,075145	0,065483	0,115449	0,256004	0,188061	314,6217	95,68558	2774,882
122400	5,70864E-07	6,987372	1,366905	0,057981	6,99091	0,35503	9186,594	61,03958	1408,606	0,008696	0,075145	0,065483	0,115449	0,25727	0,188061	314,6379	95,24611	2762,137
126000	5,70864E-07	7,192883	1,395892	0,05921	6,99091	0,35503	9186,594	61,03958	1408,606	0,008696	0,075145	0,065483	0,115449	0,2585	0,188061	314,6535	94,82322	2749,873
129600	5,70864E-07	7,398394	1,424063	0,060405	6,99091	0,35503	9186,594	61,03958	1408,606	0,008696	0,075145	0,065483	0,115449	0,259695	0,188061	314,6685	94,41583	2738,059
133200	5,70864E-07	7,603905	1,451462	0,061568	6,99091	0,35503	9186,605	61,03964	1408,607	0,008696	0,075145	0,065483	0,115449	0,260857	0,188061	314,683	94,02295	2726,665
136800	5,70864E-07	7,809416	1,47813	0,062699	6,99091	0,35503	9186,605	61,03964	1408,607	0,008696	0,075145	0,065483	0,115449	0,261988	0,188061	314,697	93,64367	2715,666
140400	5,70864E-07	8,014927	1,504106	0,063801	6,99091	0,35503	9186,605	61,03964	1408,607	0,008696	0,075145	0,065483	0,115449	0,26309	0,188061	314,7105	93,27717	2705,038
144000	5,70864E-07	8,220438	1,529423	0,064874	6,99091	0,35503	9186,605	61,03964	1408,607	0,008696	0,075145	0,065483	0,115449	0,264164	0,188061	314,7236	92,92271	2694,758
147600	5,70864E-07	8,425949	1,554116	0,065922	6,99091	0,35503	9186,605	61,03964	1408,607	0,008696	0,075145	0,065483	0,115449	0,265211	0,188061	314,7363	92,57958	2684,808
151200	5,70864E-07	8,63146	1,578214	0,066944	6,99091	0,35503	9186,605	61,03964	1408,607	0,008696	0,075145	0,065483	0,115449	0,266233	0,188061	314,7485	92,24715	2675,167
154800	5,70864E-07	8,836971	1,601744	0,067942	6,99091	0,35503	9186,605	61,03964	1408,607	0,008696	0,075145	0,065483	0,115449	0,267231	0,188061	314,7604	91,92485	2665,821
158400	5,70864E-07	9,042482	1,624734	0,068917	6,99091	0,35503	9186,605	61,03964	1408,607	0,008696	0,075145	0,065483	0,115449	0,268206	0,188061	314,7719	91,61212	2656,751
162000	5,70864E-07	9,247993	1,647207	0,069871	6,99091	0,35503	9186,605	61,03964	1408,607	0,008696	0,075145	0,065483	0,115449	0,26916	0,188061	314,7831	91,30847	2647,946
165600	5,70864E-07	9,453504	1,669185	0,070803	6,99091	0,35503	9186,605	61,03964	1408,607	0,008696	0,075145	0,065483	0,115449	0,270092	0,188061	314,794	91,01344	2639,39
169200	5,70864E-07	9,659015	1,690692	0,071715	6,99091	0,35503	9186,605	61,03964	1408,607	0,008696	0,075145	0,065483	0,115449	0,271004	0,188061	314,8046	90,72658	2631,071
172800	5,70864E-07	9,864526	1,711745	0,072608	6,99091	0,35503	9186,605	61,03964	1408,607	0,008696	0,075145	0,065483	0,115449	0,271897	0,188061	314,8149	90,44752	2622,978

Table A. 5 Results analytical calculations for the optimal distance between pipe and concrete (0.02 mm) under heating conditions.

t	a	x	E(x)	Rsol	Pr	v	Re	Nu(ref)	h	R fluide	R tube	R eq	R beton	R tot	m	T	q	Q
3600	5,71E-07	0,205511	-2,15946	-0,0916	6,99091	1,22449	12186,298	92,94772	3983,474	0,005711	0,12908	0,05831	0,127446	0,170638	0,188061	280,8296	-72,6698	-2107,42
7200	5,71E-07	0,411022	-1,46631	-0,0622	6,99091	1,22449	12186,298	92,94772	3983,474	0,005711	0,12908	0,05831	0,127446	0,200039	0,188061	280,469	-62,8902	-1823,82
10800	5,71E-07	0,616533	-1,06084	-0,045	6,99091	1,22449	12186,298	92,94772	3983,474	0,005711	0,12908	0,05831	0,127446	0,217238	0,188061	280,2998	-58,3006	-1690,72
14400	5,71E-07	0,822044	-0,77316	-0,0328	6,99091	1,22449	12186,298	92,94772	3983,474	0,005711	0,12908	0,05831	0,127446	0,229441	0,188061	280,1939	-55,4306	-1607,49
18000	5,71E-07	1,027555	-0,55002	-0,02333	6,99091	1,22449	12186,298	92,94772	3983,474	0,005711	0,12908	0,05831	0,127446	0,238906	0,188061	280,1187	-53,3918	-1548,36
21600	5,71E-07	1,233066	-0,3677	-0,0156	6,99091	1,22449	12186,298	92,94772	3983,474	0,005711	0,12908	0,05831	0,127446	0,24664	0,188061	280,0613	-51,8341	-1503,19
25200	5,71E-07	1,438577	-0,21355	-0,00906	6,99091	1,22449	12186,298	92,94772	3983,474	0,005711	0,12908	0,05831	0,127446	0,253178	0,188061	280,0153	-50,5863	-1467
28800	5,71E-07	1,644088	-0,08001	-0,00339	6,99091	1,22449	12186,298	92,94772	3983,474	0,005711	0,12908	0,05831	0,127446	0,258843	0,188061	279,9772	-49,5529	-1437,03
32400	5,71E-07	1,849599	0,03777	0,001602	6,99091	1,22449	12186,298	92,94772	3983,474	0,005711	0,12908	0,05831	0,127446	0,263839	0,188061	279,9449	-48,6759	-1411,6
36000	5,71E-07	2,055109	0,14313	0,006071	6,99091	1,22449	12186,298	92,94772	3983,474	0,005711	0,12908	0,05831	0,127446	0,268308	0,188061	279,9169	-47,9172	-1389,6
39600	5,71E-07	2,26062	0,23844	0,010114	6,99091	1,22449	12186,298	92,94772	3983,474	0,005711	0,12908	0,05831	0,127446	0,272351	0,188061	279,8923	-47,251	-1370,28
43200	5,71E-07	2,466131	0,32545	0,013805	6,99091	1,22449	12186,298	92,94772	3983,474	0,005711	0,12908	0,05831	0,127446	0,276041	0,188061	279,8705	-46,6588	-1353,11
46800	5,71E-07	2,671642	0,40549	0,0172	6,99091	1,22449	12186,298	92,94772	3983,474	0,005711	0,12908	0,05831	0,127446	0,279437	0,188061	279,8509	-46,127	-1337,68
50400	5,71E-07	2,877153	0,4796	0,020344	6,99091	1,22449	12186,298	92,94772	3983,474	0,005711	0,12908	0,05831	0,127446	0,28258	0,188061	279,8331	-45,6453	-1323,71
54000	5,71E-07	3,082664	0,54859	0,02327	6,99091	1,22449	12186,298	92,94772	3983,474	0,005711	0,12908	0,05831	0,127446	0,285507	0,188061	279,8169	-45,2058	-1310,97
57600	5,71E-07	3,288175	0,61313	0,026008	6,99091	1,22449	12186,298	92,94772	3983,474	0,005711	0,12908	0,05831	0,127446	0,288244	0,188061	279,802	-44,8023	-1299,27
61200	5,71E-07	3,493686	0,67376	0,028579	6,99091	1,22449	12186,298	92,94772	3983,474	0,005711	0,12908	0,05831	0,127446	0,290816	0,188061	279,7883	-44,4297	-1288,46
64800	5,71E-07	3,699197	0,73092	0,031004	6,99091	1,22449	12186,298	92,94772	3983,474	0,005711	0,12908	0,05831	0,127446	0,29324	0,188061	279,7755	-44,0841	-1278,44
68400	5,71E-07	3,904708	0,78498	0,033297	6,99091	1,22449	12186,298	92,94772	3983,474	0,005711	0,12908	0,05831	0,127446	0,295534	0,188061	279,7637	-43,7621	-1269,1
72000	5,71E-07	4,110219	0,83628	0,035473	6,99091	1,22449	12186,298	92,94772	3983,474	0,005711	0,12908	0,05831	0,127446	0,297709	0,188061	279,7526	-43,4609	-1260,37
75600	5,71E-07	4,31573	0,88507	0,037542	6,99091	1,22449	12186,298	92,94772	3983,474	0,005711	0,12908	0,05831	0,127446	0,299779	0,188061	279,7421	-43,1782	-1252,17
79200	5,71E-07	4,521241	0,93159	0,039516	6,99091	1,22449	12186,298	92,94772	3983,474	0,005711	0,12908	0,05831	0,127446	0,301752	0,188061	279,7323	-42,9121	-1244,45
82800	5,71E-07	4,726752	0,97604	0,041401	6,99091	1,22449	12186,298	92,94772	3983,474	0,005711	0,12908	0,05831	0,127446	0,303638	0,188061	279,7231	-42,6609	-1237,17
86400	5,71E-07	4,932263	1,0186	0,043206	6,99091	1,22449	12186,298	92,94772	3983,474	0,005711	0,12908	0,05831	0,127446	0,305443	0,188061	279,7143	-42,4231	-1230,27
90000	5,71E-07	5,137774	1,05942	0,044938	6,99091	1,22449	12186,298	92,94772	3983,474	0,005711	0,12908	0,05831	0,127446	0,307175	0,188061	279,706	-42,1975	-1223,73
93600	5,71E-07	5,343285	1,09864	0,046602	6,99091	1,22449	12186,298	92,94772	3983,474	0,005711	0,12908	0,05831	0,127446	0,308838	0,188061	279,6981	-41,983	-1217,51

97200	**5,71E-07**	**5,548796**	**1,13638**	**0,048203**	**6,99091**	**1,22449**	**12186,298**	**92,94772**	**3983,474**	**0,005711**	**0,12908**	**0,05831**	**0,127446**	**0,310439**	**0,188061**	**279,6905**	**-41,7787**	**-1211,58**
100800	**5,71E-07**	**5,754307**	**1,17275**	**0,049745**	**6,99091**	**1,22449**	**12186,298**	**92,94772**	**3983,474**	**0,005711**	**0,12908**	**0,05831**	**0,127446**	**0,311982**	**0,188061**	**279,6833**	**-41,5836**	**-1205,92**
104400	**5,71E-07**	**5,959818**	**1,20784**	**0,051234**	**6,99091**	**1,22449**	**12186,298**	**92,94772**	**3983,474**	**0,005711**	**0,12908**	**0,05831**	**0,127446**	**0,31347**	**0,188061**	**279,6765**	**-41,3971**	**-1200,52**
108000	**5,71E-07**	**6,165328**	**1,24174**	**0,052672**	**6,99091**	**1,22449**	**12186,298**	**92,94772**	**3983,474**	**0,005711**	**0,12908**	**0,05831**	**0,127446**	**0,314908**	**0,188061**	**279,6699**	**-41,2185**	**-1195,34**
111600	**5,71E-07**	**6,370839**	**1,27453**	**0,054063**	**6,99091**	**1,22449**	**12186,298**	**92,94772**	**3983,474**	**0,005711**	**0,12908**	**0,05831**	**0,127446**	**0,316299**	**0,188061**	**279,6636**	**-41,0473**	**-1190,37**
115200	**5,71E-07**	**6,57635**	**1,30628**	**0,055409**	**6,99091**	**1,22449**	**12186,298**	**92,94772**	**3983,474**	**0,005711**	**0,12908**	**0,05831**	**0,127446**	**0,317646**	**0,188061**	**279,6575**	**-40,8828**	**-1185,6**
118800	**5,71E-07**	**6,781861**	**1,33705**	**0,056715**	**6,99091**	**1,22449**	**12186,298**	**92,94772**	**3983,474**	**0,005711**	**0,12908**	**0,05831**	**0,127446**	**0,318951**	**0,188061**	**279,6517**	**-40,7246**	**-1181,01**
122400	**5,71E-07**	**6,987372**	**1,3669**	**0,057981**	**6,99091**	**1,22449**	**12186,298**	**92,94772**	**3983,474**	**0,005711**	**0,12908**	**0,05831**	**0,127446**	**0,320217**	**0,188061**	**279,646**	**-40,5724**	**-1176,6**
126000	**5,71E-07**	**7,192883**	**1,39589**	**0,05921**	**6,99091**	**1,22449**	**12186,298**	**92,94772**	**3983,474**	**0,005711**	**0,12908**	**0,05831**	**0,127446**	**0,321447**	**0,188061**	**279,6406**	**-40,4256**	**-1172,34**
129600	**5,71E-07**	**7,398394**	**1,42406**	**0,060405**	**6,99091**	**1,22449**	**12186,298**	**92,94772**	**3983,474**	**0,005711**	**0,12908**	**0,05831**	**0,127446**	**0,322642**	**0,188061**	**279,6354**	**-40,284**	**-1168,23**
133200	**5,71E-07**	**7,603905**	**1,45146**	**0,061568**	**6,99091**	**1,22449**	**12186,298**	**92,94772**	**3983,474**	**0,005711**	**0,12908**	**0,05831**	**0,127446**	**0,323804**	**0,188061**	**279,6304**	**-40,1472**	**-1164,27**
136800	**5,71E-07**	**7,809416**	**1,47813**	**0,062699**	**6,99091**	**1,22449**	**12186,298**	**92,94772**	**3983,474**	**0,005711**	**0,12908**	**0,05831**	**0,127446**	**0,324935**	**0,188061**	**279,6255**	**-40,0149**	**-1160,43**
140400	**5,71E-07**	**8,014927**	**1,50411**	**0,063801**	**6,99091**	**1,22449**	**12186,298**	**92,94772**	**3983,474**	**0,005711**	**0,12908**	**0,05831**	**0,127446**	**0,326037**	**0,188061**	**279,6208**	**-39,8869**	**-1156,72**
144000	**5,71E-07**	**8,220438**	**1,52942**	**0,064874**	**6,99091**	**1,22449**	**12186,298**	**92,94772**	**3983,474**	**0,005711**	**0,12908**	**0,05831**	**0,127446**	**0,327111**	**0,188061**	**279,6162**	**-39,7629**	**-1153,13**
147600	**5,71E-07**	**8,425949**	**1,55412**	**0,065922**	**6,99091**	**1,22449**	**12186,298**	**92,94772**	**3983,474**	**0,005711**	**0,12908**	**0,05831**	**0,127446**	**0,328158**	**0,188061**	**279,6118**	**-39,6428**	**-1149,64**
151200	**5,71E-07**	**8,63146**	**1,57821**	**0,066944**	**6,99091**	**1,22449**	**12186,298**	**92,94772**	**3983,474**	**0,005711**	**0,12908**	**0,05831**	**0,127446**	**0,329181**	**0,188061**	**279,6075**	**-39,5262**	**-1146,26**
154800	**5,71E-07**	**8,836971**	**1,60174**	**0,067942**	**6,99091**	**1,22449**	**12186,298**	**92,94772**	**3983,474**	**0,005711**	**0,12908**	**0,05831**	**0,127446**	**0,330179**	**0,188061**	**279,6033**	**-39,413**	**-1142,98**
158400	**5,71E-07**	**9,042482**	**1,62473**	**0,068917**	**6,99091**	**1,22449**	**12186,298**	**92,94772**	**3983,474**	**0,005711**	**0,12908**	**0,05831**	**0,127446**	**0,331154**	**0,188061**	**279,5992**	**-39,3031**	**-1139,79**
162000	**5,71E-07**	**9,247993**	**1,64721**	**0,069871**	**6,99091**	**1,22449**	**12186,298**	**92,94772**	**3983,474**	**0,005711**	**0,12908**	**0,05831**	**0,127446**	**0,332107**	**0,188061**	**279,5953**	**-39,1962**	**-1136,69**
165600	**5,71E-07**	**9,453504**	**1,66919**	**0,070803**	**6,99091**	**1,22449**	**12186,298**	**92,94772**	**3983,474**	**0,005711**	**0,12908**	**0,05831**	**0,127446**	**0,333039**	**0,188061**	**279,5915**	**-39,0923**	**-1133,68**
169200	**5,71E-07**	**9,659015**	**1,69069**	**0,071715**	**6,99091**	**1,22449**	**12186,298**	**92,94772**	**3983,474**	**0,005711**	**0,12908**	**0,05831**	**0,127446**	**0,333952**	**0,188061**	**279,5877**	**-38,9911**	**-1130,74**
172800	**5,71E-07**	**9,864526**	**1,71175**	**0,072608**	**6,99091**	**1,22449**	**12186,298**	**92,94772**	**3983,474**	**0,005711**	**0,12908**	**0,05831**	**0,127446**	**0,334845**	**0,188061**	**279,5841**	**-38,8925**	**-1127,88**

Table A. 6 Results analytical calculations for the optimal distance between pipe and concrete (0.02 mm) under cooling conditions.

t	a	x	E(x)	Rsol	Pr	v	Re	Nu(ref)	h	R fluide	R tube	R eq	R beton	R tot	m	T	q	Q
3600	5,71E-07	0,205511	-2,15946	-0,0916	6,99091	1,22449	17060,81755	100,1585	4292,507	0,005299	0,12908	0,05831	0,127446	0,170227	0,188061	313,017573	139,1897	4036,503
7200	5,71E-07	0,411022	-1,46631	-0,0622	6,99091	1,22449	17060,81755	100,1585	4292,507	0,005299	0,12908	0,05831	0,127446	0,199628	0,188061	313,709577	120,4228	3492,262
10800	5,71E-07	0,616533	-1,06084	-0,045	6,99091	1,22449	17060,81755	100,1585	4292,507	0,005299	0,12908	0,05831	0,127446	0,216827	0,188061	314,034192	111,6194	3236,962
14400	5,71E-07	0,822044	-0,77316	-0,0328	6,99091	1,22449	17060,81755	100,1585	4292,507	0,005299	0,12908	0,05831	0,127446	0,22903	0,188061	314,237146	106,1153	3077,345
18000	5,71E-07	1,027555	-0,55002	-0,02333	6,99091	1,22449	17060,81755	100,1585	4292,507	0,005299	0,12908	0,05831	0,127446	0,238495	0,188061	314,381293	102,2061	2963,977
21600	5,71E-07	1,233066	-0,3677	-0,0156	6,99091	1,22449	17060,81755	100,1585	4292,507	0,005299	0,12908	0,05831	0,127446	0,246229	0,188061	314,491417	99,2196	2877,368
25200	5,71E-07	1,438577	-0,21355	-0,00906	6,99091	1,22449	17060,81755	100,1585	4292,507	0,005299	0,12908	0,05831	0,127446	0,252767	0,188061	314,579625	96,82742	2807,995
28800	5,71E-07	1,644088	-0,08001	-0,00339	6,99091	1,22449	17060,81755	100,1585	4292,507	0,005299	0,12908	0,05831	0,127446	0,258431	0,188061	314,652666	94,84656	2750,55
32400	5,71E-07	1,849599	0,03777	0,001602	6,99091	1,22449	17060,81755	100,1585	4292,507	0,005299	0,12908	0,05831	0,127446	0,263428	0,188061	314,714657	93,16539	2701,796
36000	5,71E-07	2,055109	0,14313	0,006071	6,99091	1,22449	17060,81755	100,1585	4292,507	0,005299	0,12908	0,05831	0,127446	0,267897	0,188061	314,768276	91,71125	2659,626
39600	5,71E-07	2,26062	0,23844	0,010114	6,99091	1,22449	17060,81755	100,1585	4292,507	0,005299	0,12908	0,05831	0,127446	0,271939	0,188061	314,815359	90,43438	2622,597
43200	5,71E-07	2,466131	0,32545	0,013805	6,99091	1,22449	17060,81755	100,1585	4292,507	0,005299	0,12908	0,05831	0,127446	0,27563	0,188061	314,857212	89,29935	2589,681
46800	5,71E-07	2,671642	0,40549	0,0172	6,99091	1,22449	17060,81755	100,1585	4292,507	0,005299	0,12908	0,05831	0,127446	0,279026	0,188061	314,894796	88,28009	2560,123
50400	5,71E-07	2,877153	0,4796	0,020344	6,99091	1,22449	17060,81755	100,1585	4292,507	0,005299	0,12908	0,05831	0,127446	0,282169	0,188061	314,928836	87,35693	2533,351
54000	5,71E-07	3,082664	0,54859	0,02327	6,99091	1,22449	17060,81755	100,1585	4292,507	0,005299	0,12908	0,05831	0,127446	0,285096	0,188061	314,959893	86,51468	2508,926
57600	5,71E-07	3,288175	0,61313	0,026008	6,99091	1,22449	17060,81755	100,1585	4292,507	0,005299	0,12908	0,05831	0,127446	0,287833	0,188061	314,988407	85,74137	2486,5
61200	5,71E-07	3,493686	0,67376	0,028579	6,99091	1,22449	17060,81755	100,1585	4292,507	0,005299	0,12908	0,05831	0,127446	0,290405	0,188061	315,014732	85,02745	2465,796
64800	5,71E-07	3,699197	0,73092	0,031004	6,99091	1,22449	17060,81755	100,1585	4292,507	0,005299	0,12908	0,05831	0,127446	0,292829	0,188061	315,039153	84,36515	2446,589
68400	5,71E-07	3,904708	0,78498	0,033297	6,99091	1,22449	17060,81755	100,1585	4292,507	0,005299	0,12908	0,05831	0,127446	0,295123	0,188061	315,061906	83,7481	2428,695
72000	5,71E-07	4,110219	0,83628	0,035473	6,99091	1,22449	17060,81755	100,1585	4292,507	0,005299	0,12908	0,05831	0,127446	0,297298	0,188061	315,083186	83,17099	2411,959
75600	5,71E-07	4,31573	0,88507	0,037542	6,99091	1,22449	17060,81755	100,1585	4292,507	0,005299	0,12908	0,05831	0,127446	0,299368	0,188061	315,103158	82,62937	2396,252
79200	5,71E-07	4,521241	0,93159	0,039516	6,99091	1,22449	17060,81755	100,1585	4292,507	0,005299	0,12908	0,05831	0,127446	0,301341	0,188061	315,121959	82,11949	2381,465
82800	5,71E-07	4,726752	0,97604	0,041401	6,99091	1,22449	17060,81755	100,1585	4292,507	0,005299	0,12908	0,05831	0,127446	0,303227	0,188061	315,139709	81,63812	2367,505
86400	5,71E-07	4,932263	1,0186	0,043206	6,99091	1,22449	17060,81755	100,1585	4292,507	0,005299	0,12908	0,05831	0,127446	0,305032	0,188061	315,156509	81,1825	2354,292
90000	5,71E-07	5,137774	1,05942	0,044938	6,99091	1,22449	17060,81755	100,1585	4292,507	0,005299	0,12908	0,05831	0,127446	0,306764	0,188061	315,172449	80,75023	2341,757
93600	5,71E-07	5,343285	1,09864	0,046602	6,99091	1,22449	17060,81755	100,1585	4292,507	0,005299	0,12908	0,05831	0,127446	0,308427	0,188061	315,187603	80,33923	2329,838

97200	**5,71E-07**	**5,548796**	**1,13638**	**0,048203**	**6,99091**	**1,22449**	**17060,81755**	**100,1585**	**4292,507**	**0,005299**	**0,12908**	**0,05831**	**0,127446**	**0,310028**	**0,188061**	**315,202041**	**79,94768**	**2318,483**
100800	**5,71E-07**	**5,754307**	**1,17275**	**0,049745**	**6,99091**	**1,22449**	**17060,81755**	**100,1585**	**4292,507**	**0,005299**	**0,12908**	**0,05831**	**0,127446**	**0,311571**	**0,188061**	**315,215822**	**79,57396**	**2307,645**
104400	**5,71E-07**	**5,959818**	**1,20784**	**0,051234**	**6,99091**	**1,22449**	**17060,81755**	**100,1585**	**4292,507**	**0,005299**	**0,12908**	**0,05831**	**0,127446**	**0,313059**	**0,188061**	**315,228997**	**79,21666**	**2297,283**
108000	**5,71E-07**	**6,165328**	**1,24174**	**0,052672**	**6,99091**	**1,22449**	**17060,81755**	**100,1585**	**4292,507**	**0,005299**	**0,12908**	**0,05831**	**0,127446**	**0,314497**	**0,188061**	**315,241613**	**78,8745**	**2287,361**
111600	**5,71E-07**	**6,370839**	**1,27453**	**0,054063**	**6,99091**	**1,22449**	**17060,81755**	**100,1585**	**4292,507**	**0,005299**	**0,12908**	**0,05831**	**0,127446**	**0,315888**	**0,188061**	**315,253713**	**78,54637**	**2277,845**
115200	**5,71E-07**	**6,57635**	**1,30628**	**0,055409**	**6,99091**	**1,22449**	**17060,81755**	**100,1585**	**4292,507**	**0,005299**	**0,12908**	**0,05831**	**0,127446**	**0,317235**	**0,188061**	**315,265333**	**78,23124**	**2268,706**
118800	**5,71E-07**	**6,781861**	**1,33705**	**0,056715**	**6,99091**	**1,22449**	**17060,81755**	**100,1585**	**4292,507**	**0,005299**	**0,12908**	**0,05831**	**0,127446**	**0,31854**	**0,188061**	**315,276506**	**77,92822**	**2259,918**
122400	**5,71E-07**	**6,987372**	**1,3669**	**0,057981**	**6,99091**	**1,22449**	**17060,81755**	**100,1585**	**4292,507**	**0,005299**	**0,12908**	**0,05831**	**0,127446**	**0,319806**	**0,188061**	**315,287264**	**77,63648**	**2251,458**
126000	**5,71E-07**	**7,192883**	**1,39589**	**0,05921**	**6,99091**	**1,22449**	**17060,81755**	**100,1585**	**4292,507**	**0,005299**	**0,12908**	**0,05831**	**0,127446**	**0,321036**	**0,188061**	**315,297633**	**77,35527**	**2243,303**
129600	**5,71E-07**	**7,398394**	**1,42406**	**0,060405**	**6,99091**	**1,22449**	**17060,81755**	**100,1585**	**4292,507**	**0,005299**	**0,12908**	**0,05831**	**0,127446**	**0,322231**	**0,188061**	**315,307638**	**77,08394**	**2235,434**
133200	**5,71E-07**	**7,603905**	**1,45146**	**0,061568**	**6,99091**	**1,22449**	**17060,81755**	**100,1585**	**4292,507**	**0,005299**	**0,12908**	**0,05831**	**0,127446**	**0,323393**	**0,188061**	**315,317302**	**76,82186**	**2227,834**
136800	**5,71E-07**	**7,809416**	**1,47813**	**0,062699**	**6,99091**	**1,22449**	**17060,81755**	**100,1585**	**4292,507**	**0,005299**	**0,12908**	**0,05831**	**0,127446**	**0,324524**	**0,188061**	**315,326645**	**76,56847**	**2220,486**
140400	**5,71E-07**	**8,014927**	**1,50411**	**0,063801**	**6,99091**	**1,22449**	**17060,81755**	**100,1585**	**4292,507**	**0,005299**	**0,12908**	**0,05831**	**0,127446**	**0,325626**	**0,188061**	**315,335686**	**76,32327**	**2213,375**
144000	**5,71E-07**	**8,220438**	**1,52942**	**0,064874**	**6,99091**	**1,22449**	**17060,81755**	**100,1585**	**4292,507**	**0,005299**	**0,12908**	**0,05831**	**0,127446**	**0,3267**	**0,188061**	**315,344443**	**76,08579**	**2206,488**
147600	**5,71E-07**	**8,425949**	**1,55412**	**0,065922**	**6,99091**	**1,22449**	**17060,81755**	**100,1585**	**4292,507**	**0,005299**	**0,12908**	**0,05831**	**0,127446**	**0,327747**	**0,188061**	**315,352932**	**75,85558**	**2199,812**
151200	**5,71E-07**	**8,63146**	**1,57821**	**0,066944**	**6,99091**	**1,22449**	**17060,81755**	**100,1585**	**4292,507**	**0,005299**	**0,12908**	**0,05831**	**0,127446**	**0,328769**	**0,188061**	**315,361166**	**75,63227**	**2193,336**
154800	**5,71E-07**	**8,836971**	**1,60174**	**0,067942**	**6,99091**	**1,22449**	**17060,81755**	**100,1585**	**4292,507**	**0,005299**	**0,12908**	**0,05831**	**0,127446**	**0,329768**	**0,188061**	**315,36916**	**75,41547**	**2187,049**
158400	**5,71E-07**	**9,042482**	**1,62473**	**0,068917**	**6,99091**	**1,22449**	**17060,81755**	**100,1585**	**4292,507**	**0,005299**	**0,12908**	**0,05831**	**0,127446**	**0,330743**	**0,188061**	**315,376926**	**75,20486**	**2180,941**
162000	**5,71E-07**	**9,247993**	**1,64721**	**0,069871**	**6,99091**	**1,22449**	**17060,81755**	**100,1585**	**4292,507**	**0,005299**	**0,12908**	**0,05831**	**0,127446**	**0,331696**	**0,188061**	**315,384476**	**75,00011**	**2175,003**
165600	**5,71E-07**	**9,453504**	**1,66919**	**0,070803**	**6,99091**	**1,22449**	**17060,81755**	**100,1585**	**4292,507**	**0,005299**	**0,12908**	**0,05831**	**0,127446**	**0,332628**	**0,188061**	**315,39182**	**74,80094**	**2169,227**
169200	**5,71E-07**	**9,659015**	**1,69069**	**0,071715**	**6,99091**	**1,22449**	**17060,81755**	**100,1585**	**4292,507**	**0,005299**	**0,12908**	**0,05831**	**0,127446**	**0,333541**	**0,188061**	**315,398969**	**74,60708**	**2163,605**
172800	**5,71E-07**	**9,864526**	**1,71175**	**0,072608**	**6,99091**	**1,22449**	**17060,81755**	**100,1585**	**4292,507**	**0,005299**	**0,12908**	**0,05831**	**0,127446**	**0,334434**	**0,188061**	**315,405931**	**74,41826**	**2158,13**

Table A. 7 Results analytical calculations for the optimal pipe angular position (α=30°) under heating conditions.

t	a	x	E(x)	Rsol	Pr	v	Re	Nu(ref)	h	R fluide	R tube	R eq	R beton	R tot	m	T	q	Q
3600	5,71E-07	0,205511	-2,15946	-0,0916	6,99091	1,22449	17060,81755	121,6581	5213,921	0,004363	0,12908	0,054263	0,134882	0,176727	0,188061	280,745996	-70,4026	-2041,67
7200	5,71E-07	0,411022	-1,46631	-0,0622	6,99091	1,22449	17060,81755	121,6581	5213,921	0,004363	0,12908	0,054263	0,134882	0,206128	0,188061	280,406109	-61,185	-1774,36
10800	5,71E-07	0,616533	-1,06084	-0,045	6,99091	1,22449	17060,81755	121,6581	5213,921	0,004363	0,12908	0,054263	0,134882	0,223327	0,188061	280,245612	-56,8323	-1648,14
14400	5,71E-07	0,822044	-0,77316	-0,0328	6,99091	1,22449	17060,81755	121,6581	5213,921	0,004363	0,12908	0,054263	0,134882	0,23553	0,188061	280,14492	-54,1016	-1568,95
18000	5,71E-07	1,027555	-0,55002	-0,02333	6,99091	1,22449	17060,81755	121,6581	5213,921	0,004363	0,12908	0,054263	0,134882	0,244995	0,188061	280,073242	-52,1577	-1512,57
21600	5,71E-07	1,233066	-0,3677	-0,0156	6,99091	1,22449	17060,81755	121,6581	5213,921	0,004363	0,12908	0,054263	0,134882	0,252729	0,188061	280,018391	-50,6702	-1469,43
25200	5,71E-07	1,438577	-0,21355	-0,00906	6,99091	1,22449	17060,81755	121,6581	5213,921	0,004363	0,12908	0,054263	0,134882	0,259267	0,188061	279,974399	-49,4771	-1434,84
28800	5,71E-07	1,644088	-0,08001	-0,00339	6,99091	1,22449	17060,81755	121,6581	5213,921	0,004363	0,12908	0,054263	0,134882	0,264931	0,188061	279,937932	-48,4881	-1406,16
32400	5,71E-07	1,849599	0,03777	0,001602	6,99091	1,22449	17060,81755	121,6581	5213,921	0,004363	0,12908	0,054263	0,134882	0,269928	0,188061	279,906955	-47,6481	-1381,79
36000	5,71E-07	2,055109	0,14313	0,006071	6,99091	1,22449	17060,81755	121,6581	5213,921	0,004363	0,12908	0,054263	0,134882	0,274397	0,188061	279,880141	-46,9209	-1360,71
39600	5,71E-07	2,26062	0,23844	0,010114	6,99091	1,22449	17060,81755	121,6581	5213,921	0,004363	0,12908	0,054263	0,134882	0,27844	0,188061	279,85658	-46,2819	-1342,18
43200	5,71E-07	2,466131	0,32545	0,013805	6,99091	1,22449	17060,81755	121,6581	5213,921	0,004363	0,12908	0,054263	0,134882	0,28213	0,188061	279,835624	-45,7136	-1325,69
46800	5,71E-07	2,671642	0,40549	0,0172	6,99091	1,22449	17060,81755	121,6581	5213,921	0,004363	0,12908	0,054263	0,134882	0,285526	0,188061	279,816796	-45,203	-1310,89
50400	5,71E-07	2,877153	0,4796	0,020344	6,99091	1,22449	17060,81755	121,6581	5213,921	0,004363	0,12908	0,054263	0,134882	0,288669	0,188061	279,799735	-44,7403	-1297,47
54000	5,71E-07	3,082664	0,54859	0,02327	6,99091	1,22449	17060,81755	121,6581	5213,921	0,004363	0,12908	0,054263	0,134882	0,291596	0,188061	279,784162	-44,318	-1285,22
57600	5,71E-07	3,288175	0,61313	0,026008	6,99091	1,22449	17060,81755	121,6581	5213,921	0,004363	0,12908	0,054263	0,134882	0,294333	0,188061	279,769859	-43,9301	-1273,97
61200	5,71E-07	3,493686	0,67376	0,028579	6,99091	1,22449	17060,81755	121,6581	5213,921	0,004363	0,12908	0,054263	0,134882	0,296905	0,188061	279,75665	-43,5718	-1263,58
64800	5,71E-07	3,699197	0,73092	0,031004	6,99091	1,22449	17060,81755	121,6581	5213,921	0,004363	0,12908	0,054263	0,134882	0,299329	0,188061	279,744391	-43,2394	-1253,94
68400	5,71E-07	3,904708	0,78498	0,033297	6,99091	1,22449	17060,81755	121,6581	5213,921	0,004363	0,12908	0,054263	0,134882	0,301623	0,188061	279,732966	-42,9295	-1244,96
72000	5,71E-07	4,110219	0,83628	0,035473	6,99091	1,22449	17060,81755	121,6581	5213,921	0,004363	0,12908	0,054263	0,134882	0,303798	0,188061	279,722278	-42,6397	-1236,55
75600	5,71E-07	4,31573	0,88507	0,037542	6,99091	1,22449	17060,81755	121,6581	5213,921	0,004363	0,12908	0,054263	0,134882	0,305868	0,188061	279,712245	-42,3676	-1228,66
79200	5,71E-07	4,521241	0,93159	0,039516	6,99091	1,22449	17060,81755	121,6581	5213,921	0,004363	0,12908	0,054263	0,134882	0,307841	0,188061	279,702796	-42,1113	-1221,23
82800	5,71E-07	4,726752	0,97604	0,041401	6,99091	1,22449	17060,81755	121,6581	5213,921	0,004363	0,12908	0,054263	0,134882	0,309727	0,188061	279,693874	-41,8694	-1214,21
86400	5,71E-07	4,932263	1,0186	0,043206	6,99091	1,22449	17060,81755	121,6581	5213,921	0,004363	0,12908	0,054263	0,134882	0,311532	0,188061	279,685428	-41,6403	-1207,57
90000	5,71E-07	5,137774	1,05942	0,044938	6,99091	1,22449	17060,81755	121,6581	5213,921	0,004363	0,12908	0,054263	0,134882	0,313264	0,188061	279,677412	-41,4229	-1201,26
93600	5,71E-07	5,343285	1,09864	0,046602	6,99091	1,22449	17060,81755	121,6581	5213,921	0,004363	0,12908	0,054263	0,134882	0,314927	0,188061	279,66979	-41,2162	-1195,27

97200	5,71E-07	5,548796	1,13638	0,048203	6,99091	1,22449	17060,81755	121,6581	5213,921	0,004363	0,12908	0,054263	0,134882	0,316528	0,188061	279,662527	-41,0192	-1189,56
100800	5,71E-07	5,754307	1,17275	0,049745	6,99091	1,22449	17060,81755	121,6581	5213,921	0,004363	0,12908	0,054263	0,134882	0,318071	0,188061	279,655593	-40,8312	-1184,1
104400	5,71E-07	5,959818	1,20784	0,051234	6,99091	1,22449	17060,81755	121,6581	5213,921	0,004363	0,12908	0,054263	0,134882	0,319559	0,188061	279,648962	-40,6514	-1178,89
108000	5,71E-07	6,165328	1,24174	0,052672	6,99091	1,22449	17060,81755	121,6581	5213,921	0,004363	0,12908	0,054263	0,134882	0,320997	0,188061	279,642612	-40,4792	-1173,9
111600	5,71E-07	6,370839	1,27453	0,054063	6,99091	1,22449	17060,81755	121,6581	5213,921	0,004363	0,12908	0,054263	0,134882	0,322388	0,188061	279,636521	-40,314	-1169,1
115200	5,71E-07	6,57635	1,30628	0,055409	6,99091	1,22449	17060,81755	121,6581	5213,921	0,004363	0,12908	0,054263	0,134882	0,323735	0,188061	279,63067	-40,1553	-1164,5
118800	5,71E-07	6,781861	1,33705	0,056715	6,99091	1,22449	17060,81755	121,6581	5213,921	0,004363	0,12908	0,054263	0,134882	0,32504	0,188061	279,625043	-40,0027	-1160,08
122400	5,71E-07	6,987372	1,3669	0,057981	6,99091	1,22449	17060,81755	121,6581	5213,921	0,004363	0,12908	0,054263	0,134882	0,326306	0,188061	279,619625	-39,8558	-1155,82
126000	5,71E-07	7,192883	1,39589	0,05921	6,99091	1,22449	17060,81755	121,6581	5213,921	0,004363	0,12908	0,054263	0,134882	0,327536	0,188061	279,614402	-39,7141	-1151,71
129600	5,71E-07	7,398394	1,42406	0,060405	6,99091	1,22449	17060,81755	121,6581	5213,921	0,004363	0,12908	0,054263	0,134882	0,328731	0,188061	279,609362	-39,5774	-1147,75
133200	5,71E-07	7,603905	1,45146	0,061568	6,99091	1,22449	17060,81755	121,6581	5213,921	0,004363	0,12908	0,054263	0,134882	0,329893	0,188061	279,604493	-39,4454	-1143,92
136800	5,71E-07	7,809416	1,47813	0,062699	6,99091	1,22449	17060,81755	121,6581	5213,921	0,004363	0,12908	0,054263	0,134882	0,331024	0,188061	279,599785	-39,3177	-1140,21
140400	5,71E-07	8,014927	1,50411	0,063801	6,99091	1,22449	17060,81755	121,6581	5213,921	0,004363	0,12908	0,054263	0,134882	0,332126	0,188061	279,595228	-39,1941	-1136,63
144000	5,71E-07	8,220438	1,52942	0,064874	6,99091	1,22449	17060,81755	121,6581	5213,921	0,004363	0,12908	0,054263	0,134882	0,3332	0,188061	279,590814	-39,0744	-1133,16
147600	5,71E-07	8,425949	1,55412	0,065922	6,99091	1,22449	17060,81755	121,6581	5213,921	0,004363	0,12908	0,054263	0,134882	0,334247	0,188061	279,586535	-38,9584	-1129,79
151200	5,71E-07	8,63146	1,57821	0,066944	6,99091	1,22449	17060,81755	121,6581	5213,921	0,004363	0,12908	0,054263	0,134882	0,33527	0,188061	279,582384	-38,8458	-1126,53
154800	5,71E-07	8,836971	1,60174	0,067942	6,99091	1,22449	17060,81755	121,6581	5213,921	0,004363	0,12908	0,054263	0,134882	0,336268	0,188061	279,578353	-38,7365	-1123,36
158400	5,71E-07	9,042482	1,62473	0,068917	6,99091	1,22449	17060,81755	121,6581	5213,921	0,004363	0,12908	0,054263	0,134882	0,337243	0,188061	279,574437	-38,6303	-1120,28
162000	5,71E-07	9,247993	1,64721	0,069871	6,99091	1,22449	17060,81755	121,6581	5213,921	0,004363	0,12908	0,054263	0,134882	0,338196	0,188061	279,57063	-38,527	-1117,28
165600	5,71E-07	9,453504	1,66919	0,070803	6,99091	1,22449	17060,81755	121,6581	5213,921	0,004363	0,12908	0,054263	0,134882	0,339128	0,188061	279,566926	-38,4266	-1114,37
169200	5,71E-07	9,659015	1,69069	0,071715	6,99091	1,22449	17060,81755	121,6581	5213,921	0,004363	0,12908	0,054263	0,134882	0,340041	0,188061	279,56332	-38,3288	-1111,53
172800	5,71E-07	9,864526	1,71175	0,072608	6,99091	1,22449	17060,81755	121,6581	5213,921	0,004363	0,12908	0,054263	0,134882	0,340934	0,188061	279,559808	-38,2335	-1108,77

Table A. 8 Results analytical calculations for the optimal pipe angular position (α=30°) under cooling conditions.

t	a	x	E(x)	Rsol	Pr	v	Re	Nu(ref)	h	R fluide	R tube	R eq	R beton	R tot	m	T	q	Q
3600	5,71E-07	0,205511	-2,15946	-0,0916	6,99091	1,22449	17060,81755	100,1585	4292,507	0,005299	0,12908	0,054263	0,134882	0,177663	0,188061	313,212207	133,9113	3883,429
7200	5,71E-07	0,411022	-1,46631	-0,0622	6,99091	1,22449	17060,81755	100,1585	4292,507	0,005299	0,12908	0,054263	0,134882	0,207065	0,188061	313,856013	116,4515	3377,095
10800	5,71E-07	0,616533	-1,06084	-0,045	6,99091	1,22449	17060,81755	100,1585	4292,507	0,005299	0,12908	0,054263	0,134882	0,224264	0,188061	314,160304	108,1993	3137,778
14400	5,71E-07	0,822044	-0,77316	-0,0328	6,99091	1,22449	17060,81755	100,1585	4292,507	0,005299	0,12908	0,054263	0,134882	0,236466	0,188061	314,3513	103,0195	2987,566
18000	5,71E-07	1,027555	-0,55002	-0,02333	6,99091	1,22449	17060,81755	100,1585	4292,507	0,005299	0,12908	0,054263	0,134882	0,245932	0,188061	314,487305	99,33109	2880,602
21600	5,71E-07	1,233066	-0,3677	-0,0156	6,99091	1,22449	17060,81755	100,1585	4292,507	0,005299	0,12908	0,054263	0,134882	0,253665	0,188061	314,591406	96,50792	2798,73
25200	5,71E-07	1,438577	-0,21355	-0,00906	6,99091	1,22449	17060,81755	100,1585	4292,507	0,005299	0,12908	0,054263	0,134882	0,260204	0,188061	314,674913	94,24322	2733,053
28800	5,71E-07	1,644088	-0,08001	-0,00339	6,99091	1,22449	17060,81755	100,1585	4292,507	0,005299	0,12908	0,054263	0,134882	0,265868	0,188061	314,744146	92,36566	2678,604
32400	5,71E-07	1,849599	0,03777	0,001602	6,99091	1,22449	17060,81755	100,1585	4292,507	0,005299	0,12908	0,054263	0,134882	0,270864	0,188061	314,802963	90,77055	2632,346
36000	5,71E-07	2,055109	0,14313	0,006071	6,99091	1,22449	17060,81755	100,1585	4292,507	0,005299	0,12908	0,054263	0,134882	0,275333	0,188061	314,853882	89,38965	2592,3
39600	5,71E-07	2,26062	0,23844	0,010114	6,99091	1,22449	17060,81755	100,1585	4292,507	0,005299	0,12908	0,054263	0,134882	0,279376	0,188061	314,898627	88,17618	2557,109
43200	5,71E-07	2,466131	0,32545	0,013805	6,99091	1,22449	17060,81755	100,1585	4292,507	0,005299	0,12908	0,054263	0,134882	0,283067	0,188061	314,938428	87,09679	2525,807
46800	5,71E-07	2,671642	0,40549	0,0172	6,99091	1,22449	17060,81755	100,1585	4292,507	0,005299	0,12908	0,054263	0,134882	0,286462	0,188061	314,974191	86,12691	2497,681
50400	5,71E-07	2,877153	0,4796	0,020344	6,99091	1,22449	17060,81755	100,1585	4292,507	0,005299	0,12908	0,054263	0,134882	0,289606	0,188061	315,006599	85,24801	2472,192
54000	5,71E-07	3,082664	0,54859	0,02327	6,99091	1,22449	17060,81755	100,1585	4292,507	0,005299	0,12908	0,054263	0,134882	0,292532	0,188061	315,036181	84,44575	2448,927
57600	5,71E-07	3,288175	0,61313	0,026008	6,99091	1,22449	17060,81755	100,1585	4292,507	0,005299	0,12908	0,054263	0,134882	0,29527	0,188061	315,063354	83,70883	2427,556
61200	5,71E-07	3,493686	0,67376	0,028579	6,99091	1,22449	17060,81755	100,1585	4292,507	0,005299	0,12908	0,054263	0,134882	0,297841	0,188061	315,088451	83,02822	2407,818
64800	5,71E-07	3,699197	0,73092	0,031004	6,99091	1,22449	17060,81755	100,1585	4292,507	0,005299	0,12908	0,054263	0,134882	0,300266	0,188061	315,111741	82,39659	2389,501
68400	5,71E-07	3,904708	0,78498	0,033297	6,99091	1,22449	17060,81755	100,1585	4292,507	0,005299	0,12908	0,054263	0,134882	0,302559	0,188061	315,133449	81,80789	2372,429
72000	5,71E-07	4,110219	0,83628	0,035473	6,99091	1,22449	17060,81755	100,1585	4292,507	0,005299	0,12908	0,054263	0,134882	0,304735	0,188061	315,153758	81,25712	2356,457
75600	5,71E-07	4,31573	0,88507	0,037542	6,99091	1,22449	17060,81755	100,1585	4292,507	0,005299	0,12908	0,054263	0,134882	0,306804	0,188061	315,172823	80,74007	2341,462
79200	5,71E-07	4,521241	0,93159	0,039516	6,99091	1,22449	17060,81755	100,1585	4292,507	0,005299	0,12908	0,054263	0,134882	0,308778	0,188061	315,190777	80,25317	2327,342
82800	5,71E-07	4,726752	0,97604	0,041401	6,99091	1,22449	17060,81755	100,1585	4292,507	0,005299	0,12908	0,054263	0,134882	0,310663	0,188061	315,207731	79,79337	2314,008
86400	5,71E-07	4,932263	1,0186	0,043206	6,99091	1,22449	17060,81755	100,1585	4292,507	0,005299	0,12908	0,054263	0,134882	0,312469	0,188061	315,223783	79,35805	2301,383
90000	5,71E-07	5,137774	1,05942	0,044938	6,99091	1,22449	17060,81755	100,1585	4292,507	0,005299	0,12908	0,054263	0,134882	0,3142	0,188061	315,239016	78,94495	2289,403
93600	5,71E-07	5,343285	1,09864	0,046602	6,99091	1,22449	17060,81755	100,1585	4292,507	0,005299	0,12908	0,054263	0,134882	0,315864	0,188061	315,253502	78,55208	2278,01

97200	**5,71E-07**	**5,548796**	**1,13638**	**0,048203**	**6,99091**	**1,22449**	**17060,81755**	**100,1585**	**4292,507**	**0,005299**	**0,12908**	**0,054263**	**0,134882**	**0,317465**	**0,188061**	**315,267307**	**78,17771**	**2267,154**
100800	**5,71E-07**	**5,754307**	**1,17275**	**0,049745**	**6,99091**	**1,22449**	**17060,81755**	**100,1585**	**4292,507**	**0,005299**	**0,12908**	**0,054263**	**0,134882**	**0,319007**	**0,188061**	**315,280485**	**77,82032**	**2256,789**
104400	**5,71E-07**	**5,959818**	**1,20784**	**0,051234**	**6,99091**	**1,22449**	**17060,81755**	**100,1585**	**4292,507**	**0,005299**	**0,12908**	**0,054263**	**0,134882**	**0,320496**	**0,188061**	**315,293087**	**77,47856**	**2246,878**
108000	**5,71E-07**	**6,165328**	**1,24174**	**0,052672**	**6,99091**	**1,22449**	**17060,81755**	**100,1585**	**4292,507**	**0,005299**	**0,12908**	**0,054263**	**0,134882**	**0,321934**	**0,188061**	**315,305157**	**77,15122**	**2237,385**
111600	**5,71E-07**	**6,370839**	**1,27453**	**0,054063**	**6,99091**	**1,22449**	**17060,81755**	**100,1585**	**4292,507**	**0,005299**	**0,12908**	**0,054263**	**0,134882**	**0,323325**	**0,188061**	**315,316735**	**76,83724**	**2228,28**
115200	**5,71E-07**	**6,57635**	**1,30628**	**0,055409**	**6,99091**	**1,22449**	**17060,81755**	**100,1585**	**4292,507**	**0,005299**	**0,12908**	**0,054263**	**0,134882**	**0,324671**	**0,188061**	**315,327855**	**76,53565**	**2219,534**
118800	**5,71E-07**	**6,781861**	**1,33705**	**0,056715**	**6,99091**	**1,22449**	**17060,81755**	**100,1585**	**4292,507**	**0,005299**	**0,12908**	**0,054263**	**0,134882**	**0,325977**	**0,188061**	**315,338551**	**76,24559**	**2211,122**
122400	**5,71E-07**	**6,987372**	**1,3669**	**0,057981**	**6,99091**	**1,22449**	**17060,81755**	**100,1585**	**4292,507**	**0,005299**	**0,12908**	**0,054263**	**0,134882**	**0,327243**	**0,188061**	**315,34885**	**75,96629**	**2203,022**
126000	**5,71E-07**	**7,192883**	**1,39589**	**0,05921**	**6,99091**	**1,22449**	**17060,81755**	**100,1585**	**4292,507**	**0,005299**	**0,12908**	**0,054263**	**0,134882**	**0,328472**	**0,188061**	**315,358778**	**75,69704**	**2195,214**
129600	**5,71E-07**	**7,398394**	**1,42406**	**0,060405**	**6,99091**	**1,22449**	**17060,81755**	**100,1585**	**4292,507**	**0,005299**	**0,12908**	**0,054263**	**0,134882**	**0,329667**	**0,188061**	**315,368359**	**75,43719**	**2187,679**
133200	**5,71E-07**	**7,603905**	**1,45146**	**0,061568**	**6,99091**	**1,22449**	**17060,81755**	**100,1585**	**4292,507**	**0,005299**	**0,12908**	**0,054263**	**0,134882**	**0,33083**	**0,188061**	**315,377615**	**75,18617**	**2180,399**
136800	**5,71E-07**	**7,809416**	**1,47813**	**0,062699**	**6,99091**	**1,22449**	**17060,81755**	**100,1585**	**4292,507**	**0,005299**	**0,12908**	**0,054263**	**0,134882**	**0,331961**	**0,188061**	**315,386566**	**74,94344**	**2173,36**
140400	**5,71E-07**	**8,014927**	**1,50411**	**0,063801**	**6,99091**	**1,22449**	**17060,81755**	**100,1585**	**4292,507**	**0,005299**	**0,12908**	**0,054263**	**0,134882**	**0,333063**	**0,188061**	**315,395228**	**74,70852**	**2166,547**
144000	**5,71E-07**	**8,220438**	**1,52942**	**0,064874**	**6,99091**	**1,22449**	**17060,81755**	**100,1585**	**4292,507**	**0,005299**	**0,12908**	**0,054263**	**0,134882**	**0,334137**	**0,188061**	**315,403619**	**74,48097**	**2159,948**
147600	**5,71E-07**	**8,425949**	**1,55412**	**0,065922**	**6,99091**	**1,22449**	**17060,81755**	**100,1585**	**4292,507**	**0,005299**	**0,12908**	**0,054263**	**0,134882**	**0,335184**	**0,188061**	**315,411753**	**74,26036**	**2153,55**
151200	**5,71E-07**	**8,63146**	**1,57821**	**0,066944**	**6,99091**	**1,22449**	**17060,81755**	**100,1585**	**4292,507**	**0,005299**	**0,12908**	**0,054263**	**0,134882**	**0,336206**	**0,188061**	**315,419646**	**74,04632**	**2147,343**
154800	**5,71E-07**	**8,836971**	**1,60174**	**0,067942**	**6,99091**	**1,22449**	**17060,81755**	**100,1585**	**4292,507**	**0,005299**	**0,12908**	**0,054263**	**0,134882**	**0,337204**	**0,188061**	**315,427308**	**73,83851**	**2141,317**
158400	**5,71E-07**	**9,042482**	**1,62473**	**0,068917**	**6,99091**	**1,22449**	**17060,81755**	**100,1585**	**4292,507**	**0,005299**	**0,12908**	**0,054263**	**0,134882**	**0,338179**	**0,188061**	**315,434754**	**73,6366**	**2135,461**
162000	**5,71E-07**	**9,247993**	**1,64721**	**0,069871**	**6,99091**	**1,22449**	**17060,81755**	**100,1585**	**4292,507**	**0,005299**	**0,12908**	**0,054263**	**0,134882**	**0,339133**	**0,188061**	**315,441992**	**73,44029**	**2129,769**
165600	**5,71E-07**	**9,453504**	**1,66919**	**0,070803**	**6,99091**	**1,22449**	**17060,81755**	**100,1585**	**4292,507**	**0,005299**	**0,12908**	**0,054263**	**0,134882**	**0,340065**	**0,188061**	**315,449034**	**73,24931**	**2124,23**
169200	**5,71E-07**	**9,659015**	**1,69069**	**0,071715**	**6,99091**	**1,22449**	**17060,81755**	**100,1585**	**4292,507**	**0,005299**	**0,12908**	**0,054263**	**0,134882**	**0,340977**	**0,188061**	**315,45589**	**73,06339**	**2118,838**
172800	**5,71E-07**	**9,864526**	**1,71175**	**0,072608**	**6,99091**	**1,22449**	**17060,81755**	**100,1585**	**4292,507**	**0,005299**	**0,12908**	**0,054263**	**0,134882**	**0,34187**	**0,188061**	**315,462567**	**72,8823**	**2113,587**

Appendice B

Appendice B. 1 Analytical Framework and Parametric Calculations (Part 03).

Table B. 1 Results analytical calculations for the optimal pipe configuration (Triangular cross-section) under heating conditions.

T	α	x	E(x)	Rsol	Pr	v	Re	Nu	H	R p,f	R p	Req	R c	R tot	m	Tout	q	Q
3600	5,70864E-07	0,20551	-2,1595	-0,0916	6,99091	0,600003	8240,417	67,9674	2942,312	0,00613	0,063393	0,05467	0,13412	0,112043	0,18806	282,0329	979,4834	28405,02
7200	5,70864E-07	0,41102	-1,4663	-0,0622	6,99091	0,600003	8240,417	67,9674	2942,312	0,00613	0,063393	0,05467	0,13412	0,141445	0,18806	312,0936	164,2467	4763,153
10800	5,70864E-07	0,61653	-1,0608	-0,045	6,99091	0,600003	8240,417	67,9674	2942,312	0,00613	0,063393	0,05467	0,13412	0,158644	0,18806	312,6819	148,2943	4300,534
14400	5,70864E-07	0,82204	-0,7732	-0,0328	6,99091	0,600003	8240,417	67,9674	2942,312	0,00613	0,063393	0,05467	0,13412	0,170846	0,18806	313,0344	138,734	4023,285
18000	5,70864E-07	1,02755	-0,55	-0,02333	6,99091	0,600003	8240,417	67,9674	2942,312	0,00613	0,063393	0,05467	0,13412	0,180312	0,18806	313,278	132,1269	3831,68
21600	5,70864E-07	1,23307	-0,3677	-0,0156	6,99091	0,600003	8240,417	67,9674	2942,312	0,00613	0,063393	0,05467	0,13412	0,188045	0,18806	313,4605	127,1782	3688,167
25200	5,70864E-07	1,43858	-0,2135	-0,00906	6,99091	0,600003	8240,417	67,9674	2942,312	0,00613	0,063393	0,05467	0,13412	0,194584	0,18806	313,6044	123,2744	3574,958
28800	5,70864E-07	1,64409	-0,08	-0,00339	6,99091	0,600003	8240,417	67,9674	2942,312	0,00613	0,063393	0,05467	0,13412	0,200248	0,18806	313,7222	120,0815	3482,364
32400	5,70864E-07	1,8496	0,03777	0,001602	6,99091	0,600003	8240,417	67,9674	2942,312	0,00613	0,063393	0,05467	0,13412	0,205244	0,18806	313,8211	117,3994	3404,583
36000	5,70864E-07	2,05511	0,14313	0,006071	6,99091	0,600003	8240,417	67,9674	2942,312	0,00613	0,063393	0,05467	0,13412	0,209713	0,18806	313,9059	115,0997	3337,892
39600	5,70864E-07	2,26062	0,23844	0,010114	6,99091	0,600003	8240,417	67,9674	2942,312	0,00613	0,063393	0,05467	0,13412	0,213756	0,18806	313,9798	113,0957	3279,774
43200	5,70864E-07	2,46613	0,32545	0,013805	6,99091	0,600003	8240,417	67,9674	2942,312	0,00613	0,063393	0,05467	0,13412	0,217447	0,18806	314,045	111,3261	3228,456
46800	5,70864E-07	2,67164	0,40549	0,0172	6,99091	0,600003	8240,417	67,9674	2942,312	0,00613	0,063393	0,05467	0,13412	0,220842	0,18806	314,1033	109,7464	3182,647
50400	5,70864E-07	2,87715	0,4796	0,020344	6,99091	0,600003	8240,417	67,9674	2942,312	0,00613	0,063393	0,05467	0,13412	0,223986	0,18806	314,1557	108,3234	3141,377
54000	5,70864E-07	3,08266	0,54859	0,02327	6,99091	0,600003	8240,417	67,9674	2942,312	0,00613	0,063393	0,05467	0,13412	0,226912	0,18806	314,2034	107,0313	3103,907
57600	5,70864E-07	3,28818	0,61313	0,026008	6,99091	0,600003	8240,417	67,9674	2942,312	0,00613	0,063393	0,05467	0,13412	0,22965	0,18806	314,2469	105,8502	3069,656
61200	5,70864E-07	3,49369	0,67376	0,028579	6,99091	0,600003	8240,417	67,9674	2942,312	0,00613	0,063393	0,05467	0,13412	0,232221	0,18806	314,287	104,7643	3038,164
64800	5,70864E-07	3,6992	0,73092	0,031004	6,99091	0,600003	8240,417	67,9674	2942,312	0,00613	0,063393	0,05467	0,13412	0,234646	0,18806	314,324	103,7606	3009,059
68400	5,70864E-07	3,90471	0,78498	0,033297	6,99091	0,600003	8240,417	67,9674	2942,312	0,00613	0,063393	0,05467	0,13412	0,236939	0,18806	314,3583	102,8288	2982,036
72000	5,70864E-07	4,11022	0,83628	0,035473	6,99091	0,600003	8240,417	67,9674	2942,312	0,00613	0,063393	0,05467	0,13412	0,239115	0,18806	314,3904	101,9601	2956,844
75600	5,70864E-07	4,31573	0,88507	0,037542	6,99091	0,600003	8240,417	67,9674	2942,312	0,00613	0,063393	0,05467	0,13412	0,241184	0,18806	314,4203	101,1474	2933,274
79200	5,70864E-07	4,52124	0,93159	0,039516	6,99091	0,600003	8240,417	67,9674	2942,312	0,00613	0,063393	0,05467	0,13412	0,243158	0,18806	314,4485	100,3844	2911,147

82800	**5,70864E-07**	**4,72675**	**0,97604**	**0,041401**	**6,99091**	**0,600003**	**8240,417**	**67,9674**	**2942,312**	**0,00613**	**0,063393**	**0,05467**	**0,13412**	**0,245043**	**0,18806**	**314,475**	**99,66601**	**2890,314**
86400	**5,70864E-07**	**4,93226**	**1,0186**	**0,043206**	**6,99091**	**0,600003**	**8240,417**	**67,9674**	**2942,312**	**0,00613**	**0,063393**	**0,05467**	**0,13412**	**0,246848**	**0,18806**	**314,5**	**98,98778**	**2870,646**
90000	**5,70864E-07**	**5,13777**	**1,05942**	**0,044938**	**6,99091**	**0,600003**	**8240,417**	**67,9674**	**2942,312**	**0,00613**	**0,063393**	**0,05467**	**0,13412**	**0,24858**	**0,18806**	**314,5236**	**98,34586**	**2852,03**
93600	**5,70864E-07**	**5,34328**	**1,09864**	**0,046602**	**6,99091**	**0,600003**	**8240,417**	**67,9674**	**2942,312**	**0,00613**	**0,063393**	**0,05467**	**0,13412**	**0,250244**	**0,18806**	**314,5461**	**97,73691**	**2834,37**
97200	**5,70864E-07**	**5,5488**	**1,13638**	**0,048203**	**6,99091**	**0,600003**	**8240,417**	**67,9674**	**2942,312**	**0,00613**	**0,063393**	**0,05467**	**0,13412**	**0,251845**	**0,18806**	**314,5674**	**97,15802**	**2817,583**
100800	**5,70864E-07**	**5,75431**	**1,17275**	**0,049745**	**6,99091**	**0,600003**	**8240,417**	**67,9674**	**2942,312**	**0,00613**	**0,063393**	**0,05467**	**0,13412**	**0,253387**	**0,18806**	**314,5878**	**96,60664**	**2801,593**
104400	**5,70864E-07**	**5,95982**	**1,20784**	**0,051234**	**6,99091**	**0,600003**	**8240,417**	**67,9674**	**2942,312**	**0,00613**	**0,063393**	**0,05467**	**0,13412**	**0,254876**	**0,18806**	**314,6072**	**96,08051**	**2786,335**
108000	**5,70864E-07**	**6,16533**	**1,24174**	**0,052672**	**6,99091**	**0,600003**	**8240,417**	**67,9674**	**2942,312**	**0,00613**	**0,063393**	**0,05467**	**0,13412**	**0,256314**	**0,18806**	**314,6257**	**95,57763**	**2771,751**
111600	**5,70864E-07**	**6,37084**	**1,27453**	**0,054063**	**6,99091**	**0,600003**	**8240,417**	**67,9674**	**2942,312**	**0,00613**	**0,063393**	**0,05467**	**0,13412**	**0,257705**	**0,18806**	**314,6435**	**95,09623**	**2757,791**
115200	**5,70864E-07**	**6,57635**	**1,30628**	**0,055409**	**6,99091**	**0,600003**	**8240,417**	**67,9674**	**2942,312**	**0,00613**	**0,063393**	**0,05467**	**0,13412**	**0,259051**	**0,18806**	**314,6605**	**94,63471**	**2744,407**
118800	**5,70864E-07**	**6,78186**	**1,33705**	**0,056715**	**6,99091**	**0,600003**	**8240,417**	**67,9674**	**2942,312**	**0,00613**	**0,063393**	**0,05467**	**0,13412**	**0,260357**	**0,18806**	**314,6768**	**94,19164**	**2731,558**
122400	**5,70864E-07**	**6,98737**	**1,3669**	**0,057981**	**6,99091**	**0,600003**	**8240,417**	**67,9674**	**2942,312**	**0,00613**	**0,063393**	**0,05467**	**0,13412**	**0,261623**	**0,18806**	**314,6925**	**93,76576**	**2719,207**
126000	**5,70864E-07**	**7,19288**	**1,39589**	**0,05921**	**6,99091**	**0,600003**	**8240,417**	**67,9674**	**2942,312**	**0,00613**	**0,063393**	**0,05467**	**0,13412**	**0,262852**	**0,18806**	**314,7076**	**93,35588**	**2707,321**
129600	**5,70864E-07**	**7,39839**	**1,42406**	**0,060405**	**6,99091**	**0,600003**	**8240,417**	**67,9674**	**2942,312**	**0,00613**	**0,063393**	**0,05467**	**0,13412**	**0,264047**	**0,18806**	**314,7222**	**92,96098**	**2695,868**
133200	**5,70864E-07**	**7,60391**	**1,45146**	**0,061568**	**6,99091**	**0,600003**	**8240,417**	**67,9674**	**2942,312**	**0,00613**	**0,063393**	**0,05467**	**0,13412**	**0,26521**	**0,18806**	**314,7362**	**92,58008**	**2684,822**
136800	**5,70864E-07**	**7,80942**	**1,47813**	**0,062699**	**6,99091**	**0,600003**	**8240,417**	**67,9674**	**2942,312**	**0,00613**	**0,063393**	**0,05467**	**0,13412**	**0,266341**	**0,18806**	**314,7498**	**92,21233**	**2674,158**
140400	**5,70864E-07**	**8,01493**	**1,50411**	**0,063801**	**6,99091**	**0,600003**	**8240,417**	**67,9674**	**2942,312**	**0,00613**	**0,063393**	**0,05467**	**0,13412**	**0,267443**	**0,18806**	**314,7629**	**91,85694**	**2663,851**
144000	**5,70864E-07**	**8,22044**	**1,52942**	**0,064874**	**6,99091**	**0,600003**	**8240,417**	**67,9674**	**2942,312**	**0,00613**	**0,063393**	**0,05467**	**0,13412**	**0,268516**	**0,18806**	**314,7756**	**91,51316**	**2653,882**
147600	**5,70864E-07**	**8,42595**	**1,55412**	**0,065922**	**6,99091**	**0,600003**	**8240,417**	**67,9674**	**2942,312**	**0,00613**	**0,063393**	**0,05467**	**0,13412**	**0,269564**	**0,18806**	**314,7879**	**91,18035**	**2644,23**
151200	**5,70864E-07**	**8,63146**	**1,57821**	**0,066944**	**6,99091**	**0,600003**	**8240,417**	**67,9674**	**2942,312**	**0,00613**	**0,063393**	**0,05467**	**0,13412**	**0,270586**	**0,18806**	**314,7997**	**90,85788**	**2634,878**
154800	**5,70864E-07**	**8,83697**	**1,60174**	**0,067942**	**6,99091**	**0,600003**	**8240,417**	**67,9674**	**2942,312**	**0,00613**	**0,063393**	**0,05467**	**0,13412**	**0,271584**	**0,18806**	**314,8113**	**90,54519**	**2625,811**
158400	**5,70864E-07**	**9,04248**	**1,62473**	**0,068917**	**6,99091**	**0,600003**	**8240,417**	**67,9674**	**2942,312**	**0,00613**	**0,063393**	**0,05467**	**0,13412**	**0,272559**	**0,18806**	**314,8225**	**90,24176**	**2617,011**
162000	**5,70864E-07**	**9,24799**	**1,64721**	**0,069871**	**6,99091**	**0,600003**	**8240,417**	**67,9674**	**2942,312**	**0,00613**	**0,063393**	**0,05467**	**0,13412**	**0,273513**	**0,18806**	**314,8333**	**89,94711**	**2608,466**
165600	**5,70864E-07**	**9,4535**	**1,66919**	**0,070803**	**6,99091**	**0,600003**	**8240,417**	**67,9674**	**2942,312**	**0,00613**	**0,063393**	**0,05467**	**0,13412**	**0,274445**	**0,18806**	**314,8439**	**89,6608**	**2600,163**
169200	**5,70864E-07**	**9,65901**	**1,69069**	**0,071715**	**6,99091**	**0,600003**	**8240,417**	**67,9674**	**2942,312**	**0,00613**	**0,063393**	**0,05467**	**0,13412**	**0,275357**	**0,18806**	**314,8541**	**89,3824**	**2592,09**
172800	**5,70864E-07**	**9,86453**	**1,71175**	**0,072608**	**6,99091**	**0,600003**	**8240,417**	**67,9674**	**2942,312**	**0,00613**	**0,063393**	**0,05467**	**0,13412**	**0,27625**	**0,18806**	**314,8641**	**89,11153**	**2584,234**

Table B. 2 Results analytical calculations for the optimal pipe configuration (Triangular cross-section) under cooling conditions.

t	α	x	E(x)	Rsol	Pr	v	Re	Nu	H	R p,f	R p	Req	R c	R tot	m	Tout	q	Q
3600	5,70864E-07	0,20551	-2,1595	-0,0916	6,99091	0,600003	8240,417	55,95608	2422,341	0,007446	0,063393	0,05467	0,13412	0,113359	0,18806	310,803	199,2477	5778,182
7200	5,70864E-07	0,41102	-1,4663	-0,0622	6,99091	0,600003	8240,417	55,95608	2422,341	0,007446	0,063393	0,05467	0,13412	0,142761	0,18806	312,1431	162,9058	4724,269
10800	5,70864E-07	0,61653	-1,0608	-0,045	6,99091	0,600003	8240,417	55,95608	2422,341	0,007446	0,063393	0,05467	0,13412	0,159959	0,18806	312,7222	147,2004	4268,811
14400	5,70864E-07	0,82204	-0,7732	-0,0328	6,99091	0,600003	8240,417	55,95608	2422,341	0,007446	0,063393	0,05467	0,13412	0,172162	0,18806	313,0697	137,7761	3995,508
18000	5,70864E-07	1,02755	-0,55	-0,02333	6,99091	0,600003	8240,417	55,95608	2422,341	0,007446	0,063393	0,05467	0,13412	0,181627	0,18806	313,3101	131,2578	3806,477
21600	5,70864E-07	1,23307	-0,3677	-0,0156	6,99091	0,600003	8240,417	55,95608	2422,341	0,007446	0,063393	0,05467	0,13412	0,189361	0,18806	313,4902	126,3728	3664,811
25200	5,70864E-07	1,43858	-0,2135	-0,00906	6,99091	0,600003	8240,417	55,95608	2422,341	0,007446	0,063393	0,05467	0,13412	0,1959	0,18806	313,6323	122,5176	3553,009
28800	5,70864E-07	1,64409	-0,08	-0,00339	6,99091	0,600003	8240,417	55,95608	2422,341	0,007446	0,063393	0,05467	0,13412	0,201564	0,18806	313,7486	119,3633	3461,535
32400	5,70864E-07	1,8496	0,03777	0,001602	6,99091	0,600003	8240,417	55,95608	2422,341	0,007446	0,063393	0,05467	0,13412	0,20656	0,18806	313,8464	116,7128	3384,671
36000	5,70864E-07	2,05511	0,14313	0,006071	6,99091	0,600003	8240,417	55,95608	2422,341	0,007446	0,063393	0,05467	0,13412	0,211029	0,18806	313,9302	114,4397	3318,75
39600	5,70864E-07	2,26062	0,23844	0,010114	6,99091	0,600003	8240,417	55,95608	2422,341	0,007446	0,063393	0,05467	0,13412	0,215072	0,18806	314,0033	112,4583	3261,291
43200	5,70864E-07	2,46613	0,32545	0,013805	6,99091	0,600003	8240,417	55,95608	2422,341	0,007446	0,063393	0,05467	0,13412	0,218763	0,18806	314,0678	110,7085	3210,546
46800	5,70864E-07	2,67164	0,40549	0,0172	6,99091	0,600003	8240,417	55,95608	2422,341	0,007446	0,063393	0,05467	0,13412	0,222158	0,18806	314,1254	109,1462	3165,239
50400	5,70864E-07	2,87715	0,4796	0,020344	6,99091	0,600003	8240,417	55,95608	2422,341	0,007446	0,063393	0,05467	0,13412	0,225301	0,18806	314,1773	107,7385	3124,417
54000	5,70864E-07	3,08266	0,54859	0,02327	6,99091	0,600003	8240,417	55,95608	2422,341	0,007446	0,063393	0,05467	0,13412	0,228228	0,18806	314,2244	106,4603	3087,348
57600	5,70864E-07	3,28818	0,61313	0,026008	6,99091	0,600003	8240,417	55,95608	2422,341	0,007446	0,063393	0,05467	0,13412	0,230966	0,18806	314,2675	105,2917	3053,46
61200	5,70864E-07	3,49369	0,67376	0,028579	6,99091	0,600003	8240,417	55,95608	2422,341	0,007446	0,063393	0,05467	0,13412	0,233537	0,18806	314,3071	104,2172	3022,297
64800	5,70864E-07	3,6992	0,73092	0,031004	6,99091	0,600003	8240,417	55,95608	2422,341	0,007446	0,063393	0,05467	0,13412	0,235962	0,18806	314,3438	103,2239	2993,494
68400	5,70864E-07	3,90471	0,78498	0,033297	6,99091	0,600003	8240,417	55,95608	2422,341	0,007446	0,063393	0,05467	0,13412	0,238255	0,18806	314,3778	102,3017	2966,748
72000	5,70864E-07	4,11022	0,83628	0,035473	6,99091	0,600003	8240,417	55,95608	2422,341	0,007446	0,063393	0,05467	0,13412	0,240431	0,18806	314,4095	101,4418	2941,813
75600	5,70864E-07	4,31573	0,88507	0,037542	6,99091	0,600003	8240,417	55,95608	2422,341	0,007446	0,063393	0,05467	0,13412	0,2425	0,18806	314,4391	100,6373	2918,481
79200	5,70864E-07	4,52124	0,93159	0,039516	6,99091	0,600003	8240,417	55,95608	2422,341	0,007446	0,063393	0,05467	0,13412	0,244474	0,18806	314,467	99,88195	2896,576
82800	5,70864E-07	4,72675	0,97604	0,041401	6,99091	0,600003	8240,417	55,95608	2422,341	0,007446	0,063393	0,05467	0,13412	0,246359	0,18806	314,4932	99,17072	2875,951
86400	5,70864E-07	4,93226	1,0186	0,043206	6,99091	0,600003	8240,417	55,95608	2422,341	0,007446	0,063393	0,05467	0,13412	0,248164	0,18806	314,518	98,49919	2856,476
90000	5,70864E-07	5,13777	1,05942	0,044938	6,99091	0,600003	8240,417	55,95608	2422,341	0,007446	0,063393	0,05467	0,13412	0,249896	0,18806	314,5414	97,86356	2838,043
93600	5,70864E-07	5,34328	1,09864	0,046602	6,99091	0,600003	8240,417	55,95608	2422,341	0,007446	0,063393	0,05467	0,13412	0,25156	0,18806	314,5637	97,26055	2820,556

97200	**5,70864E-07**	**5,5488**	**1,13638**	**0,048203**	**6,99091**	**0,600003**	**8240,417**	**55,95608**	**2422,341**	**0,007446**	**0,063393**	**0,05467**	**0,13412**	**0,25316**	**0,18806**	**314,5848**	**96,68728**	**2803,931**
100800	**5,70864E-07**	**5,75431**	**1,17275**	**0,049745**	**6,99091**	**0,600003**	**8240,417**	**55,95608**	**2422,341**	**0,007446**	**0,063393**	**0,05467**	**0,13412**	**0,254703**	**0,18806**	**314,6049**	**96,14121**	**2788,095**
104400	**5,70864E-07**	**5,95982**	**1,20784**	**0,051234**	**6,99091**	**0,600003**	**8240,417**	**55,95608**	**2422,341**	**0,007446**	**0,063393**	**0,05467**	**0,13412**	**0,256192**	**0,18806**	**314,6241**	**95,62012**	**2772,984**
108000	**5,70864E-07**	**6,16533**	**1,24174**	**0,052672**	**6,99091**	**0,600003**	**8240,417**	**55,95608**	**2422,341**	**0,007446**	**0,063393**	**0,05467**	**0,13412**	**0,25763**	**0,18806**	**314,6425**	**95,12204**	**2758,539**
111600	**5,70864E-07**	**6,37084**	**1,27453**	**0,054063**	**6,99091**	**0,600003**	**8240,417**	**55,95608**	**2422,341**	**0,007446**	**0,063393**	**0,05467**	**0,13412**	**0,25902**	**0,18806**	**314,6601**	**94,6452**	**2744,711**
115200	**5,70864E-07**	**6,57635**	**1,30628**	**0,055409**	**6,99091**	**0,600003**	**8240,417**	**55,95608**	**2422,341**	**0,007446**	**0,063393**	**0,05467**	**0,13412**	**0,260367**	**0,18806**	**314,6769**	**94,18804**	**2731,453**
118800	**5,70864E-07**	**6,78186**	**1,33705**	**0,056715**	**6,99091**	**0,600003**	**8240,417**	**55,95608**	**2422,341**	**0,007446**	**0,063393**	**0,05467**	**0,13412**	**0,261672**	**0,18806**	**314,6931**	**93,74914**	**2718,725**
122400	**5,70864E-07**	**6,98737**	**1,3669**	**0,057981**	**6,99091**	**0,600003**	**8240,417**	**55,95608**	**2422,341**	**0,007446**	**0,063393**	**0,05467**	**0,13412**	**0,262939**	**0,18806**	**314,7087**	**93,32724**	**2706,49**
126000	**5,70864E-07**	**7,19288**	**1,39589**	**0,05921**	**6,99091**	**0,600003**	**8240,417**	**55,95608**	**2422,341**	**0,007446**	**0,063393**	**0,05467**	**0,13412**	**0,264168**	**0,18806**	**314,7237**	**92,92118**	**2694,714**
129600	**5,70864E-07**	**7,39839**	**1,42406**	**0,060405**	**6,99091**	**0,600003**	**8240,417**	**55,95608**	**2422,341**	**0,007446**	**0,063393**	**0,05467**	**0,13412**	**0,265363**	**0,18806**	**314,7381**	**92,52994**	**2683,368**
133200	**5,70864E-07**	**7,60391**	**1,45146**	**0,061568**	**6,99091**	**0,600003**	**8240,417**	**55,95608**	**2422,341**	**0,007446**	**0,063393**	**0,05467**	**0,13412**	**0,266525**	**0,18806**	**314,752**	**92,15256**	**2672,424**
136800	**5,70864E-07**	**7,80942**	**1,47813**	**0,062699**	**6,99091**	**0,600003**	**8240,417**	**55,95608**	**2422,341**	**0,007446**	**0,063393**	**0,05467**	**0,13412**	**0,267657**	**0,18806**	**314,7654**	**91,78819**	**2661,858**
140400	**5,70864E-07**	**8,01493**	**1,50411**	**0,063801**	**6,99091**	**0,600003**	**8240,417**	**55,95608**	**2422,341**	**0,007446**	**0,063393**	**0,05467**	**0,13412**	**0,268758**	**0,18806**	**314,7784**	**91,43605**	**2651,645**
144000	**5,70864E-07**	**8,22044**	**1,52942**	**0,064874**	**6,99091**	**0,600003**	**8240,417**	**55,95608**	**2422,341**	**0,007446**	**0,063393**	**0,05467**	**0,13412**	**0,269832**	**0,18806**	**314,791**	**91,09541**	**2641,767**
147600	**5,70864E-07**	**8,42595**	**1,55412**	**0,065922**	**6,99091**	**0,600003**	**8240,417**	**55,95608**	**2422,341**	**0,007446**	**0,063393**	**0,05467**	**0,13412**	**0,27088**	**0,18806**	**314,8031**	**90,76562**	**2632,203**
151200	**5,70864E-07**	**8,63146**	**1,57821**	**0,066944**	**6,99091**	**0,600003**	**8240,417**	**55,95608**	**2422,341**	**0,007446**	**0,063393**	**0,05467**	**0,13412**	**0,271902**	**0,18806**	**314,8149**	**90,44607**	**2622,936**
154800	**5,70864E-07**	**8,83697**	**1,60174**	**0,067942**	**6,99091**	**0,600003**	**8240,417**	**55,95608**	**2422,341**	**0,007446**	**0,063393**	**0,05467**	**0,13412**	**0,2729**	**0,18806**	**314,8264**	**90,13621**	**2613,95**
158400	**5,70864E-07**	**9,04248**	**1,62473**	**0,068917**	**6,99091**	**0,600003**	**8240,417**	**55,95608**	**2422,341**	**0,007446**	**0,063393**	**0,05467**	**0,13412**	**0,273875**	**0,18806**	**314,8374**	**89,83551**	**2605,23**
162000	**5,70864E-07**	**9,24799**	**1,64721**	**0,069871**	**6,99091**	**0,600003**	**8240,417**	**55,95608**	**2422,341**	**0,007446**	**0,063393**	**0,05467**	**0,13412**	**0,274828**	**0,18806**	**314,8482**	**89,54351**	**2596,762**
165600	**5,70864E-07**	**9,4535**	**1,66919**	**0,070803**	**6,99091**	**0,600003**	**8240,417**	**55,95608**	**2422,341**	**0,007446**	**0,063393**	**0,05467**	**0,13412**	**0,275761**	**0,18806**	**314,8587**	**89,25975**	**2588,533**
169200	**5,70864E-07**	**9,65901**	**1,69069**	**0,071715**	**6,99091**	**0,600003**	**8240,417**	**55,95608**	**2422,341**	**0,007446**	**0,063393**	**0,05467**	**0,13412**	**0,276673**	**0,18806**	**314,8688**	**88,98383**	**2580,531**
172800	**5,70864E-07**	**9,86453**	**1,71175**	**0,072608**	**6,99091**	**0,600003**	**8240,417**	**55,95608**	**2422,341**	**0,007446**	**0,063393**	**0,05467**	**0,13412**	**0,277566**	**0,18806**	**314,8787**	**88,71537**	**2572,746**

Appendice C

Appendice C. 1 Estimation of the number of simulations for GEP study.

Part 1: Variation of Reynolds Number

- Reynolds numbers: 4 (500, 1000, 1500, 2000)
- Mesh: Default (1 mesh)
- Conditions: Heating and Cooling (2)
  - ❑ **Number of simulations:**4 (Re) × 1 (mesh) × 2 = **8 simulations**
  - ❑ **Total computation time estimate:**8 simulations × 12 hours = **96 hours=4days**

Part 2: Geometric Variants

- Pile diameter: 3 (400 mm, 600 mm, 800 mm)
- Pipe diameter: 3 (14 mm, 20 mm, 26 mm)
- Spacing: 4 (0.02 mm, 0.05 mm, 0.1 mm, 0.15 mm)
- Pipe angle: 3 (0°, 30°, 60°)
- Mesh sensitivity: 5 grids
- Conditions: Heating and Cooling (2)
- Reynolds number: 1
  - ❑ **Number of simulations :** 2 × (3+3+4+3) =26+5+3=**34 simulations**
  - ❑ **Total computation time estimate:** 34 × 48 hours = **1632 hours** ÷24 =**68 days**

Part 3: Pipe Geometries and Mesh Sensitivity

- Pipe geometries: 3 (circular, square, triangular)
- Mesh grids: 5 (but same grids applied for each geometry)
- Conditions: Heating and Cooling (2)
- Reynolds number: 1

❑ **Number of simulations:** 3 × 5 × 2 × 1 = **30 simulations**

❑ **Total computation time estimate:** 30 × 48 hours = **1440 hours** ÷ 24 =**60 days**

Total Estimated Simulations

8 + 34 + 30 = 72 simulations

Total computation time

96 + 1632+ 1440 = 3168 hours ÷ 24 =132 days

Appendice D

Appendice D. 1 Scientific production.

D.1/ Paper

S. Boudjaza, A. Chehhat , A. Kaddour , Y. Menni , S. Larguech , B.M. Alshammari , L. Kolsi, "Three-dimensional thermomechanical modeling of geothermal energy piles with U-tube heat exchangers of different cross-sectional shapes", Case Studies in Thermal Engineering, vol. 74, p. 106846, 2025, https://doi.org/10.1016/j.csite.2025.106846

Case Studies in Thermal Engineering 74 (2025) 106846

Contents lists available at ScienceDirect

Case Studies in Thermal Engineering

journal homepage: www.elsevier.com/locate/csite

Three-dimensional thermomechanical modeling of geothermal energy piles with U-tube heat exchangers of different cross-sectional shapes

Samia Boudjaza [a,b], Abdelmadjid Chehhat [a,c], Abdelmadjid Kaddour [d], Younes Menni [e,f,*], Samia Larguech [g], Badr M. Alshammari [h], Lioua Kolsi [i,**]

[a] Department of Mechanical Engineering, Faculty of Science and Technology, University of Khenchela, 40000, Khenchela, Algeria
[b] Laboratory of Engineering and Science of Advanced Materials (ISMA), University of Khenchela, 40000, Khenchela, Algeria
[c] LESET Laboratory, University of Batna 2, Batna, 05000, Algeria
[d] Unité de Recherche Appliquée en Energies Renouvelables, URAER, Centre de Développement des Energies Renouvelables, CDER, 47133, Ghardaïa, Algeria
[e] Department of Mechanical Engineering, Institute of Technology, University Center Salhi Ahmed Naama (Ctr. Univ. Naama), P.O. Box 66, Naama, 45000, Algeria
[f] College of Technical Engineering, National University of Science and Technology, Dhi Qar, 64001, Iraq
[g] Department of Electrical Engineering, College of Engineering, Princess Nourah bint Abdulrahman University, P.O. Box 84428, Riyadh, 11671, Saudi Arabia
[h] Department of Electrical Engineering, College of Engineering, University of Ha'il, Ha'il City, 81451, Saudi Arabia
[i] Department of Mechanical Engineering, College of Engineering, University of Ha'il, Ha'il City, 81451, Saudi Arabia

ARTICLE INFO

Keywords:
Geothermal energy pile
Thermomechanical analysis
Heat exchanger geometry
Thermal performance
Energy foundation systems

ABSTRACT

This study explores the thermomechanical performance of a three-dimensional (3D) geothermal energy pile (GEP) system, emphasizing the optimization of heat exchanger (HE) geometry to improve both thermal efficiency and structural integrity. As GEPs offer a promising avenue for integrating renewable geothermal energy into building foundations, their design must balance energy performance with mechanical stability. A finite volume-based numerical model is developed, employing second-order spatial and temporal discretization and the Pressure-Implicit with Splitting of Operators (PISO) algorithm for pressure–velocity coupling. A segregated solution strategy with under-relaxation is used to ensure numerical stability and convergence. The model simulates a concrete-encased U-shaped HE embedded in clayey soil, with three cross-sectional geometries: circular, square, and triangular. Simulation outcomes are validated against analytical predictions and benchmarked with experimental and numerical data from the literature. Among the tested geometries, the triangular HE demonstrates superior thermal and structural performance under both mechanical and thermomechanical loading conditions. Compared to the circular configuration, the triangular U-pipe enhances cooling efficiency by reducing outlet temperature by 1.2 % and increasing heat extraction by 8.6 %. In heating mode, it raises the outlet temperature by 0.6 % but lowers the heat transfer rate by 4.8 %, underscoring the need for season-specific or hybrid designs. Thermomechanically, the triangular configuration exhibits the highest axial compressive stress in summer, increasing by 6.36 %, while in winter, it shows a 4.75

* Corresponding author.Department of Mechanical Engineering, Institute of Technology, University Center Salhi Ahmed Naama (Ctr. Univ. Naama), P.O. Box 66, Naama, 45000, Algeria.
** Corresponding author.
E-mail addresses: menni.younes@cuniv-naama.dz (Y. Menni), l.kolsi@uoh.edu.sa (L. Kolsi).

https://doi.org/10.1016/j.csite.2025.106846
Received 29 April 2025; Received in revised form 19 July 2025; Accepted 7 August 2025
Available online 9 August 2025

D. 2/ Scientific publications

D. 2 . 1/ International conferences

S. Boudjaza, A.Chehhat, B. Rebai, “Fluid flow and Performances of Geothermal Energy Pile (GEP) Using CFD”, 1st International Conference on Materials Sciences and Technology (Mat Science-2022), Dec,13-15th, 2022, Abbes Laghrour University , Khenchela, Algeria.

S. Boudjaza, A.Chehhat, B. Rebai, “Analysis of pipe diameter changes on the long-term performance of an energy pile system”, 3 rd International Workshop on structural Mechanics and Materials (IWSMM’24), April, 23-24,2024, Mostefa Ben Boulaid Batna 2 University , Algeria.

S. Boudjaza, A.Chehhat, B. Rebai, “ Numerical investigation of pile diameter on geothermal energy pile GEP system for summer and winter periods” Séminaire International sur L’Energétique et les Energies Renouvelables (SIEER 2025), Avril , 22-23, 2025, Université Batna 1, Algeria.

D. 2 . 2/ National conferences

S. Boudjaza, A.Chehhat, B. Rebai," Etude du comportement thermomécanique d'un pieu énergétique par CFD", First National Conference on Thermal Engineering Renewable and Conventional Processes (NCTE22), October, 25th , 2022, Mostefa Ben Boulaid Batna 2 University , Algeria.

S. Boudjaza, A.Chehhat, B. Rebai,"Analysis on the change of distance between the outer diameter of the pipe and the pile by the long-term performance of the energy pile", First National Conference on Mechanical Engineering (NCME'23) , May, 10,2023, Mostefa Ben Boulaid Batna 2 University , Algeria.

S. Boudjaza, A.Chehhat, B. Rebai,"Analysis of the Thermal-Mechanical Response of an Energy Geostructures (GEP) for heating and cooling", Séminaire National sur L'Energétique et les Energies Renouvelables (SNEER 2024), Avril , 22, 2024, Université Batna 1, Algeria.

S. Boudjaza, A.Chehhat, B. Rebai,"CFD Analysis of Ground Changes Effect on the Long-term Performance of a Geothermal Energy Pile", The 7th Students Symposium on Engineering Application of Mechanics (SSENAM'7) " Environment And Socio -Economic Impact", April, 29-30, 2024, Abbes Laghrour University , Khenchela, Algeria.

S. Boudjaza, A.Chehhat, B. Rebai,"Impact of Heat Exchanger Cross -Sectional Geometry on the Thermo-Mechanical Performance of Geothermal Energy Piles (GEPs) During Winter and Summer Periods", Second National Conference on Mechanical Engineering (NCME'25) , November , 26th, 2025, at Mechanical Engineering Department, Mostefa Ben Boulaid Batna 2 University , Algeria.

Thème de Thèse : Etude des performances des pieux à énergie géothermique par l'utilisation de la CFD

Auteurs : Samia BOUDJAZA, Département de génie mécanique, Université de Khenchela.
Spécialité : Energétique.
Rapporteur : Abdelmadjid CHEHHAT
Co-rapporteur : Billel REBAI

RESUME

Les pieux géothermiques (GEP), qui intègrent des éléments structurels de fondation avec des échangeurs de chaleur souterrains, représentent une solution durable et efficace pour le chauffage et le refroidissement des bâtiments, en exploitant la température relativement stable du sol en profondeur. Cette étude propose une analyse paramétrique et multiphysique complète du comportement thermique et thermo-mécanique des GEP en conditions de fonctionnement saisonnières. Elle est divisée en trois parties principales, en s'appuyant sur des simulations numériques avancées réalisées dans ANSYS Workbench. Dans la première partie, la réponse thermique transitoire des GEP en été et en hiver est analysée à l'aide de la dynamique des fluides numérique (CFD) dans ANSYS Fluent, en évaluant l'impact de différents régimes d'écoulement (nombres de Reynolds de 500 à 2000) sur la température de sortie et le taux de transfert de chaleur. Les résultats indiquent que des vitesses d'écoulement plus élevées augmentent le taux de transfert de chaleur, mais réduisent l'efficacité de l'échange thermique en raison d'un temps de séjour du fluide plus court. La deuxième partie est consacrée à une optimisation paramétrique en CFD de plusieurs paramètres géométriques clés : le diamètre du pieu, le diamètre de l'échangeur thermique, l'espacement entre le tuyau et le béton, et l'orientation angulaire du tuyau. Appuyées par un modèle analytique, les simulations permettent d'identifier la configuration optimale (diamètre de pieu de 400 mm, diamètre de tuyau de 26 mm, espacement de 20 mm, et orientation de 30°), offrant de meilleures performances thermiques en mode chauffage comme en mode refroidissement. Une forte corrélation entre les résultats CFD et analytiques confirme la validité du modèle. La troisième partie concerne une analyse thermo-mécanique couplée, évaluant la réponse structurelle des GEP avec des géométries de tuyaux en U de forme circulaire, carrée et triangulaire, à travers un couplage bidirectionnel entre ANSYS Fluent (entrée thermique) et Static Structural (analyse mécanique). Les résultats montrent que la géométrie des tuyaux influence de manière significative à la fois le transfert thermique et la

répartition des contraintes. La configuration triangulaire présente une efficacité de refroidissement supérieure grâce à une convection interne améliorée, mais engendre des concentrations de contraintes localisées qui nécessitent une attention structurelle. Les charges thermiques saisonnières induisent des schémas de contraintes axiales et de cisaillement dépendants de la géométrie, avec un déplacement maximal situé systématiquement à la base du pieu. Dans l'ensemble, cette étude multiphysique basée sur la CFD met en évidence l'influence cruciale des paramètres de conception et des conditions saisonnières sur l'efficacité thermique et la fiabilité mécanique des systèmes GEP, fournissant des recommandations pratiques pour le développement de solutions géothermiques à la fois performantes et durables dans les climats soumis à de fortes variations de température.

Mots-clés : Énergie géothermique, Pieu géothermique (GEP), Simulation numérique, Modélisation analytique, Échangeur de chaleur.

عنوان الأطروحة : دراسة أداء الركائز الجوفية الطاقوية باستخدام المحاكاة العدديّة CFD

الطالبة : سامية بوجزة ، قسم الهندسة الميكانيكية ، جامعة عباس لغرور خنشلة.

التخصص : الطاقوية

المقرّر : عبد المجيد شحاط

المشرف المشارك : بلال ربعي

الملخص

تُمثّل الأكوام الحرارية الجوفية(GEPs) ، التي تدمج العناصر الهيكلية لأساسات المباني مع المبادلات الحرارية الأرضية، حلاً مستدامًا وفعّالًا لتدفئة وتبريد المباني، من خلال الاستفادة من درجة حرارة التربة المستقرة نسبيًا في الطبقات العميقة. تقدم هذه الدراسة تحليلًا شاملًا ومعمّقًا متعدد المتغيرات ومتعدد الفيزياء للسلوكين الحراري والحراري-الميكانيكي للأكوام الجوفية تحت ظروف تشغيل موسمية، وذلك باستخدام محاكاة رقمية متقدمة .ANSYS Workbench . في الجزء الأول، تم تحليل الاستجابة الحرارية العابرة للأكوام الجوفية خلال فصلي الصيف والشتاء باستخدام ديناميكيات الموائع الحسابية (CFD)في برنامجANSYS Fluent ، مع تقييم تأثير اختلاف أنظمة الجريان (أعداد رينولدز من 500 إلى 2000) على درجة حرارة المائع عند المخرج ومعدل انتقال الحرارة. أظهرت النتائج أن زيادة سرعة الجريان تؤدي إلى تحسين معدل انتقال الحرارة، لكنها تقلل من كفاءة التبادل الحراري نتيجة لانخفاض زمن مكوث المائع داخل النظام. يركز الجزء الثاني على تحسين بارامتري هندسي باستخدامCFD ، يشمل أبعادًا رئيسية مثل قطر الكومة، قطر المبادل الحراري، المسافة الفاصلة بين الأنابيب والخرسانة، والزاوية المحيطية لتركيب الأنابيب. وبالاعتماد على النمذجة التحليلية، حددت المحاكاة التكوين الأمثل (قطر كومة 400 مم، قطر أنبوب 26 مم، تباعد 20 مم، وزاوية 30 درجة)، مما أدى إلى تحسين الأداء الحراري في وضعي التدفئة والتبريد. كما أظهرت النتائج توافقًا كبيرًا بين النماذج العددية والنظرية، مما يؤكد صحة النموذج المُعتمد . أما الجزء الثالث، فيتضمن تحليلًا حراريًا-ميكانيكيًا مزدوج الاتجاه، لدراسة السلوك الإنشائي للأكوام ذات أنابيب على شكل حرفU ، وبمقاطع دائرية، مربعة، ومثلثة، من خلال الربط بين ANSYS Fluent(للبيانات الحرارية) و ANSYS Static Structural(للتحليل الميكانيكي). أظهرت النتائج أن شكل المقطع الهندسي للأنبوب يؤثر بشكل كبير على كل من انتقال الحرارة وتوزيع الإجهادات. وقد بيّن التكوين الثلاثي كفاءة تبريد أعلى بفضل تحسين الحمل الحراري الداخلي، ولكنه يُسبب تركّزًا موضعيًا للإجهادات، مما يتطلب اعتبارات إنشائية خاصة. كما تتسبب الأحمال الحرارية الموسمية في أنماط مختلفة من الإجهادات المحورية وقصّية تعتمد على شكل الأنبوب، مع تسجيل أقصى إزاحة دائمًا عند قاعدة

الكومة. بشكل عام، تُبرز هذه الدراسة المتعددة الفيزياء والمعتمدة على المحاكاة العددية (CFD) التأثير الحاسم للمعايير التصميمية وظروف التشغيل الموسمية على كفاءة الأداء الحراري والموثوقية الإنشائية لأنظمة الأكوام الحرارية الجوفية، وتُقدّم إرشادات عملية لتطوير حلول طاقية جيوحرارية فعّالة ومستدامة في المناخات ذات التغيرات الحرارية الكبيرة.

الكلمات المفتاحية :الطاقة الجيوحرارية، الأكوام الحرارية الجوفية (GEP)، المحاكاة العددية، النمذجة التحليلية، المبادلات الحرارية.

Thesis Title: Performance Study of Geothermal Energy Piles Using CFD Simulation
Author: Samia BOUDJAZA, Department of Mechanical Engineering, University of Khenchela
Speciality: Energetics
Supervisor : Abdelmadjid CHEHHAT
Co-supervisor : Billel REBAI

ABSTRACT

Geothermal energy piles (GEPs), which integrate structural foundation elements with ground heat exchangers, represent a sustainable and efficient solution for building heating and cooling by harnessing the relatively stable subsurface soil temperature. This study offers a comprehensive parametric and multi-physics investigation into both the thermal and thermo-mechanical behavior of GEPs under seasonal operating conditions. It is divided into three main parts, using advanced numerical simulations within ANSYS Workbench. In the first part, the transient thermal response of GEPs during summer and winter is analyzed using Computational Fluid Dynamics (CFD) in ANSYS Fluent, assessing the impact of varying flow regimes (Reynolds numbers from 500 to 2000) on outlet temperature and heat transfer rate. Results indicate that higher flow velocities increase the heat transfer rate but reduce thermal exchange efficiency due to shorter fluid residence time. The second part focuses on parametric CFD optimization of key geometric parameters, pile diameter, heat exchanger diameter, pipe-to-concrete spacing, and pipe angular orientation. Supported by analytical modeling, simulations identify the optimal configuration (400 mm pile diameter, 26 mm pipe diameter, 20 mm spacing, and 30° orientation), yielding improved thermal performance in both heating and cooling scenarios. Strong correlation between CFD and analytical results confirms the model's validity. The third part involves a coupled thermo-mechanical analysis, evaluating the structural response of GEPs with circular, square, and triangular U-shaped pipe geometries through two-way coupling between ANSYS Fluent (thermal input) and Static Structural (mechanical analysis). Findings reveal that pipe geometry significantly influences both heat transfer and stress distribution. The triangular configuration demonstrates superior cooling efficiency due to enhanced internal convection but introduces localized stress concentrations that require structural consideration. Seasonal thermal loads induce geometry-dependent axial and shear stress patterns, with maximum displacement consistently occurring at the pile base. Overall,

this CFD-based, multi-physics study highlights the critical influence of design parameters and seasonal conditions on the thermal efficiency and mechanical reliability of GEP systems, offering practical guidance for the development of energy-efficient and resilient geothermal solutions in climates with significant temperature fluctuations.

Keywords: Geothermal energy, Geothermal energy pile (GEP), Numerical simulation, Analytical modelling, Heat exchanger.